Profiling deubiquitylase activity during the cell cycle reveals phosphorylation-dependent regulation of USP7 activity at G_1/S.

Sarah Darling

Thesis submitted in accordance with the requirements of the University of Liverpool for the degree of Doctor in Philosophy

April 2017

Profiling deubiquitylase activity during the cell cycle reveals phosphorylation-dependent regulation of USP7 activity at G_1/S.

Sarah Darling

Abstract

Ubiquitylation is a well-defined regulator of the cell cycle, as temporal degradation of cell cycle effectors is essential to ensure unidirectional progression. A family of approximately 100 deubiquitylases (DUBs) antagonise ubiquitylation and therefore may also play important roles in cell cycle progression. Several DUBs have been associated with the governance of checkpoint transitions through RNA interference screens, yet the periodic regulation of DUB catalytic activity remains unexplored. This project aimed to generate the first global study of cell cycle-dependent DUB regulation.

Active site-directed ubiquitin probes were incubated with extracts from synchronised A549 cell populations enriched for key cell cycle phases. Those DUBs with accessible and reactive active sites were detected by specific immunoblotting, or unbiased triple-labelled mass spectrometry, to comprehensively profile global DUB activity throughout the cell cycle. Twenty-three DUBs were identified, most exhibited differential activity during the cell cycle and interestingly there was pervasive downregulation of DUB activity during mitosis. Further analysis revealed clusters of DUBs that were co-regulated during the cell cycle, the largest of which exhibited increased activity during S-phase coupled with a notable reduction in activity at mitosis. This periodic profile of DUB activity was observed for USP7. A comparative analysis of USP7 abundance and activity identified proportionally increased activity during G_1/S; this coincided with an increase USP7 phosphorylation at serine 18 (S18).

GFP-tagged USP7 constructs were generated harbouring non-phosphorylatable (S18A) or phospho-mimetic (S18E) mutations to investigate the role of phosphorylation in a cellular context. Exogenously expressed USP7-S18A, but not USP7-S18E, exhibited decreased reactivity towards active site-directed ubiquitin probes. Furthermore, both USP7-S18A and catalytically inactive USP7-C223S displayed increased cytoplasmic localisation compared to wild type USP7. This suggests activity-dependent localisation that could alter the availability of USP7 for certain substrates. Importantly, the role of S18 phosphorylation was elucidated in an *in vitro* setting using bacterially expressed USP7. CK2 phosphorylation directly potentiated USP7 catalytic activity, increasing cleavage of K48-linked tetra-ubiquitin chains and ubiquitin-AMC compared to the non-phosphorylated USP7. Enzyme kinetics demonstrated 5-fold higher activity towards ubiquitin-AMC, predominantly through increased K_{cat}. This is the first report that S18-phosphorylation of USP7 fundamentally augments catalytic activity. In a cellular context, this is elevated at G_1/S, affects subcellular compartmentalisation and may alter affinity towards specific substrates.

Acknowledgements

I would like to dedicate this thesis to my grandparents, the late Josephine and Charles Maund, who I miss dearly. In particular, my forever interested, encouraging and always enthusiastic grandmother Josie: she was always keen to know what I was doing and how I was proceeding, although it is likely that she has never fully understood what it was all about!

I am grateful to my parents, Adele and Richard, and my brother Steven, who have provided me with moral and unconditional emotional support throughout my life. A special mention must go to my mum, my eternal cheerleader, who has been with me every step of the way with an inspirational comment always on hand. I am also indebted to my exceptionally supportive boyfriend, David Blackstock, who in addition to keeping me sane over these final few months, has always been a source of love, happiness and uncontrollable laughter.

I would like to express my sincere gratitude to my supervisor Prof. Judy Coulson. In addition to the continuous support during my Ph.D., she provided me an opportunity to work in her laboratory many years ago as an undergraduate, which ignited my desire to become a research scientist. Her guidance, patience and immense knowledge have been invaluable throughout the seven years we have worked together. I could not have imagined having a better mentor for my Ph.D.

I give thanks to Prof. Ian Prior, Prof. Michael Clague and Prof. Sylvie Urbé for their guidance and inspiration throughout my Ph.D. and to all my colleagues on 5th floor (past and present). A special mention must go to Jenna Kenyani and Alice Howarth, your friendship inside and outside of the laboratory has made the past few years thoroughly enjoyable. I would also like to thank Monica Faronato, Joe Sacco and Andrew Fielding for being encouraging and supportive teachers. Finally, I thank, in no particular order, Zohra, Neil, Matthew, Rachel, Vruti, Jenny, Emma, Fi, Yvonne, Claire, Han, Ewan, Amos and Dora for making 5th floor such a fantastic place to work.

Thank you for all your encouragement!

Contents

List of figures

List of tables

List of appendices

List of abbreviations

Abbreviation	Description
A	Alanine
A549	Adenocarcinoma cell line
ACTB	Actin
ADRM1	Adhesion regulating molecule 1
Ahx	Aminohexanoic acid
AKT	RAC-alpha serine/threonine-protein kinase
AMP	Adenosine monophosphate
AMPK	AMP-activated kinase
AMSH	Associated molecule with the SH3 domain of STAM
APC/C	Anaphase-promoting complex/cyclosome
APF-1	ATP-dependent proteolysis factor 1
ASXL1	Additional sex combs-like protein 1
ATG (8/12)	Autophagy-related protein (8/12)
ATM	Ataxia-telangiectasia mutated
ATP	Adenosine triphosphate
ATR	Ataxia-telangiectasia and Rad3-related protein
ATXN3	Spinocerebellar ataxia type 3 protein
AU	Relative fluorescence
BAP1	BRCA1-associated protein 1
BCA	Bicinchoninic acid
BCL-3	B-cell lymphoma 3 protein
BRCC36	BRCA1/BRCA2-containing complex subunit 36
BSA	Bovine serum albumin
BUB3	Budding uninhibited by benzimidazoles 3
BUBR1	BUB1-related kinase
β-TrCp	β-transducin repeat containing protein
C223S-USP7	Catalytically inactive USP7
CCN (A/B/D/E)	Cyclin (A/B/D/E)
CDC (20/25)	Cell division cycle protein (20/25)
CDH1	CDC20 homolog 1
CDK (1/2/4/6)	Cyclin-dependent kinase (1/2/4/6)
CHFR	Checkpoint with Forkhead and Ring Finger
CHIP	C-terminus of the Heat-shock cognate 70-Interacting Protein
CK2	Casein kinase 2
CO_2	Carbon dioxide
CRLs	Cullin Ring ubiquitin E3 ligases
CSN	COP9 signalosome
CYLD	Cylindromatosis
D	Aspartic acid
DAPI	Diamidino-2-phenylindole
DAXX	Death domain-associated protein
DDR	DNA damage response

Abbreviation	Description
DEUBAD	Deubiquitylase adaptor
DMEM	Dulbecco's modified Eagle's medium
DTT	Dithiothreitol
DUB	Deubiquitylase
DUSP	Domain in USP
E	Glutamic acid
ECACC	European Collection of Cell Cultures
ERAD	ER-associated protein degradation
ESCRT	Endosomal sorting complex required for transport
FBS	Foetal Bovine Serum
FAT10	HLA-F adjacent transcript
FC	Flow cytometry
FCP1	TFIIF-associating C-terminal domain phosphatase
FSG	Fish skin gelatin
FT	Flow through
GMPS	Guanosine monophosphate synthase
H	Histidine
HA	Haemagglutinin
HACE1	HECT domain and ankryin repeat containing E3 protein ligase 1
HCF-1	Host cell factor-1
HDAC	Histone deacetylase
HECT	Homologous to the E6AP carboxyl terminus
HEPES	4-(2-hydroxyethyl)-1-piperazineethanesulfonic acid
HIF	Hypoxia-inducible factor
HOIP	HOIL-1 interacting protein
I	Isoleucine
iBAQ	Intensity-based absolute quantification
INO80G	INO80 complex subunit G
ISG15	Interferon-stimulated gene 15
JAMM	JAB1/MPN/MOV34
JOSs	Josephins
K	Lysine
K48-Ub_4	K48-linked tetra-ubiquitin chain
K_{cat}	Catalytic turnover
K_m	Substrate binding affinity
LC-MS/MS	Liquid chromatography-Mass Spectrometry
LPP	Lambda phosphatase
LUBAC	Linear ubiquitin chain assembly complex
M	Methionine
MAD2	Mitotic arrest deficient 2
MCC	Mitotic checkpoint complex
MDM2	Mouse double minute 2
MINDY	MIU-containing novel DUB
MIU	Motif-interacting with Ub

Abbreviation	Description
MJD	Machado Joseph disease
MM	Multiple myeloma
MPN	Mpr1-Pad1-N-terminal
MRC-PPU	MRC Protein Phosphorylation and Ubiquitylation Unit
mRNA	Messenger RNA
MYT	Membrane-associated tyrosine- and threonine-specific cdc2-inhibitory kinase
MS	Mass spectrometry
NB	Neuroblastoma
NEAA	Non-essential amino acids
NEDD8	Neural precursor cell expressed developmentally down-regulated protein 8
NEMO	NF-κB essential modulator
NF-κB	Nuclear factor kappa-light-chain enhancer of activated B cells
NKI	Netherlands Cancer Institute
NLS	Nuclear localisation signal
OTPNT1	Non-targeting control
OUT	Ovarian tumour protease
P53	Cellular tumour antigen P53
PBS	Phosphate-buffered saline
PCNA	Proliferating cell nuclear antigen
PFA	Paraformaldehyde
PH	Pleckstrin homology
PHOSIDA	Phosphorylation Site Database
PI	Propidium iodide
PIM	PUB interacting motif
PLK1	Polo-like kinase 1
P	Proline
PPM1G	Protein phosphatase magnesium-dependent 1 gamma
PSMB5	B5-subunit of the proteasome
PSMD14	26S proteasome non-ATPase regulatory subunit 14
PTEN	Phosphatase and tensin homolog
PTM	Post-translational modification
PUB	PNGase/UBA/UBX
QPCR	Quantitative real-time RT-PCR
R	Arginine
Rb	Retinoblastoma protein
RBR	RING-betweenRING-RING
RING	Really interesting new gene
RNAi	RNA-interference
RNF168	RING finger protein 168
RT	Reverse transcription
PCR	Polymerase Chain Reaction
S	Serine

Abbreviation	Description
S18A-USP7	Non-phosphorylatable USP7
S18E-USP7	Phospho-mimetic USP7
SAC	Spindle assembly checkpoint
SCF	Skp-Cullin-Fbox
SDS-PAGE	SDS polyacrylamide gel electrophoresis
SILAC	Stable isotope labelling of amino acids in cell culture
STAM	Signal transducing adaptor molecule
snRNP	Small nuclear ribonucleo protein
siRNA	Short interfering RNA
SUMO	Small ubiquitin-related modifier
T	Threonine
TCR	T-cell receptor
TFA	Trifluoroacetic acid
TGF-β	Transforming growth factor-β
TNFAIP3	Tumour necrosis factor alpha-induced protein 3
TRAF	TNF receptor-associated factor
TRIKA2	TRAF6-regulated IκB kinase activator 2
TRIM21	Tripartite motif-containing protein 21
UAF1	USP1-associated factor 1
Ub	Ubiquitin
UBA domains	Ubiquitin associated domains
Ub-AMC	Ubiquitin 7-amido-4-methylcoumarin
Ub-based probes	Ubiquitin-based active site-directed probes
UBE2 (C/O/S)	Ubiquitin-conjugating enzyme E2 (C/O/S)
UBE3C	Ubiquitin protein ligase E3C
UBL domain	Ubiquitin-like domain
Ub-PA	C-terminally propargylated ubiquitin
Ub-VME	Ubiquitin-vinylmethyl ester
UCH	Ubiquitin C-terminal hydrolase
UIM	Ubiquitin interacting motif
UPS	Ubiquitin proteasome system
USP	Ubiquitin specific protease
URM1	Ubiquitin-related modifier 1
UFM1	Ubiquitin fold modifier 1
VAMP8	Vesicle-associated membrane protein 8
W	Tryptophan
WEE1	WEE1-like protein kinase
WT-USP7	Wild type USP7
Y	Tyrosine
ZAP70	Z-chain-associated protein of 70kDa
ZnF domain	Zinc-finger domain

Chapter 1

Introduction

1.1 The Ubiquitin Code

1.1.1 The history of ubiquitin

In 1975, a small heat stable polypeptide was isolated from bovine thymus tissue and found to be ubiquitously expressed in all tissues studied, and so was named ubiquitin (Goldstein et al., 1975; Schlesinger et al., 1975). This new protein was shown to interact with and covalently attach to a chromatin-associated protein, histone H2A (Goldknopf and Busch, 1977). However, the importance of this conjugation was not yet realised. A seemingly unrelated study also isolated a new protein, ATP-dependent proteolysis factor 1 (APF-1), which was found to regulate proteolytic degradation when APF-1 was covalently conjugated to proteins (Ciechanover et al., 1980; Hershko et al., 1980).

It was later discovered, after biochemical comparison of the two newly isolated proteins, that APF-1 and ubiquitin were one and the same (Wilkinson et al., 1980). This observation confirmed that one protein, ubiquitin, linked two very different aspects of cell biology: gene transcription and protein degradation, sparking the idea that this small polypeptide may be a fundamental part of a complex regulatory network that governs numerous facets of cell biology.

Since this seminal work in the 1980's, a wealth of research has uncovered the myriad cellular roles for ubiquitin and the host of proteins within this complex regulatory network, thousands of proteins have been identified to regulate ubiquitin signalling in cells, additionally a comprehensive study has revealed tens of thousands of ubiquitylation sites within the human proteome (Kim et al., 2011).

1.1.2 The ubiquitin genes

Four separate genes encode ubiquitin: UbB, UbC, UBA52 and RPS27a, each of which contributes to the total amount of cellular ubiquitin, or the "free ubiquitin pool" (Monia et al., 1989; Wiborg et al., 1985). However, it has been predicted that UbC is the major contributor to this pool, with approximately 40% of free ubiquitin encoded for by the UbC gene (Heride et al., 2014; Kaiser et al.,

2011). Each gene generates a precursor polypeptide that must be processed to produce functional ubiquitin monomers. UbB and UbC encode polyubiquitin strands with head-to-tail fused ubiquitin repeats of three or nine ubiquitins respectively. Conversely, UBA52 and RPS27a only encode one ubiquitin polypeptide, and it is fused through its C-terminus to a ribosomal subunit protein (Monia et al., 1989). Once processed, a 76 amino acid globular ubiquitin protein is produced.

Interestingly, despite variance at the DNA level, ubiquitin is an extremely highly conserved polypeptide with only 3 amino acids varying between the yeast and human peptide sequences (Phillips and Corn, 2015). This confirms that nearly every amino acid and the three-dimensional structure created plays a specific and important role in ubiquitin signalling.

1.1.3 Ubiquitin and ubiquitin-like modifiers

Ubiquitin is a member of the ß-grasp family, as its compact three-dimensional structure encompasses a single α-helix flanked by two pairs of sequential ß-sheets (Vijay-Kumar et al., 1987). This compact folded structure presents a number of sites important for ubiquitin function including protein interaction and the formation of polyubiquitin chains. Ubiquitin exists in three forms within the cell, as previously mentioned there is a pool of “free” ubiquitin which accounts for approximately 23% of the total amount of cellular ubiquitin (Kaiser et al., 2011). Ubiquitin can also exist in an “activated” state, in which it is linked through a thioester bond to enzymes within the ubiquitin conjugation cascade (see Section 1.1.4). Finally, “conjugated” ubiquitin, which represents any ubiquitin molecule that has been covalently bound to cellular proteins. The human genome also encodes a number of ubiquitin-like proteins, or UBLs, these alternative modifications include: small ubiquitin-related modifier (SUMO), neural precursor cell expressed developmentally down-regulated protein 8 (NEDD8), interferon-stimulated gene 15 (ISG15), HLA-F adjacent transcript (FAT10), autophagy-related protein 8 (ATG8), autophagy-related protein 12 (ATG12), ubiquitin-related modifier 1 (URM1) and ubiquitin fold modifier 1

(UFM1). These are all structurally similar to ubiquitin and modify cellular proteins in a similar, yet distinct, manner (Cappadocia and Lima, 2017).

The post-translational covalent attachment of an ubiquitin moiety to a substrate protein is named “ubiquitylation”. This process involves the covalent conjugation of the flexible C-terminus of ubiquitin (glycine 76) to the ε-amino group of a lysine (K) residue. In its most basic form, ubiquitylation is the covalent addition of one ubiquitin moiety to a K residue on a target protein, termed “monoubiquitylation”. Similarly, a protein can be monoubiquitylated numerous times on separate residues, termed “multi-monoubiquitylation”.

Ubiquitin itself possesses seven K residues: K6, K11, K27, K29, K33, K48 and K63 (Figure 1.1A and B). These internal K residues enable the formation of polyubiquitin chains in which additional ubiquitin monomers are tagged onto one of the seven internal Ks or the N-terminal methionine (M1) to form an ubiquitin polymer, termed “polyubiquitylation”. Furthermore, there are multiple versions of polyubiquitin present within the ubiquitin signalling network. Although some ubiquitin polymers are restricted to a single K linkage, termed “homotypic” polyubiquitylation, there are “heterotypic” ubiquitin polymers that incorporate multiple K linkages, which can also be “branched” so that a single ubiquitin molecule is ubiquitylated on more than one site. Evidently, the world of ubiquitylation is multifaceted and each layer relies upon different families of proteins to either write, read or erase this “ubiquitin code” as comprehensively reviewed in (Akutsu et al., 2016; Swatek and Komander, 2016). A simplified view of the complexity within the ubiquitin code is illustrated in Figure 1.2.

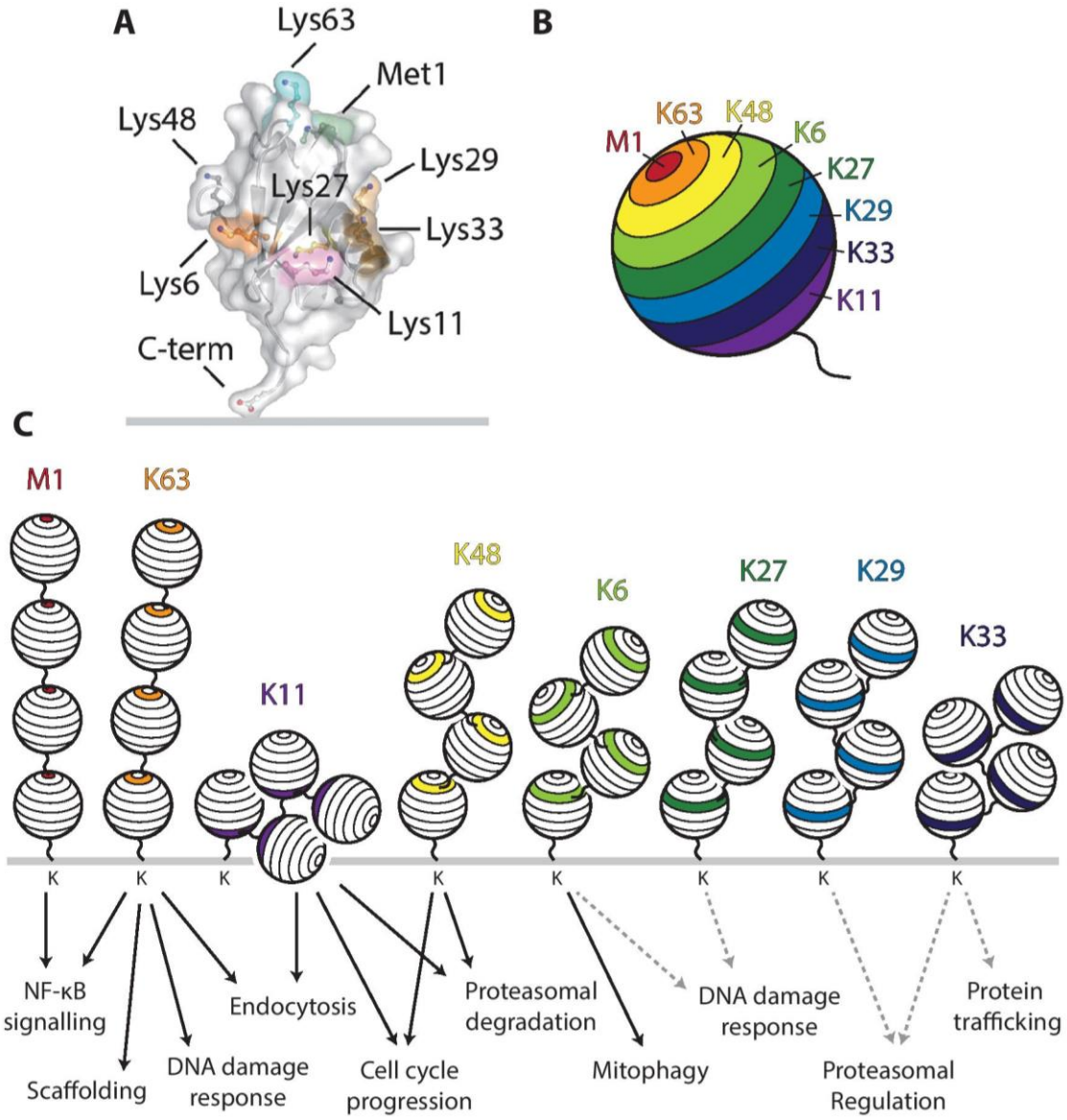

Figure 1.1: Ubiquitin Chain linkages and their associated signalling pathways.
A-B: Ubiquitin has seven internal lysines and an N-terminal methionine, all of which can be modified by ubiquitin to form polyubiquitin chains, A is schematically represented in B. **C:** The signalling pathways affected by linkage-specific ubiquitin signalling.

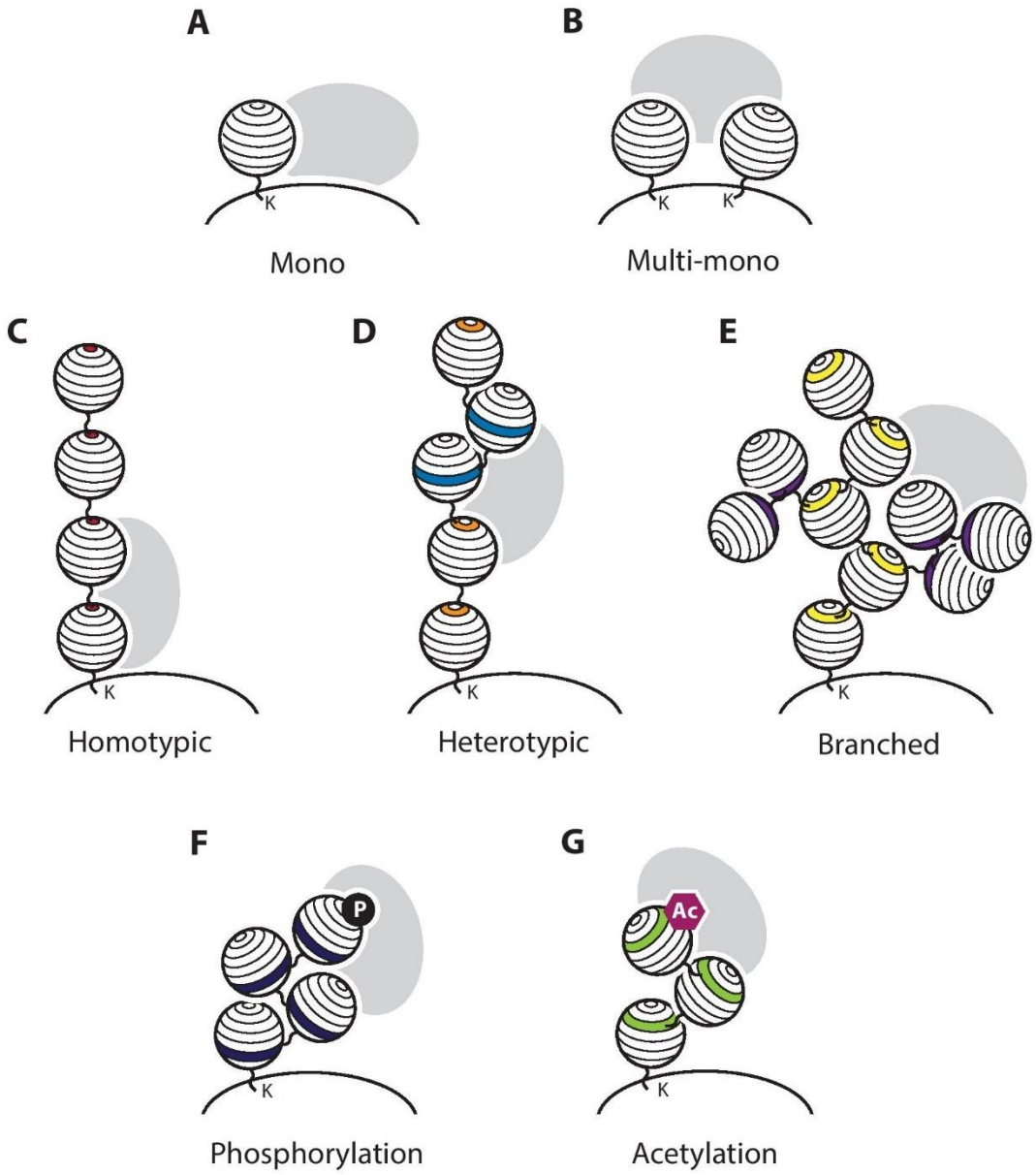

Figure 1.2: The increasing complexity of the ubiquitin code.
A-E: Different ubiquitin chain topologies. A: Monoubiquitylation, B: Multi-monoubiquitylation, C: Homotypic polyubiquitylation, D: Heterotypic polyubiquitylation, E: Branched ubiquitin polymers. F and G: Post-translational modifications of ubiquitin: Phosphorylation (F) and Acetylation (G). Grey ellipses represent proteins that interact with these different ubiquitin signals.

1.1.4 Ubiquitylation: Writing the Ubiquitin Code

Despite vast diversity in ubiquitylated substrates, the steps catalysed by the ubiquitylation machinery are highly conserved. Ubiquitylation is a multi-step process in which an ubiquitin monomer is sequentially relayed between three different enzymes prior to its covalent addition to target proteins. These proteins are the E1 ubiquitin activating enzyme, the E2 ubiquitin conjugating

enzyme and the E3 ubiquitin protein ligase. As reviewed in Clague et al (2015), the human genome encodes for eight E1 enzymes, approximately forty E2 enzymes (Li et al., 2008; Stewart et al., 2016), more than six hundred E3 ligases (Li et al., 2008), a clear depiction of the complexity involved in functional ubiquitylation.

As illustrated in Figure 1.3, the process begins with the C-terminal carboxylate of glycine 76 being adenylated by the E1 enzyme in an adenosine triphosphate (ATP)-dependent process. Subsequently, a conserved nucleophilic cysteine residue within the E1 activating enzyme displaces the residual adenosine monophosphate (AMP) from this adenylate intermediate. This forms a thioester bond between the ubiquitin C-terminus and the E1 enzyme (Ciechanover et al., 1982; Hershko and Ciechanover, 1998). This process is then repeated, the binding and ensuing acetylation of a second ubiquitin monomer results in a ternary complex, in which the E1 is now asymmetrically bonded with two ubiquitin molecules, one covalently as a thioester conjugate and one non-covalently as an adenylate intermediate. The now activated ubiquitin moiety is transferred from the ternary complex to the active site cysteine of an E2 conjugating enzyme in a transthioesterification, or transthiolation, reaction (Hershko and Ciechanover, 1998; Hershko et al., 1983).

The final step in this ubiquitylation cascade is the E3 ligase-mediated conjugation of the C-terminal tail of ubiquitin to a lysine residue on a target protein. The E3 enzymes regulate the specificity within this pathway, recruiting particular downstream targets to the E2 enzymes and facilitating the transfer of the ubiquitin moiety. There are three types of E3 ligase each classified using characteristic protein domains and their mechanism of ubiquitin transfer: the really interesting new gene (RING) E3 ligases, the homologous to the E6AP carboxyl terminus (HECT) E3 ligases and the RING-between-RING (RBR) E3 ligases (Morreale and Walden, 2016). The RING family of E3 ubiquitin ligases (Metzger et al., 2014), including U-box and multimeric E3 complexes, are the most common type of E3. They are catalytically inert and so function by mediating the direct transfer of ubiquitin to the substrate. They act as a scaffold to bring the ubiquitin-bound E2 enzyme within proximity of the specific target protein. Conversely, HECT (Rotin and Kumar, 2009) and RBR (Spratt et al., 2014) E3

ligases employ a two-step mechanism of action where the ubiquitin is first transferred to a catalytic cysteine within the catalytic domain prior to its transfer to the target protein. For all E3 families the ubiquitin-charged E2 enzymes are recruited to the N-terminal domains, and the C-terminal protein domains possess the catalytic cysteine required for ubiquitin transfer.

Outlined above are the mechanisms involved in conjugating an ubiquitin monomer to a target protein. Monoubiquitylation can have a profound effect on protein function by either changing its cellular distribution or regulating its catalytic activity. However, as alluded to in Section 1.1.3, ubiquitin can form homotypic and heterotypic polymers, and particular E2/E3s extend ubiquitin chains through specific linkages (reviewed in (Clague et al., 2015)). These chains are essential for correct downstream signalling.

1.1.5 Ubiquitin signalling: Interpreting the Ubiquitin Code

As reviewed in (Scott et al., 2015), proteins modified with ubiquitin are recognised by a specific subset of interactors, these proteins often possess ubiquitin interacting motifs (UIMs) or ubiquitin associated domains (UBA domains) to help them interact with specific ubiquitin moieties. These proteins also bind downstream effectors and so link an ubiquitylation event with a physiological outcome. Many of these ubiquitin binding proteins have a preference for specific ubiquitin monomers and polymers, these different forms of ubiquitylation are often associated with different cellular functions. More recently, the signalling pathways associated with ubiquitin chain diversity have been comprehensively reviewed in (Swatek and Komander, 2016) revealing the vast array of cellular processes regulated through ubiquitylation (Figure 1.1C).

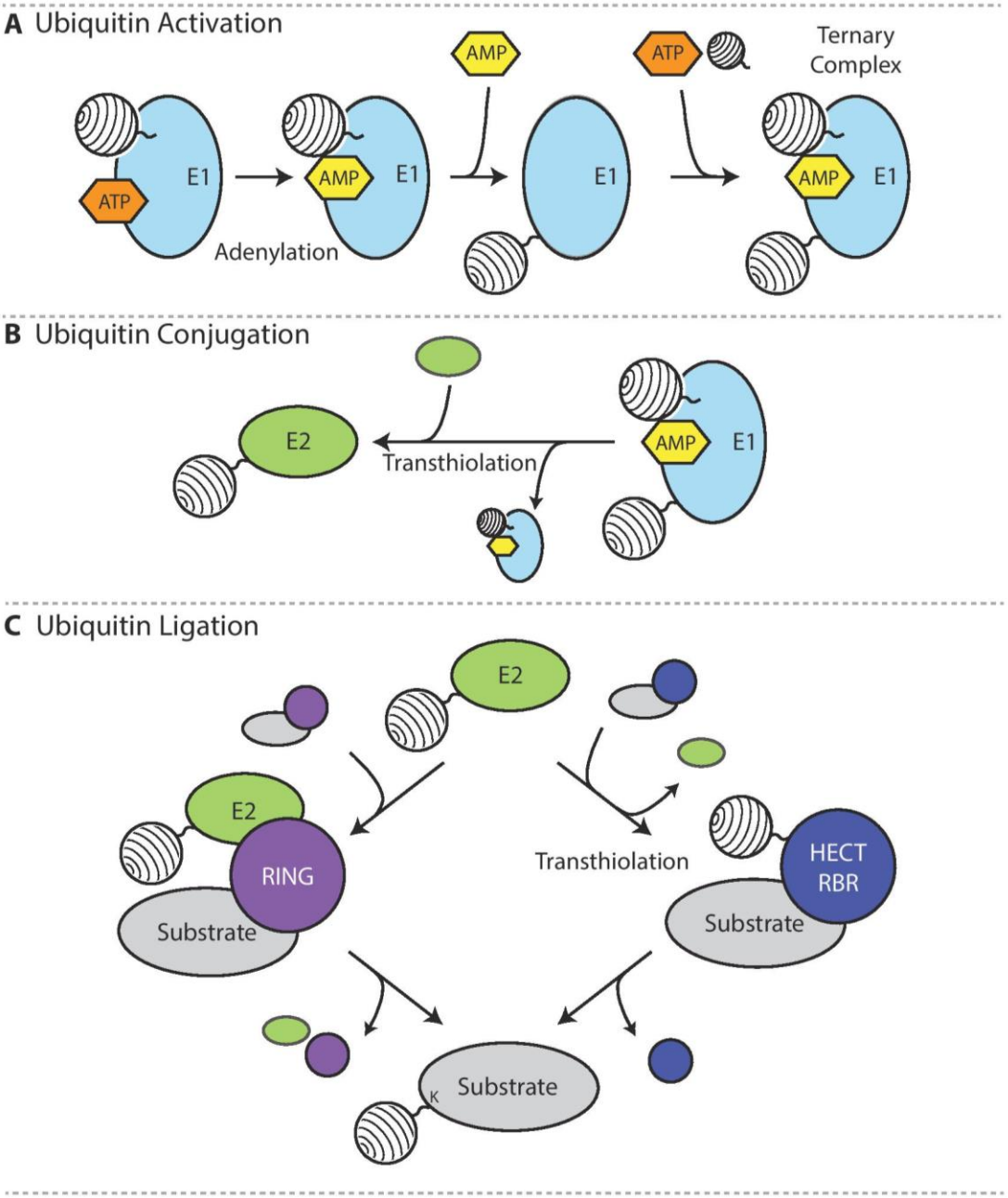

Figure 1.3: The Ubiquitin Conjugation Pathway.

A: Ubiquitin Activation. The process begins with ATP-dependent formation of an adenylate intermediate and the subsequent formation of a thioester bond between the C-terminus of ubiquitin and a catalytic cysteine in the E1 enzyme active site. The process is repeated to form the asymmetrically bound ternary complex possessing an activated ubiquitin moiety. **B: Ubiquitin Conjugation**. By transthiolation, the activated ubiquitin monomer is transferred to the catalytic cysteine of an E2 conjugating enzyme. **C: Ubiquitin ligation to a substrate protein.** Ubiquitin transfer to a substrate occurs in an E3-dependent manner. RING E3 ligases (purple) catalyses the reaction by bringing an E2 enzyme and the substrate into proximity. HECT and RBR E3 ligases (dark blue) employ a two-step process, where the ubiquitin monomer is transferred on to the E3 prior to its conjugation to a substrate.

1.1.5.1 K48 ubiquitin chains

In the not-too-distant past, polyubiquitylation was a euphemism for K48-linked and K63-linked ubiquitin chains, as these were most extensively researched and so best understood. K48-linked ubiquitin chains are the most abundant ubiquitin chain type present in cells, often making up at least 50% of all ubiquitin chains (Swatek and Komander, 2016). K48-linked ubiquitin was first identified on proteins targeted to the proteasome, moreover K48 was demonstrated to be the only essential internal ubiquitin lysine in *Saccharomyces cerevisiae* because of this role in proteasomal-mediated protein degradation (Finley et al., 1994). Further biochemical investigation suggested that a K48-linked tetra-ubiquitin chain was the minimum chain length required for proteasomal targeting (Thrower et al., 2000). However, more recent studies revealed that two K48-linked di-ubiquitins are more efficient for proteasomal targeting than the K48 tetra-ubiquitin chain (Lu et al., 2015), suggesting that the K48-mediated proteolytic signal is not as simple as once thought.

1.1.5.2 K63 ubiquitin chains

Like K48-linked ubiquitin chains, K63-linked polyubiquitylation has been extensively studied. Yet unlike K48, K63 ubiquitin polymers do not target proteins for proteasomal degradation, with K63 modified proteins often directed to endosomal-lysosomal structures instead (Nathan et al., 2013). K63 polymers preferentially interact with components of the endosomal sorting complex required for transport (ESCRT) machinery, preventing K63 modified proteins from binding to proteasomes (Nathan et al., 2013). K63 chains were classically shown to regulate nuclear factor kappa-light-chain enhancer of activated B cells (NF-κB) signalling (Chen and Sun, 2009). Upon receptor stimulation, TNF receptor-associated factor 6 (TRAF6) a RING E3 ligase is recruited to the cellular membrane and catalyses the addition of K63-linked polyubiquitin chains to adjacent adaptor proteins, including itself. These K63-linked polyubiquitin chains act as scaffolds recruiting upstream NF-κB signalling effectors, including the ubiquitin-dependent TRAF6-regulated IκB kinase activator 2 (TRIKA2), a kinase complex that initiates a cascade of phosphorylation events that result in the nuclear translocation of NF-κB and subsequent target gene transcription (Wang et al., 2001). It was subsequently identified that K63-linked ubiquitin

polymers were not the only chain type involved in this signalling pathway, with downstream signalling proteins scaffolded on M1-linked linear ubiquitin chains as well (Rahighi et al., 2009). K63-linked polyubiquitylation has also been linked to a number of additional signalling pathways, including DNA repair and endocytosis (Chen and Sun, 2009).

1.1.5.3 Linear (M1) ubiquitin chains

Like K63 chains, linear ubiquitin chains act as protein scaffolds mediating the interaction of key effectors in cell signalling pathways. The discovery of linear ubiquitin chains was crucial in furthering the biological understanding of ubiquitin-mediated regulation of NF-κB signalling. Initially, the linear ubiquitin chain assembly complex (LUBAC) was identified, the first E3 ligase that exclusively assembled M1-linked ubiquitin chains (Kirisako et al., 2006). Subsequently, NF-κB essential modulator (NEMO) was shown to specifically interact with these LUBAC generated linear ubiquitin chains, directly linking M1-linked polyubiquitin with NF-κB signalling (Rahighi et al., 2009).

1.1.5.4 K6 ubiquitin chains

In contrast to a number of ubiquitin chain types, K6 polymers are not enriched upon proteasomal inhibition, suggesting that these polymers mediate non-degradative signalling (Kim et al., 2011). Due to the lack of K6-specific detection methods, distinct cellular roles for K6 ubiquitin polymers are not well understood. However, K6 ubiquitin chains have been associated with the DNA damage response after UV-induced genotoxic stress (Elia et al., 2015). Additional studies have linked K6 ubiquitin chains to mitochondrial homeostasis, as cells expressing K6 ubiquitin mutants exhibiting delayed mitophagy (Cunningham et al., 2015).

1.1.5.5 K11 ubiquitin chains

Like M1-linked chains, the physiological roles of K11 polyubiquitin signalling are extensively studied and so better understood. In asynchronous cells, only approximately 2% of all ubiquitin chains are K11-linked, but substantially

increased K11 chain formation is seen at mitosis (Wickliffe et al., 2011). The best characterised role for K11-linked ubiquitin is as an additional proteasomal degradation signal. However, contrary to the initial hypothesis, homotypic K11 chains are poor substrates for proteasomal degradation, and instead are incorporated into branched heterotypic K48/K11 polymers to promote the degradation of cell cycle effectors (Grice et al., 2015). K11-linked chains have also been associated with the hypoxia signalling response by regulating hypoxia-inducible factors (HIFs) HIF-1α and HIF-2α (Bremm et al., 2014; Moniz et al., 2015). Interestingly, K11-linked ubiquitin chains induced HIF-1α degradation in a proteasomal independent mechanism, suggesting that K11-linked ubiquitin chains can mediate multiple mechanisms of protein degradation (Bremm et al., 2014).

1.1.5.6 K27 ubiquitin chains

K27-linked ubiquitin chains are the least understood ubiquitin polymer type. To date, there are no known proteins containing K27-specific ubiquitin binding domains, making it harder to attribute biological functions for this linkage type. However, recent reports have linked K27-linked ubiquitin with two E3 ligases: ring finger protein 168 (RNF168) and HECT domain and ankryin repeat containing E3 protein ligase 1 (HACE1) (Gatti et al., 2015; Palicharla and Maddika, 2015). These findings have associated K27-linked ubiquitylation with the DNA damage response, protein secretion and autophagic flux (Gatti et al., 2015; Liu et al., 2014; Palicharla and Maddika, 2015).

1.1.5.7 K29 ubiquitin chains

In contrast to K6-linked ubiquitin polymers, K29-linked ubiquitin chains were enriched upon proteasomal inhibition, inferring that K29-linked polymers signal for proteasomal-dependent protein degradation (Kim et al., 2011). However, more recent reports have suggested a different theory. K29-linked ubiquitin chains are assembled by the ubiquitin protein ligase E3C (UBE3C), a proteasomal associated HECT E3 ligase (Besche et al., 2014; You and Pickart, 2001). This ligase was found to modify the proteasomal subunit adhesion regulating molecule 1 (ADRM1), also referred to as RPN13, with K29-linked chains during

periods of proteasomal stress (Besche et al., 2014), instead suggesting the K29 ubiquitin linkages play a regulatory role in proteasomal function.

1.1.5.8 K33 ubiquitin chains

K33-linked ubiquitin chains also appear to relay non-degradative signals, instead these linkages regulate the T-cell receptor (TCR) and AMP-activated kinase (AMPK)-related kinase signalling pathways. In TCR signalling, K33-linked ubiquitin prevented the ζ-chain-associated protein of 70kDa (ZAP70) kinase from interacting with the TCR, and so reduced downstream signalling (Huang et al., 2010). Members of the AMPK-related kinase family exhibited decreased kinase activity upon K33-linked polyubiquitylation (Al-Hakim et al., 2008). More recently, K33-linked chains have been shown to regulate anterograde protein trafficking within the *trans*-Golgi network (Yuan et al., 2014).

1.1.5.9 Additional layers of complexity in ubiquitin signalling

As alluded to in Sections 1.1.5.5, K48/K11 heterotypic ubiquitin polymers can also regulate cell signalling pathways. In addition to this, heterotypic K63/M1 polymers have been shown to regulate the NF-κB signalling response. Interestingly, when K29-linked polymers are enriched from cells, they are often found as part of heterotypic chains (Kristariyanto et al., 2015). The influence of heterotypic and branched chain ubiquitin signalling adds yet more complexity to the ubiquitin code (Figure 1.2).

As recently reviewed in (Swatek and Komander, 2016), ubiquitin itself is subject to post-translational modification and polyubiquitin chains are becoming more complex. The ubiquitin monomer has been shown to be phosphorylated, acetylated and sumoylated, each modification regulating the behaviour of ubiquitin in a different way. There are eleven predicted phosphorylation sites on ubiquitin, although to date only one, serine 65 (S65), is thought to be functionally important (Wauer et al., 2015). Originally, S65 phosphorylation was shown to promote mitophagy, acting as a recruitment platform for mitophagy adaptors at mitochondrial membranes (Kane et al., 2014; Kazlauskaite et al.,

2014; Koyano et al., 2014). Since this discovery, S65 phosphorylation of ubiquitin has been shown to affect its structure, polyubiquitin chain assembly and ubiquitin chain hydrolysis, this has been comprehensively discussed in (Wauer et al., 2015).

Acetylation of K residues on ubiquitin monomers is also suggested to affect the formation and disassembly of polyubiquitin chains, again reviewed in (Swatek and Komander, 2016). As the authors suggest, these PTMs have significantly expanded the complexity of the ubiquitin code (Figure 1.2), revealing that there is yet more to uncover about ubiquitin as a post-translational modification.

1.2 The Deubiquitylases: Erasing the Ubiquitin Code

The reversible nature of ubiquitylation as a post-translational modification lends itself to dynamic signalling within the cells, as each modification event can be quickly reversed cancelling the signal. The group of isopeptidases responsible for erasing the ubiquitin code are the deubiquitylases or DUBs (Figure 1.4).

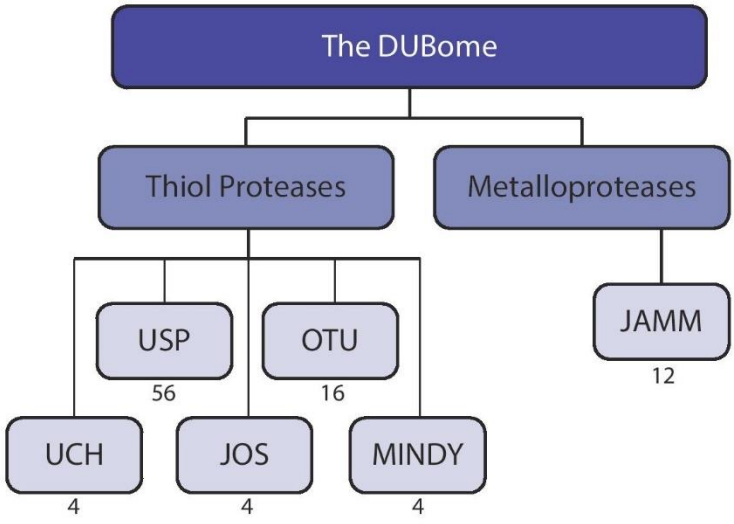

Figure 1.4: The architecture of the DUBome.
Deubiquitylates are divided into two classes of enzymes: Thiol proteases and metalloproteases. These classes are further subdivided into 6 DUB families: ubiquitin specific proteases (USPs), ubiquitin C-terminal hydrolases (UCHs), ovarian tumour proteases (OTUs), Josephins (JOSs), motif-interacting with Ub (MIU)-containing novel DUB family (MINDYs) and JAB1/MPN/MOV34 family (JAMMs). The number of members in each family in noted underneath.

1.2.1 DUB function

As discussed in (Komander et al., 2009), DUB activity can be outlined by three main functions, each of which helps to maintain an adequate pool of free ubiquitin ready for immediate conjugation. Firstly, as outlined in Section 1.1.2, ubiquitin is synthesised *de novo* as fusion proteins, either ribosomal protein-fused or strings of consecutive ubiquitins, that must be cleaved by DUBs in order to produce free ubiquitin monomers. Secondly, working in direct opposition to E3 ligases, DUBs can remove ubiquitin chains from substrate proteins, which leads to the reversal of the ubiquitin signal. This is nicely exemplified through protein stabilisation after the DUB-mediated removal of K48-linked ubiquitin chains. Finally, DUBs can edit the signal through ubiquitin chain trimming. Here, the remodelling of ubiquitin chain linkages can alter the fate of substrate proteins, although the extent to which DUBs play a role in remodelling is less well studied.

1.2.2 The DUB families

The human genome encodes approximately one hundred DUBs, that have been further sub-categorised into six DUB families based upon the homology of their catalytic domains: ubiquitin specific proteases (USPs), ubiquitin C-terminal hydrolases (UCHs), ovarian tumour proteases (OTUs), Josephins (JOSs), motif-interacting with Ub (MIU)-containing novel DUB family (MINDYs) and JAB1/MPN/MOV34 family (JAMMs).

Two different DUB catalytic mechanisms have been determined and so these six families can be additionally grouped into either metalloproteases (the JAMMs) or thiol proteases (the USPs, UCHs, OTUs, JOSs and MINDYs). The metalloproteases require a zinc ion to facilitate the activation of water molecules for the subsequent ubiquitin chain hydrolysis. Conversely, the thiol proteases harbour a catalytic triad comprising cysteine, histidine and aspartate residues that coordinate to perform a nucleophilic attack of the ubiquitin peptide bond. This process is outlined in more detail in Section 3.1.

1.2.2.1 USPs

The USP family is by far the largest DUB family, with 56 members (Figure 1.4). Structurally, USPs have been likened to an open hand, containing folds resembling palm, thumb and finger subunits to aid in the catalysis of ubiquitin bonds. In addition to the conserved catalytic domain, the DUBs within the USP family express a diverse array of accessory domains, including ubiquitin-like (UBL) domains, pleckstrin homology (PH) domains and zinc-finger ubiquitin binding (ZnF) domains that can influence DUB activity or localisation and so regulate their behaviour within the cell (Clague et al., 2013; Komander et al., 2009). In general, the USPs are a promiscuous group of DUBs as the majority are able to cleave multiple different ubiquitin chain linkages, with only Cylindromatosis (CYLD), USP1L and USP18 exhibiting strong specificity for K63-linked, SUMO and ISG15 conjugated substrates respectively (Malakhov et al., 2002; Ritorto et al., 2014; Schulz et al., 2012).

1.2.2.2 UCHs

With only four members, the UCH family is one of the smallest (Figure 1.4). However, UCHL1 and UCHL3 are some of the most abundantly expressed DUBs across a number of cell lines (Geiger et al., 2012; Schwanhäusser et al., 2011). Interestingly, structural studies suggest that both UHCL1 and UCHL3 have limited deubiquitylating activity towards complex ubiquitin-substrate structures due to a short crossover loop sitting directly over their active site (Boudreaux et al., 2010; Johnston et al., 1999). In agreement with this, an *in vitro* study has confirmed that UCHL1 and UCHL3 demonstrate negligible activity towards all polyubiquitin chains (Ritorto et al., 2014). And so, it has been proposed that these two abundant UCHs may play a role in processing *de novo* ubiquitin chains to replenish the free ubiquitin pool. The other two members of the UCH family, the proteasome-associated UCHL5 and cancer-associated BRCA1-associated protein 1 (BAP1), are larger proteins with a more permissive loop region enabling interactions with ubiquitylated substrates (Clague et al., 2013).

1.2.2.3 OTUs

While the OTUs are thiol proteases, like the USPs, UCHs, JOSs and MINDYs, the catalytic mechanism varies slightly as some OTUs only harbour a catalytic diad and do not require a third catalytic residue to stabilise the histidine (Komander and Barford, 2008). Furthermore, due to slight variations in catalytic domain architectures, the OTU subfamily has since been further divided into 3 subfamilies: the Otubains, the OTUs and the A20-like OTUs. Interestingly, a number of the OTUs exist as inactive *apo*-enzymes in which their catalytic residues are not efficiently aligned (Edelmann et al., 2009). This is the case for OTUB1, a highly abundant DUB that potently suppresses K63-linked ubiquitylation during DNA damage independently of its catalytic activity (Juang et al., 2012).

1.2.2.4 JOSs

With only four members the JOSs are one of the smallest families. The JOSs are also known as the Machado Joseph disease (MJD) DUB family due to their association with the spinocerebellar ataxia disease (Clague et al., 2013). The disease is characterised by an aberrant form of the Spinocerebellar ataxia type 3 protein (ATXN3) DUB, which contains an expanded poly-glutamate region. Whilst the Josephins remain a poorly understood family, ATXN3 the best studied of the four, has been identified as a transcriptional repressor for multiple genes including the tumour suppressor PTEN (Evert et al., 2006; Sacco et al., 2014).

1.2.2.5 MINDYs

The MINDYs are a newly discovered family of DUBs, first identified to have deubiquitylating activity in a recent study that investigated a small group of four uncharacterised proteins (Abdul Rehman et al., 2016). MINDY-1 (or FAM36A as it was previously known) was shown to contain tandem MIUs that specifically interact with and cleave long K48-linked polyubiquitin chains (Abdul Rehman et al., 2016; Kristariyanto et al., 2017). Interestingly, upon solving the structure for MINDY-1, it was shown to have a novel variant of the thiol protease fold that is completely dissimilar to the four other thiol protease families (Abdul Rehman et al., 2016).

1.2.2.6 JAMMs

The JAMMs comprise sixteen DUBs that belong to a larger superfamily of highly conserved proteins, the Mpr1-Pad1-N-terminal (MPN) family. As outlined above, these are the only DUB family to rely upon a zinc ion to coordinate the cleavage of the ubiquitin bond, this is dependent upon their signature "H-x-H-P-$x_{(6)}$-S-$x_{(2)}$-D" motif (Clague et al., 2013; Maytal-Kivity et al., 2002). JAMMs tend to be found in large protein complexes, including the 19S regulatory proteasome lid complex (26S proteasome non-ATPase regulatory subunit 14 (PSMD14)), DNA repair complexes (BRCA1/BRCA2-containing complex subunit 36 (BRCC36)), the ESCRT machinery (associated molecule with the SH3 domain of STAM (AMSH)) and the COP9 signalosome (CSN) (CSN5) (Clague et al., 2013). Interestingly, a number of these complex bound DUBs exhibit specificity towards K63-linked ubiquitin chains, a higher proportion of specificity than can be seen in any of the other five families (Ritorto et al., 2014).

1.3. Regulation of DUB activity: highly complex networks

The number of encoded DUBs is relatively small in relation to the high proportion of ubiquitylated proteins present within the cell. Despite this it is thought that most DUBs only act upon a specific subset of target proteins within the cell. Certain DUBs, especially within the OTU and JAMM families, exhibit an exquisite specificity to one ubiquitin chain linkage (Komander et al., 2009; Mevissen et al., 2013), which limits their activity towards a discrete set of ubiquitylated substrates. However, a preference for cleaving specific ubiquitin chain types is not sufficient to regulate a DUB's interaction with a specific target protein, as a myriad of proteins can be labelled with the same types of ubiquitin polymer. Moreover, a large number of DUBs, particularly within the USP family, are promiscuous with the ability to cleave multiple ubiquitin chain types and interact with a range of target proteins. Therefore, it is evident that DUBs require tight regulation to prevent non-specific deubiquitylation and possible derailment of normal physiology.

To cope with this, cells have developed a plethora of strategies to regulate DUB activity and ensure their interaction with target proteins occurs at the correct time and in the correct place. These strategies can be divided into three main groups, which temporally, spatially, or quantitatively regulate DUBs.

The first layer of regulation occurs at the transcriptional level. DUBs, like all proteins expressed in the cell, are subject to regulation through transcriptional control. DUB expression levels are known to vary between cell and tissue type, as well as to become aberrantly expressed under pathophysiological conditions (Clague et al., 2013). The second layer of regulation comes from intramolecular factors, specifically the role that internal protein domains and protein structure have on DUB activity. The third, and most complex, layer of regulation comprises all the external factors that may regulate DUBs, in particular the role that protein interactions and post-translational modifications play in this multi-faceted system of DUB regulation.

1.3.1 Intramolecular factors

Due to complex protein folding and tertiary structure a number of DUBs are innately capable of regulating their own activity. Here, protein domains and short peptide loops can positively or negatively modulate DUB function, through occlusion of the active site, attraction of target proteins, interaction with protein complexes or by directly effecting the rate of catalysis.

1.3.1.1 Intramolecular protein domains

As outlined in Section 1.2.2, each DUB family contains a shared and highly conserved catalytic domain, in addition to this DUBs can harbour a wide range of accessory domains and these are not all restricted to certain families. A comprehensive overview of DUB domain architecture was recently outlined in (Clague et al., 2013) where the authors depict the multi-domain structure for each DUB. These domains have the capacity to regulate many aspects of DUB physiology including substrate recognition, subcellular localisation and recruitment of regulatory interactors. The two most common across all DUB

families, or the DUBome, are UBL domains and ZnF domains. These are especially prevalent in the USP family.

ZnF domains interact with the ubiquitin C-terminal di-glycine motif and so are well suited to monitor and interact with free ubiquitin monomers and polymers (Sahtoe and Sixma, 2015). The catalytic activity of USPs that contain functional ZnF domains is often potentiated through the interaction of the di-glycine motif and the internal ZnF domain. This is true of USP5, a DUB that interacts with free polyubiquitin chains. Upon ubiquitin interaction with the ZnF domains in USP5, USP5 catalytic activity towards the ubiquitin substrate increases (Bonnet et al., 2008).

UBL domains (UBLs) are structurally similar to ubiquitin, sharing the same β-grasp fold, but lack the di-Gly motif at the C-terminus (Clerici et al., 2014). As not all UBLs share the same amino acid sequence, it is unsurprising that they have all evolved to perform different functions. Within the USP family, UBLs have been shown to play a role in sub-cellular recruitment and localisation as well as in directly regulating catalytic activity.

1.3.1.1.1 UBL-mediated DUB localisation

USP14, a proteasome-associated DUB, can rescue proteins from proteasomal degradation through removal of ubiquitin at the proteasome. This last minute removal of ubiquitin chains also helps to maintain the homeostasis of the free ubiquitin pool. USP14 possesses an N-terminal UBL domain. Biochemical analysis has revealed that this UBL domain is essential for the correct recruitment of USP14 to the 19S regulatory cap of the proteasome (Hu et al., 2005).

1.3.1.1.2 UBL-mediated DUB catalytic activity

USP7 is an excellent case study to illustrate how internal UBLs can modulate the catalytic activity of a DUB. USP7 possesses five UBLs, all situated after the catalytic domain towards the C-terminus of the protein (Faesen et al., 2011a).

These five UBLs can be divided into two groups, UBL-123 and UBL-45, each playing a different role in USP7 activation. Early structural analysis of the isolated USP7 catalytic domain revealed that native USP7 exists in an inactive state, with the residues in the catalytic triad grossly misaligned (Hu et al., 2002). More recent developments to this structural story have revealed that the C-terminal tail and UBL-45 interact with a "switching loop", a small loop that rests adjacent to the active site. This interaction, and the associated structural rearrangement, potentiated USP7 activity via the realignment of the catalytic triad (Faesen et al., 2011a). In addition to this, a regulatory role has recently been found for the extended charged α-helix that joins the USP7 catalytic domain to the UBL-123 region. Again, structural analysis revealed that the polarity, rigidity and length of this connector helix was essential for the correct structural rearrangement of UBL-123 and subsequent catalytic potentiation of USP7 via UBL-45 (Kim et al., 2016).

USP7 is not the only DUB to be catalytically regulated through internal UBL domains. USP4 contains an internal UBL domain directly adjacent to the N-terminal domain in USP (DUSP) domain. This DUSP-UBL is essential in regulating USP4 activity through promoting efficient ubiquitin dissociation from the catalytic cleft. The catalytic domain of USP4 has an unusually high affinity for ubiquitin, which would prevent rapid ubiquitin release and so impede catalytic turnover. However, the DUSP-UBL interacts with specific residues in a switching loop near the USP4 catalytic cleft. This interaction rearranges the switching loop and so promotes ubiquitin dissociation, and increases catalytic turnover (Clerici et al., 2014).

1.3.1.2 Auto-inhibition of DUBs

As exemplified by USP7 (Hu et al., 2002), some native DUBs only possess minimal deubiquitylating activity due to misaligned residues within the active site. However, this is not the only form of auto-inhibition identified within the DUBome. Some DUBs, including USP14 and CSN5, are structurally inhibited by small polypeptide loops that occlude the catalytic site and prevent deubiquitylation (Sahtoe and Sixma, 2015). Large-scale structural inhibition has

also been demonstrated to play an auto-inhibitory role. USP19 exhibits a novel method of auto-inhibition, USP19 functions as a part of the endoplasmic reticulum-associated protein degradation (ERAD) pathway. Despite being the only DUB to contain a C-terminal transmembrane domain, USP19 is primarily localised to the cytosol. Biochemical analysis showed that the C-terminal transmembrane domain interacted with the catalytic domain of USP19, inhibiting its activity, whilst in the cytosol (Lee et al., 2014). In some cases, the auto-inhibition does not abolish DUB activity instead only limiting it. As discussed in Section 1.2.2.2, UCHL1 and UCHL3 possess very short crossover loops that sit over their catalytic cleft limiting their interaction with specific substrates (Clague et al., 2013; Heideker and Wertz, 2015).

1.3.2 External factors

As outlined in Section 1.3.1, DUBs utilise a number of intramolecular mechanisms to regulate their function. Furthermore, other proteins within the cell can manipulate these mechanisms in an additional layer of regulation.

1.3.2.1 Substrate-dependent Activation

Interestingly, ubiquitin binding itself can modulate DUB activity. Whilst some native DUBs have correctly aligned active sites, certain DUBs are folded in such a manner that the three residues of the catalytic triad are misaligned so inhibiting high DUB activity. This has been elegantly described for UCHL1 and USP7, two highly abundant DUBs that require conformational rearrangement to reach their full catalytic activity.

UCHL1 harbours an exosite, an ubiquitin binding site away from the active site. Upon ubiquitin binding to this distal exosite, a cascade of conformational rearrangements properly align the catalytic triad into a productive conformation (Boudreaux et al., 2010). As briefly mentioned, the catalytic triad is grossly misaligned within the USP7 catalytic domain and folding of the mobile C-terminus can instigate a structural rearrangement to increase USP7 activity. In addition to this, ubiquitin binding was shown to be sufficient to promote these

structural rearrangements and correctly align the catalytic triad as well as exposing the switching loop (Faesen et al., 2011a; Hu et al., 2002; Rouge et al., 2016).

Ultimately, this ubiquitin-driven regulation of DUB activity has low specificity and so it is often coupled with additional layers of regulation. A more specific facet of substrate-mediated activation comes from interacting with specific target proteins, so that the ubiquitylated substrate itself can directly affect catalysis. Again, this is most often achieved through structural rearrangements that relieve auto-inhibition of the interacting DUB.

One such example of substrate-mediated DUB activation involves a less classical function of DUBs in cells, in which a DUB removes an ubiquitin-like modification rather than ubiquitin. There are a wide range of ubiquitin-like modifiers (Section 1.1.3), and this example refers to NEDD8 and its role in activating ubiquitin E3 Cullin Ring Ligases (CRLs). The deneddylating DUB CSN5 is one subunit of the CSN multimeric complex (Cope et al., 2002). In its native state, the active site of CSN5 is covered by an inhibitory loop, inactivating itself (Lingaraju et al., 2014). However, upon CSN interaction with a NEDD8-modified CRL, separate subunits of the CSN (CSN4 and CSN6) undergo conformational rearrangement to properly bind the CRL. These large structural changes within the CSN complex relieve the auto-inhibition of CSN5, permitting the deneddylation of the CRL substrate, in a substrate binding-dependent manner (Lingaraju et al., 2014).

1.3.2.2 Sub-cellular recruitment and localisation

Sub-cellular DUB localisation is increasingly appreciated as a regulatory mechanism that can either increase or decrease DUB activity towards specific substrates. It is often observed that as DUBs are recruited to multimeric complexes, or bound to scaffold proteins, they are allosterically regulated through protein-protein interactions.

A prime example of location-mediated allosteric regulation of DUBs can be found at the 19S regulatory cap of the proteasome, where three DUB localise: USP14, UCHL5 and PSMD14. Upon binding to the 19S cap and interaction with the ADRM1 subunit, UCHL5 activity increases. The deubiquitylase adaptor (DEUBAD) domain within ADRM1 allosterically stabilises the crossover loop within the UCHL5 active site and additionally alleviates the auto-inhibitory position of the UCHL5 C-terminus (Sahtoe et al., 2015). In a similar manner, prior to incorporation to the proteasome, USP14 is auto-inhibited by two loops that sit over the ubiquitin binding pocket. Then once bound to the 19S cap of the proteasome, via the N-terminal UBL domain, USP14 structurally rearranges repositioning the inhibitory loops and enabling the C-terminal tail of ubiquitin access to the active site for catalysis (Hu et al., 2005).

Another prime example of a DUB that is regulated through recruitment to cellular structures is AMSH. AMSH is directly localised to the endosome, being recruited specifically to the ESCRT machinery, and so is actively involved in receptor recycling or degradation through the endocytic pathway. The first stage of receptor internalisation relies upon the ESCRT-0 complex and it is here, through an interaction with signal transducing adaptor molecule (STAM), that AMSH acts (Clague and Urbe, 2006). AMSH activity in the endocytic pathway is dependent upon its interaction with STAM, via a SH3 domain. When this SH3-dependent interaction is perturbed AMSH no longer promoted the lysosomal receptor degradation, resulting in the accumulation of internalised receptors (Sierra et al., 2010).

A global cellular response that requires the proper recruitment of DUBs is the DNA damage response (DDR). For example, upon DNA damage, proliferating cell nuclear antigen (PCNA) is monoubiquitylated and coordinates a signalling response to promote DNA repair. USP1, in complex with USP1-associated factor 1 (UAF1), is recruited to these sites of damage to deubiquitylate PCNA and so negatively regulates the PCNA-induced DNA damage response, preventing the prolonged recruitment of error-prone DNA polymerases (Kee and Huang, 2015).

1.3.2.3 Allosteric Activity Modulation

Allosteric regulation, in contrast to substrate-mediated regulation, describes a regulator's ability to modulate DUB activity without binding to the DUB active site. Instead, they interact at a separate binding site to modulate DUB function. This kind of allosteric regulation is prevalent in large protein complexes, as described for the roles of the CSN and the proteasome in regulating CSN5, or USP14 and UCHL5 activity, respectively. For these examples, the DUBs exhibit low activity in isolation, yet can attain full catalytic potential when correctly associated with their allosteric regulators within these macro-molecular complexes.

Allosteric regulation is not confined to these multi-modular protein complexes; a simple protein-protein interaction is capable of vastly changing DUB function. USP1 activity and stability is dependent upon interaction with its cofactor, the WD40-repeat containing protein UAF1 (Garcia-Santisteban et al., 2013). Alone, the activity of USP1 is minimal, attaining full catalytic potential requires UAF1-induced structural and biochemical changes within the active site of USP1, in which the UAF1 interaction increases the basicity of the catalytic histidine (Villamil et al., 2012a). Multiple DUBs can be regulated through complexing with WD40-repeat containing proteins. For instance, UAF1 is also capable of regulating the activity of USP12 and USP46 (Cohn et al., 2009), two DUBs that are closely related to USP1. Again, the allosteric interaction with UAF1 potentiates their catalytic activity, though to a lesser extent than seen for USP1 (Faesen et al., 2011b).

BAP1, an important tumour suppressor, is also allosterically activated like its UCH family member UCHL5. BAP1 interacts with the transcription-related protein additional sex combs-like protein 1 (ASXL1) to deubiquitylate histone H2A in BAP1's emerging role in transcriptional regulation. ASXL1 contains a DEUBAD domain that upon interaction increases BAP1's affinity for ubiquitin and so increases catalytic turnover (Sahtoe et al., 2016). Interestingly, this allosteric potentiation of BAP1 by the ASXL1 DEUBAD domain is mechanistically similar to

the ADRM1-mediated activation of UCHL5 at the proteasome (Sahtoe et al., 2016; Sahtoe et al., 2015).

The role of guanosine monophosphate synthase (GMPS), a metabolic enzyme, in potentiating USP7 activity is another well-characterised example of allosteric activation. Full USP7 activity is dependent upon the interaction of the C-terminal tail with a switching loop in the USP7 active site, as this promotes a conformational rearrangement to realign the catalytic triad within the USP7 active site (Faesen et al., 2011a) (Section 1.3.1.1.2). The interaction between GMPS and the UBL-123 domain in USP7 stabilises USP7 in this active conformation, and so GMPS allosterically increases USP7 activity (Faesen et al., 2011a). This will be discussed in more detail in Section 5.1.

Allosteric inhibition of DUB activity is less prevalent than activation. One of the best understood examples comes from the inhibition of UCHL5 by the INO80 complex subunit G (INO80G). This is of particular interest, as it reveals how the same protein domain (DEUBAD domain) can both positively and negatively regulate the same DUB (UCHL5) in a context-dependent manner. Whilst UCHL5 is often considered to be a proteasomal DUB, it has a less well-defined role in chromatin remodelling, via the INO80 complex, during DNA repair. However, the deubiquitylating activity of UCHL5 is inhibited in this complex, in an INO80G-dependent manner (Yao et al., 2008). Interestingly, like ADRM1 and ASXL1, INO80G contains a DEUBAD domain. As described above DEUBAD domains allosterically increase activity of UCHL5 and BAP1. However, the interaction of INO80G DEUBAD domain with UCHL5 directly inhibited activity by occupying the ubiquitin docking site. This occlusion was dependent upon a unique hairpin structure that is not present in ADRM1 and ASXL1 (Sahtoe et al., 2015).

1.3.2.4 Post-translational Modifications

Post-translational modifications (PTMs) are a versatile and reversible means to modify protein function. DUBs are subject to heavy post-translational

modification, in which phosphorylation, ubiquitylation and sumoylation have been identified as additional regulators of DUB function.

1.3.2.4.1 Ubiquitylation

It is an emerging theme that DUBs and other members of the ubiquitin proteasome system (UPS) are capable of regulating each other, often in complex feedback loops. The most extreme example of coupled DUB and E3 ligase activity is demonstrated by tumour necrosis factor alpha-induced protein 3 (TNFAIP3), or as it is commonly known A20 or OTUD7C, and its dual ubiquitin editing functions. A20 has a well-defined role in the pro-inflammatory response through its regulation of NF-κB. Interestingly, this protein coordinates its deubiquitylating activity, via a K63-specific OTU domain, with its K48-specific ubiquitin ligase activity, via A20-like ZnFs, within the same protein (Heyninck and Beyaert, 2005). Therefore, upon interaction with target proteins, A20 can edit the ubiquitin signal, removing K63-linked ubiquitin chains and replacing them with K48-linked ubiquitin polymers (Heyninck and Beyaert, 2005).

Ubiquitylation, particularly monoubiquitylation, can also directly activate or inhibit DUB activity in cells. ATXN3 is ubiquitylated at lysine 117 (K117) by the E3 ligase C-terminus of the Heat-shock cognate 70-Interacting Protein (CHIP) (Todi et al., 2009). K117 is adjacent to the catalytic histidine (H119), the monoubiquitylation event within the catalytic cleft promotes ATXN3 activity, although the exact structural or biochemical mechanisms involved are not fully understood (Todi et al., 2009). A similar monoubiquitylation-dependent increase in activity has also been identified for another JOS family member, JOSD1 (Seki et al., 2013).

Monoubiquitylation can also negatively regulate DUB activity. UCHL1 undergoes multiple monoubiquitylation events at lysine 4 (K4), lysine 65 (K65), lysine 71 (K71) and lysine 157 (K157) (Meray and Lansbury, 2007). Structurally, these residues are within close proximity to the active site and so it was unsurprising that these PTMs affect catalytic activity. Multi-monoubiquitylation of UCHL1

impairs its ability to interact with substrates and bind ubiquitin. Interestingly, UCHL1 is able to self-regulate this process via auto-deubiquitylation in a regulatory feedback loop (Meray and Lansbury, 2007).

Monoubiquitylation can also affect DUB function through regulation of sub-cellular compartmentalisation. BAP1 is a predominantly nuclear DUB, it harbours a C-terminal nuclear localisation signal (NLS) that transports it into the nucleus and within proximity of its chromatin-associated network of proteins (Mashtalir et al., 2014). BAP1 is multi-monoubiquitylated within the NLS by the E2/E3 hybrid ubiquitin-conjugating enzyme E2 O (UBE2O). These ubiquitylation events promote the translocation of BAP1 from the nucleus into the cytosol, negatively regulating its activity towards nuclear proteins. Like UCHL1, BAP1 has the ability to self-regulate this subcellular compartment shuttling by auto-deubiquitylation (Mashtalir et al., 2014). Additionally, auto-deubiquitylation is also important for proper USP4 and USP15 activity (Wijnhoven et al., 2015).

1.3.2.4.2 Sumoylation

The ubiquitin-like modifier SUMO can also regulate DUB activity, although this is less extensively studied. CYLD, a NF-κB associated USP DUB, can be sumoylated at lysine 40 (K40), which decreases CYLD catalytic activity towards its substrates without perturbing CYLD stability, subcellular localisation or substrate affinity (Kobayashi et al., 2015). Two other examples of USPs that are negatively regulated by sumoylation are the paralogs USP25 and USP28 (Meulmeester et al., 2008; Zhen et al., 2014). Both USPs are sumoylated within their N-terminal region, which possesses two UIMs. These UIMs are important for efficient binding and cleavage of ubiquitin chains, sumoylation of these regions negatively regulates deubiquitylating activity of USP25 and USP28 (Meulmeester et al., 2008; Zhen et al., 2014).

1.3.2.4.3 Phosphorylation

There is extensive crosstalk between ubiquitin and phosphorylation signalling networks. As with any protein in the cell, phosphorylation has the capacity to activate as well as inhibit DUB activity. The first example of phosphorylation-dependent DUB activity described the casein kinase 2 (CK2)-mediated phosphorylation of OTUD5 (also known as DUBA). OTUD5 is a regulator of the innate immune response, capable of suppressing type 1 interferon production (Huang et al., 2012). Biochemical analyses revealed that unmodified OTUD5 is inactive, yet phosphorylation at serine 177 (S177) was sufficient to activate the enzyme. Additional structural analysis determined that S177 phosphorylation alone did not induce a conformational change within the adjacent catalytic domain. However, upon ubiquitin binding, S177 phosphorylated OTUD5 did undergo structural rearrangement, suggesting that S177 phosphorylation was critical for OTUD5 activity through promoting its interaction with ubiquitin (Huang et al., 2012). Another example of a DUB activated by phosphorylation is USP10. USP10 is phosphorylated on serine 76 (S76) by AMPK; S76 phosphorylation increases USP10 activity, increasing its ability to deubiquitylate AMPK (Deng et al., 2016). Interestingly, deubiquitylated AMPK exhibits increased kinase activity and so USP10-AMPK activation results in a feed-forward activation loop (Deng et al., 2016).

Phosphorylation is a principal regulator of cell cycle progression (see Section 1.5), and has also been shown to temporally regulate DUB activity in this context. Phosphorylation regulates the complex interplay between USP37 and an E3 ligase, the anaphase-promoting complex/cyclosome (APC/C) complexed with the CDC20 homolog 1 (CDH1) cofactor (APC/C^{CDH1}), in a cell cycle-specific manner. Cyclin-dependent kinase 2 (CDK2)-mediated phosphorylation of USP37 at serine 628 (S628) increases its catalytic activity in a G_1/S-specific manner. Phosphorylated and therefore fully active USP37 can antagonise the APC/C^{CDH1} mediated degradation of cyclin A (CCNA), enabling S-phase entry (Huang et al., 2011).

Phosphorylation can also affect DUB activity by promoting interactions with allosteric regulators. As outlined in section 1.3.2.3, USP1 activity is dependent upon its interaction with the UAF1 cofactor (Villamil et al., 2012a). Moreover, it was discovered that UAF1 interaction and potentiation of USP1 activity was dependent upon a phosphorylation event. Biochemical analyses revealed that cyclin-dependent kinase 1 (CDK1) phosphorylated USP1 at serine 313 (S313) within the UAF1 binding domain, directly promoting the interaction of USP1 and its cofactor (Villamil et al., 2012b). In addition to promoting allosteric interactions, phosphorylation can promote DUB activity towards specific substrates. Phosphorylation of USP7 at serine 18 (S18) increases its activity specifically towards mouse double minute 2 (MDM2), whereas dephosphorylated USP7 preferentially interacts with and deubiquitylates cellular tumour antigen P53 (P53) (Khoronenkova et al., 2012).

Inhibitory phosphorylation events also regulate DUBs. OTULIN, an OTU family member with specificity for linear ubiquitin chains, is a negative regulator of the NF-κB response. OTULIN antagonises the LUBAC E3 ligase, via a direct interaction with the LUBAC subunit HOIL-1 interacting protein (HOIP) (Elliott and Komander, 2016). This association is dependent upon the N-terminal PNGase/UBA/UBX (PUB) domain in HOIP interacting with the PUB-interacting motif (PIM) in OTULIN. Phosphorylation of tyrosine 56 (Y56) perturbs this interaction, preventing OTULIN from interacting with its target proteins (Schaeffer et al., 2014). USP8 is also negatively regulated by phosphorylation. Phosphorylation of serine 680 (S680) within the linker domain of USP8 promotes its interaction with 14-3-3 scaffold proteins. 14-3-3 bound USP8 has decreased activity, as it is sequestered away from its target proteins. Mitotic dephosphorylation of S680 allows dissociation from 14-3-3s, increasing USP8 activity during the final stages of cell division (Mizuno et al., 2007).

Phosphorylation, like monoubiquitylation, can mediate the redistribution of DUBs between subcellular compartments. Both USP4 and USP10 shuttle between the cytosol and the nucleus in a phosphorylation-dependent manner. USP4 is a predominantly cytoplasmic DUB until its phosphorylation at serine 445 (S445) by

RAC-alpha serine/threonine-protein kinase (AKT) (Zhang et al., 2012). This phosphorylation event results in the export of USP4 from the nucleus into the cytosol, here it localises with the transforming growth factor-ß (TGF-ß) receptor at the plasma membrane to induce TGF-ß signalling (Zhang et al., 2012). Conversely, USP10 is commonly localised to the cytosol where it stabilises cytosolic P53. Upon DNA-damage, USP10 is phosphorylated at tyrosine 42 (Y42) and serine 337 (S337) by the ataxia-telangiectasia mutated (ATM) kinase. This DNA damage-dependent phosphorylation enables USP10 to translocate into the nucleus and stabilise nuclear P53 levels for the DNA damage response (Yuan et al., 2010).

In summary, regulation of DUB activity is a multi-faceted system that comprises and interlinks intramolecular regulation and external influences. These mechanisms modulate all aspects of DUB behaviour from the biochemistry within the active site to subcellular localisation. It is becoming more apparent, as the research into DUB regulation grows, that DUBs are regulated through multiple mechanistic layers, which in combination ensure that DUBs are only active at the correct time and in the correct place. Therefore, preventing non-specific deubiquitylation and subsequent aberrant signalling pathways that can lead to cellular pathophysiology.

1.4 Deubiquitylases and disease

1.4.1 Mutations in the code

Over seventy DUBs have to date been associated with the progression of human diseases, as outlined in an extensive review that linked DUBs to various human pathologies, including neurodegenerative diseases, numerous cancers, heart failure, infertility and depression (Clague et al., 2013). The authors collated bioinformatic data from Oncomine and COSMIC databases to determine which DUBs were mutated or otherwise deregulated in these diseases (Clague et al., 2013).

1.4.1.1 Cancer associated DUB mutation

The majority of DUBs highlighted in the data collated by (Clague et al., 2013) were implicated in cancer. Whilst DUB function has been associated with nearly all cellular events, there are distinct trends in DUB function that cluster around three main cellular processes: DNA damage response pathways, cell cycle checkpoint control and regulation of gene expression (both transcriptional and epigenetic). Whilst, these are functionally separate events, they are often interconnected and when aberrantly regulated result in tumour formation and cancer progression, so therefore a high proportion of DUBs are associated with this disease. Here I will highlight a few selected examples of DUBs and describe how their deregulation affects tumorigenicity.

A few DUBs are generically mutated in cancer tissues. This is best exemplified by A20, which is mutated in 9% of all cancers (Clague et al., 2013) based on COSMIC datasets (Forbes et al., 2010). The constitutive activation of NF-κB pathways is linked to tumourigenesis and malignancies in multiple lymphomas. As a negative regulator of the NF-κB signalling pathway, A20 is considered a tumour suppressor gene in these cancers. Moreover, it is subject to chromosomal deletions and inactivating mutations that drive tumorigenicity in several subtypes of lymphoma (Honma et al., 2009; Sacco et al., 2010).

Interestingly, there are only a few DUBs for which genetic mutation drives cancer progression. BAP1 has been identified as a tumour suppressor (Jensen and Rauscher, 1999) and more recently as a prognostic marker for certain cancers (Luchini et al., 2016). BAP1 is mutated in 8% of all cancers (Clague et al., 2013; Forbes et al., 2010), most commonly mutated in metastasising uveal melanoma (85%) (Harbour et al., 2010), mesothelioma (22%) (Bott et al., 2011) and other melanocytic tumours (Carbone et al., 2013; Harbour et al., 2010). Furthermore, germline mutations in BAP1 have been linked to a cancer predisposition syndrome in which an increased susceptibility for malignancies is coupled with a poor prognosis (Testa et al., 2011; Wiesner et al., 2011). Mutations, including frameshift, nonsense and missense mutations, span the entire BAP1 coding sequence (Carbone et al., 2013; Forbes et al., 2010). Often,

these mutations result in the loss of BAP1 function. This can occur through loss nuclear expression (due to the deletion of the C-terminal NLS), a severe protein truncation (leaving only a partial catalytic domain) or a catalytic site mutation all of which critically impair catalytic function. This markedly disrupts BAP1-mediated epigenetic regulation and leaves an open question about how aberrant cytosolic BAP1 activity may affect cellular physiology.

1.4.1.2 Genetic association of DUBs with neurological diseases

A number of genetic mutations in DUB genes have been associated with the development of neurodegenerative conditions. UCHL1 has been associated with numerous degenerative diseases, including Parkinson's disease (Maraganore et al., 2004), where a heterozygous I93M mutation was identified to decrease UCHL1 activity causing the aberrant accumulation of neuronal proteins in the brain (Nishikawa et al., 2003). UCHL1 has also been linked with Alzheimer's disease (Choi et al., 2004) and childhood-onset multisystem neurodegenerative syndrome (Bilguvar et al., 2013).

In addition to these prevalent neurodegenerative diseases, some DUBs have been associated with rarer neurological conditions. Spinocerebellar Ataxia Type 3, also known as MJD, is the most common form of inherited ataxia. This disease locus encodes the DUB ATXN3, which can acquire pathogenic polyQ expansions that result in large AXTN3 aggregates forming within the cell (Ellisdon et al., 2007; Kawaguchi et al., 1994). Intracellular ATXN3 aggregates sequester wild type ATXN3, ubiquitin, transcription factors and heat shock proteins. It is thought that the functional depletion of all these proteins contributes to the development of disease, however the exact mechanisms are yet to be fully deciphered (Costa Mdo and Paulson, 2012).

As outlined with these few examples, and in numerous reviews (Clague et al., 2013; Heideker and Wertz, 2015; Pinto-Fernandez and Kessler, 2016), it is becoming increasingly evident that ubiquitin signalling is intricately linked with the progression of many diseases. Only a few DUBs, like BAP1, A20, UCHL1 and

ATXN3 can be considered genetic drivers of disease. Instead, the majority of DUBs act as mediators where alterations in their protein levels or catalytic activity are capable of affecting disease-associated cellular processes. Even as mediators, inhibiting these DUBs to ameliorate their pathogenic functions could have a profound therapeutic effect, and so DUBs are beginning to take centre-stage as druggable cancer targets.

1.4.2 DUBs as druggable targets

Due to their far-reaching influence over nearly all aspects of cellular physiology, DUBs and other components of the UPS have been targeted for pharmacological inhibition, as recently reviewed in (Ndubaku and Tsui, 2015; Paiva et al., 2017).

The proteasome was the first UPS target to be exploited for cancer therapeutics. Proteasomal inhibition affects a cancer cell's ability to regulate the cell cycle, apoptosis, DNA repair and ER stress, ultimately resulting in cancer cell death. Bortezomib was the first proteasome inhibitor to be used in clinical practice (Crawford et al., 2011). However, certain cancers are developing an acquired resistance to bortezomib by up-regulating other proteins within the proteasome to combat the bortezomib-mediated inhibition of the ß5-subunit of the proteasome (PSMB5) (Lu and Wang, 2013). Researchers have started to consider combination therapies with upstream UPS regulators, like DUBs, that could help overcome bortezomib resistance for cancer therapy (Farshi et al., 2015).

Interestingly, inhibition of proteasome-associated DUBs, USP14 and UCHL5, may help overcome bortezomib resistance in specific cancers, including multiple myeloma (MM). The small molecule b-AP15 specifically inhibits the deubiquitylating activity of the 19S proteasomal cap, without inhibiting other cellular DUBs (D'Arcy et al., 2011; Tian et al., 2014). Proteasomes treated with b-AP15 no longer function, resulting in an increase of polyubiquitylated substrates in cells. In addition, b-AP15 arrests cell proliferation, via downregulation of cell cycle effectors, and induces apoptosis of MM cells,

regardless of their P53 expression status, enabling cell death in bortezomib-resistant MM cells (Tian et al., 2014).

Of all the DUBs, USP7 has garnered the most interest with respect to inhibitor development, as one of its main functions is the direct and indirect regulation of the tumour suppressor P53. High throughput screening of small molecule-based inhibitor libraries was used to identify compounds that inhibited USP7 activity in the low micromolar range. Multiple studies have identified and evaluated possible compounds: HBX 41,108 (Colland et al., 2009), HBX 19,818 and HBX 28,258 (Reverdy et al., 2012) and PR-619 and P22077 (Altun et al., 2011). PR-619 was found to be a broad inhibitor of DUB activity, potently inhibiting members of USP, UCH and JOS families (Altun et al., 2011). Whereas P22077, and a more recently developed related analogue P5091, are selective and potent competitive inhibitors of USP7 (half maximal effective concentration (EC_{50}) of 8μM and 4.2μM, respectively (Ndubaku and Tsui, 2015)). Although these inhibitors exhibit higher selectivity than previous small molecule compounds, both inhibit the USP7 paralog USP47 with similar micromolar efficiency. Both P22077 and P9051 have been used *in vivo* to target aberrant USP7 signalling in MM and neuroblastoma (NB) models. In MM cell models, P9051 decreased USP7 deubiquitylating activity in an MDM2-P53 pathway-dependent manner, inducing apoptosis in the inhibitor-treated MM cells and helping to overcome bortezomib resistance (Chauhan et al., 2012). Moreover, P22077 suppressed xenograph tumour growth in NB mouse models (Fan et al., 2013).

Interestingly, the trends in targeting the UPS proteins are shifting towards allosteric inhibition, rather than the more classical active site-directed approach (Paiva et al., 2017). Allosteric regulation of these enzymes has proved to be more selective than their active site-directed counterparts, as well as having decreased susceptibility for acquired resistance. An innovative example of this comes from the allosteric inhibition of USP1. A high throughput screen of small molecular inhibitors for USP1 observed that the best compounds, Pimozide and GW7647, inhibited though a non-competitive means (Chen et al., 2011). Surprisingly, the mechanism of inhibition did not perturb USP1 interaction with

its cofactor UAF1, as dimer formation was not affected (Chen et al., 2011). Instead, it is thought that these USP1 inhibitors bind to an allosteric site, possibly on the UAF1 subunit, to decrease USP1 activity (Paiva et al., 2017).

Described above are just a few of the DUB inhibitors that are being discovered and investigated within the UPS scientific community. It is promising to see evidence for anti-tumour efficacy and compounds that may overcome resistance to current cancer therapeutics. It is hoped that with the increased diversity in compound screening libraries, the development of robust high-throughput assays for testing and the assessment of compound pharmacokinetics that the number of potent and specific DUB inhibitors that qualify for clinical trials will increase.

1.5 Ubiquitylation control cell cycle

1.5.1 The objective of the cell cycle

The cell cycle is the coordination of cellular events to duplicate the genetic material and divide the cellular contents to create two identical daughter cells. The cycle is split into four stages. After division into daughter cells, cells undergo an initial growth phase (G_1), followed by the replication of the genome (S-phase), a second growth phase (G_2) prepares the cell for division and assembles cytoskeletal structures and finally the genetic material divides between the daughter cells during mitosis (M-phase).

The orderly and unidirectional progression of the cell cycle through these phases is dependent upon the periodic activation and inactivation of cell cycle effectors, most notably the cyclin-dependent kinases (CDKs). These are an evolutionary conserved family of protein kinases considered to be the engine that drives the cell cycle. Accordingly, the activities of these kinases are tightly regulated through a myriad of mechanisms including protein-protein interactions, phosphorylation and ubiquitylation. By definition, these kinases are dependent upon their interaction with a family of regulatory proteins, the cyclins (CCNs). Without this interaction the CDK possesses minimal kinase

activity, preventing it from phosphorylating target proteins. The cell ensures the unidirectional progression of the cell cycle by periodically transcribing the cyclins at specific stages during cell cycle progression, and rapidly degrading/inactivating them as the cell passes into the next phase. The periodic activity of CCN-CDK complexes has been depicted in Figure 1.5. The cell cycle can be viewed as a poised system with effectors, like the CCN-CDK complexes, actively inhibited until an initial activation step. Subsequently, positive feed-forward signalling loops rapidly and fully activate these complexes reinforcing transitions between cell cycle phases. This activation is countered by an equally rapid inactivation, which is often mediated by proteolysis of the cell cycle effectors, ensuring the unidirectional progression of the cell cycle (Rhind and Russell, 2012).

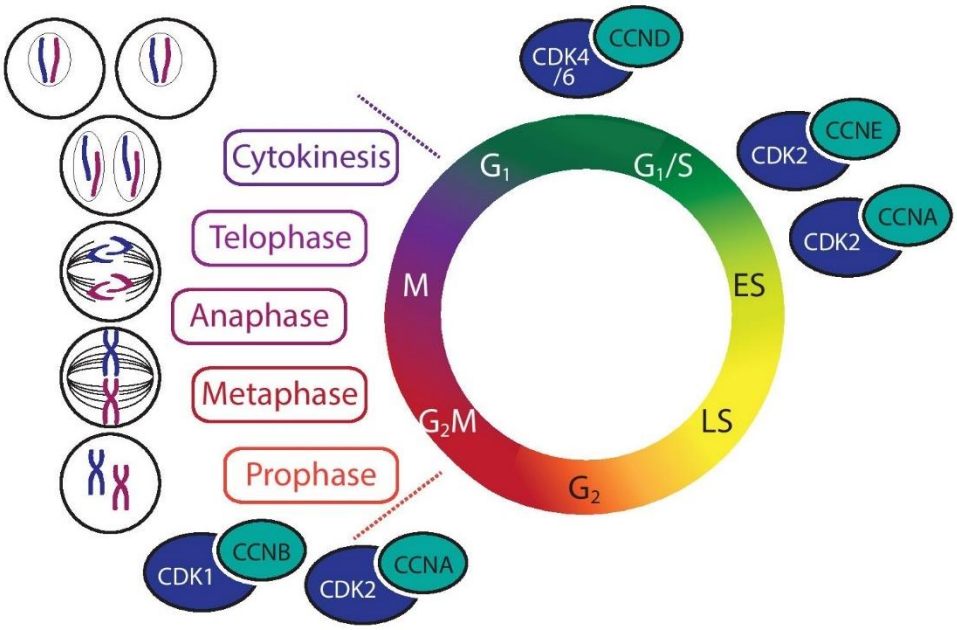

Figure 1.5: The stages of the cell cycle and cyclin-CDK complexes.
The cell cycle, with the individual stages of mitosis, is schematically represented with cyclin-CDK complexes linked to their associated cell cycle phase.

1.5.2 Checkpoint control

Once initiated, the cell cycle can be viewed as a series of autonomic cellular events that cascade until the eventual division into two daughter cells. However, brakes have been inbuilt into this system, called checkpoints, to temporarily halt the cell cycle to assess whether the cell has accurately

completed one phase of the cell cycle before it can enter the next. These checkpoints ensure that each daughter cell will be a direct replica with an intact genome and the correct array of intracellular components. The plethora of regulatory mechanisms mediating cell cycle control is too extensive to comprehensively discuss here, instead two critical checkpoints and the role ubiquitylation plays in their control are outlined below.

1.5.2.1 The G_1 restriction point and retinoblastoma protein

Upon entering G_1, cells are not committed to a subsequent round of cell division, instead they have the option to exit the cell cycle into quiescence, or G_0, a resting phase where the cell exists in a dormant non-cycling state. Entry into the cell cycle relies upon the signalling of extracellular mitogenic growth factors. If there is sufficient mitogenic signalling the cell can overcome a restriction point that is situated towards the end of the G_1 growth phase and is now committed to a further round of cell division independent of any additional extracellular signals.

Mitogen-dependent initiation of the cell cycle is mediated through the transcription and expression of cyclin D family members (CCNDs), this has been comprehensively reviewed in (Blagosklonny and Pardee, 2002). The accumulation of CCNDs acts as a mitogenic sensor to help the cell assess whether it can satisfy the restriction point. Growth factor-stimulated signalling pathways regulate CCND in a number of ways: transcriptional induction of the CCND gene, stabilisation and reduced turnover of the CCND protein, translocation of CCND to the nucleus, and finally promoting its interaction with CDK-4 and CDK-6 to form a catalytic kinase complex (Aktas et al., 1997; Diehl et al., 1997). Once active, CCND-CDK4/6 complexes accumulate in the nucleus and phosphorylate target proteins, including retinoblastoma protein (Rb).

As the mediator of the restriction point, Rb governs entry into S-phase. It does this through its interaction with the E2F transcription factor that induces the transcription of a number of S-phase genes. Hypo-phosphorylated Rb inhibits E2F

by blocking the trans-activation domain, preventing the transcription of E2F-dependent S-phase genes (Helin et al., 1993). Hypo-phosphorylated Rb can also recruit additional proteins that repress E2F activity. One of these mechanisms involves a histone deacetylase (HDAC), an enzyme essential in chromatin remodelling, which represses E2F-mediated transcription through inducing chromatin remodelling at E2F promoter sites (Brehm et al., 1998).

Prior to the accumulation of CCND-CDK4/6 complexes, Rb remains in this hypo-phosphorylated state and prevents the cell from entering S-phase. Upon CCND1-CDK4/6 activation, Rb becomes increasingly phosphorylated resulting in its dissociation from E2F. The newly liberated E2F transcription factor transcribes S-phase genes including cyclin E (CCNE) and CCNA, these cyclins in complex with CDK2 continue to hyper-phosphorylate Rb in a positive feedback loop. Consequently, Rb phosphorylation is no longer reliant upon CCND and mitogen-dependent signalling pathways, and so the cell can pass through the restriction point into the G_1 to S phase transition (G_1/S) (Blagosklonny and Pardee, 2002).

In addition to phosphorylation, Rb is regulated by ubiquitylation. Rb, more specifically hypo-phosphorylated Rb, has been identified as a target of the E3 ligase MDM2 in response to cellular stress (Delston et al., 2011; Xiao et al., 1995). MDM2-mediated ubiquitylation promotes the degradation of Rb via the ubiquitin-dependent 26S proteasome as well as the ubiquitin-independent 20S proteasome (Sdek et al., 2005; Uchida et al., 2005). This stalls the cell cycle and can promote apoptosis. The DUB USP7 directly antagonises MDM2-mediated polyubiquitylation of Rb (Bhattacharya and Ghosh, 2014), stabilising the Rb protein so that during normal physiological conditions hypo-phosphorylated Rb can mediate the transition through the restriction point.

1.5.2.2 The DNA damage checkpoint and P53

The key to successful cell division comes from maintaining the integrity of the genome during DNA replication in S-phase. There are a number of quality control mechanisms in place to ensure any damage to the genome is repaired prior to

cell division, guaranteeing the correct genetic content is passed to the daughter cells.

As with regulation of the G_1 restriction point, the interplay of phosphorylation and ubiquitylation is also important when regulating the DNA damage response. If DNA is damaged during the growth phases of the cell cycle (G_1 and G_2), a checkpoint is activated to stall the cell cycle until the appropriate DNA repair pathways can be activated. This response revolves around the cellular P53. Under normal cellular conditions, P53 is continuously synthesized but maintained at a low level through polyubiquitylation and proteasomal degradation. MDM2, the E3 ligase involved in Rb stability, inhibits P53 function in two ways. Firstly, MDM2 binds to P53 at its N-terminal transactivation domain preventing P53-induced transcription (Lin et al., 1994) and secondly, MDM2 directly polyubiquitylates P53 resulting in its degradation (Fuchs et al., 1998).

Interestingly USP7, the same DUB that stabilises Rb, can directly antagonise MDM2-mediated polyubiquitylation of P53 (Li et al., 2002). However, in an additional layer of regulation, USP7 can directly deubiquitylate the auto-polyubiquitylated MDM2, hence stabilising the E3 ligase as well as its substrate (Brooks et al., 2007). Moreover, USP7 exhibits a preference for deubiquitylating MDM2 over P53 in unstressed cells, stabilising MDM2 and therefore ensuring P53 levels are maintained at a low level (Brooks et al., 2007).

Under genotoxic stress these regulatory mechanisms are reversed. At sites of damage, sensors facilitate the activation of ATM and ataxia-telangiectasia and Rad3-related protein (ATR) protein kinases. These kinases, and other DNA damage-activated kinases, phosphorylate the N-terminus of P53 (Lakin and Jackson, 1999). These phosphorylation events abolish the interaction between P53 and MDM2, preventing K48-linked polyubiquitylation and so increasing P53 levels and inducing the transcription of P53 target genes (Lakin and Jackson, 1999). Again, USP7 provides an additional layer of regulation to guarantee an increase in P53 levels. Upon DNA damage, USP7 is dephosphorylated by protein

phosphatase magnesium-dependent 1 gamma (PPM1G) reducing USP7 activity towards MDM2, and causing increased auto-polyubiquitylation of MDM2 and its subsequent degradation (Khoronenkova et al., 2012). Moreover, during periods of genotoxic stress, USP7 forms a deubiquitylating complex with GMPS and P53 that potentiates USP7 deubiquitylation of P53 (Reddy et al., 2014), again stabilising P53 so that it can stall the cell cycle and initiate DNA repair pathways. One example of P53-mediated cell cycle arrest involves the P53 target gene that encodes for the CDK inhibitor-1 ($p21^{CIP1/WAF1}$), upon accumulation $p21^{CIP1/WAF1}$ interacts with and inhibits CCNA-CDK2 and CCNE-CDK2 complexes (Harper et al., 1993). Once inhibited, the cyclin-CDK complexes can no longer hyper-phosphorylate Rb and ultimately arrests the cell cycle in G_1.

1.5.3 Mitosis

After the complete replication of the genome and sufficient cell growth the cell enters mitosis. The main objective of mitosis is to separate the two copies of the genome so that each daughter cell inherits the correct chromosome complement. To achieve this, the cell undergoes a sequence of dramatic cellular events separated into distinct phases: prophase, metaphase, anaphase, telophase and cytokinesis (depicted in Figure 1.5). During prophase, the onset of mitosis is initially marked by chromosomal condensation of the replicated DNA into sister chromatid pairs. This is rapidly followed with the breakdown of the nuclear envelope in pro-metaphase, allowing the microtubule network to interact with the chromatid pairs forming the mitotic spindle. During metaphase, the spindle-bound chromosomes are aligned on the metaphase plate, an imaginary line that centrally dissects the cell. Once correctly aligned with all checkpoints satisfied, anaphase can initiate. Here, the sister chromatids are separated, pulled to opposite poles of the cell through the contraction of specific chromatid-bound microtubules. Telophase is the reversal of events performed during prophase and pro-metaphase and so the nuclear envelope reforms and the daughter chromosomes begin to decondense. With mitosis now complete, the cell enters the final phase of cell division, cytokinesis. Here, the cell pinches to separate the two daughter nuclei and upon division creates two identical cells (Rhind and Russell, 2012).

1.5.3.1 Cyclin-Dependent Kinase 1: The mitotic engine

Much like the restriction point at the end of G_1, once the cell has entered mitosis the cell is now committed and a rapid cellular response prepares the cell for division. The key event stimulating mitotic entry is the activation of the cyclin B (CCNB)-CDK1 complex. This activity of this complex is heavily regulated to prevent the cell entering mitosis prior to satisfying the checkpoints in S-phase and G_2. Firstly, CCNB is periodically transcribed with its transcript level peaking in G_2, preventing any early interaction with CDK1. However, the initial complex formed between CCNB and CDK1 exhibits little kinase activity due to the inhibitory phosphorylation CDK1 at threonine 14 (T14) and tyrosine 15 (Y15) by membrane-associated tyrosine- and threonine-specific cdc2-inhibitory kinase (MYT1) and WEE1-like protein kinase (WEE1), respectively (Mueller et al., 1995; Parker and Piwnica-Worms, 1992). By late G_2, there is a reservoir of inert CCNB-CDK1 complexes awaiting activation by the phosphatase cell division cycle 25 (CDC25). Upon initial activation, CDK1 phosphorylates and activates more CDC25, whilst simultaneously inhibiting WEE1 (Hoffmann et al., 1993; Watanabe et al., 2004). This results in a rapid and complete activation of the CCNB-CDK1 reservoir to promote mitotic entry and activate numerous mitotic effectors. In addition to the CCNB-CDK1 complex, CCNA can also mediate mitotic entry through activating the transcription of mitotic effector proteins (Laoukili et al., 2005).

Again, the interplay between phosphorylation and ubiquitylation is essential in driving unidirectional progression through each phase. CCNB-CDK1-phosphorylates WEE1 at its phosphodegron (Watanabe et al., 2004), a motif that in response to phosphorylation events signals for degradation of the protein. The WEE1 phosphodegron promotes interaction with the E3 ligase Skp, Cullin, F-box containing complex with ß-transducin repeat containing protein ($SCF^{-\beta TrCP}$) resulting in K48-linked polyubiquitylation and subsequent proteasomal degradation of WEE1 (Watanabe et al., 2004). Phosphodegron-mediated ubiquitylation of proteins is prevalent throughout the cell cycle, mediating rapid temporal degradation of numerous cell cycle effectors.

1.5.3.2 Mitotic exit: The Anaphase Promoting Complex/Cyclosome

The onset of anaphase signifies mitotic exit; this process is orchestrated by the APC/C multi-subunit E3 ubiquitin ligase. The APC/C is only activated once all the chromosomes have correctly attached the mitotic spindle and the spindle assembly checkpoint (SAC) is satisfied. Substrate targeting by the APC/C is dependent upon temporal interactions with its two co-activator proteins: cell division cycle protein 20 (CDC20) and CDH1 (Kramer et al., 2000). The APC/C first associates with CDC20 (APC/C^{CDC20}), this interaction governs the pro-metaphase to anaphase shift, whereas the subsequent interaction with CDH1 (APC/C^{CDH1}) occurs during anaphase and coordinates mitotic exit into early G_1 (Kramer et al., 2000).

Significantly for mitotic progression, APC/C^{CDC20} targets Securin for polyubiquitylation and degradation (Stemmann et al., 2001). Securin inhibits Separase, a protease that cleaves the cohesin complexes that hold the sister chromatids to the mitotic spindle during metaphase (Hornig et al., 2002). Once activated, Separase permits the separation of sister chromatids at the onset of anaphase. The APC/C^{CDC20} also targets both the mitotic cyclins CCNA and CCNB resulting in their rapid degradation and terminates mitotic entry signals (den Elzen and Pines, 2001; Sudakin et al., 1995). The APC/C^{CDC20}-mediated decrease in cellular CCNB levels returns CDK1 to an inactive state, this alleviates the CDK1-mediated inhibition of CDH1 (Crasta et al., 2008). The APC/C^{CDH1} complex targets a number of cell cycle effectors for proteasomal degradation, including numerous mitotic kinases and so drives mitotic exit (Lindon and Pines, 2004; Littlepage and Ruderman, 2002; Stewart and Fang, 2005).

The APC/C is a particularly interesting E3 ligase as it possesses the ability to polyubiquitylate target proteins with K48-linked, K11-linked and K11/K48 branched ubiquitin chains in an E2-dependent manner. The two E2 enzymes that regulate the APC/C heterotypic chain formation are ubiquitin-conjugating enzyme E2 C (UBE2C) and ubiquitin-conjugating enzyme E2 S (UBE2S) (Williamson et al., 2011; Wu et al., 2010). UBE2C acts as the initiating E2 enzyme

and has the capacity to generate K11-, K48- (and K63)-linked ubiquitin polymers. In contrast, UBE2S specifically conjugates K11-linked ubiquitin chains and as the elongating E2 enzyme expands the UBE2C-conjugated ubiquitin with blocks of K11-linked ubiquitin polymers. Interestingly, these K11/K48-linked branched chains enhanced degradation via promoting substrate recognition by the proteasome (Grice et al., 2015; Meyer and Rape, 2014).

1.5.4 DUBs in the cell cycle

As outlined above the role of ubiquitylation is essential in governing the unidirectional progression across multiple phases and checkpoints during the cell cycle. However, the role of DUBs and their antagonistic activity towards E3 ligase-mediated signalling can also be essential in regulating the cell cycle (Fournane et al, 2013). Accordingly, the activity of DUBs during cell cycle progression is of increasing interest. To date, a number of DUBs have been linked to signalling processes and their associated cell cycle phases, as depicted in Figure 1.6. A number of these DUB-dependent regulatory mechanisms are outlined below.

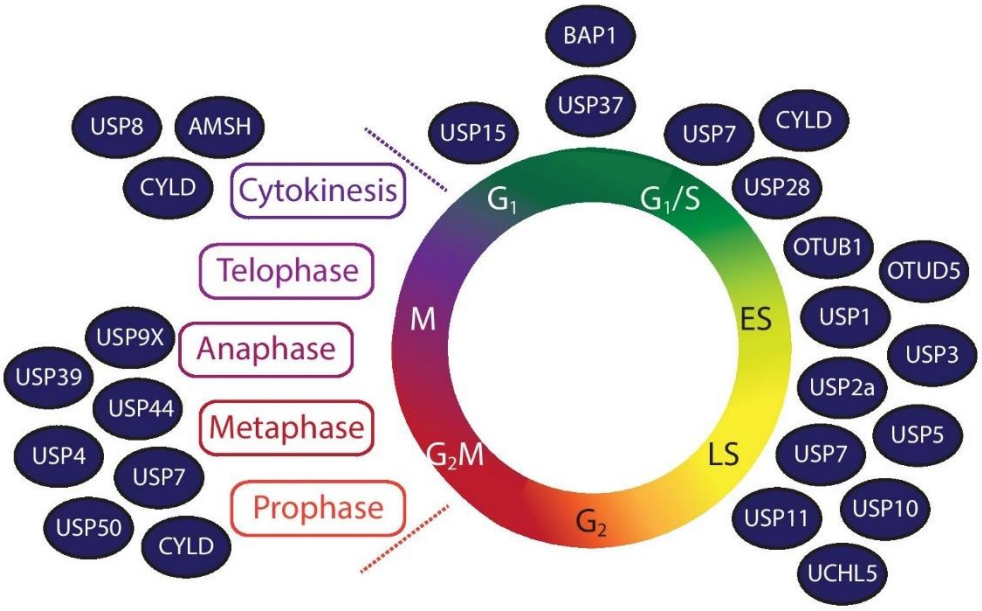

Figure 1.6: DUBs associated with the cell cycle.
The cell cycle, with the individual stages of mitosis, is schematically represented with DUBs and their associated cell cycle phases.

1.5.4.1 G_1 and S-phase

Some DUBs regulate cell cycle events by counterbalancing specific cell cycle-associated E3 ligases (Stegmeier et al., 2007). This includes the aforementioned USP7, which deubiquitylates a number of MDM2 substrates. Additionally, multiple DUBs, including USP44, USP37 and USP22, have all been shown to directly antagonise APC/C mediated polyubiquitylation of cell cycle effectors as well as indirectly affecting APC/C activity by regulating its co-activators (Huang et al., 2011; Lin et al., 2015; Stegmeier et al., 2007a).

Though the APC/C is considered to be most active during the onset of anaphase, its activity in complex with CDH1 continues into G_1. During G_1, the APC/C^{CDH1} polyubiquitylates CCNA, targeting it for degradation in order to prevent the cell from entering S-phase (Huang et al., 2011). USP37 regulates the activity of the APC/C^{CDH1} during G_1 through a direct interaction with the CDH1 co-activator. USP37 binds to APC/C^{CDH1}, via the CDH1 subunit, and removes polyubiquitin chains from CCNA (Huang et al., 2011). CCNA levels are stabilised and so USP37 directly regulates S-phase entry by antagonising the activity of the APC/C^{CDH1}.

DUBs can also regulate G_1 progression by stabilising transcription factors, as previously exemplified by USP7 and its influence over E2F transcriptional activity in Section 1.5.2.1 (Bhattacharya and Ghosh, 2014). USP7 is not the only DUB to govern the cells transition from G_1 to S-phase in this manner. BAP1 also indirectly regulates the activity of E2F during G_1, via its deubiquitylation of the transcriptional regulator host cell factor-1 (HCF-1) (Eletr and Wilkinson, 2011; Machida et al., 2009).

1.5.4.2 DNA damage checkpoints

A further aspect of cell cycle control where DUB activity plays a significant role is in response to DNA damage. Again, USP7 was previously highlighted as the original DUB associated with the P53-dependent DDR (Li et al., 2002). Since then a host of other DUBs have been associated with this response: USP2a (Stevenson et al., 2007), USP5 (Dayal et al., 2009), USP10 (Yuan et al., 2010), USP11 (Ke et

al., 2014), OTUB1 (Sun et al., 2012) and OTUD5 (Luo et al., 2013). In addition, DUBs have also been associated with several other DDR pathways. As outlined in section 1.3.2.2, USP1 can mediate the DNA damage response (Kee and Huang, 2015). Some DUBs exhibit a more global effect on DDR pathways, a screen for DUBs involved in DNA damage revealed that UCHL5 was recruited to sites of DNA damage in addition to being involved in double strand break resection (Nishi et al., 2014).

An RNA-interference(RNAi)-based study observed that upon depletion of USP3 there was a delay in S-phase entry coupled with an increase in double strand DNA breaks and a subsequent increase in DDR signalling (Nicassio et al., 2007). USP3 was shown to directly interact with and deubiquitylate ubiquitylated histones (Ub-H2A and Ub-H2B). Upon DNA damage, there is an increase of Ub-H2A at DNA damage foci, this promotes the dynamic recruitment of USP3 to DNA damage sites. Here, USP3 deubiquitylates H2A, and possibly other DDR effectors, to coordinate DNA repair (Nicassio et al., 2007).

1.5.4.3 Mitosis and Cytokinesis

USP44 was one of the first DUBs to be linked to mitotic progression, regulating the metaphase-anaphase transition (Stegmeier et al., 2007a). As outlined in Section 1.5.3.2, anaphase entry is promoted by the APC/C; to prevent premature chromatid separation, the APC/C is inhibited by sequestering its initial co-activator CDC20. Three proteins are involved in this inhibitory process: mitotic arrest deficient 2 (MAD2), BUB1-related kinase (BUBR1) and budding uninhibited by benzimidazoles 3 (BUB3), they comprise the mitotic checkpoint complex (MCC) (Sudakin et al., 2001). MAD2, in complex with BUB1 and BUB3, sequesters CDC20 at microtubule-unattached chromosomes, preventing the APC/C^{CDC20} complex from activating until these chromosomes are correctly attached to the mitotic spindle (Sudakin et al., 2001). UBE2C-medaited ubiquitylation of CDC20 by the APC/C promotes the dissociation of these inhibitory MAD2-CDC20 complexes (Reddy et al., 2007). USP44 directly antagonises UBE2C-mediated ubiquitylation of CDC20, and so stabilises the interaction between MAD2 and CDC20 (Stegmeier et al., 2007a). Taken together,

these results suggest that USP44 plays a protective role at the SAC. Interestingly, temporal phosphorylation of USP44 has been shown to regulate its activity in a cell cycle specific manner. After the SAC has been satisfied, USP44 is dephosphorylated by TFIIF-associating C-terminal domain phosphatase (FCP1) (Visconti et al., 2012). Dephosphorylated USP44 exhibited decreased activity towards CDC20, promoting CDC20 dissociation from the MCC and so enables mitotic exit in complex with APC/C (Visconti et al., 2012).

USP44 is not the only DUB known to regulate the SAC and its protective role in the metaphase-anaphase transition. Another RNA interference screen searching for additional regulators of the SAC discovered that a decrease in the levels of USP39 resulted in chromosome segregation defects (van Leuken et al., 2008). USP39 regulates splicing of pre-messenger RNA (mRNA) as a component of the U4/U6.U5 tri-small nuclear ribonucleo proteins (snRNP) spliceosomal complex. Depletion of USP39 resulted in a decrease in levels of Aurora B mRNA transcript, and as a result decreased Aurora B protein levels in cycling cells (van Leuken et al., 2008). The mitotic kinase Aurora B is a key regulator of the attachment of the sister chromatids to microtubules in the mitotic spindle. Therefore, USP39 is essential in maintaining Aurora B kinase levels throughout metaphase to ensure the equal division of chromosomes during anaphase.

USP9X also mediates the correct attachment of chromosomes to the mitotic spindle. Aurora B exists in a complex with Survivin, both functioning to ensure the proper attachment and alignment of chromosomal pairs to the metaphase plate (Vader et al., 2006). The ubiquitylation status of Survivin mediates its interaction with chromosomes; USP9X-mediated deubiquitylation is required for dissociation of Survivin from the chromosomes once correctly aligned (Vong et al., 2005).

USP8 and AMSH, two DUBs that are usually recruited to endosomes, also have an important role in cytokinesis. The scission of the two daughter cells uses the same molecular machinery used for the scission of vesicles in the endosomal

pathway: the ESCRT machinery. USP8 and AMSH, in concert with components of the ESCRT machinery, facilitate membrane scission to complete cytokinesis (Mukai et al., 2008). Vesicle-associated membrane protein 8 (VAMP8) was observed to co-localise with USP8 and AMSH during cytokinesis, moreover it was identified as a target for deubiquitylation. However, the significance of VAMP8 deubiquitylation for proper cytokinesis progression was not elucidated (Mukai et al., 2008).

1.5.4.4 DUBs with multiple roles in cell cycle progression

Some DUBs could be considered as multifunctional regulators of cell cycle progression as they are involved in signalling processes in multiple phases of the cell cycle. CYLD, a well-established tumour suppressor, was also one of the first DUBs associated with cell cycle progression (Stegmeier et al., 2007b). Since then CYLD has been linked to a number of cell cycle events. CYLD plays a protective role during G_1, ensuring the cell does not prematurely enter S-phase. CYLD forms an inhibitory interaction with the transcription factor B-cell lymphoma 3 protein (BCL-3). CYLD deubiquitylates BCL-3 inhibiting its nuclear translocation and so decreases the transcription of BCL-3 target genes (Massoumi et al., 2006). CCND is a BCL-3 target gene, therefore CYLD indirectly decreases CCND levels in cycling cells preventing cells from passing through the restriction point (Massoumi et al., 2009).

CYLD has also been shown to colocalise with and stabilise microtubules, through an interaction with acetylated α-tubulin (Wickstrom et al., 2010). The acetylation of α-tubulin is associated with stabilisation of microtubules; deacetylation of α-tubulin is performed by the histone deacetylase 6 (HDAC6) and results in microtubule destabilisation and depolymerisation (Matsuyama et al., 2002). CYLD directly interacts with the catalytic domain of HDAC6, inhibiting α-tubulin deacetylation and therefore CYLD indirectly increases the stability of microtubules. CYLD's governance of microtubule stability plays a role in spindle orientation during metaphase (Yang et al., 2014) and regulates the rate of cytokinesis (Wickstrom et al., 2010). Moreover, this association with microtubules assists CYLD during G_1. Upon co-localising with acetylated α-

tubulin, CYLD accumulates at the peri-nuclear region; this promotes its inhibitory interaction with BCL-3 to restrict CCND transcription (Wickstrom et al., 2010). In addition, CYLD can regulate mitotic entry possibly through the activation of the mitotic kinase polo-like kinase 1 (PLK1) (Stegmeier et al., 2007b).

As discussed in Section 1.5.2, USP7 has multiple roles in governing S-phase entry by stabilising the transcription factors Rb and P53. In addition to this, USP7 plays an important role in maintaining genomic stability during mitosis. USP7 was shown to interact with and stabilise BUB3, a component of the MCC. Upon depletion of USP7, BUB3 levels decreased; this resulted in genomic instability through the improper segregation of chromosomes during mitosis (Giovinazzi et al., 2014). Additionally, as discussed in more detail in Section 5.1, USP7 also regulates genomic instability during mitosis by stabilising an E3 ligase, Checkpoint with Forkhead and Ring Finger (CHFR) (Giovinazzi et al., 2013).

In this chapter I have reviewed the post-translational modifier ubiquitin and the complexity of signals that can be created by this single protein. I have also discussed the cellular machinery that mediates the addition and removal of ubiquitin signals from proteins, with a particular focus on DUBs and the myriad of mechanisms employed to regulate their activity. Finally, I have introduced the principles of cell cycle regulation, reliant on phosphorylation and ubiquitylation to execute sharp, irreversible transitions.

1.6 Project Aims

1.6.1 Outstanding question

A number of DUBs have been linked, either directly or indirectly, to correct cell cycle progression. The majority of investigations have focussed on a specific cell cycle effector or a specific DUB, with a few studies performing DUBome-wide RNAi screens assessing the role of DUBs at certain cell cycle checkpoints, including DNA damage repair and the G_2/M transition (Aressy et al., 2010; Nishi et al., 2014; Stegmeier et al., 2007a; Stegmeier et al., 2007b; van Leuken et al., 2008). However, the latter are biased towards identification of DUBs whose activity is required for cell cycle progression, and depletion strategies are unlikely to identify functionally important DUB inactivation. In addition, periodic regulation through the cell cycle has been studied for only a few selected DUBs. Importantly, there has yet to be any systematic investigation of how the expression and activity of the DUBome is modulated during the cell cycle. Addressing this challenge was the initial objective of my thesis.

DUB activity needs to be tightly regulated within cells to ensure they act only against the appropriate targets when required, and I have reviewed our current knowledge of the mechanisms employed. A number of studies have used unbiased techniques to assess differential DUB activity, however these screens often assay the activity of purified recombinant DUBs towards synthetic substrates *in vitro* (Faesen et al., 2011b; Mevissen et al., 2013; Ritorto et al., 2014). However, such *in vitro* studies cannot accurately reflect the activity of DUBs within the cellular milieu, where their activity can be externally modulated in many ways. In order to monitor DUBs during such a dynamic and tightly regulated process as the cell cycle, it is important to extract active DUBs from an *in vivo* cell model. Here I have taken advantage of ubiquitin active site-directed probes (reviewed in Section 3.1) to monitor DUB activity. This approach enriches for DUBs to monitor their expression, and should more accurately reflect the many of the layers of DUB regulation.

1.6.2 Specific Aims

My objective was to employ a novel screen to profile regulation of the DUBome through the cell cycle, and to further characterise regulation of a selected DUB.

The specific aims of this study were initially to:

- Develop an unbiased and quantitative technique to assay the expression/activity of endogenous DUBs within synchronised cell lysates using DUB activity probes (Chapter 3).
- Apply this DUB activity assay to perform the first unbiased profile of DUB expression/activity across multiple cell cycle phases by mass spectrometry (Chapter 4).
- Identify DUBs exhibiting cell cycle-dependent oscillation in expression/activity and characterise how this is temporally regulated (Chapter 4 and 5).

On completion of these initial aims, I selected USP7 for further study. My final aim was to:

- Elucidate how phosphorylation of USP7, which peaks at G_1/S, regulates its cellular behaviour and *in vitro* enzymatic activity (Chapter 6).

Chapter 2

Materials and Methods

2.1 Cell Biology

2.1.1 Cell Culture

A549 and U2OS cell lines were obtained from the European Collection of Cell Cultures (ECACC) for use in this project. U2OS cells are classically used for cell cycle research, however their high transfection efficiency and large surface area made them ideal for later GFP expression studies. A549 cells were employed throughout this project, as all preliminary research and protocol development was performed in this cell line. Both cell lines were cultured under normal physiological conditions, in a humidified incubator at 37°C with 5% carbon dioxide (CO_2). Cell lines were maintained in high glucose (4.5g/L) Dulbecco's modified Eagle's medium (DMEM) supplemented with 10% heat inactivated Foetal Bovine Serum (FBS) and 1% MEM non-essential amino acids (NEAA) (all Gibco, Thermo-Fisher, MA, USA). Cells were routinely passaged every 48 or 72 hours, see Table 2.1. Upon reaching 80% confluency in 10cm^2 dishes, cells were washed with phosphate-buffered saline (PBS) to remove any traces of serum. Cells were lifted from the plastic-ware following minimal incubation with 0.05% trypsin-EDTA (Gibco, Thermo-Fisher) and re-seeded into new dishes using the ratio described in Table 2.1. All plastic-ware used for culturing cells was obtained from Corning, NY, USA.

	Incubation periods	
Cell Lines	**48-hour**	**72-hour**
A549	1:5	1:7
U2OS	1:4	1:6

Table 2.1 Split ratios applied for cell line maintenance for 48 and 72-hour incubations.

2.1.2 Cell synchronisation

A549 cells were subject to two synchronisation protocols in order to obtain synchronised populations from each stage of the cell cycle. A double thymidine block was employed to obtain G_1/S, S-phase and G_2 cell populations, whereas a single thymidine block coupled with a subsequent nocodazole treatment was used to purify mitotic and early G_1 cell populations.

2.1.2.1 Double thymidine block

A549 cells were seeded in varying densities dependent upon the area of the culture dish (Table 2.2). Cells were allowed to adhere overnight prior to an 18-hour 2mM thymidine incubation (Sigma-Aldrich, Dorset, UK). Cells were released into fresh, fully supplemented, DMEM after one wash in pre-warmed PBS and re-incubated at 37°C for eight hours. Subsequently, cells were subjected to a second 17-hour 2mM thymidine incubation to fully arrest cells at the G_1/S boundary. For early and late S-phase cell populations cells were released in to fresh media for 2.5 hours and 5.5 hours, respectively. For G_2 synchronised populations, cells were re-incubated for 7.5 hours prior to lysis.

2.1.2.2 Single thymidine, single nocodazole block

Cells synchronised under these experimental conditions only undergo one cell division and so increased numbers of cells were required at seeding to achieve 80% confluency at lysis (Table 2.2). Again, cells were allowed to adhere overnight before cells were supplemented with 2mM thymidine for 24 hours to hold the majority of cells at G_1/S. As above, cells were washed once in pre-warmed PBS, prior to a 14-hour overnight incubation in full DMEM supplemented with 100ng/mL nocodazole (Sigma-Aldrich) to arrest cells in pro-metaphase. To select for a purified mitotic population, rounded cells were knocked off the dish and collected and washed twice in pre-warmed PBS. Pro-metaphase cells were lysed immediately; mitotic cell populations cells were re-incubated for 30 minutes at 37°C and to enrich for cells in G_1, cells were released for 3 hours to exit mitosis and enter early G_1.

	Synchronisation protocols	
Dish size	**Double thymidine**	**Single thymidine**
$6cm^2$	4.0×10^5	6.0×10^5
$10cm^2$	1.0×10^6	1.5×10^6
$15cm^2$	2.5×10^6	3.25×10^6

Table 2.2 Cell seeding densities for cell synchronisation protocols.

2.1.3 Stable Isotope Labelling with Amino Acids (SILAC) labelling of A549 cells

ECACC A549 cells were grown and maintained for a minimum of eight passages in three variations of 'SILAC media' (light, medium and heavy) to ensure full incorporation of differentially labelled arginine and lysine amino acids. SILAC media comprised arginine and lysine free DMEM, 10% dialyzed FBS (both Dundee Cell Products, Dundee, UK) and was supplemented with the following amino acids: Light SILAC medium: L-lysine (Lys 0), L-arginine (Arg 0) and L-proline (Pro 0). Medium SILAC medium: L-lysine-2H4 (Lys 4), L-arginine-U–13C6 (Arg 6) and L-proline (Pro 0). Heavy SILAC medium: L-lysine- U–13C6-15N2 (Lys 8), L-arginine-U–13C6–15N4 (Arg 10) and L-proline (Pro 0). The supplemented amino acids were added for a final concentration of 84mg/L arginine, 146mg/L lysine and 200mg/L proline (all obtained from Sigma-Aldrich).

2.1.4 RNA interference

Both U2OS and A549 cells were used for RNAi experiments, they were seeded at an appropriate density for a five-day experiment and short interfering RNA (siRNA) transfections were performed 24 hours post-seeding. Dependent on the cell line used transfections were performed using two different transfection reagents following the manufacturers guidelines. Oligofectamine was used for A549 cells (in 10cm^2 dishes for non-denaturing lyses) or Lipofectamine RNAiMAX was used for U2OS cells (in 6-well plates for whole cell lysates) (both from Invitrogen, Thermo-Fisher).

For both transfections two solutions were prepared, the first of which (solution A) was made up of siRNA (stock concentration of 20μM) diluted in OptiMEM (Gibco, Thermo-Fisher) and the second (solution B) consisted of the transfection reagent diluted in OptiMEM (see table 2.3 for detailed volumes). Following a 5-minute incubation, the two solutions were mixed and incubated at room temperature for 20 minutes prior being added drop-wise to the cells. A final siRNA concentration of 50nM (Oligofectamine) or 10nM (RNAiMAX) was used. Four-hours post-transfection, FBS was added to a final concentration of 10% and

incubated overnight before replacing with fresh full media. The sequences of the siRNAs used are shown in Table 2.4.

Cell line	Solution	Volumes
A549	Solution A	15.5µL siRNA oligo 1.1mL OptiMEM
	Solution B	24µL oligofectamine 110.5µL OptiMEM
U2OS	Solution A	0.5µL siRNA oligo 179.5µL OptiMEM
	Solution B	2µL RNAiMAX 18µL OptiMEM

Table 2.3: Composition of RNAi transfection solutions for A549 and U2OS siRNA transfections.

siRNA oligo	Sequence
OTP NT1	non-targeting siRNA control D-001810-01
siUSP7_1	5'-AAGCGUCCCUUUAGCAUUA-3'
siUSP7_3	5'-UAAGGACCCUGCAAAUUAU-3'
siGMPS_6	5'-ACAGAGAACUUGAGUGUAU-3'
siGMPS_7	5'-GAGAUAGUGUAGACAAAGU-3'

Table 2.4: siRNA oligo sequences for all transfected oligos.
All oligos were purchased from Dharmacon, GE Healthcare Life Sciences, Buckinghamshire, UK.

2.1.5 Plasmid transfection

Both U2OS and A549 cells were used for overexpression experiments, they were seeded at an appropriate density for a three-day experiment. Plasmid transfections were performed 24 hours post-seeding, and incubated for 24 hours prior to lysis/fixation. Dependent on the cell line, transfections used two different transfection reagents: for A549 cells Lipofectamine LTX supplemented with PLUS reagent (both from Invitrogen, Thermo-Fisher) was used and for U2OS cells GeneJuice (Novagen, Merck-Millipore, Hertfordshire, UK) was used. Each cell line required different concentrations of exogenous DNA for optimum transfection efficiency. Transfection reagents were added at a 3:1 ratio of transfection reagent:DNA (v/v) (see Table 2.5 for specific volumes).

Cell line	Dish size	Plasmid	Transfection Reagent	OptiMEM
U2OS	6-well	0.3µg (+0.7µg Bluescript)	3µL GeneJuice	500µL
A549	10cm^2	8µg	24µL Lipofectamine LTX +8µL PLUS reagent	1mL
	15cm^2	21µg	63µL Lipofectamine LTX +21µL PLUS reagent	2mL

Table 2.5: Composition of DNA concentrations and transfection solutions for A549 and U2OS DNA transfections.

2.1.6 Cell lysis

2.1.6.1 Laemmli lysis

For whole cell lysates, cells were lysed in Laemmli buffer (50mM Tris-Base (pH 6.8), 2% SDS, 10% glycerol (v/v)). Cells were grown in 6-well plates or 10cm^2 dishes and were washed twice in PBS before lysis. The PBS was aspirated from the cells and pre-heated Laemmli buffer (110°C) was added to each sample, 100-150µl (for 6-well plates) or 600-800µL (for 10cm dishes). The samples were immediately transferred onto a dry heat block at 110°C and scraped with a rubber policeman. The lysate was then collected and transferred to a heat-durable screw cap tube. All samples were then incubated for a further 10 minutes at 110°C with vigorous vortexing every 2 minutes.

2.1.6.2 Non-denaturing homogenisation

A549 cells were lysed in a non-denaturing lysis buffer (50mM Tris-base (pH 7.5), 5mM $MgCl_2$, 250mM sucrose, 1mM dithiothreitol (DTT), 2mM ATP) for use in active site-directed ubiquitin-based probe activity assays (see Section 2.4.5). Cells were washed twice in PBS prior to being scraped off the dish and collected by centrifugation (300g, 2 minutes). Cell pellets were resuspended in 100-300µL ice-cold non-denaturing lysis buffer (volume was varied dependent on cell number) and homogenised by progressively passing through 23G, 26G and 30G needles. Phosphatase inhibitors (PhosStop, Roche, Basel, Switzerland) were added to each sample after the homogenisation process was completed. Lysates were cleared by centrifugation (20,000g, 20 minutes, 4°C).

2.1.6.3 E1A lysis

For lysates that were to be used in phosphatase assays, cells were lysed in E1A lysis buffer (50mM HEPES (pH 7.5), 250mM NaCl, 0.5% NP-40). Cells from a confluent 10cm^2 dish were washed twice in warm PBS, then trypsinised (0.05% Trypsin-EDTA) and collected by centrifugation (300g, 2 minutes). Cell pellets were resuspended in ice-cold E1A lysis buffer and incubated at 4^{o}C with vortexing every two minutes.

2.1.6.4 NP-40 lysis

For immunoprecipitation experiments, A549 cells were lysed in NP-40 lysis buffer (0.5% NP40 (w/v), 25mM Tris (pH 7.5), 100mM NaCl, 50mM NaF, 2mM $MgCl_2$, 1mM EGTA, containing protease inhibitor cocktail tablets and PhosStop inhibitor tablets (both from Roche)). Cells were placed on ice and washed twice with ice cold PBS. NP-40 lysis buffer was added directly to the dish and the cells were lysed for 15 minutes with gentle rocking. The lysate was collected and then cleared by centrifugation (16,000g, 10 minutes, 4°C).

2.1.7 Flow cytometry

The cell cycle phases of synchronised A549 cells was validated through flow cytometry (FC) using propidium iodide (PI, Sigma-Aldrich) to determine cellular DNA content. Pellets of synchronised cell populations were gently resuspended in ice-cold molecular grade ethanol (75% final ethanol concentration). Once fixed, synchronised cells were centrifuged (1000g, 10 minutes, 4^{o}C) and washed twice in PBS. Washed cells were pelleted, as before, and resuspended in 400µL PI, supplemented with 4µg RNase A (Sigma-Aldrich), to stain cellular DNA. Stained cells were incubated for 30 minutes at 37^{o}C, protected from light and subsequently stored at 4^{o}C until analysis. The fluorescence of single cells for each synchronised cell population was quantified using a BD FACScalibur™ system (BD Biosciences, Oxford, UK) using the FL-2 filter to measure PI fluorescence.

2.1.8 Cell Imaging

U2OS cells were seeded at low density directly onto glass coverslips in a 6-well plate, this resulted in 40-50% confluency after a 72 hour experiment. Cells were washed twice with warm PBS and immediately fixed in 4% paraformaldehyde (PFA), after 15 minutes the fixative was removed and cells were washed twice in PBS. Subsequently, cells were incubated with 50mM ammonium chloride for 20 minutes. Again, the cells were washed twice with PBS prior to a 5 minute incubation with 0.1% triton X-100 to permeabilised cell membranes. Cells expressed Green Fluorescent Protein (GFP) and so did not require additional staining protocols, therefore cover slips were mounted on to glass slides using Moviol supplemented with 4′,6-diamidino-2-phenylindole (DAPI) at 1:10,000. Slides were stored at 4^{o}C prior to imaging on a Nikon Eclipse Ti (CFI Plan Apochromat 40× N.A. 0.95, W.D. 0.14mm) microscope.

2.2 Protein Biochemistry

2.2.1 Protein assays and sample preparation

The protein concentration of all cell lysates was determined using a bicinchoninic acid (BCA) protein assay kit (Pierce, Thermo-Fisher). They were performed according to the manufacturer's instructions, using bovine serum albumin (BSA) to generate a standard curve. Absorbance was read using a GloMAX Multi plate reader (Promega, WI, USA). Following the protein assay, cell lysates were adjusted to equal protein concentrations using the original lysis buffer. Whole cell lysates, for immunoblotting, were adjusted to equal volumes with Leammli lysis buffer and supplemented with 10X loading buffer (312.5mM Tris-base pH 6.8, 50% glycerol (w/v), 1M DTT and 1% bromophenol blue). Samples were then boiled for 10 minutes at 98^{o}C prior to storage at -20^{o}C. Homogenised cell lysates were immediately snap frozen in liquid nitrogen and stored at -80^{o}C prior to use in activity assays (Section 2.4.5). Similarly, NP-40 lysates (for immunoprecipitation experiments) and E1A lysates (for phosphatase assays) were snap frozen in liquid nitrogen if not used immediately.

2.2.2 SDS polyacrylamide gel electrophoresis (SDS-PAGE)

SDS-PAGE was performed using Mini Gels poured using a BioRad Mini-Protean® 3 system (BioRad, CA, USA) or using precast NuPAGE® Novex™ Bis-Tris 4-12%

gradient gels on a XCell SureLock™ Mini-Cell or Bolt® Mini Gel system or (all Invitrogen, Thermo-Fisher). NuPAGE® gradient gels were only used for samples from *in vitro* assay reactions. Otherwise, protein samples were separated on self-poured polyacrylamide gels. The percentage concentration of acrylamide used was determined by the target protein molecular weight, 8% and 10% acylamide gels were used in this project.

Equal amounts of each sample were loaded, alongside two molecular weight markers: Perfect Protein (Novagen, Merck-Millipore) and Rainbow Marker (GE Healthcare Life Sciences). Self-poured gels were run at 200V for approximately 1 hour in electrophoresis running buffer containing 50mM TrisHCl, 38mM glycine and 0.1% SDS. NuPAGE® gradient gels were run according to manufacturer's instructions in diluted NuPAGE® MOPS buffer containing 200µL NuPAGE® antioxidant at 200V for approximately 1 hour (both Invitrogen, Thermo-Fisher).

2.2.3 Immunoblotting

Following separation by SDS-PAGE, proteins were transferred onto nitrocellulose membrane in fresh transfer buffer (25 mM tris-glycine, 20% Methanol) using a Genie blotter apparatus (Idea Scientific, MN, USA) with a fixed voltage of 24V for 60-90 minutes, dependent on the molecular weight of the target protein. Proteins were stained using Ponceau-S (Sigma-Aldrich) to assess the transfer and protein loading efficiency. Blots were then incubated in a blocking buffer of either 5% marvel milk, 5% BSA or 0.5% fish skin gelatin (FSG) in TBS-T (20mM Tris-base (pH 7.6), 137mM NaCl, supplemented with 0.1% Tween-20) for an hour. Primary antibodies were added in the same blocking buffer and the blots were incubated on a rocker for either 1-2 hours at room temperature or overnight at 4^{o}C. Concentrations and conditions for each antibody are described in Table 2.6. After primary incubation, immunoblots were washed twice in TBS-T before the addition of a secondary antibody (Table 2.7), which was again diluted in the same buffer. Secondary antibodies were incubated for 1 hour at room temperature, the blots were washed twice in TBS-T and twice in TBS (20mM Tris-base (pH 7.6), 137mM NaCl) for 10 minutes with rocking. Immunoblotted

proteins were visualised on a LI-COR Odyssey® 2.1 scanning system which produced 16-bit images from each scan for further analysis.

Protein	Catalogue Number	Company	Species	Buffer	Dilution
Actin	ab6276	Abcam	Mouse	5% milk	1:10,000
	A2066	Sigma	Rabbit	5% milk	1:2000
HA	MMS-101P	Covance	Mouse	5% milk	1:2000
GFP	Gift from Prof. Ian Prior		Sheep	5% milk	1:2000
Ub	U5379	Sigma	Rabbit	0.5% FSG	
Cyclin B1	05-373	Merck-Millipore	Mouse	5% milk	1:2000
Cyclin E1	HE12	CST	Mouse	5% milk	1:1000
pCDK1	9111	CST	Rabbit	5% BSA	1:1000
pRb	9308	CST	Rabbit	5% BSA	1:1000
Rb	9309	CST	Mouse	5% milk	1:1000
pP53	9284	CST	Rabbit	5% BSA	1:1000
P53	sc-126	Santa Cruz	Mouse	5% milk	1:1000
USP7	ab4080	Abcam	Rabbit	5% milk	1:1000
	05-1946	Merck-Millipore	Mouse	5% milk	1:1000
pS18-USP7	ABC225	Merck-Millipore	Rabbit	5% BSA	1:500
Non-pS18-USP7	ABC226	Merck-Millipore	Rabbit	5% BSA	1:500
USP8	HA004869	Sigma	Rabbit	5% milk	1:2000
USP11	A301-613A	Bethyl	Rabbit	5% milk	1:2000
USP15	H00009958-M01	Abnova	Mouse	5% milk	1:1000
USP9X	A301-350A	Bethyl	Rabbit	5% milk	1:2000
USP47	A301-048A	Bethyl	Rabbit	5% milk	1:2000
UCHL1	ab27053	Abcam	Rabbit	5% BSA	1:500
UCHL5	3904-1	Epitomics	Rabbit	5% milk	1:10,000
BAP1	sc-28383	Santa Cruz	Mouse	5% milk	1:400
YOD1	sc-79663	Santa Cruz	Goat	5% BSA	1:200
ATXN3	650401	BioLegend	Mouse	5% BSA	1:2000
GMPS	16376-1-AP	Protein-Tech	Rabbit	5% milk	1:2000

Table 2.6: All primary antibodies used in this project.

Secondary	IRDye	Catalogue Number	Company	Dilution
Donkey α-mouse	680LT	926-68020	LI-COR	1:20,000
	800CW	926-32212		1:15,000
Donkey α-rabbit	680LT	926-68023		1:20,000
	800CW	926-32213		1:15,000
Donkey α-sheep	800CW	926-32214		1:15,000

Table 2.7: All secondary antibodies used in this project.

2.2.4 Immunoprecipitation

Snap-frozen NP-40 lysates were thawed on ice and, if required, concentration adjusted to 1mg/mL using NP-40 lysis buffer. Whilst thawing, beads were washed twice in NP-40 lysis buffer. Two types of beads were used in this project: HA-conjugated agarose beads (33µL beads per sample) (Sigma-Aldrich) and GFP-NanoTrap beads (prepared in house by Dr A. Fielding, 10µL per sample). Equal amounts of lysate (1mg) were incubated with the specified beads for approximately 16 hours at 4°C. Beads were pelleted in a bench-top centrifuge (10,000rpm, 4°C) and the supernatant, or flow through, was aspirated and stored at -80°C. Pelleted beads were washed three times in a wash buffer (0.5% NP-40 (w/v), 25mM Tris-base (pH 7.5), 100mM NaCl, 50mM NaF, 2mM $MgCl_2$, containing protease and phosphatase inhibitor cocktail tablets) prior to a final wash in a detergent-free wash buffer (10mM Tris (pH7.5), 2mM $MgCl_2$). To elute bound proteins, beads were resuspended in 2% SDS for 5 minutes at 95°C, with vigorous vortexing every minute. The supernatant was collected and supplemented with 5X sample buffer (15% SDS, 312.5mM Tris-base (pH 6.8), 50% glycerol (w/v), 16% ß-mercaptoethanol, 1% bromophenol blue) prior to SDS-PAGE.

2.3 Molecular Biology

2.3.1 RNA extraction

Total RNA extraction was performed using an RNeasy Mini kit and QIAshredder columns (Qiagen, Manchester, UK) following the manufacturer's instructions and including all optional steps. The RNA was eluted in nuclease-free water and the concentration of each sample was determined using a ND-1000 NanoDrop spectrophotometer (Thermo-Fisher). As well as determining the concentration

of RNA (ng/µL) also provided absorbance ratios for 260/280 and 260/230 to assess the purity of each sample, these were routinely >2.0. RNA was stored at -20°C.

2.3.2 Reverse transcription (RT)

Equal amounts of RNA (1µg) were reverse transcribed using RevertAid H-minus M-MuLV reverse transcriptase (Fermentas, Thermo-Fisher). A mix containing 1µg RNA, 0.5µg of oligo dT primer (Promega) and nuclease-free molecular grade water was incubated at 70°C for 5 minutes, and subsequently snap-chilled on ice. Each reaction was then supplemented with: 4µl of 5x reverse transcription buffer (Fermentas, Thermo-Fisher), 2µl PCR nucleotide mix (containing 10mM dATP, dCTP, dGTP and dTTP each (Promega)), 0.5µl RNasin (Promega) and 1.5µl of nuclease-free water. The reaction mix was incubated at 37°C for 5 minutes, prior to the addition of 1µl of M-MuLV reverse transcriptase (Fermentas, Thermo-Fisher). The reaction was then incubated at 42°C for 1 hour and then followed by a denaturation step at 70°C for 10 minutes. cDNA samples were immediately snap-chilled on ice for 5 minutes, then diluted five-fold in nuclease-free water prior to long-term storage at -20°C.

2.3.3 End-point reverse transcription Polymerase Chain Reaction (RT-PCR)

To determine the expression levels of USP7 splice variants, cDNA from A549, U2OS and HeLa cells were amplified with primers that were designed in-house to bind to isoform-specific regions in the 5' end or 5' UTRs (see table 2.8 and Figure 6.1). End-point PCR reactions were performed using HotStarTaq *Plus* DNA polymerase (Qiagen). Equal volumes of cDNA (2µL) were supplemented with 3µL primer (1.5µL forward, 1.5µL reverse of 20µM stock concentration, final concentration 2µM), HotStarTaq *Plus* Mastermix (15µL) and nuclease-free water (10µL). The reaction mix was first incubated at 94°C for 15 minutes to activate the DNA polymerase. This was followed by a 40 cycle 3-step incubation programme: 94°C for 1 minute, 60°C for 1 minute, 72°C for 1 minute. The PCR products were then incubated for a further 10 minutes at 72°C as a polishing step to ensure all products were fully elongated.

Primer		Sequence
USP7-001	For	5'-GAGCAGCAGTTGAGCGAGCC-3'
	Rev	5'-GGTGTGGTCTGTCTGGATAAAAGC-3'
USP7-004	For	5'-ATTCTATGCAGTCACTCTGATGTGG-3'
	Rev	5'-GGTGTGGTCTGTCTGGATAAAAGC-3'
USP7-002	For	5'-GAATGTTTGAAACCTGGGAGCG-3'
	Rev	5'- GGCTGAACTTTTGGCAGGAGG-3'
USP7-201	For	5'-TGCAGAGATGGCTGGGAACC-3'
	Rev	5'-GGCTGAACTTTTGGCAGGAGG-3'
USP7-all	For	5'-ATGGCCTGGAGTGAAGTGACC-3'
	Rev	5'-CGGTTGGCATCATGTACACAGC-3'
USP7 (general)	For	5'-ACTTTGAGCCACAGCCCGGTAATA-3'
	Rev	5'-GCCTTGAACACACCAGCTTGGAAA-3'
ACTB	For	5'-CACCTTCTACAATGAGCTGCGTGTG-3'
	Rev	5'-ATAGCACAGCCTGGATAGCAACGTAC-3'
CCNB1	For	5'-GCTCTTCTCGGCGTGCTGC-3'
	Rev	5'-CCTGCCATGTTGATCTTCG-3'
CCNE	For	5'-CCTTATGGTATACTTGCTGCT-3'
	Rev	5'-CCACTGATACCCTGAAACC-3'

Table 2.8: A list of all primers used in PCR in this project.

2.3.4 Quantitative real-time RT-PCR (QPCR)

QPCR reactions were performed in triplicate using a CFX Connect real-time PCR detection system and SYBR green supermix (both BioRad). Each reaction contained 1µl of cDNA, 0.15µl forward and reverse primers (20µM stock concentration, final concentration 2µM) and 5µl of SYBR green supermix (2X). Reactions were made up to a final volume of 10µL with nuclease-free distilled water. Triplicate samples were arranged on a white-walled 96-well PCR plate and firmly sealed with a plastic cover (both BioRad). An initial enzyme activation incubation at 95°C for 30 seconds preceded 40 cycles using a 2-step program (95°C for 5 seconds, 60°C for 30 seconds). Data were analysed using BioRad software to generate cycle threshold (Ct) values, early in the exponential amplification phase. Ct values were determined for each sample and compared to the reference gene (actin, ACTB) using the $2^{-\Delta\Delta Ct}$ method.

2.3.5 Cloning USP7 into pCR4-TOPO vector system

USP7-001 sequence (NM_003470.2) was cloned from a GFP-tagged USP7 plasmid and inserted into the pCR4-TOPO system prior to being shuttled into the

Gateway cloning system (both Invitrogen, Thermo-Fisher). All the primers used to generate siRNA resistant versions of USP7, USP7-C223S, USP7-S18A and USP7-S18E are listed in Table 2.9. The PCR reactions performed to amplify USP7 into pCR4-TOPO vector used the high fidelity DNA polymerase PfuUltra II Fusion to prevent unwanted mutations. These reactions mixed 50-100ng plasmid DNA with 1µL PfuUltra II Polymerase, 5µL PfuUltra HF buffer (both Agilent Technologies, CA, USA), 1µL dNTPs (Promega) (10mM concentration of each dNTP) and 0.625µL forward and reverse primer. This reaction mix is made to a final volume of 50µL with nuclease-free water. The reaction mix was first incubated at 95°C for 2 minutes to activate the DNA polymerase. This was followed by a 30 cycle 3-step incubation programme: 95°C for 30 seconds, 60°C for 30 seconds, 72°C for 3 minutes and a final incubation of 10 minutes at 72°C.

After each PCR reaction a small volume of PCR product (5µL) was resolved on a 0.8% agarose gel to verify the correct size product was amplified. The USP7 PCR product was ligated into the pCR4-TOPO vector by following the manufacture's instruction for the Blunt-End TOPO Cloning Kit (Invitrogen, Thermo-Fisher). The ligated plasmid was transformed in TOP10 competent cells (Invitrogen, Thermo-Fisher) and incubated at 37°C overnight on LB agar plates supplemented with 100µg/mL ampicillin. Continuing to follow the suggested protocol, colonies were picked and amplified overnight in LB media supplemented with 100µg/mL ampicillin at 37°C with gentle shaking (220rpm). Plasmid DNA was extracted and purified from the bacteria using a QiaPrep Spin Mini kit (Qiagen), following the manufacturer's instructions until the final step. Plasmid DNA was eluted in nuclease-free water rather than the suggested buffer as these plasmid were to be used in further rounds of PCR-based cloning. All plasmids were validated though DNA digests and sent for final sequencing confirmation (DNA Sequencing and Services, Dundee, UK).

2.3.6 Site-directed mutagenesis

To generate the three USP7 mutants (C223S, S18A and S18E) and make all USP7 constructs resistant to a specific USP7 siRNA oligo (siUSP7_3), I performed multiple rounds of QuikChange site-directed mutagenesis. As outlined above,

PCR reactions using specifically designed primers were performed with a high-fidelity DNA polymerase. The PCR reaction mix remained unchanged, however the PCR incubation program was amended. The cycle number was reduced to 18 cycles of 94°C for 30 seconds, 55°C for 30 seconds and 68°C for 8 minutes. PCR reactions were then immediately placed on ice whilst 10U DpnI was added to each reaction to digest the methylated template DNA (90 minutes at 37°C). The PCR products were immediately transformed into DH5α competent cells (Invitrogen, Thermo-Fisher), rather than TOP10s, but plasmid DNA was amplified and purified using the methods described above.

Primer		Sequence
USP7 (Gateway Cloning)	For	5'-GGACAAGTTTGTACAAAAAAGCAGGCTCAAGATCTA TGAACCACCAGCAGCAG-3'
	Rev	5'-GGACCACTTTGTACAAGAAAGCTGGGTGCTCGAGTC AGATTTTAATGGCCTT-3'
USP7-C223S	For	5'-GAATCAGGGAGCGACTTCTTACATGAACAGCCTGC-3'
	Rev	5'-GCAGGCTGTTCATGTAAGAAGTCGCTCCCTGATTC-3'
USP7-S18A	For	5'-CGAGCAGCAGTTGGCCGAGCCCGAGGAC-3'
	Rev	5'-TCCTCGGGCTCGGCCAACTGCTGCTC-3'
USP7-S18E	For	5'-CGAGCAGCAGTTGAGCGGAGCCGAGGACATGGAGATG-3'
	Rev	5'-CATCTCCATGTCCTCGGGCTCCTCCAACTGCTGCTCGC-3'
USP7 siRes	For	5'-AACAGATCCTAAGGATCCTGCTAACTACATTCTTCATGC-3'
	Rev	5'-GCATGAAGAATGTAGTTAGCAGGATCCTTAGGATCTGTT-3'

Table 2.9: All primers used for cloning in this project.

2.3.7 Gateway Cloning

Once the four siRNA resistant pCR4-TOPO-USP7 constructs had been generated, they were N-terminally tagged with GFP using the Gateway cloning system. The first step transfers the USP7 sequence from linearized pCR4-TOPO plasmids into a Gateway Entry vector (Invitrogen, Thermo-Fisher). Following the manufacturer's instructions BP Clonase was employed to perform the BP reaction shuttling the siRNA resistant USP7 sequences into the Gateway vector pDON223. The second step transfers the USP7 sequence from this entry vector into a destination vector expressing GFP at the 5' end of USP7 to produce an N-terminally GFP-tagged USP7 protein when expressed in cells. Again, following the manufacturer's instructions LR Clonase was employed to perform the LR

reaction shuttling USP7 into the final destination vector (pEGFPC_GW). At each stage, the recombined plasmids were transformed into DH5α competent cells and purified using the QiaPrep Spin Mini Kit as described above. GFP-tagged USP7 constructs (pEGFPC_USP7_WT/C223S/ S18A/S18E) were sent for sequence analysis and once confirmed prepped on a larger scale using HiSpeed Plasmid Midi Kit (Qiagen) for transfection into eukaryotic cells.

2.3.8 Agarose gel electrophoresis

End-point PCR products, USP7 plasmids and plasmid digest products were analysed by agarose gel electrophoresis. Agarose gels were prepared by adding electrophoresis grade agarose to 0.5X TBE buffer (45mM Tris-borate, 1mM EDTA) (Sigma-Aldrich). Large DNA products were separated on 0.8% agarose gels, whereas smaller PCR products were separated on 2% agarose gels. The agarose mixture was gently heated in a microwave to dissolve the agarose, this solution once cooled was then supplemented with ethidium bromide (0.5 µg/mL) before being poured and left to set. Samples were made up in 5X sample buffer (BioLine, London, UK), loaded onto the gel and run at 120V for approximately an hour in the same 0.5X TBE buffer. DNA bands were visualised using a GeneFlash UV transilluminator (Syngene, Cambridge, UK).

2.4 *In vitro* assays

2.4.1 *In vitro* phosphorylation

2.4.1.1 *In vitro* phosphorylation of CK2 synthetic substrate

Phosphorylation assays were performed in a kinase reaction buffer (50mM Tris pH 7.5, 10mM $MgCl_2$, 1mM DTT). CK2 phosphorylation was initially tested on a synthetic substrate peptide (Signal Chem, Vancouver, Canada), 100mM synthetic substrate peptide was incubated with increasing amounts of recombinant CK2 (MRC-PPU, Dundee, UK) (0-1.1µM) and 10µM ATP. Reactions were incubated for 60 minutes at room temperature prior to being aliquoted, in triplicate, into a white walled 96-well plate (BioRad). Phosphorylation efficiency was analysed using a Kinase-Glo assay kit (Promega), following the manufacturer's instructions. Kinase-Glo reagent was added to each reaction and incubated for

10 minutes at room temperature prior to luminescence analysis on a GloMAX plate reader (Promega).

2.4.1.2 *In vitro* phosphorylation of recombinant USP7-FL

To phosphorylate purified USP7-FL (NKI, the Netherlands), 1 pmol USP7-FL was resuspended in 10µL kinase buffer and was supplemented with 11.9 pmol (0.5µg) of recombinant CK2 (MRC-PPU) and 10-200µM ATP. Reactions were incubated at 30°C for 30 minutes with gentle shaking (300rpm in a thermoshaker) and either taken forward into additional *in vitro* DUB activity assays described below, or supplemented with 5X sample buffer and the USP7 phospho-status analysed via SDS-PAGE.

2.4.2 *In vitro* dephosphorylation

Lambda phosphatase (LPP) was employed to dephosphorylate both recombinant USP7-FL or proteins from an E1A cell lysate to test LPP efficiency. Phosphatase assays were traditionally performed in a 4-(2-hydroxyethyl)-1-piperazineethanesulfonic acid (HEPES)-based buffer (50mM HEPES (pH 7.5), 100mM NaCl, 1mM DTT) but the kinase buffer was Tris-based and it was preferable to reduce any variables between kinase and phosphatase assays. Therefore, an initial experiment using E1A lysate was performed comparing LPP efficiency in the HEPES-based buffer and a Tris-based buffer (50mM Tris pH 7.5, 10mM $MgCl_2$, 1mM DTT).

2.4.2.1 *In vitro* dephosphorylation of cell lysates

Equal amounts of E1A lysate (30µg) were resuspended in either HEPES-based or Tris-based phosphatase buffer. Reactions were supplemented with 1mM $MnCl_2$ and either 400U LPP (1µL) (both NEB, MA, USA) or a vehicle control. Reactions were incubated at 30°C for 30 minutes with gently mixing (300rpm on thermoshaker). Each sample was supplemented with 5mM EDTA and incubated at 65°C for 1 hour to terminate the phosphatase reaction. Samples were additionally supplemented with 5X sample buffer and boiled for 5 minutes at 95°C to prepare for SDS-PAGE.

2.4.2.2 *In vitro* dephosphorylation of recombinant USP7-FL

To dephosphorylate USP7-FL, 1 pmol USP7-FL was resuspended in the Tris-based phosphatase buffer additionally supplemented with 400U LPP and 1mM $MnCl_2$. Like the kinase assay, phosphatase reactions were incubated for 30 min (30°C, 300rpm) then either taken forward into other *in vitro* assays or incubated with 5mM EDTA for 1 hour at 65°C to terminate the reaction and prepared for SDS-PAGE as described above.

2.4.3 *In vitro* inhibition of USP7

P22077 (#662142, Merck-Millipore) is an USP7-selective inhibitor. P22077-inhibited USP7 would act as a negative control for each *in vitro* USP7 activity assay. The specificity of P22077 was analysed through a secondary reaction with HA-Ub-VME (see Section 2.4.5) where USP7 and UCHL5 activity were measured post-incubation with P22077.

2.4.3.1 *In vitro* inhibition of DUBs in cell lysates

Equal amounts (40µg) of non-denatured A549 cell lysate were resuspended in kinase buffer and supplemented with a high concentration of P22077 (200µM) or a DMSO vehicle control. It should be noted that such high concentrations have been shown to non-specifically inhibit other cellular DUBs (Altun et al., 2011). Reactions were incubated for 30 minutes (30°C, 300rpm) in-keeping with the kinase and phosphatase protocols. DUB activity was analysed in a HA-Ub-VME (see Sections 2.4.5) time course experiment, samples were separated into 4x10µg samples and supplemented with 50ng HA-Ub-VME (1:200 probe: protein concentration) and incubated for increasing periods of time prior to termination using 5X sample buffer and boiling.

2.4.3.2 *In vitro* inhibition of recombinant USP7-FL

For inhibition of recombinant USP7-FL, 1pmol was resuspended in kinase buffer and supplemented with 200µM P22077. Incubations were performed at 30°C for 30 minutes with gentle shaking (300rpm). Samples were either taken forward

into subsequent *in vitro* assays or prepared for SDS-PAGE by addition of 5X sample buffer.

2.4.4 Constitution of activity probes

All active site-directed ubiquitin-based probes (Ub-based probes) were purchased from UbiQ Bio (Amsterdam, The Netherlands) and received as a lyophilised powder. Stocks were initially resuspended in DMSO (Sigma-Aldrich) for a stock concentration of 20mg/ml. DMSO stocks were further diluted in 50mM Tris-Base (pH 7.5) to a concentration of 0.5mg/mL. Repeated freeze-thaw cycles decrease the efficacy of Ub-based probes and so these were aliquoted into small volumes prior to long-term storage at -80°C

2.4.5 Ub-based probe activity assays

2.4.5.1 Ub-based probe assays in cell lysates

Snap-frozen homogenised lysates were thawed on ice and, if required, the concentration adjusted using non-denaturing lysis buffer. Equal amounts of cell lysate (15µg, unless otherwise indicated) was incubated with 75ng HA-Ub-VME (UbiQ-035), HA-Ub-PA (UbiQ-078) or Ub-PA (UbiQ-057) giving a 1:200 ratio of probe:protein, for the specified period of time (within a range of 30 seconds to 45 minutes) at 37°C with shaking at 300rpm. For exogenously expressed USP7, an increased probe:protein ratio of 1:50 was used for each reaction. Each experiment was performed with a 'no probe' vehicle control of 1µL 50mM Tris-base (pH 7.5). Reactions were terminated by the addition of 5X sample buffer and samples heated at 95°C for 5 minutes prior to analysis by SDS-PAGE.

2.4.5.2 Ub-based probes with recombinant DUBs

Ub-VME assays were initially performed using the catalytic domain of USP2 (USP2cc) to optimise the *in vitro* reaction conditions for the limited amount of USP7-FL. Equal amounts of USP2cc (100nM) were incubated with increasing concentrations of Ub-VME over a time course. Adding 5X sample buffer, vortexing and heating samples to 95°C for 5 minutes terminated reactions prior to analysis via SDS-PAGE. For USP7-FL, untreated, phosphorylated,

dephosphorylated or inhibited USP7 (100nM) was resuspended in non-denaturing lysis buffer and was incubated with 250nM of HA-Ub-VME for 5 or 45 minutes at 37°C with gentle shaking (300rpm). To terminate reactions, 5X sample buffer was added and samples heated at 95°C for 5 min prior to analysis by SDS-PAGE

2.4.6 K48-linked tetra-ubiquitin chain (K48-Ub_4) assay

K48-Ub_4 assays were initially performed using USP2cc to optimise the *in vitro* reaction for the limited amount of USP7-FL. Equal amounts of K48-Ub_4 (250ng) (Boston BioChem) was incubated with increasing concentration of USP2cc over a time course of 5 minutes to 16 hours. Adding 5X sample buffer, vortexing and heating samples to 95°C for 5 minutes terminated reactions prior to analysis via SDS-PAGE. For USP7-FL, untreated, phosphorylated, dephosphorylated or inhibited USP7 (100nM) was resuspended in DUB reaction buffer (50mM Tris (pH 7.5), 10mM $MgCl_2$, 1mM DTT, 25mM KCl) and was incubated with 250ng of K48-Ub_4 for 30 minutes or 6 hours at 37°C with gentle shaking (300rpm). To terminate reactions, 5x sample buffer was added and samples heated at 95°C for 5 min prior to analysis by SDS-PAGE.

2.4.7 Ub-AMC assay

Ub-AMC *in vitro* assays were performed with USP2cc prior to recombinant USP7-FL. USP2cc (1nM, 10nM or 100nM) was resuspended in Ub-AMC reaction buffer (50mM Tris (pH 7.5), 10mM $MgCl_2$, 10mM DTT, 0.5% Tween-20 (w/v)). Triplicate reactions were supplemented with 2μM Ub-AMC (UbiQ-001) and incubated in a white-walled 96-well plate (BioRad) at 30°C over a 60 minute time course. AMC fluorescence was measured using a GloMax Multi plate reader (Promega) (Excitation: 365nm, emission: 410nm) periodically during the incubation. Relative Fluorescence Units (RFU) were converted to molar concentrations using an AMC (Boston BioChem) standard curve. For analysis of USP7-FL activity, untreated, phosphorylated, dephosphorylated or inhibited USP7 (10nM) was resuspended in Ub-AMC reaction buffer and aliquoted into a 96-well plate in triplicate. Each reaction was supplemented with Ub-AMC (0.5-8μM) and incubated at 30°C for 90 minutes. AMC fluorescence was measured periodically as described above.

2.5 Proteomics

2.5.1 HA-Ub-VME immunoprecipitation, in-gel digest and sample prep

Equal amounts of synchronised A549 lysates (1µg) were incubated with HA-Ub-VME (UbiQ-035) at a final concentration ratio of 1:200 probe:protein and incubated for 45 minutes at 37°C with gentle shaking (300rpm). A vehicle control reaction was used for each synchronised lysate. Reactions were terminated by the addition of SDS to a final concentration of 0.4% (v/v). HA-Ub-VME reactive DUBs were then subjected to HA immunoprecipitation following the protocol outlined in Section 2.2.4.

The immunoprecipitation eluate was separated on NuPAGE Novex 4–12% Bis-Tris Gels (Invitrogen, Thermo-Fisher) for 1 hour at 200V. The gel was stained using a Colloidal Blue staining kit (Invitrogen, Thermo-Fisher), following the manufactures' guidelines. Each lane was cut into 24 slices, chopped into approximately $1mm^3$ cubes and placed in LoBind tubes (Eppendorf, Sigma-Aldrich). Gel pieces were de-stained using a 50% acetonitrile / 50% 100mM ammonium bicarbonate solution for 10 minutes at 37°C with shaking (300rpm). The de-staining process was repeated at least once until all the stain was removed. Next, samples were reduced by incubating with 10mM DTT for 1 hour at 56°C with shaking (900rpm) and subsequently alkylated with 50mM iodoacetamide (30 minutes, room temp). Once reduced and alkylated, gel cubes were completely dehydrated with acetonitrile. The gel cubes were then incubated with mass spectrometry grade Trypsin Gold (Promega) for 18 hours at 37°C. Trypsin was resuspended in 50mM acetic acid and further diluted to 10ng/µl in 40mM ammonium bicarbonate / 9% Acetonitrile.

The following morning, peptides were extracted from the gel pieces by incubation in acetonitrile for 30 minutes at 30°C. The supernatant was transferred to a fresh Lo-bind tube, and the remaining gel pieces were incubated for a further 40 minutes (2 x 20 minutes) with 1% formic acid to fully extract all peptides. Finally, acetonitrile was added to the gel pieces and incubated for 10

minutes, before the supernatant was collected. The gel debris was pelleted in a centrifuge for 15 minutes (20,000g) and the final supernatant collected and transferred to the new tube. Samples were dried by evaporation in a Speedvac and the peptide pellet resuspended in 1% formic acid. Finally, samples were centrifuged for 15 minutes (20,000g) to pellet any gel debris, before being transferred to glass vials and stored at -20°C prior to analysis by mass spectrometry.

2.5.2 Sepharose-Ub-PA immunoprecipitation, on bead digest and sample prep

Homogenised cell lysates from each stage of the cell cycle were thawed on ice, and made to equal concentrations with non-denaturing lysis buffer. 1mg cleared lysate was mixed with 16mg pre-washed sepharose-Ub-PA or sepharose-Ub-76 beads (NKI, The Netherlands, made by Dr. Ekkebus) and incubated for 3 hours at 37°C with gentle shaking (300rpm). Reactions were terminated by addition of SDS to a final concentration of 0.4% (v/v). Prior to being mixed, the individual samples were reduced in 10mM DTT and alkylated in 50mM chloroacetamide (as described in Section 2.5.1). The SILAC triplets were then mixed at equal volumes (1:1:1) and then fully denatured in 8M urea. Immobilized proteins were subject to on-bead Lys-C/Trypsin digestion (Promega) for 3 hours at 37°C. Samples were diluted 6-fold to reduce the urea concentration and activate trypsin, then incubated for a further 12 hours at 37°C. The supernatants were collected and the digested peptides were then desalted on C18-Stage tip columns prepared in-house. Once desalted, eluates were dried in a SpeedVac and resuspended in 1% formic acid as described in Section 2.5.1 for loading onto the mass spectrometer.

2.5.3 Liquid chromatography-Mass Spectrometry (LC-MS/MS)

Peptides were separated using a nanoACQUITY UPLC system (Waters, Hertfordshire, UK), coupled to an LTQ Orbitrap XL mass spectrometer (Thermo-Fisher) with a Proxeon nano-electrospray source. 5µl of the resuspended peptide samples was injected into a the column: 180µm x 20mm, 5µm BEH-C18 symmetry trapping column (Waters) at a rate of 15µl/minute before being resolved on a 25cm × 75µm BEH-C18 column (Waters) for maximum separation, in a

acetonitrile gradient in 0.1% formic acid, with a flow rate of 400 nl/min. Full scan MS spectra (*m/z* 300–2000) were generated at 30,000 resolution, and the top five most intense ions were fragmented and subjected to MS/MS in the linear quadrapole ion trap (collision energy 35%, 30ms). All spectra were acquired using Xcalibur software (version 2.0.7; Thermo-Fisher) prior to in-depth analysis of RAW files for peptide identification.

2.6 Bioinformatics and Statistical Analysis

2.6.1 Peptide identification using MaxQuant

RAW files from LC-MS/MS were processed using MaxQuant version 1.4.1.2 (http://www.maxquant.org). The ipi.HUMAN protein database was uploaded to MaxQuant to enable protein identification, where only one unique peptide was required for identification rather than two, the usual standard for high-confidence protein identification. Oxidation was set as the variable modification and carbamidomethylation was set as the fixed modification. RAW files for each SILAC-triplexed experiment was loaded individually then MaxQuant was used to analyse all datasets together and generate one file containing all identified proteins and their identified intensities from individual experiments. The table produced contained intensities and fold changes for each peptide identified in light, medium and heavy fractions.

2.6.2 Hierarchal Clustering Analysis

To identify patterns within datasets, data (Log_2 ratios for proteomic data and mined phosphorylation data (from PHOSIDA)) were input into Multi Experiment Viewer 4.8 (Version 10.2). A two-colour array was generated with a blue-pink colour scale with ±1.0 fold change set as the colour scale limit. Hierarchal clustering analysis was performed by the average linkage method using the Pearson correlation as the metric function.

2.6.3 Statistical analysis

Statistical analyses were performed for all experiments that were performed independently at least three times using GraphPad Prism 6. For experiments

with 5 or more samples a one-way ANOVA was performed, coupled with Tukey's post-hoc test. A paired t-test was used when analysing the statistical significance of the means of two populations.

Chapter 3

Evaluating ubiquitin-based probes as a tool to measure deubiquitylase activity throughout the cell cycle.

3.1 Introduction

There has to date been no report of a systematic approach to profile DUB activity during cell cycle progression. A number of previous studies have identified DUBs with roles at specific stages during the cell cycle. The majority of these have focused on the involvement of DUBs in DNA damage responses or during mitosis (Fournane et al., 2012; Pinto-Fernandez and Kessler, 2016). Experimental methods have largely relied on RNAi-mediated depletion, either using an unbiased screen approach, implementing siRNA/shRNA libraries targeting all the DUBs or a biased approach, targeting a specific DUB of interest. Readouts are typically altered cell cycle dynamics e.g. checkpoint slippage or increased mitotic index (Aressy et al., 2010; Stegmeier et al., 2007a; Stegmeier et al., 2007b; van Leuken et al., 2008). The use of RNAi to study cell cycle progression has limitations, as efficient depletion of a protein can require up to 120 hours, dependent on the protein half-life. Furthermore, if that protein is required for the dynamic progression of the cell cycle, undergoing multiple cell divisions without that protein can be toxic to the cell making any phenotypic analysis problematic. With this in mind it is important to find new techniques to study the role of DUBs in cell cycle progression.

Active site-directed probes have been used with great success in profiling the activity of enzyme families in cell lysates, including kinases and GTPases (Villamor et al., 2013). A pioneering investigation described the development of ubiquitin-based, active site-directed probes (Ub-based probes) that specifically targeted active DUBs (Borodovsky et al., 2002). Through their implementation these activity probes provided the first recorded proof of *in vivo* catalytic activity for a number of DUBs, including many of the USP family (Borodovsky et al., 2002). Furthermore, they have proved indispensable in the discovery of new DUBs. This is best exemplified by the discovery of the OTU family as active DUBs (Borodovsky et al., 2002), a family previously overlooked as candidate DUBs due to a lack of sequence homology with known DUB catalytic domains. Additionally, Ub-based probes have uncovered novel pathogenic DUBs encoded by both viruses, such as Herpes Simplex Virus (Kattenhorn et al., 2005), and parasites, including Toxoplasma gondii (Frickel et al., 2007) and Plasmodium falciparum (Artavanis-Tsakonas et al., 2006). More recent endeavours have utilised Ub-

based probes as an effective tool to profile newly developed DUB inhibitors for potency and selectivity (Altun et al., 2011; Edelmann et al., 2011).

Historically, the use of intein-based chemical ligation generated a number of ubiquitin derived suicide probes (Borodovsky et al., 2002). The C-terminal glycine of monomeric ubiquitin was covalently bound to a diverse range of electrophilic traps. On incubation with cell lysates, each probe demonstrated different binding efficiencies across the DUBome. Michael acceptor-derived probes showed a broader binding profile, with ubiquitin-vinylmethyl ester (Ub-VME) binding to the largest number of DUBs (Borodovsky et al., 2002; de Jong et al., 2012).

The electrophilic traps manipulate the chemistry of the DUB active site in order to form an irreversible covalent bond with the catalytic cysteine. Only five of the six DUB families rely upon a cysteine for the scission of isopeptide bonds. Therefore these Ub-based probes cannot interact with the JAMM family of DUBs, which rely on a zinc ion for their catalytic activity (Clague et al., 2013). The catalytic mechanism of cysteine protease DUBs pivot around a highly conserved catalytic triad: cysteine, histidine and aspartate/asparagine residues. A detailed overview of this mechanism can be found in a recent review (Clague et al., 2013), from which Figure 3.1 is adapted.

The histidine primes the active site through lowering the pK_a, and subsequent deprotonation of the catalytic cysteine. The deprotonated thiol group, by means of a nucleophilic attack, forms an acyl intermediate in which a covalent bond is formed between the catalytic cysteine and the carboxyl group of ubiquitin (Figure 3.1B). It is this intermediate that the Ub-based probes mimic within the DUB active site. The C-terminal VME warhead forms an irreversible vinyl-thioether bond (Figure 3.1D), mimicking the thioester intermediate depicted in Figure 3.1C.

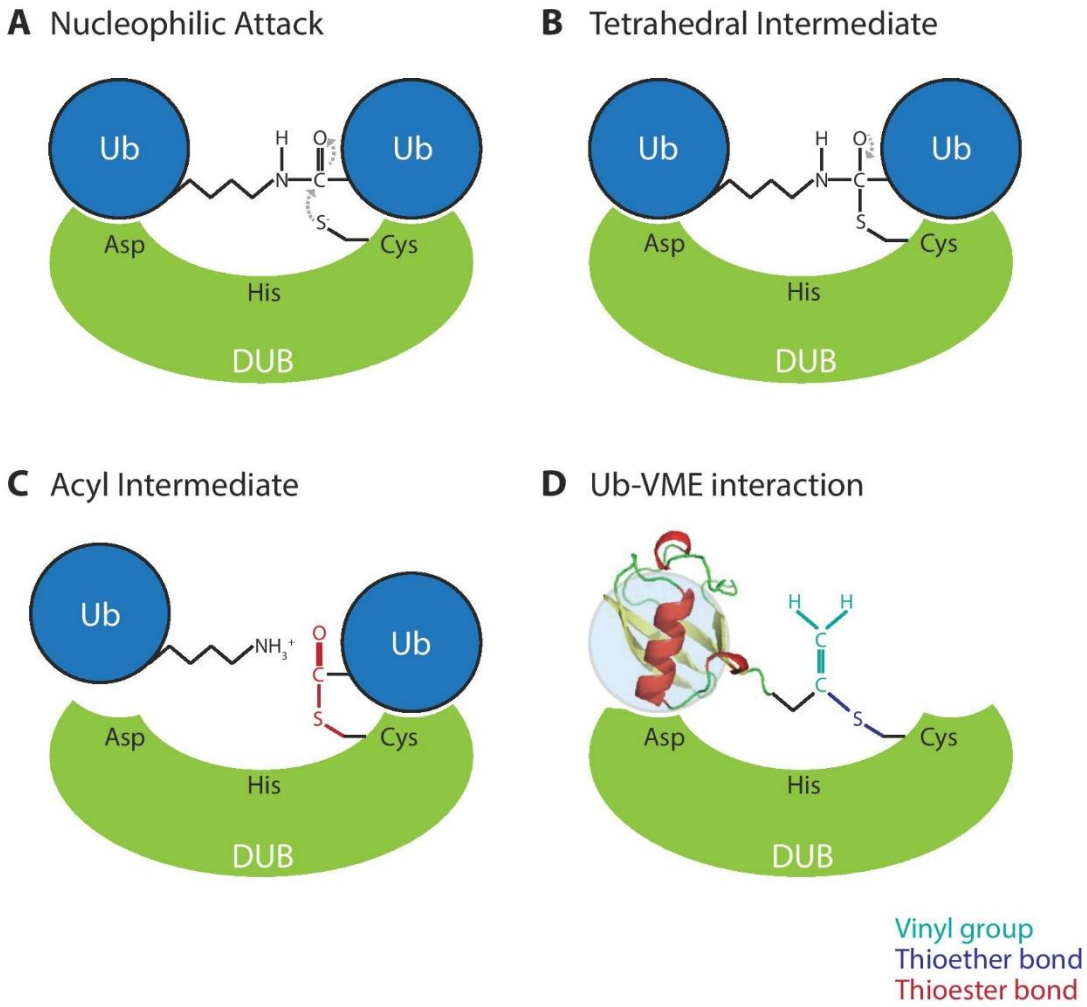

Figure 3.1: Ubiquitin-based activity probes exploit the biochemistry of the DUB active site.

A: A nucleophilic attack on the ubiquitin carboxyl group is coordinated by the catalytic cysteine. **B:** The covalent bond formed in A results in a tetrahedral intermediate. **C:** Upon scission of the isopeptide bond a thioester intermediate is formed. **D:** Manipulation of DUB active site biochemistry by active site-directed ubiquitin probes (Ub-VME).

3.2 Aims

3.2.1 To determine whether Ub-based probes can effectively analyse endogenous DUB activity

The Ub-based probes are an innovative method of analysing DUB activity and have been successfully employed to measure the activity of both endogenous and recombinant DUBs. My first objective is to establish whether Ub-based probes can be a viable candidate to measure endogenous DUB activity in an adenocarcinoma cell (A549) model and optimise these activity assays for unbiased global profiling of DUB activity.

3.2.2 To develop a synchronisation protocol to enrich for cells in different cell cycle phases

The overall aim of this project is to profile DUB activity during cell cycle progression, and so my second aim is to establish an efficient synchronisation protocol to generate A549 populations enriched for each phase of the cell cycle.

3.2.3 To analyse differential DUB activity throughout the cell cycle using Ub-based probes

And finally, once these protocols have been validated and optimised, I intend to perform the first unbiased DUB activity screen using Ub-based probes to investigate any differential DUB activity between synchronised cell lysates.

3.3 Using Ub-VME as a tool for screening DUB activity in the adenocarcinoma cell line A549

Ub-VME is composed of a synthetic ubiquitin monomer joined via a double aminohexanoic acid (Ahx-Ahx) linker region to an electrophilic warhead (VME) (Figure 3.2A). Upon binding the VME group forms an irreversible bond with the catalytic cysteine in a DUB active site (Figure 3.1D). As I intended to use the Ub-VME activity probe to globally profile DUBs, I used Ub-VME modified with an N-terminal haemagglutinin (HA) tag. The HA tag would enable me to collectively investigate the activity of all DUBs that interacted with Ub-VME, via immunoblotting or immunoprecipitation using HA-reactive antibodies.

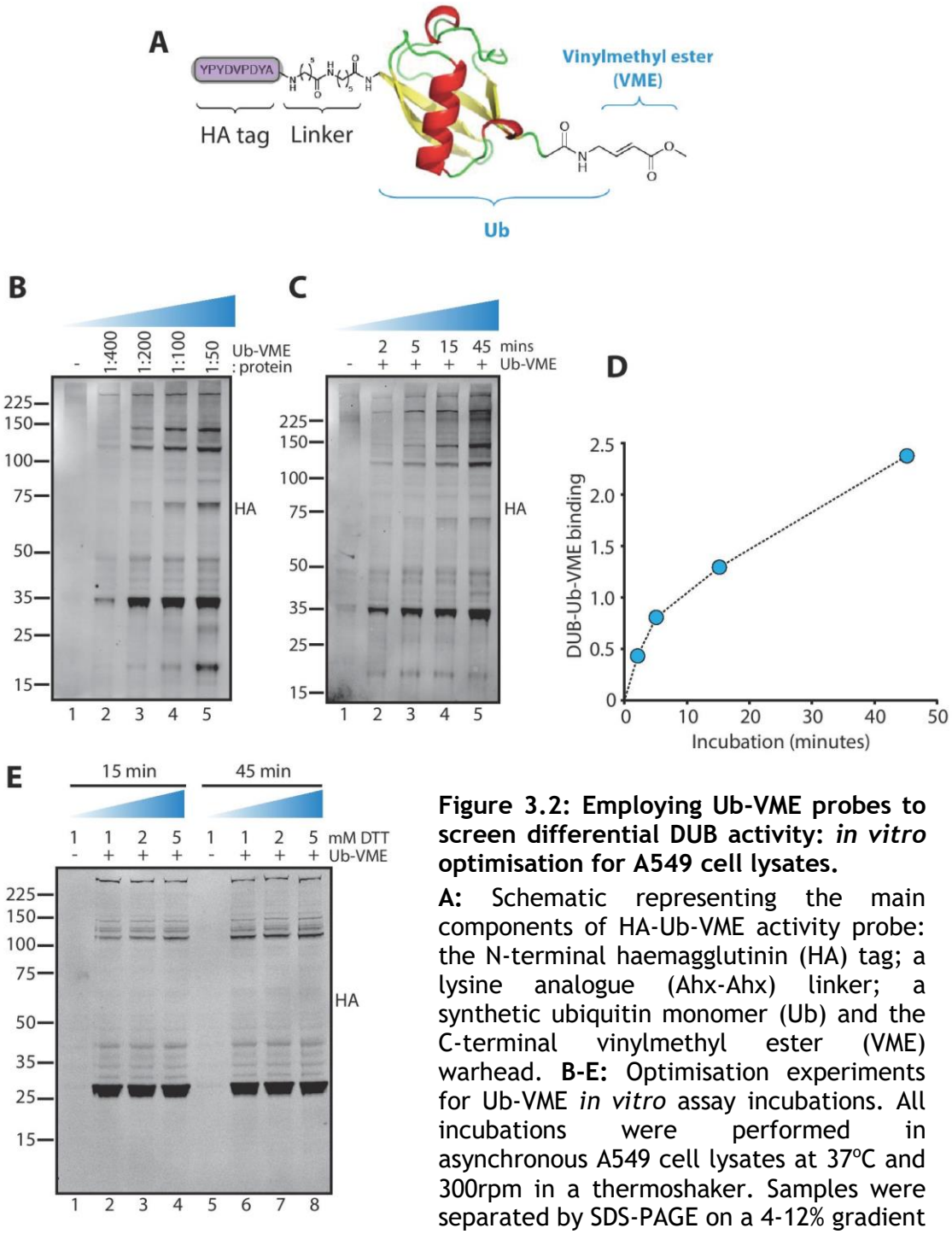

Figure 3.2: Employing Ub-VME probes to screen differential DUB activity: *in vitro* optimisation for A549 cell lysates.

A: Schematic representing the main components of HA-Ub-VME activity probe: the N-terminal haemagglutinin (HA) tag; a lysine analogue (Ahx-Ahx) linker; a synthetic ubiquitin monomer (Ub) and the C-terminal vinylmethyl ester (VME) warhead. **B-E:** Optimisation experiments for Ub-VME *in vitro* assay incubations. All incubations were performed in asynchronous A549 cell lysates at 37°C and 300rpm in a thermoshaker. Samples were separated by SDS-PAGE on a 4-12% gradient gel and immunoblotted for HA to visualise the global extent of DUB-Ub-VME binding. **B:** Titration of Ub-VME concentration. Equal amounts of extract (15µg) were incubated with increasing amounts of Ub-VME for 15 minutes. **C:** Time dependency. 15µg lysate was incubated with 75ng Ub-VME (1:200) for increasing periods of time. **D:** The 1:200 HA-Ub-VME concentration was not rate limiting over a 45 minute incubation. HA staining for each incubation in C was normalised to actin and plotted over time. **E:** Additional DTT had no effect on Ub-VME binding efficiency. Equal volumes of lysate were incubated with increasing concentrations of DTT and equilibrated for 15 minutes prior to the addition of Ub-VME (1:200). After a 15 or 45 minute incubation, the reaction was terminated.

As outlined in section 3.2, my objective was to globally profile DUB activity in A549 cells and be able to distinguish any differences in activity for individual DUBs between different phases of the cell cycle. To achieve this I needed to develop an *in vitro* Ub-VME incubation protocol that was both robust and sensitive enough to analyse subtle fluctuations in "DUB activity", which is more accurately defined as DUB reactivity towards the Ub-VME probe.

As Ub-VME acts as a suicide substrate for the DUB active site, the binding of the ubiquitin monomer is covalent. This was a key aspect to recognise when planning these *in vitro* incubations. If Ub-VME were incubated with a DUB for a prolonged period of time it would eventually bind to completion, in which all of the available DUB would become covalently Ub-VME bound. This would provide an accurate measure of DUB abundance but would not be amenable for measuring any fluctuations in DUB activity. Therefore, in order to analyse variations in DUB activity the *in vitro* incubation would have to result in sub-maximal binding, in which approximately 50% of the available DUB becomes Ub-VME bound. With only a portion of the available DUB covalently bound, it would enable increases or decreases in DUB reactivity to Ub-VME between conditions to be analysed.

To elicit this sub-maximal binding response, I had to carefully consider two variables: the concentration of Ub-VME and the *in vitro* incubation length. The concentration of Ub-VME has to be sufficient so that it does not limit DUB binding, otherwise this would prevent any increase in DUB activity from being observed. Similarly, the *in vitro* incubation length must be short enough so that not all of the available DUB becomes Ub-VME bound. If all of the available DUB has been saturated by Ub-VME binding, this would mask any increase in DUB activity from being analysed.

However, not only are DUBs expressed at different levels in A549 cells, but they also harbour varying levels of catalytic activity (Clague et al., 2015). This means that the *in vitro* incubation conditions that would elicit a sub-maximal binding response from one DUB could result in a maximal, or saturated, binding response

from a second DUB. I performed optimisation experiments to find a set of *in vitro* incubation conditions; they were designed to find a compromise that would give the best chance of distinguishing differences between as many DUB activity profiles as possible.

3.3.1 Validation and optimisation of Ub-VME as a method to globally profile endogenous DUB activity

My first set of experiments aimed to find an appropriate concentration of Ub-VME. Asynchronous A549 cell extracts were incubated with increasing concentrations of Ub-VME from 2.5ng Ub-VME/1µg protein (1:800 or 0.24µM) to 20ng Ub-VME/1µg protein (1:50 or 1.96µM) (Figure 3.2B) for 15 minutes. This range was selected based on published experiments, in which a molarity of 0.5-1µM was used (de Jong et al., 2012). Immunoblotting for the N-terminal HA tag allowed the Ub-VME binding profile to be visualised. Each HA immuno-reactive band in Figure 3.2 represents one or more cysteine protease DUBs that have covalently bound to HA-Ub-VME. Increasing the concentration of Ub-VME led to an increase in the HA signal (Figure 3.2B). Certain DUBs, particularly those with strong HA staining, showed only marginal increases in Ub-VME binding between ratios of 1:100 (lane 4) and 1:50 (lane 5). This is best exemplified by the HA immuno-reactive band at 35kDa. Interestingly, a band at approximately 250kDa with weaker HA staining exhibited a similar HA-Ub-VME binding profile. This inferred that A549 cells both express high abundance DUBs that readily bind to the Ub-VME probe, as well as less abundant DUBs that are highly reactive to Ub-VME. The binding profiles of these highly Ub-VME reactive DUBs suggest that high concentrations of Ub-VME result in saturation of DUB binding even with short incubation times. Conversely, other DUBs only exhibit detectable binding at high concentrations of Ub-VME after a 15 minute incubation (lane 5), for instance the HA immuno-reactive band at 70kDa.

As predicted, global DUB activity profiling cannot easily be achieved using a single Ub-VME concentration. The HA profile from the 1:200 condition (lane 3) exhibited a high level of global DUB reactivity to Ub-VME and importantly DUB

binding was not fully saturated during the incubation. This provided a useable probe: protein ratio for initial screening experiments.

My second set of experiments aimed to define an appropriate incubation time, at which DUB binding to Ub-VME would not become saturated and the concentration of 1:200 (Ub-VME: protein) would not be limiting. Asynchronous A549 cell extracts were incubated with a set amount of Ub-VME (1:200) for increasing lengths of time from 2 to 45 minutes. The time course experiment, depicted in Figure 3.2C, illustrates the effect of increasing incubation time on Ub-VME binding. DUB binding to Ub-VME increased with longer incubation times. As with the probe titration (Figure 3.2B) the highly reactive DUBs were completely bound at earlier time points; whilst lower reactive DUBs required longer incubation periods to bind to the Ub-VME probe (Figure 3.2C). The profile from the 15 minute incubation (lane 4) displayed a high level of DUB binding without reaching saturation for the 1:200 probe concentration and therefore this incubation period was taken forward as the standard protocol. Additional incubation periods, for example a shorter 5 minute incubation were also selected to monitor DUB reactivity to Ub-VME over time.

Having settled on the optimum conditions for the standard Ub-VME incubation protocol, it was important to confirm that under these conditions the concentration of Ub-VME (1:200) did not limit binding. To confirm this I quantified the level of DUB reactivity by analysing HA densitometry at each time point over the 45 minute time course. As shown in Figure 3.2D, DUBs continued to bind progressively up to the 45 minute time point, indicating that at the 1:200 Ub-VME: protein ratio is not limiting in these *in vitro* experiments.

One further point for consideration in these activity assays is the concentration of DTT. Upon cell lysis, DTT as a strong reducing agent is essential to reverse any protein oxidisation. This is of particular importance when studying DUB activity as the catalytic cysteine is preferentially oxidised, reducing its capacity to catalyse the bond between ubiquitin chains. The standard concentration used

during cell homogenisation is 1mM, which should be sufficient to reverse any oxidisation. I performed an experiment titrating the DTT concentration from 1mM to 5mM, however increasing concentrations of DTT had minimal effect on global DUB binding to the Ub-VME probe (Figure 3.2E).

In summary, based on these data, optimal *in vitro* conditions for initial global activity profiling were selected as: 5ng Ub-VME per 1µg protein (1:200 ratio), 15 minute incubation at 37°C, 1mM DTT. These conditions have been tailored to prevent saturation for highly reactive DUBs. Nonetheless, upon identifying a DUB of interest these optimisation experiments should be repeated. This would ensure the *in vitro* incubation conditions would not be saturating or limiting, but instead elicit a sub-maximal binding response in which approximately half of the available DUB bound to Ub-VME. This would guarantee any subtle differences in DUB reactivity to Ub-VME could be appropriately analysed.

3.3.2 Synchronisation of A549 cells

Synchronisation of A549 cells utilised a well-established protocol, previously validated in HeLa and A549 cells (Faronato et al., 2013; Olsen et al., 2010). Thymidine or nocodazole were employed to arrest cells at the G_1/S transition or at pro-metaphase (G_2/M) respectively. To enrich for specific cell cycle phases from the G_1/S transition through to G_2, a double thymidine block was applied prior to release into fresh media allowing proteins to be sequentially extracted from cells during their progression through S-phase. For the extraction of mitotic and G_1 proteins, a single thymidine block was used in conjunction with nocodazole; which as a mitotic spindle poison arrests the cells in pro-metaphase. A subsequent release into fresh media ensured the completion of mitosis and progression into G_1 (Figure 3.3A).

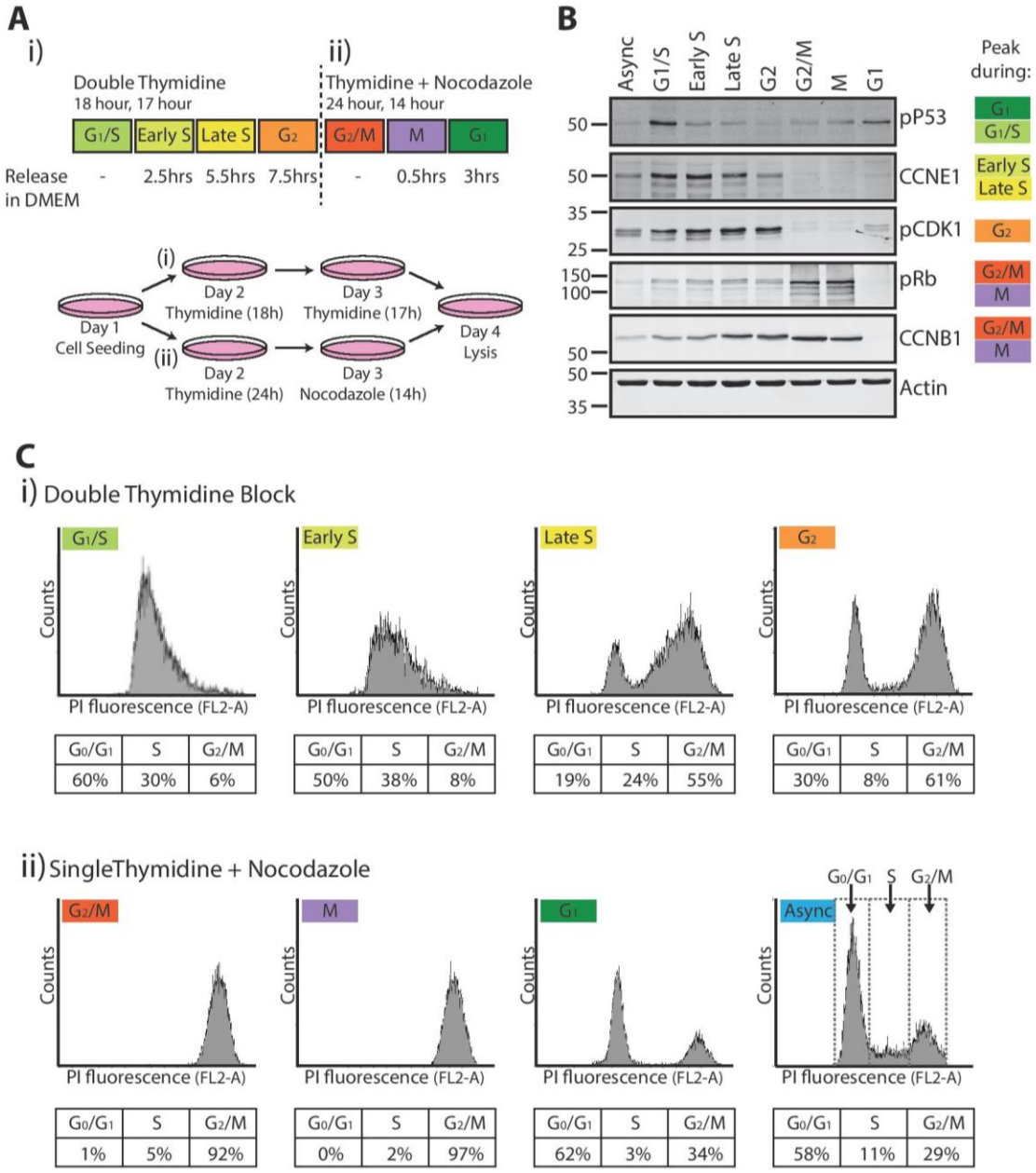

Figure 3.3: Synchronisation of A549 adenocarcinoma cells.

A: Schematic to illustrate the two protocols used to synchronise A549 cells: Double thymidine block **(i)**, Single thymidine, single nocodazole block **(ii)**. **B-C:** Validation of synchronisation protocols in A549 cells. **B:** Immunoblotting. Equal amounts of synchronised A549 cell lysates (20µg) were separated by SDS-PAGE (10%) prior to immunoblotting for the specified cell cycle markers. **C:** PI-FC. $1x10^6$ synchronised A549 cells were fixed in ethanol prior to propidium iodide (PI) staining. Flow cytometry (FC) was used to quantify DNA concentration. The FL2 sensor within the BD FACScalibur™ system measured the amount of PI fluorescence per cell. WinMDI software analysed the proportion of cells in each cell cycle phase using the regions gated in 'Async' plot. Values have been tabulated under each trace.

A combination of immunoblotting (Figure 3.3B) and flow cytometric analysis of PI-stained cells (PI-FC) (Figure 3.3C) was used to establish the enrichment of each synchronised population. Phosphorylation is a major driving force in the cell cycle, with the antagonistic action of the phosphatases aiding its unidirectional progression. Therefore, the phosphorylation status of key cell cycle effectors was analysed in conjunction with CCN levels. The role of CCNs in driving cell cycle-specific phosphorylation makes them classical cell cycle phase markers. Immunoblotting for cell cycle-specific markers confirmed the efficacy of the synchronisation protocol (Figure 3.3B). P53 is phosphorylated at serine 15 (S15) to arrest cells before S-phase, S15 is also phosphorylated during DNA damage. Phospho-P53 (pS15-P53) levels peak at G_1/S and decrease throughout S-phase and mitosis. This also indicated that these synchronisation protocols did not induce DNA damage. CCNE1 expression remained high from G_1/S through to late S phase, further confirmation that thymidine treated A549 cells progressed through G_1/S into S-phase. Phospho-CDK1 (pY15-CDK1) levels peaked at late S-phase and through into G_2, then significantly decreased upon entry into mitosis; CDK1 is a mitotic kinase that needs to be dephosphorylated in order to become active (Section 1.5.3.1). For the M-phase CCN, CCNB1, levels accumulated through G_2 and were persistently high throughout mitosis, before drastically decreasing as the cells entered G_1. This immunoblotting proved that the cell populations expressed the expected synchronisation markers.

To further explore this, PI-FC was performed to accurately profile the cell cycle distribution within each synchronised cell population. PI fluorescently labels cellular DNA enabling the direct comparison of DNA content between single cells. Those cells with two copies of DNA (G_2 and mitotic cells) have a proportionally increased fluorescent signal to cells with one copy (G_1 cells). As the DNA replicates during S-phase, there is a concurrent increase in fluorescence, so that the increase in PI staining bridges the gap between the G_1 and mitotic cell populations. Using WinDMI analysis software I quantified the proportion of cells within these three regions of interest (G_1/G_0, S-phase and G_2/M) for each synchronised cell population.

Results from a representative PI-FC experiment are shown in Figure 3.3C. As shown in the asynchronous fluorescence trace, there are two peaks of fluorescence, the first for cells with one copy of DNA (G_1/G_0) and the second for cells with two copies of DNA (G_2/M). As expected the majority of asynchronous A549 cells were in G_1 (58%) with smaller proportions in S-phase or G_2/M (11% and 29% respectively). The representative traces for the synchronised cell populations concur with the immunoblots shown in Figure 3.3B confirming efficient synchronisation protocols. In each case, the synchronised cell populations were highly enriched for cells in their respective cell cycle phase compared to the asynchronous control. Unlike immunoblotting, PI-FC provided an overview of the distribution of cells within each cell population. This revealed that in some synchronised cell populations, most notably in G_1, a proportion of arrested cells could not overcome the synchronisation block and remained 'stuck' in that cell cycle phase; 34% of nocodazole-treated cells remained in G_2/M phases after a 3 hour release. This was also seen in Late S and G_2 cell populations where 19% and 30% of cells were suspended at the G_1/S boundary after prolonged thymidine incubations. Even with these discrepancies, collectively these data show that in my hands the combination of these synchronisation protocols is an effective method to synchronise A549 cells.

3.3.3 Global DUB activity screening during the cell cycle using an unbiased Ub-VME approach coupled with immunoblotting

The current dogma states phosphorylation drives cells into mitosis, and de-phosphorylation drives mitotic exit into G_1. A parallel could be drawn between ubiquitylation and phosphorylation in their control of unidirectional cell cycle progression. Kinases temporally phosphorylate and activate mitotic proteins; similarly, E3 ligases are known to drive mitotic exit through the temporal degradation of cell cycle effectors (Section 1.5). One of the questions I wished to address using the Ub-VME activity probes was whether DUB activity was downregulated in order promote mitotic exit in cells. Furthermore, global DUB activity profiling across each stage of the cell cycle will broaden our understanding of any temporal regulation of DUB activity.

Ub-VME probes were employed across a panel of lysates prepared from synchronised A549 cells (as illustrated in Figure 3.3) to assess the abundance and activity level of DUBs at each stage of the cell cycle. These extracts were incubated with Ub-VME under the optimised conditions defined in Section 3.3.1, prior to SDS-PAGE and HA immunoblotting (Figure 3.4A). HA staining revealed differential DUB binding to Ub-VME throughout cyclic progression. Quantitation of HA immuno-reactivity revealed there was a pervasive decrease in DUB reactivity towards Ub-VME as cells entered mitosis (Figure 3.4B). This was most notable for high molecular weight DUBs, where a 41% and 51% reduction was measured by HA densitometry in G_2/M-arrested and mitotic cells respectively. Conversely, quantitation of global HA reactivity during mitosis only showed a 20% and 7% decrease; suggesting that more low molecular weight DUBs have unchanged or increased mitotic activity. This was in line with my initial hypothesis that DUBs may be inactivated or downregulated during mitosis to promote temporal ubiquitylation and drive mitotic exit. For those DUBs downregulated during mitosis, there was no significant increase in the intensity of HA staining in the G_1 extract, suggesting that DUB activity remains at a low level in early G_1. The sustained decrease in DUB activity in early G_1 could in part be an artefact of the synchronisation protocol. However, the PI-FC data show that the majority of cells in the G_1 sample (62%) had exited mitosis and entered G_1 (Figure 3.3C).

Figure 3.4

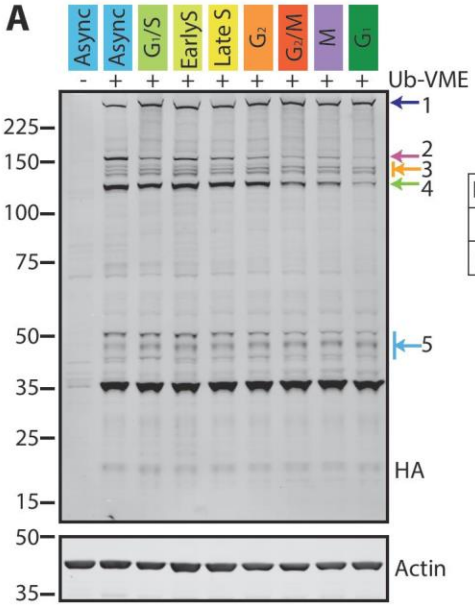

B

HA Signal	A	G_1/S	ES	LS	G_2	G_2/M	M	G_1
Full lane	1.00	0.85	0.90	0.97	0.98	0.80	0.93	0.89
High MW	1.00	1.00	0.96	0.76	0.80	0.59	0.49	0.58

D

Peak	Candidate	Observed MW	DUB-Ub-VME MW
1	USP9X	+225kDa	302kDa
2	USP7	162kDa	138kDa
3	USP15 (+)	150kDa	122kDa
4	USP5	130kDa	106kDa
5	UCHL5 (+)	50kDa	48kDa

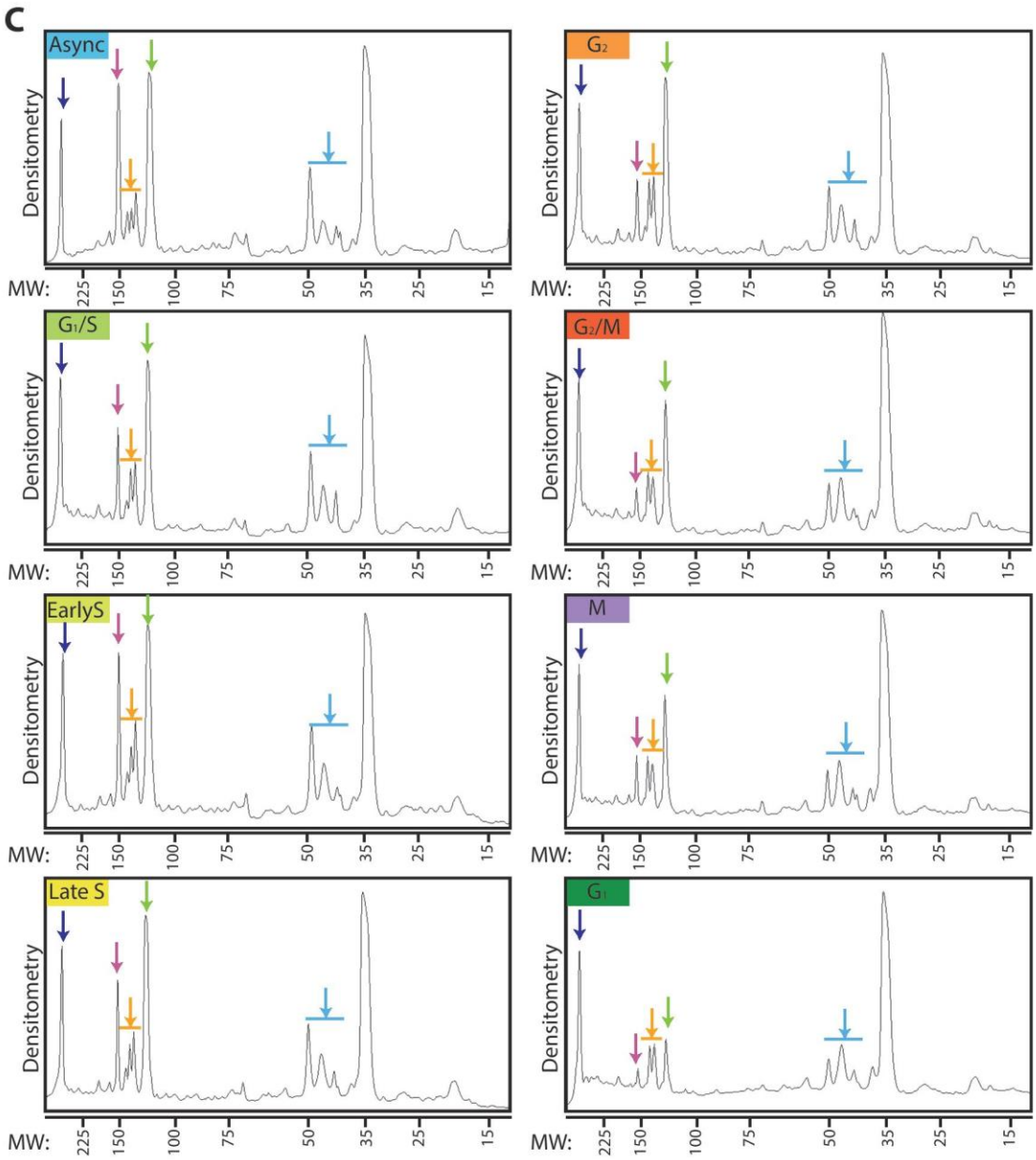

Figure 3.4: Global DUB activity was profiled using HA-Ub-VME coupled with unbiased immunoblotting.
A: Equal amounts of synchronised A549 lysates (15µg) were incubated with 75ng HA-Ub-VME probe (1:200). A vehicle control replaced the probe in a parallel asynchronous extract (labelled minus). Following 15 minute incubations, the reactions were terminated and samples separated on a 4-12% gradient gel. HA immunoblotting allowed visualisation of DUB activity profiles for each cell cycle phase. **B:** Quantitation of HA immunoreactivity for 'full lane' (15-400kDa) or 'high MW' (75-400kDa) for each synchronised population was normalised to actin and set relative to the asynchronous control. **C:** Densitometry traces of the HA immuno-staining in A were generated using Image J. Coloured arrows in A and C represent regions of interest. **D:** Candidate DUBs were designated to regions of interest (number and coloured-coordinated with arrows in A and C) based on their observed and expected Ub-VME bound molecular weights (refer to Appendix Table 1).

In addition to these general trends in DUB activity throughout the cell cycle, there were also numerous individual HA immuno-reactive bands that exhibited cell cycle-dependent reactivity towards Ub-VME (Figure 3.4B). These bands/regions are defined using coloured arrows on the HA immunoblot in Figure 3.4A. I employed Image J software to plot the HA densitometry from each HA-Ub-VME incubation against molecular weight (Figure 3.4C). This continuous line graph displays these bands/regions of interest as peaks in HA staining. The regions of interest on the immunoblot in Figure 3.4A are highlighted on the plots in Figure 3.4C using colour coordinated arrows. In an attempt to identify which DUBs exhibited differential reactivity to Ub-VME across this panel of synchronised cell extracts, I complied a comprehensive list of all the DUBs, their molecular weight, and their protein abundance (Appendix Table 1). The ranking system for protein abundance used intensity-based absolute quantification (iBAQ) data published for the A549 proteome (Geiger et al., 2012). I considered protein abundance to be an important factor when classifying these bands of interest. The synchronised cell extracts had only been incubated with Ub-VME for 15 minutes, and so any DUBs that bound and were easily detected were either highly reactive or highly abundant.

Using Appendix 1, DUBs were mapped to the bands/regions of interest in the HA immunoblot and densitometry traces (Figure 3.4A and C). The most likely candidates are summarised in Figure 3.4D. USP9X is the most likely candidate

for the highest molecular weight DUB, labelled '1' and highlighted with the dark blue arrow. Interestingly, as well as differential Ub-VME reactivity, the gel mobility of this DUB also fluctuated through the cell cycle. During Early S-phase, increased gel motility is indicative of a loss of post-translational modification. The next candidate DUB with differential Ub-VME reactivity may be USP7 (labelled '2' with the purple arrow). This DUB exhibited an oscillatory binding profile peaking at Early S, prior to a significant decrease as the cell enters mitosis. The region labelled '3' and highlighted in orange could represent a number of DUBs, of which one candidate is USP15. The pattern on the HA immunoblot (Figure 3.4A) and the corresponding traces (Figure 3.4C) clearly demonstrate three HA immuno-reactive bands. The highest molecular weight band exhibited decreased Ub-VME reactivity as cells enter G_2 and was persistently decreased during mitosis. As a DUB of interest to our group, it is already known that USP15 resolves as a doublet (Faronato et al., 2013), suggesting that either another candidate DUB or a post-translationally modified USP15 could represent the third band. USP11, a paralog of USP15, is of near identical molecular weight and is expressed at similar levels in A549 cells (Geiger et al., 2012, Appendix Table 1) and so is also a candidate. USP5 is the likely candidate for the DUB labelled '4' (green arrow); it exhibited a substantial decrease in Ub-VME reactivity during G_1. Region 5, the blue arrow, has a number of bands with differential Ub-VME reactivity, the highest molecular weight band (~50kDa) shares a similar binding profile as band 2 (predicted to be USP7) with a decrease in Ub-VME reactivity in mitosis. There are a number of candidate DUBs for this region, however as many are JAMMs they do not have the ability to bind the VME warhead (Appendix Table 1). Therefore, the most likely candidate is UCHL5, which is the most abundant of the Ub-VME reactive DUBs in A549 cells.

3.3.4 Using an unbiased proteomic approach to identify DUBs with differential Ub-VME binding

To confirm candidate DUBs suggested in Figure 3.4D for the regions of interest in the HA immunoblot (Figure 3.4A) one of two methods can be employed. First a biased immunoblotting approach that uses simultaneous multiplex detection of the candidate DUBs and the HA-tagged Ub-VME. Ultimately this approach is

limited by the availability, efficacy and specificity of DUB-specific antibodies. Unfortunately, for a number of the 90 DUBs robust antibodies were not yet commercially available. The second, an unbiased approach, uses mass spectrometry (MS) coupled with SILAC. Triplexed SILAC enables three different cell populations to be selectively labelled with isotopically heavier arginine (R) and lysine (K) residues. Comparative analysis of the mass:charge ratio for each peptide enables peptide identification for each originating cell population. This permits an unbiased quantitative comparison between HA-Ub-VME bound proteins from three differentially labelled cell populations, enriched for different cell cycle phases.

A549 cells were maintained in three media each containing differentially labelled amino acids: light (K0, R0), medium (K4, R6) and heavy (K8, R10) until incorporation of isotopically heavier arginine and lysine residues was confirmed by MS as ≥95%. Labelled A549 cells were synchronised in a triplex configuration (Figure 3.5A) that enabled quantitative comparison of G_1/S and mitotic populations with an asynchronous population. G_1/S and mitotic enriched cell populations were chosen for this initial screen as they exhibited different HA binding profiles for DUBs 2, 3, 4, and 5 (Figure 3.4). Immunoblotting for the cell cycle phase markers CCNE1 and pRb (S807/S811) was performed to verify the synchronisation of labelled A549 cells (Figure 3.5B). CCNE1 levels increased slightly in G_1/S samples compared to the asynchronous control and as expected were not present in the mitotic extracts. Conversely, the mitotic marker pRb (S807/811) was substantially increased in mitotic cell extracts compared to the G_1/S extracts and the asynchronous control. These data confirm that the synchronisation protocols validated in Section 3.3.2 efficiently enriched for G_1/S and mitotic cell populations in SILAC-labelled A549 cells (Figure 3.5B).

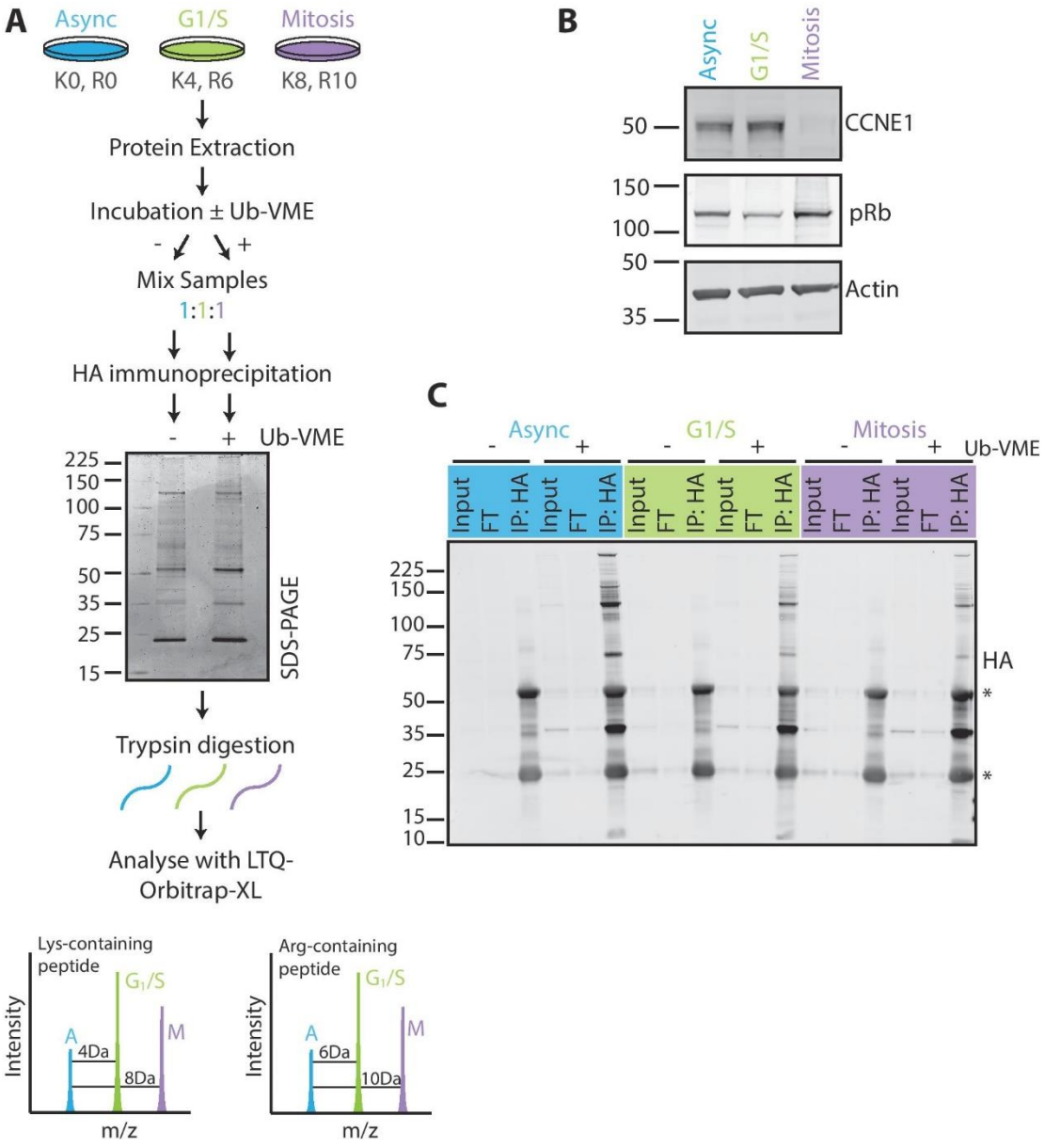

Figure 3.5: Isolation of active DUBs from synchronised lysates using HA immunoprecipitation.

A: Schematic representing the screening approach for quantitative analysis of DUB activity in G_1/S and mitotic samples. **B:** Validation of synchronisation protocol in SILAC-labelled A549 cells. A459 cells were synchronised in differentially labelled media (depicted in A). Equal amounts of lysate were separated on a 4-12% gradient gel and were subsequently immunoblotted for cell cycle phase markers CCNE1 and pRb (S807/811). **C:** Validation of HA immunoprecipitation to isolate active DUBs. 0.5mg synchronised A549 lysate was incubated with 2.5µg HA-Ub-VME (1:200) or a vehicle control. After a 45 minute incubation, reactions were terminated through the addition of SDS to a final concentration of 0.4%. Equal volumes of HA-conjugated agarose were added to each reaction and were mixed overnight at 4ºC. Post-elution, samples were separated on a 4-12% gradient gel and immunoblotted for HA reactivity. Asterisks represent the heavy (50kDa) and light (25kDa) chains of HA-IgG.

An initial screen was performed to test the feasibility of coupling HA-Ub-VME incubation with immunoprecipitation to retrieve and identify Ub-VME reactive DUBs. To maximise the number of Ub-VME bound DUBs the *in vitro* Ub-VME incubation time was increased to 45 minutes (refer to Figure 3.2C). These conditions were chosen to increase the number of DUBs identified; careful Ub-VME titration to prevent saturation of DUB binding was of less importance for this initial screen. HA immunoprecipitation was performed for all cell lysates and Ub-VME bound proteins were separated by SDS-PAGE prior to immunoblotting (Figure 3.5C). HA immunoblotting confirmed efficient pull down of many Ub-VME bound DUBs. Only heavy and light chain IgG bands were visible on immunoblotting of the vehicle control lanes. HA immuno-reactivity profiles from the immunoprecipitation eluate in Figure 3.5C reflect the previous HA profiles seen in Figure 3.4A.

Having validated the synchronisation and immunoprecipitation protocols, I next performed an unbiased screen coupling Ub-VME incubation with MS to identify DUBs with differential Ub-VME reactivity in G_1/S and mitotic cells. The workflow depicted in Figure 3.5A was performed on a large-scale for proteomic analysis (see Section 2.5.1). Labelled A549 cells were synchronised to enrich for G_1/S and mitotic cell populations alongside an unlabelled asynchronous control cell population. Each synchronised protein extract was pre-incubated with HA-Ub-VME or a vehicle control for 45 minutes and reactions were terminated prior to mixing to stop the possibility of cross-modification between samples. This prevented mitotic kinases, which are no longer spatially restricted, from interacting and phosphorylating DUBs from the G_1/S extract. This ensured that the data collected accurately represented cell cycle-specific DUB activity. Equal volumes of these pre-incubated lysates were mixed prior to HA immunoprecipitation. Eluted Ub-VME bound proteins were separated by SDS-PAGE prior to an in-gel tryptic digestion and MS analysis.

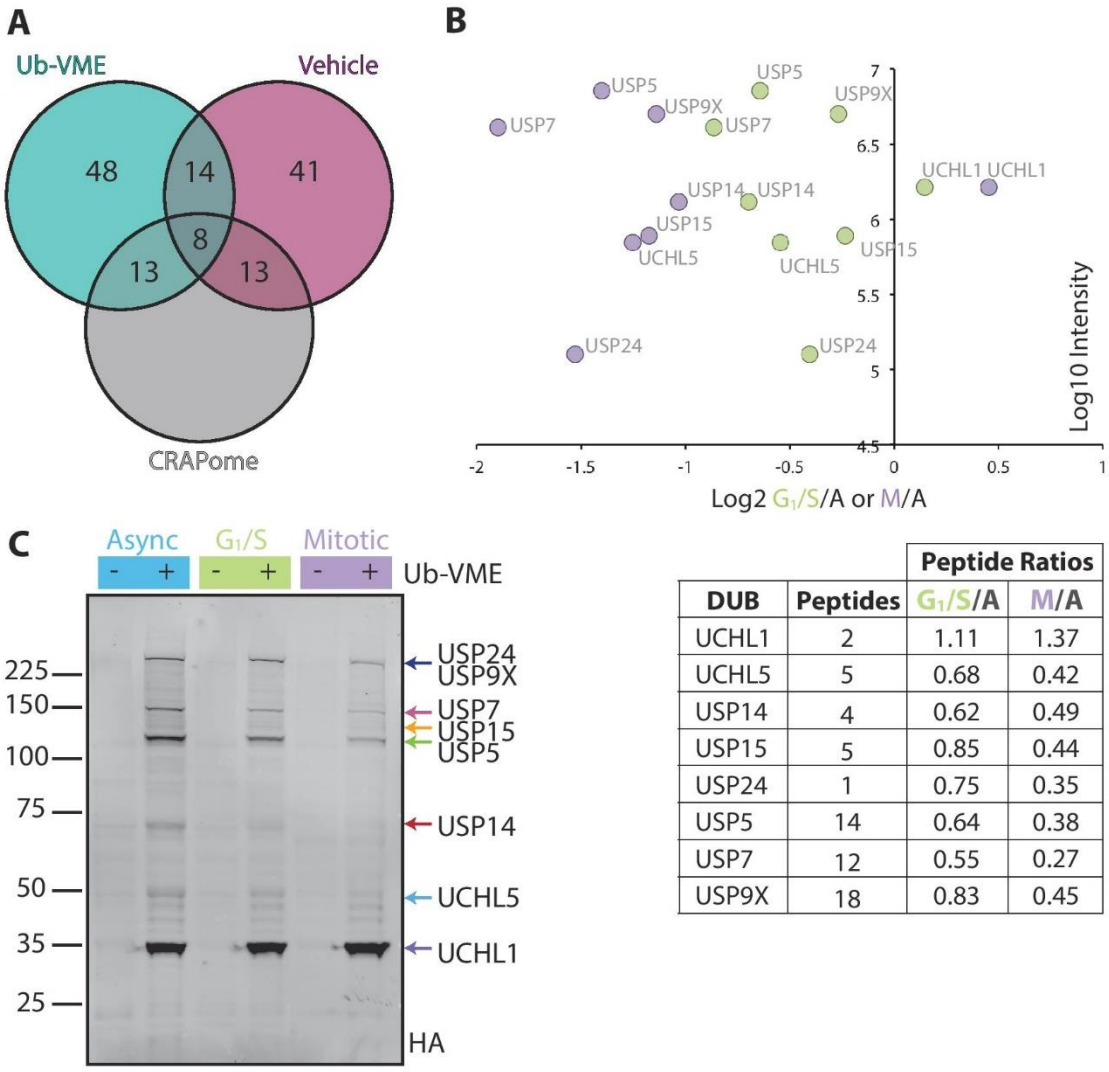

		Peptide Ratios	
DUB	Peptides	G_1/S/A	M/A
UCHL1	2	1.11	1.37
UCHL5	5	0.68	0.42
USP14	4	0.62	0.49
USP15	5	0.85	0.44
USP24	1	0.75	0.35
USP5	14	0.64	0.38
USP7	12	0.55	0.27
USP9X	18	0.83	0.45

Figure 3.6: Quantitative analysis of differential DUB activity in G_1/S and mitotic samples identified by mass spectrometry.

A: A Venn diagram illustrating the peptides identified by MS from HA-Ub-VME and vehicle control immunoprecipitations and the overlap with common contaminants from the agarose CRAPome (Mellacheruvu et al., 2013) **B:** DUBs identified from HA immunoprecipitation. Table: Ratios of peptide intensities in G_1/S and mitotic samples were normalised to the asynchronous control using Max Quant (version 1.4.1.2). Plot: Log_2 ratios from the table were plotted against intensity to visualise differential DUB activity in G_1/S and mitotic samples. Positive ratios (to right of *y*-axis) represent increased Ub-VME binding relative to asynchronous cells. Conversely, negative values (left of *y*-axis) reflect decreased Ub-VME binding. **C:** Equal amounts of synchronised A549 lysates (15µg) were incubated with 75ng HA-Ub-VME probe (1:200) for 45 minutes. The reactions were separated on a 4-12% gradient gel. HA immunoblotting enabled mapping of DUBs identified in B to their corresponding HA immuno-reactive band.

Data from two replicate MS runs identified 137 proteins across all experimental conditions (Appendix Table 2). Only 61 of these proteins were specific to the HA-Ub-VME pull down, and a further 13 of these proteins could be discounted as they are commonly identified in agarose immunoprecipitation experiments (Figure 3.6A) (Mellacheruvu et al., 2013). Of these 48 Ub-VME immobilised proteins only eight DUBs were identified. These are listed in the table in Figure 3.6B and Appendix Table 2 alongside their peptide intensity ratios. Multiple peptides were identified for each of these DUBs, except for USP24 for which only one peptide was detected. Ratios were derived from the medium (G_1/S) or heavy (M) peptide intensities relative to the light (asynchronous) control. Converted Log_2 values are graphically represented in Figure 3.6B. A decrease in Ub-VME reactivity relative to asynchronous cells is synonymous with a shift to the left along the *y*-axis; an increase in Ub-VME reactivity results in a rightward shift. All identified DUBs, except UCHL1, showed decreased reactivity towards Ub-VME in both G_1/S and mitotic lysates compared to the asynchronous control, with a more significant decrease in mitotic samples. This decrease in mitotic reactivity confirmed the results from the HA immunoblots in Figure 3.4A and 3.5C. There was a modest increase in UCHL1 reactivity to Ub-VME in mitotic cells compared to the asynchronous cell population. As UCHL1 was the most abundant DUB detected in A549 cells by iBAQ (Geiger, 2012), this modest increase in mitotic binding could help explain why there is only a 7% decrease in the full HA densitometry profile compared to the 51% decrease from the high MW densitometry **(**Figure 3.4B).

The same synchronised lysates were incubated with HA-Ub-VME under identical conditions to the proteomic screen and used for HA immunoblotting (Figure 3.6C). The eight DUBs identified from the proteomic screen have been aligned with the HA immunoblot in Figure 3.6C dependent on their Ub-VME bound molecular weight (listed in Appendix Table 1). Of these eight DUBs, five seemingly account for the regions of interest identified from the initial HA immunoblotting screen (Figure 3.4A). USP9X, USP7, USP15, USP5 and UCHL5 were matched with high confidence to the HA immunoblot in Figure 3.6C through comparison of Ub-VME reactivity profile in Figure 3.6B and molecular weight from Appendix Table 1 (see dark blue, pink, orange, green and light blue arrows

respectively). USP24 shared the same Ub-VME reactivity profile as USP9X with decreased activity in G_1/S, which decreased further in mitosis (Figure 3.6B). USP24 is only 2kDa heavier than USP9X (Appendix Table 1) and this minor difference would not resolve via immunoblotting and so the dark blue arrow also represents USP24. The final two DUBs from the proteomic screen to be mapped to the original HA immunoblotting screen were USP14 and UCHL1 (red and purple arrows respectively).

As the *in vitro* Ub-VME incubation conditions for the proteomic screen were tailored to favour increased overall Ub-VME binding to DUBs, it was possible that Ub-VME binding represented DUB abundance rather than regulated DUB activity. To address this question, I analysed the abundance and Ub-VME reactivity for five DUBs of interest. Using the same synchronised lysates, immunoblotting and quantitative densitometry was used to assess UCHL1, UCHL5, USP15, USP7 and USP9X protein abundance (Figure 3.7A). Relative to asynchronous cells, both USP7 and UCHL5 expression was lower at G_1/S and lowest at mitosis (Figure 3.7A), mirroring the Ub-VME reactivity data shown in Figure 3.6B. For USP15 and USP9X, expression was more stable across cell cycle phases (Figure 3.7A), in contrast to the Ub-VME reactivity seen in Figure 3.6B. Similarly, UCHL1 expression levels did not reflect Ub-VME reactivity. This suggests some DUB activity may be regulated independently of DUB expression.

The G_1/S and mitotic lysates were incubated with HA-Ub-VME for 45 minutes replicating the conditions used for the proteomic screen. Immunoblotting for a DUB of interest rather than the HA tag of HA-Ub-VME allows the direct visualisation of the Ub-VME bound DUB, which exhibits a 10kDa increase in molecular weight, and the remaining unbound DUB. Ub-VME reactivity was measured by monitoring the 10kDa upshift of Ub-VME bound DUBs by immunoblotting with DUB-specific antibodies (Figure 3.7B). By 45 minutes, the majority of UCHL5 and USP15 were Ub-VME bound. In contrast, UCHL1 and USP7 did not entirely bind to completion over this time course. The molecular weight of USP9X is 292kDa, for this reason the 10kDa shift resulting from Ub-VME binding

could not be resolved by electrophoresis on a 4-12% polyacrylamide gel. This prevented the analysis of Ub-VME reactivity for USP9X by immunoblotting.

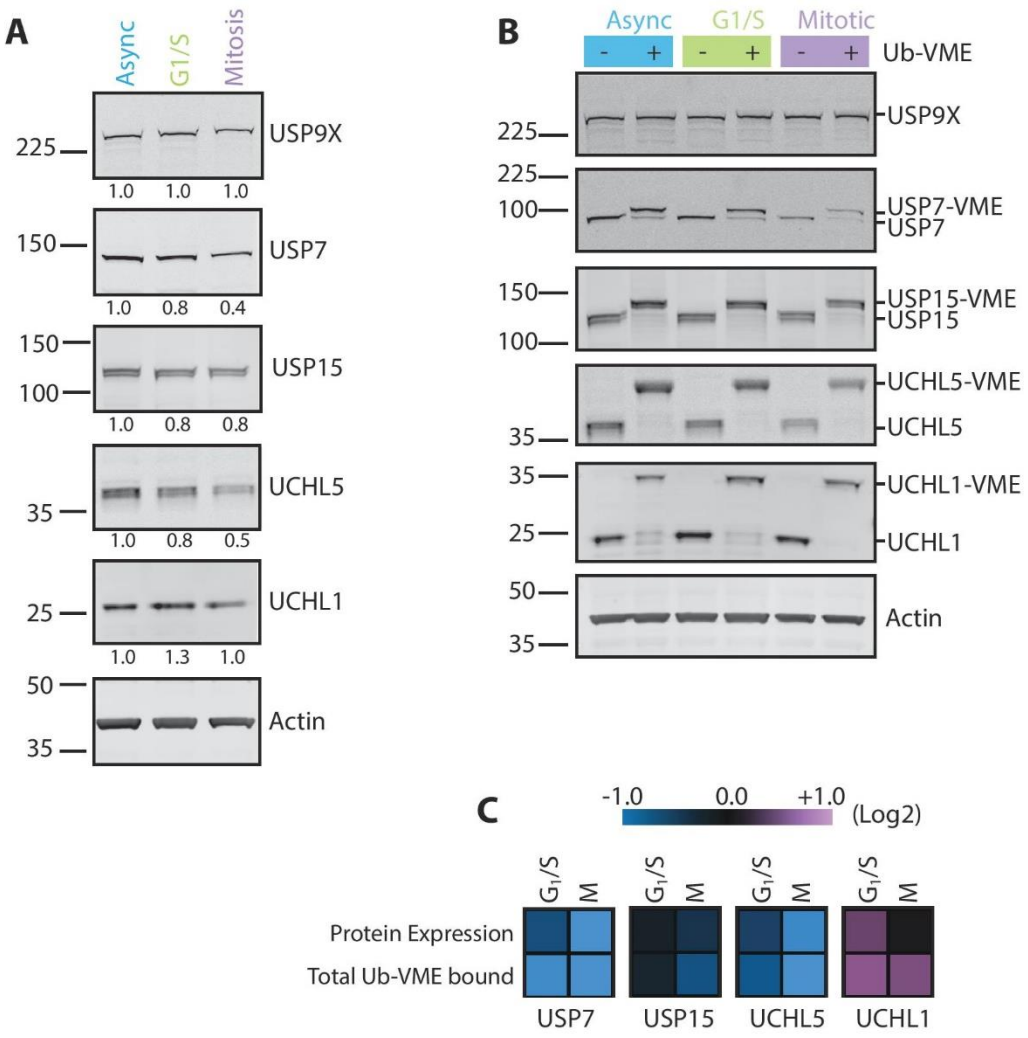

Figure 3.7: Validation of DUB abundance and activity levels in G_1/S and mitotic samples.

A: Equal amounts of synchronised lysate (15µg) were separated on a 4-12% gradient gel and were immunoblotted for five DUBs of interest identified from the screen in figure 5. DUB expression was quantified using LI-COR Image Studio software (Version 3.1.4). Values depicted underneath respective immunoblots have been normalised to actin and relative to asynchronous control. **B:** G_1/S and mitotic lysates (15µg) were incubated with 75ng HA-Ub-VME probe (1:200) or a vehicle control for 45 minutes prior to separation on a 4-12% gradient gel. Immunoblotting for the five DUBs of interest from A allowed visualisation of total amount of DUB bound Ub-VME as well as the amount of DUB that remained unbound. **C:** Differential DUB expression (from A) and Ub-VME binding (from B) in G_1/S and mitotic extracts was illustrated using individual heatmaps. Values for each DUB were normalised to an asynchronous control prior to Log_2 conversion. The pink-to-blue colour scale represents increased and decreased DUB expression/Ub-VME binding respectively.

Variation in Ub-VME binding could be regulated by DUB abundance or could instead reflect post-translational regulation of DUB activity. To assess whether DUB abundance or Ub-VME reactivity shown in Figure 3.7A and B correlated to the Ub-VME reactivity data from the screen in Figure 3.6 I calculated the fold change in protein abundance and in Ub-VME binding relative to the asynchronous control. The fold changes for USP7, USP15, UCHL5 and UCHL1 have been represented as heatmaps, where increased or decreased values compared to the asynchronous control are pink and blue respectively (Figure 3.7C). USP7 expression and Ub-VME reactivity decreased in both G_1/S and mitotic samples compared to the asynchronous control, indicating that USP7 activity could be regulated by protein abundance (Figure 3.7C). Both USP15 and UCHL5 profiles share a similar trend to the USP7 profile, with a decrease in expression levels and Ub-VME binding in mitotic cells compared to the asynchronous control. Again implying that the data obtained from the proteomic screen for USP15 and UCHL5 was indicative of DUB abundance, not of regulated DUB activity.

UCHL1 was the only DUB to exhibit increased Ub-VME binding in both G_1/S and mitotic samples relative to the asynchronous control. UCHL1 expression and Ub-VME reactivity was higher in G_1/S compared to the control. Interestingly, in mitotic extracts, there was a considerable increase in UCHL1 Ub-VME reactivity that was not coupled with an increase in protein abundance. This implies that cell cycle-specific regulation of UCHL1 activity could be independent of its cellular abundance.

3.4 Discussion

The use of active site-directed probes in synchronised cell lysates proved to be a valuable unbiased tool to study global changes in DUB activity throughout the cell cycle. A number of DUBs exhibited differential Ub-VME reactivity in synchronised A549 cell lysates, represented in Figures 3.4-3.7. Preliminary screening, using HA immunoblotting coupled with data mining, linked a number of bands with oscillations in HA immunoreactivity to candidate DUBs through comparing molecular weight and the predicted abundance in A549 (Figure 3) (Geiger et al., 2012) (Appendix Table 1). A subsequent triple-labelled proteomic approach confirmed these candidate DUBs and provided quantitative data comparing eight DUBs in G_1/S and mitotic cell populations. A more in-depth review of cell cycle-specific DUB activity data will be discussed in Chapter 7.

A549 were synchronised using a well-established protocol, which in our hands proves a reliable method of extracting lysates from synchronised populations. As depicted in Figure 3.3, the protocol is based upon pharmacological arrest of the cell cycle and timed release. Inducing cell cycle arrest has the potential to result in DNA damage. A recent large-scale proteomic study revealed that arresting the cell cycle could affect both the proteome and phospho-proteome. DNA damage, translation and metabolism pathways were altered when cells separated by centrifugal elutriation were compared to serum-starved, hydroxyurea-treated and CDK1-inhibited cells (Ly et al., 2014). Centrifugal elutriation does remove the requirement for pharmacological inhibition but is an expensive technique to develop. Instead, I employed well-established thymidine/nocodazole synchronisation methods, that have been widely used, for example in a highly cited cell cycle phospho-proteome study from Matthias Mann's laboratory (Olsen et al., 2010). I coupled this with immunoblotting for S15-phosphorylated P53 to monitor any DNA damage. Both the ATM and ATR (protein kinases that orchestrate the DNA damage response) are known to phosphorylate P53 at S15 (Meek, 2009; Meek and Anderson, 2009). Phosphorylation of P53 (pS15-P53) is an essential focal point in activating P53, priming additional phosphorylation events on P53 and in doing so stimulating a DNA damage response that arrests cells during S-phase (Dumaz et al., 1999; Loughery et al., 2014; Saito et al., 2002). Immunoblotting revealed that, in my

hands, the synchronisation protocol did not result in DNA damage as S15-P53 was only phosphorylated where expected: during G_1 and G_1/S.

Ub-based probes are often used to analyse activity levels of recombinant DUBs (Mevissen et al., 2013) or used in structural studies that investigated DUB substrate recognition (Boudreaux et al., 2010; Hu et al., 2002; Wiener et al., 2012). Data from this chapter showed that Ub-based probes could also be used imaginatively to globally profile endogenous DUB activity. That being said, this is not the first time that Ub-based probes have been used to assay activity of an endogenous DUB. An investigation into the role of USP37 in governing G_1/S entry used a targeted approach to compare endogenous USP37 activity in G_1/S and G_2/M arrested cells (Huang et al., 2011). Using HA immunoprecipitation of HA-Ub-VS reactive DUBs, Huang et al. showed that USP37 was activated at G_1/S in a phosphorylation-dependent manner.

Coupling Ub-VME reactions with HA immunoblotting provided a comprehensive overview of differential DUB activity between synchronised cell lysates (Figure 3.4). It was an important first step to highlight candidate DUBs that exhibited differential reactivity to Ub-VME in a cell cycle specific manner, although HA immunoblotting alone could not identify these DUBs of interest. A caveat of using electrophilic traps to profile enzymatic activity is that a number of cysteine proteases could theoretically bind the probe, including a number of ubiquitin processing enzymes, which also rely on a catalytic cysteine in order to transfer ubiquitin moieties to target protein. This adds a layer of complexity when analysing the HA staining in Figure 3.4A, as some bands visualised could represent other classes of cysteine proteases. For both of these reasons, it quickly became apparent that more sensitive techniques would be required for identification of Ub-VME reactive proteins.

My approach coupled HA immunoprecipitation of Ub-VME reactive DUBs with MS to identify and quantify differential DUB activity between synchronised cell lysates (Figure 3.5 and 3.6). Though this approach revealed differentially

reactive DUBs, it only identified a total of eight DUBs. Two experimental parameters may contribute to this low retrieval rate. Firstly, I selected *in vitro* Ub-VME reaction conditions that were designed to be a compromise between highly reactive and weakly reactive DUBs (Section 3.3.1). Evidently, this is limiting when investigating global DUB activity profiles. Data will be lost if the conditions are tailored to suit one group: highly reactive DUBs risk saturation or weakly reactive DUBs will not be detected if incubated under unfavourable conditions. The reaction conditions that I had chosen (1:200 Ub-VME: protein, 15 minutes, 1mM DTT from Figure 3.2) were tailored so that highly reactive or highly abundant DUBs would not bind to completion during the length of the incubation. Unfortunately, increasing the reaction length from 15 to 45 minutes for the proteomic screen did not result in a high number of DUBs retrieved (Figure 3.6, Appendix Table 2).

The second cause of this low retrieval could be that Ub-VME was not the best Ub-based probe to assay the reactivity of the five cysteine protease DUB families. A number of other Ub-based probes have been developed with a variety of electrophilic traps used to mediate the covalent interaction with active DUBs. Comprehensive testing across the range of Ub-based probes was performed at the time of development and published data revealed that, of the seven Ub-based probes, Ub-VME allowed for greater coverage for thiol protease DUB families (Borodovsky et al., 2002). Recent developments in chemistry allow total linear synthesis of Ub-based probes, this has permitted the unlimited addition of epitope tags and intermediary linker regions that make epitope tags more accessible to immuno-detection (de Jong et al., 2012). For more quantitative analysis of DUB activity, Ub-based probes have been synthetically conjugated to sepharose resin, permitting a more stringent isolation of active DUBs from cell lysates for analysis via mass spectrometry (Ekkebus et al., 2013). These advances have led to a wide array of commercially available Ub-based probes that could be used for DUB activity profiling.

C-terminally propargylated ubiquitin (Ub-PA) was an unexpected alternative to Ub-VME, which exhibited potent and selective reactivity to cysteine protease

DUBs (Ekkebus et al., 2013). It was an obvious candidate for my study to obtain more comprehensive global profiling of DUB activity throughout the cell cycle, which I will discuss in more detail in Chapter 4. In summary, data from Chapter 3 provides a strong platform from which I can re-imagine and re-optimise the Ub-based probe methodology for global DUB activity profiling, and in doing so increase the number of differentially reactive DUBs that can be retrieved and identified.

Chapter 4

Unbiased profiling reveals extensive co-regulation of DUB activity during the cell cycle.

4.1 Introduction

Ub-PA was recently identified as a novel thiol-reactive Ub-based probe. The conjugation of this terminal alkyne group to ubiquitin rendered it highly reactive towards all classes of cysteine DUBs. This electrophilic warhead manipulates the DUB active site biochemistry in a similar manner as Ub-VME (Figure 3.1D), attack of the DUB's catalytic cysteine on the alkyne group results in the formation of the vinyl-sulfide linkage (Sommer et al., 2013). This was surprising as these terminal alkyne moieties are considered to be chemically inert under physiological conditions (Ekkebus et al., 2013; Sommer et al., 2013).

This PA functionalised ubiquitin probe possessed a faster rate of binding than its predecessors, reacting with recombinant DUBs in under 1 minute (Ekkebus et al., 2013). This made it an attractive choice for more comprehensive profiling in the cell cycle screen. Furthermore, it has an increased binding affinity to the OTU DUB family compared to Ub-VME, and interacted with ATXN3 from the JOS family (Ekkebus et al., 2013). Notably, Ub-PA bound to A20, an OTU family member which was considered notoriously unreactive from previous DUB activity assays (Ekkebus et al., 2013; Lin et al., 2008; Mevissen et al., 2013). Additionally, the non-specific binding to unrelated classes of cysteine proteases appears to be reduced in Ub-PA reactions; the cysteine proteases papain and E1-activating enzyme did not react with this novel warhead (Ekkebus et al., 2013).

Ub-PA, like Ub-VME, can be conjugated to a number of N-terminal tags including affinity tags (HA or biotin) to enable recognition and retrieval of active DUBs, or to dyes (TAMRA and Cy5) to enable in-gel fluorescence detection. Additionally, Ub-PA can be directly conjugated to sepharose resin (sepharose-Ub-PA) simplifying the retrieval of Ub-PA bound DUB complexes. These qualities make Ub-PA a prime candidate probe for more comprehensive profiling of DUB activity throughout the cell cycle.

To date, only a handful of studies have used this novel probe, the majority of which have performed crystal structural analyses of DUBs in complex with Ub-PA. Using this suicide substrate, structures have been solved for USP4 (Clerici

et al., 2014), UCHL5 (Sahtoe et al., 2015), vOTU (Ekkebus et al., 2013) and the newly discovered MINDY1 (Abdul Rehman et al., 2016). The novel PA warhead has also been conjugated to a synthetic SUMO moiety as an alternative to ubiquitin, the authors showed that both SUMO-PA and Ub-PA could be employed to profile the activity of exogenously expressed cysteine proteases in cell extracts (Sommer et al., 2013). In a similar manner, Ub-PA has been used to assay the activity status of recombinant OTUs in an *in vitro* setting (Mevissen et al., 2013). However, there is yet to be a study that uses Ub-PA to quantitatively analyse endogenous DUB activity.

4.2 Aims

4.2.1 To develop a more robust method of isolating active DUBs from cell lysates

The preliminary Ub-VME proteomic screen described in Chapter 3 provided a strong foundation to develop a more comprehensive profiling assay. I established and validated effective synchronisation and SILAC-MS proteomic protocols. However, in order to analyse differential DUB reactivity through the cell cycle I need to develop a more robust method of isolating and identifying active DUBs from cell lysates. Only a small cross-section of the DUBome reacted with Ub-VME and were identified by MS using submaximal binding conditions. So, my first objective was to investigate whether a different Ub-based probe, Ub-PA, could achieve better results and increase the number of DUBs identified from each *in vitro* reaction, particularly DUBs from the OTU, JOS and MINDY families that were not represented in the preliminary Ub-VME screen (Chapter 3).

4.2.2 To perform a more comprehensive profile of DUB activity during cell cycle progression

With an improved method for isolating active DUBs I aimed to generate a more comprehensive global profile of DUB activity during the cell cycle. I will examine this dataset for patterns of regulation, to identify whether DUBs exhibit similar reactivity profiles. I will then perform a comparative analysis using collated information from existing datasets (phylogenetic, localisation, interactome and phospho-proteome studies) to determine whether intramolecular or external factors could be associated with cell cycle regulation of DUB activity.

4.3 Using Ub-PA to generate a more comprehensive profile of DUB activity throughout cell cycle progression

4.3.1 Comparing DUB reactivity towards Ub-VME and Ub-PA activity probes

Ub-PA is an ubiquitin monomer in which the C-terminal carboxylate is replaced with a propargyl group (Figure 4.1A). Ub-PA, like Ub-VME, can be N-terminally conjugated to a HA tag for recognition or retrieval of active DUBs (Figure 4.1B). Ub-PA is proposed to have improved binding kinetics in comparison to Ub-VME (Ekkebus et al., 2013) and so my first step was to validate Ub-PA binding in A549 cell lysates and test different assay conditions.

As outlined in Section 3.3, the intention when developing the Ub-VME assay was to find a standard set of *in vitro* incubation conditions that carefully balanced probe concentration and *in vitro* incubation length in order to elicit a sub-maximal binding response for as many active DUBs as possible. However, only eight DUBs were retrieved using HA immunoprecipitation (Figure 3.6). This indicated that tailoring *in vitro* Ub-VME incubation conditions to prevent saturation for highly reactive DUBs was too restrictive for global DUB activity profiling. To this end when developing the Ub-PA assay, the objective was altered with the emphasis on increasing the total number of DUBs that could be profiled. With this in mind, I performed a set of experiments to assess the effect of probe concentration and *in vitro* incubation length on Ub-PA binding (Figure 4.1C-D). These used the same range of probe concentration and incubation time as the experiments performed for Ub-VME (Figure 3.2B-C). This allowed me to directly compare DUB reactivity profiles for Ub-VME and Ub-PA probes, and in doing so I could ensure that future *in vitro* Ub-PA reactions would produce an improved global profile of DUB activity.

First, I performed the titration of HA-Ub-PA and analysed global DUB binding by HA immunoblotting (Figure 4.1C). To reiterate, each HA immuno-reactive band in these immunoblots represents one or more cysteine protease DUBs that have covalently bound to the HA-Ub-PA probe. As expected, higher concentrations of Ub-PA (Figure 4.1C, lane 5) exhibited increased HA immuno-reactivity when compared to lower concentrations of Ub-PA (Figure 4.1C, lane 2). Interestingly,

there was a substantial increase in the number of Ub-PA reactive DUBs (Figure 4.1C, Lane 5) compared to Ub-VME reactive DUBs (Figure 3.2B, Lane 5) from identical *in vitro* incubations with A549 cell lysates. These additional 23 bands are marked by green circles in Figure 4.1C. This promising observation illustrates that HA-Ub-PA has the capacity to bind a broader cross-section of the DUBome, recapitulating previously published data (Ekkebus et al., 2013).

Secondly, I performed a time course experiment, in which a set amount of HA-Ub-PA (1:200 ratio of Ub-PA:protein) was incubated with A549 cell lysates for increasing periods of time (Figure 4.1D). Ub-PA is a fast reacting probe; the majority of DUBs did not exhibit a higher level of HA-Ub-PA reactivity with longer incubation periods. This was strikingly different from the Ub-VME reactivity profile where DUB reactivity to Ub-VME increased proportionally to the length of *in vitro* incubation over the same time course (Figure 3.2C). Some DUBs did exhibit time dependent Ub-PA reactivity over the incubation time course (Figure 4.1D, blue circles), indicating that these DUBs were less reactive. More intriguingly however was the disappearance of some HA-Ub-PA bound DUBs after 45 minutes incubation in native lysates (Figure 4.1D, orange circles). This could be indicative of DUBs that need to auto-deubiquitylate to remain stable. The covalent nature of Ub-PA binding makes it a potent inhibitor of DUB activity and so any DUBs that become polyubiquitylated would no longer have the catalytic ability to remove these chains and reverse the degradation signal.

Ub-PA is reported to have a broader binding profile across the DUB families than Ub-VME, in particular showing enhanced binding to the OTU family (Ekkebus et al., 2013). To test that this holds true in our cell model, HA-Ub-VME and Ub-PA time course experiments were performed in parallel using a standard probe concentration ratio of 1:200 (probe:protein) (Figure 4.1E and F). Four DUBs were chosen to represent each of the established cysteine protease DUB families: USP15 for the USPs, BAP1 for the UCHs, YOD1 for the OTUs, and ATXN3 for JOSs.

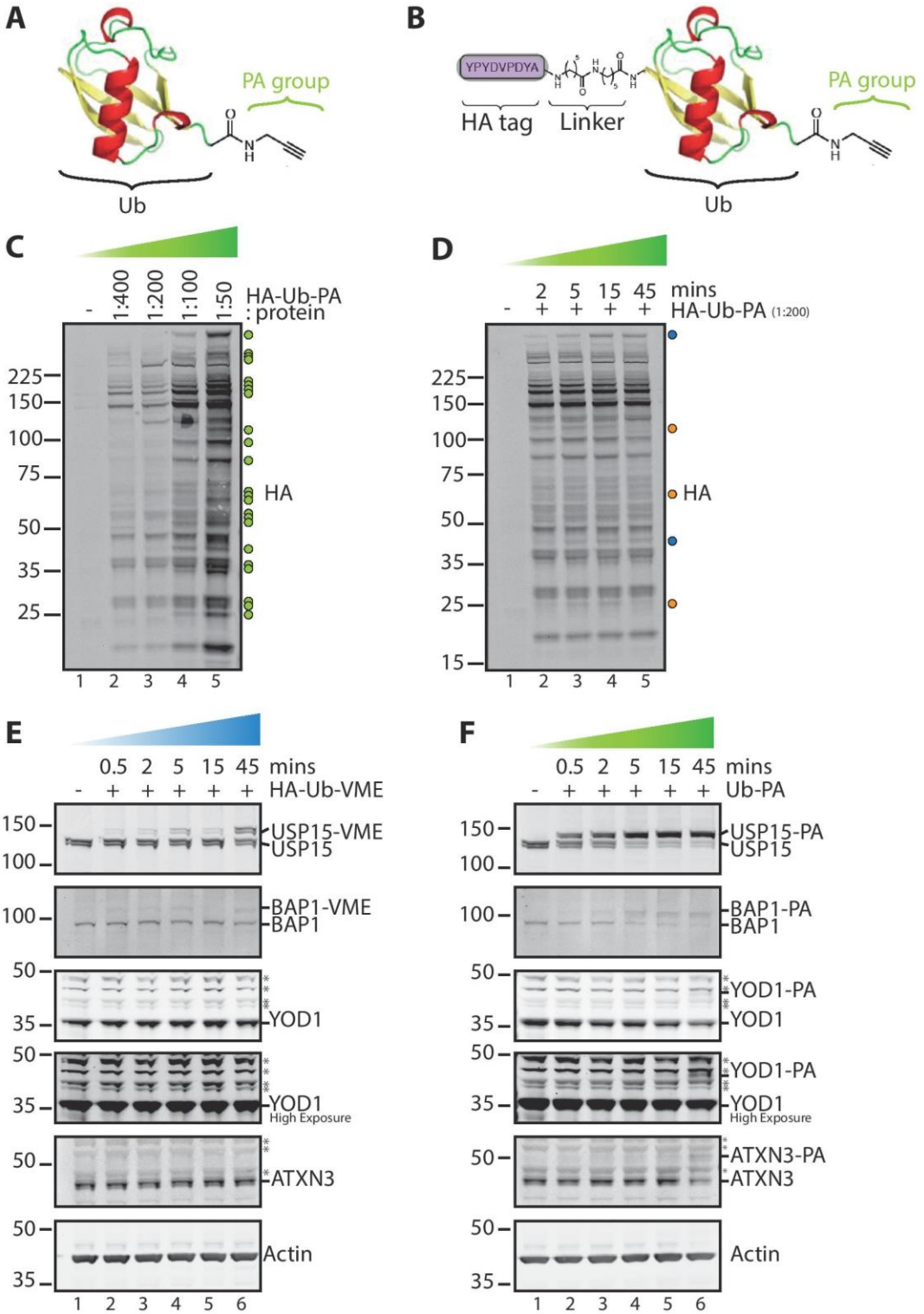

Figure 4.1: Ub-PA is a fast-reacting probe with high affinity to cysteine protease DUBs.

A and B: Illustration of two variants of an Ub-PA active site-directed probe. **A:** Ub-PA has a propargyl group covalently joined to the C-terminus of a synthetic ubiquitin monomer. **B:** HA-Ub-PA has an additional haemagglutinin (HA) recognition tag conjugated to N-terminus of ubiquitin through an Ahx-Ahx linker. **C and D:** Optimisation experiments for HA-Ub-PA *in vitro* incubation. All incubations were performed with A549 cell lysates at 37ºC and 300rpm in a thermo-shaker. Reactions were separated by SDS-PAGE on 4-12% gradient gel and immunoblotted for HA to

assess DUB reactivity. **C:** Titration of HA-Ub-PA concentration: 15µg lysate was incubated with increasing concentrations of HA-Ub-PA for 15 minutes. Green circles represent DUBs reactive to HA-Ub-PA that were not reactive to HA-Ub-VME. **D:** 15µg lysate was incubated with 75ng HA-Ub-PA (1:200) for increasing periods of time. Blue circles represent DUBs exhibiting time-dependent reactivity to HA-Ub-PA. Orange circles represent DUBs that were no longer present after a 45 minute incubation. **E and F:** Comparison of HA-Ub-VME and Ub-PA binding. 15µg A549 lysate was incubated with 75ng HA-Ub-VME **(E)** or Ub-PA **(F),** reactions were incubated over a time course. Terminated reactions were separated by SDS-PAGE and immunoblotted for representative DUBs from each family. USP: USP15, UCH: BAP1, OTU: YOD1 and JOS: ATXN3. Grey * indicates non-specific bands.

Specific immunoblotting for these DUBs enabled a comparative analysis of probe binding efficiency for these representative DUBs. Immunoblotting for a specific DUB, rather than the HA tag, allows the visualisation of both the probe-bound DUB and the residual unbound DUB. Once covalently bound to the probe, the DUB becomes approximately 10kDa heavier (10kDa for HA-Ub-VME or 8kDa for Ub-PA). Upon separation by SDS-PAGE, the heavier probe-bound DUB migrates slower than the unbound DUB, and so they resolve as two bands approximately 10kDa apart. Appearance of the heavier probe-bound DUB during the incubation time course allows comparison of binding efficiencies for DUBs to the Ub-VME and Ub-PA probes (Figure 4.1E and F).

USP15, a USP identified in the preliminary Ub-VME cell cycle screen (Chapter 3), reacted with both HA-Ub-VME and Ub-PA probes. However, Ub-PA exhibited a substantially faster binding rate, with the majority of USP15 being Ub-PA bound after 5 minutes compared to only partial binding after 45 minutes to HA-Ub-VME (compare Figure 4.1E, Lane 6 to Figure 4.1F, Lane 4). BAP1 was not identified in the previous Ub-VME proteomic screen, however after 45 minutes a small amount of BAP1 was Ub-VME bound. Like USP15, BAP1 only required 5 minutes incubation with Ub-PA to elicit a comparable binding response to that seen with Ub-VME after 45 minutes (compare Figure 4.1E, Lane 6 to Figure 4.1F, Lane 4).

In addition, Ub-PA, unlike HA-Ub-VME, was able to bind to both YOD1 and ATXN3 (compare Figure 4.1E, Lane 6 to Figure 4.1F, Lane 6). However, it required a longer incubation period for these DUBs to react with Ub-PA compared to the

USP and UCH representative DUBs. Even though both YOD1 and ATXN3 immunoblotting revealed a number of non-specific bands (marked by grey asterisks), after 45 minutes incubation with Ub-PA there was a notable appearance of DUB specific immuno-reactive bands. These bands migrated slower than the endogenous DUB, making them approximately 8kDa heavier, and there was a corresponding reduction in the level of unbound DUB (Figure 4.1F, Lane 6). This DUB-Ub-PA band was not identified in the corresponding Ub-VME incubation (Figure 4.1E, Lane 6). The affinity of both OTU and Josephin DUBs to Ub-PA likely contributes to the substantial increase in Ub-PA reactive DUBs identified in Figure 4.1C (green circles) compared to the Ub-VME reactive DUB profile.

The aim of these experiments was to identify whether incubation with Ub-PA would increase the number of active DUBs retrieved from A549 cell lysates. Collectively the data from Figure 4.1 suggest that Ub-PA was a fast reacting probe that provided more comprehensive coverage of the DUBome and therefore was a better candidate for global DUB activity profiling than Ub-VME.

4.3.2 Recognition and retrieval of Ub-PA reactive DUBs

Ub-PA can be conjugated to sepharose resin to enable facile retrieval of active DUB complexes (Ekkebus et al., 2013). To test the utility of this approach, sepharose-Ub-PA was incubated with A549 cell lysates; a schematic depicts the experimental workflow (Figure 4.2A). Sepharose pull down enabled the isolation of active DUB complexes that can be analysed using directed immunoblotting or MS dependent on the method of DUB retrieval from the sepharose beads. Two retrieval methods can be used to identify Ub-PA reactive DUBs, the first uses trifluoroacetic acid (TFA) to cleave the vinyl thioether bond between Ub-PA and a DUBs catalytic cysteine (Figure 4.2A, Option 1). This allows directed immunoblotting for DUBs of interest as well as quantitative analysis by MS. The second approach uses on-bead digestion of the immobilised DUB-Ub-PA complexes specifically for analysis by MS (Figure 4.2A, Option 2). I tested both of these approaches to see whether they could efficiently retrieve immobilised Ub-PA bound DUBs from the sepharose beads.

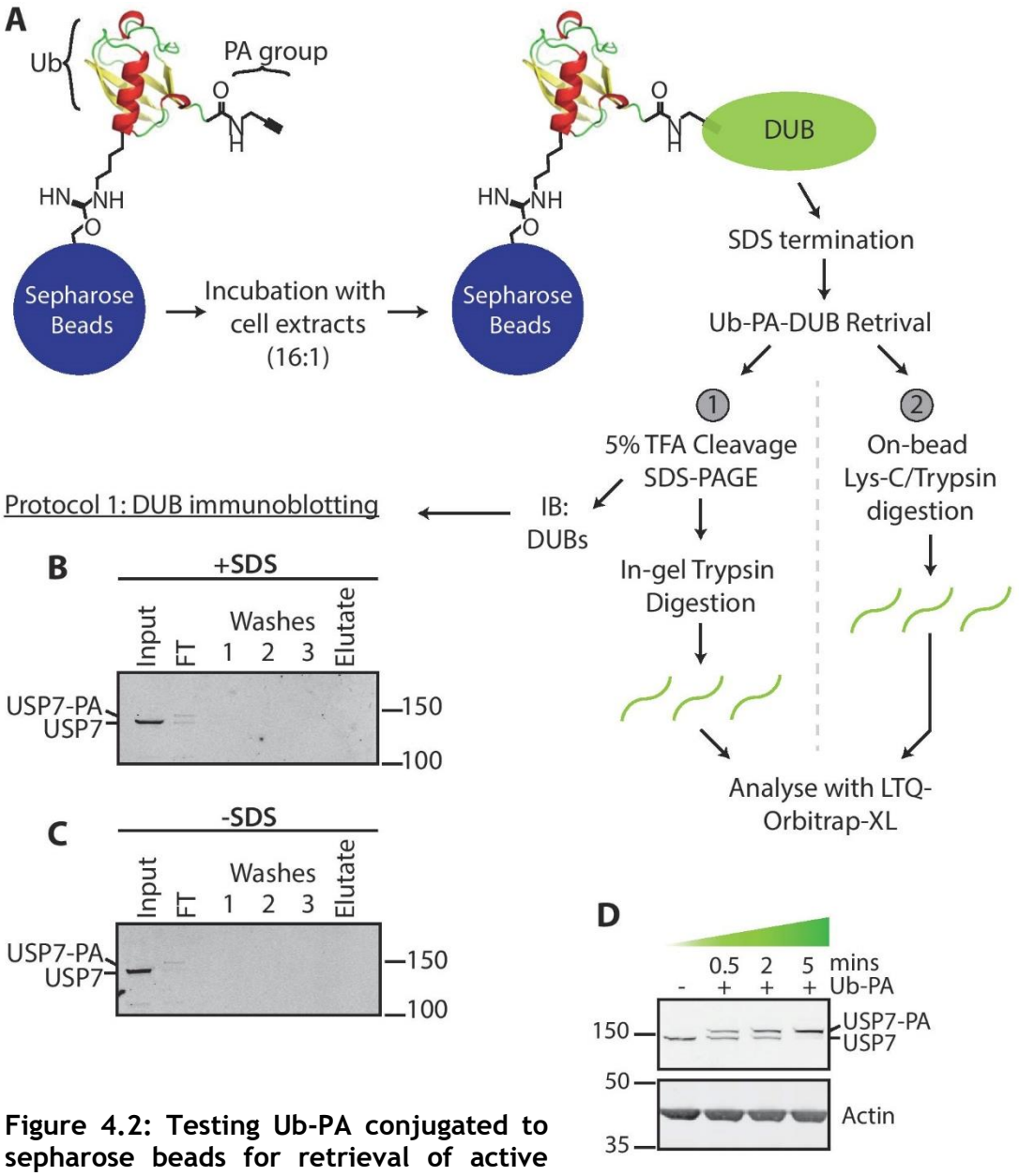

Figure 4.2: Testing Ub-PA conjugated to sepharose beads for retrieval of active DUB complexes.

A Schematic representing workflow employed to retrieve active DUBs from cell lysates using sepharose conjugated Ub-PA. Two protocols are outlined illustrating different methods used to release immobilised proteins, 5% trifluoroacetic acid incubation (TFA) **(1)** and on-bead tryptic digestion **(2)**. **B and C:** Trifluoroacetic acid is not an effective retrieval method for Ub-PA bound DUBs: Following workflow from protocol 1, A549 lysate (0.5mg) was incubated with 8mg sepharose-Ub-PA (16:1) for 3 hours at 37ºC with shaking. Reactions were supplemented with 0.4% SDS **(B)** or a vehicle control **(C)** prior to collection of sepharose beads. Immobilised proteins were dissociated from sepharose resin by a 3 hour incubation in 5% TFA. Reactions were mixed with 5x sample buffer and boiled for 5 minutes. Eluates (100%) were separated by SDS-PAGE alongside input (1%) and flow through (FT) fractions (1%) and washes (0.8% v/v). Retrieval was analysed by immunoblotting for a representative abundant DUB, USP7. **D:** USP7 can react with Ub-PA. 15µg A549 lysate was incubated with 75ng Ub-PA (1:200 probe:protein ratio) and reactions were incubated over a 5 minute time course. Terminated reactions were separated by SDS-PAGE and immunoblotted for USP7.

I first tested the TFA cleavage method (Figure 4.2A, Option 1). Post-incubation with sepharose-Ub-PA, the cell lysates were treated with 5% TFA to release immobilised DUBs from the sepharose beads. Immunoblotting for USP7 was used to analyse the efficiency of DUB retrieval using this cleavage method (Figure 4.2B). USP7 efficiently bound to the sepharose-Ub-PA beads, evident from the decreased USP7 signal in the unbound flow through (FT). However, USP7 was not observed in the eluted fraction suggesting that TFA was not able to cleave USP7 from the sepharose beads. One aspect of this method that could be affecting DUB retrieval was the SDS termination step, a standard step to prevent continued binding of probe to a DUB after the designated *in vitro* incubation period. However, SDS is often used to elute immobilised proteins from sepharose and so this termination step could result in the loss of Ub-PA reactive DUBs prior to TFA elution from the sepharose beads. To address whether the SDS termination step affected the retrieval of Ub-PA bound DUBs, a second sepharose-Ub-PA incubation was performed without the SDS termination step (Figure 4.2C). Again, even without the addition of SDS, I was unable to elute immobilised USP7 after 5% TFA incubation. The conjugation of Ub-PA to sepharose beads was previously reported to allow stringent washing procedures using 10% SDS (Ekkebus et al., 2013). Therefore, it was unsurprising that the SDS termination (0.4% SDS) had little effect on USP7 retrieval.

As this was the first time I had used USP7 in optimisation experiments, it was possible that USP7 reacted poorly with the PA warhead and that this could explain the low retrieval efficiency. To address this query, I performed a short time course experiment to determine whether USP7 reacted with the Ub-PA activity probe (Figure 4.2D). It was evident that USP7 could bind to Ub-PA even with short incubation lengths and so we concluded it was most likely that the immobilised protein was precipitated during TFA incubation.

As DUB retrieval was not possible using TFA cleavage in my hands, on-bead digestion was required to identify DUB-Ub-PA complexes (Figure 4.2A, Option 2). To this end, I established an on-bead digestion protocol based on the published in-solution digestion protocols used for complex protein samples

(Ekkebus et al., 2013) (Section 2.5.2). This used a combination of Lys-C and trypsin incubation to increase the efficacy of peptide digestion for immobilised proteins.

To ensure maximal Ub-PA tagging of DUBs for the cell cycle screen further optimisation was required. The standard conditions used in previous publications combined 50mg sepharose-Ub-PA with 3mg cell lysate providing a ratio of 16:1 sepharose-Ub-PA:protein lysate (Ekkebus et al., 2013). I compared four different experimental conditions to identify the optimal sepharose-Ub-PA:protein lysate ratio and examine whether increasing the starting amount of protein lysate would increase the number of DUBs identified (Figure 4.3A). In total, nineteen DUBs were successfully Ub-PA tagged and identified after on-bead digestion. The Venn diagram in Figure 4.3B represents the distribution of DUBs identified from each experimental condition. At the lowest ratio of sepharose-Ub-PA:protein (1.6:1), with 1mg protein lysate, only a few DUB-Ub-PA complexes were identified (orange circle). There was a 4-fold increase to 16 DUBs (yellow circle) using the recommended ratio of 16:1. Interestingly, increasing the ratio to 32:1 did not provide any further increase in the number of DUBs tagged with Ub-PA, with only 13 DUBs identified (green circle). Finally, using the 16:1 ratio of sepharose-Ub-PA:protein and doubling the amount of starting material to 2mg of cell lysate yielded 17 Ub-PA tagged DUBs (blue circle) providing no real advantage. Taking these data into account, the optimal conditions for subsequent sepharose-Ub-PA incubations were 16mg sepharose-Ub-PA and 1mg cell lysate for each experimental condition.

To put this data into context, we looked at a global proteomic study that measured protein abundance in multiple mammalian of cell lines (Geiger et al., 2012). In that study, fifty DUBs were detected and quantified by iBAQ by MS in A549 cells. Of these fifty DUBs, I identified 19 (approximately 40%) in these preliminary Ub-PA/MS experiments (Figure 4.3C). I extracted and plotted the DUB expression data for A549 cells from the Geiger proteomic dataset (Figure 4.3D) (Geiger et al., 2012). The majority of DUBs identified from the sepharose-Ub-PA pull downs are highly expressed DUBs, with only 2 of the 15 most abundant DUBs not tagged by Ub-PA (Figure 4.3D). Only the very abundant DUBs

were identified using the lowest ratio of sepharose-Ub-PA:protein lysate (1.6:1) (Figure 4.3B and D, highlighted with an asterisk) suggesting that the concentration of Ub-PA was limiting in this reaction. A 10-fold and 20-fold increase in sepharose-Ub-PA concentrations enabled Ub-PA tagging of less abundant DUBs as well as the highly abundant DUBs (Figure 4.3B and D).

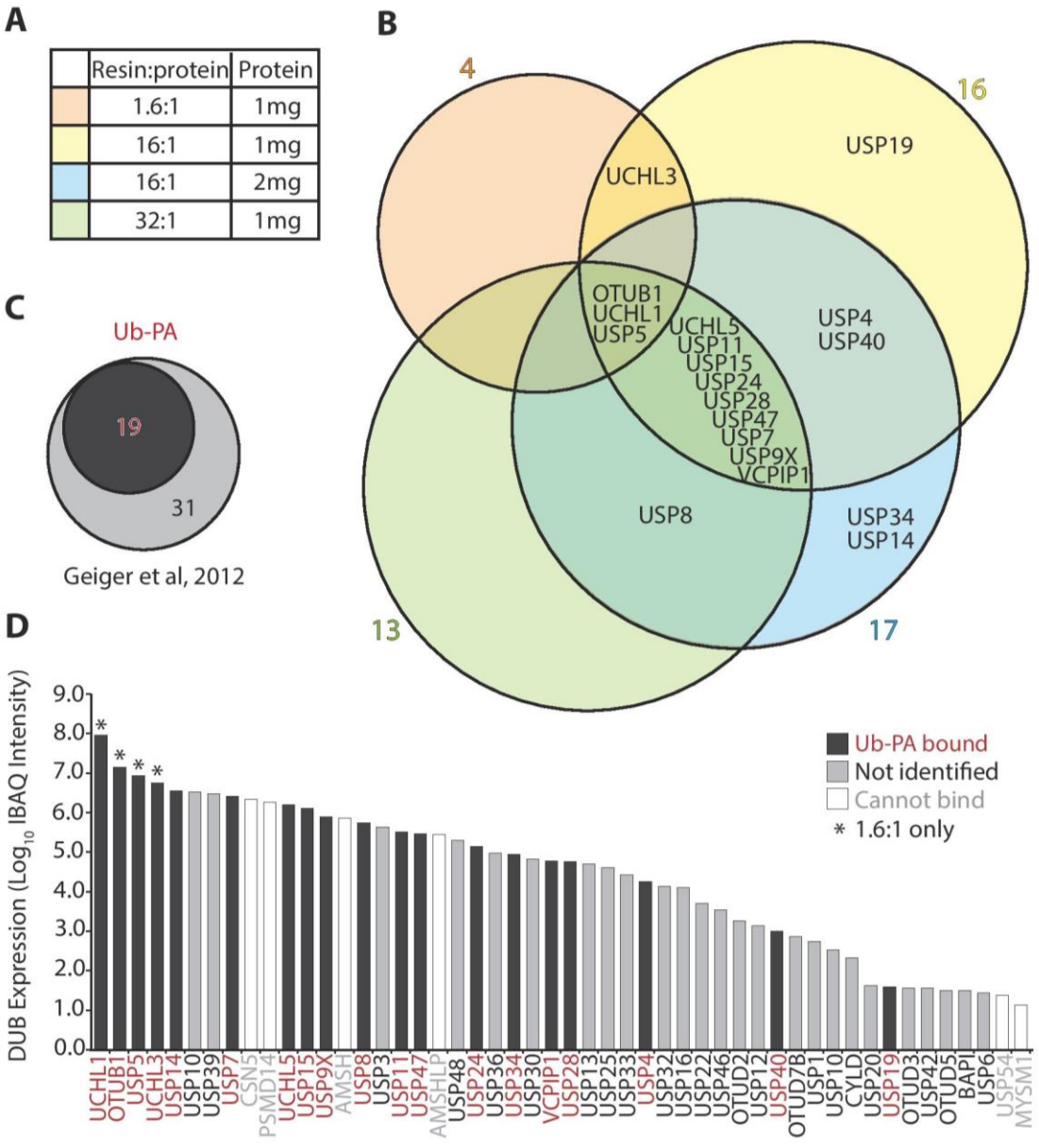

Figure 4.3: Summary of DUBs identified using sepharose-Ub-PA coupled with mass spectrometry.

A and B: Four experimental conditions used to optimise DUB reactivity to sepharose-Ub-PA. The amount of A549 cell lysate and relative concentration of sepharose-Ub-PA is tabulated in **A**. Reactions were incubated for 3 hours at 37°C with shaking; immobilised proteins were precipitated and washed prior to tandem incubations with Lys-C and trypsin. Peptides were analysed on LTQ-Orbitrap-XL. DUBs retrieved

from each experimental condition are illustrated in the Venn diagram (**B)** with each circle coloured to indicate the conditions listed in **A**. The number of DUBs identified in each condition is listed on the periphery of each circle. **C:** Venn diagram illustrating the overlap between DUBs identified at least once by Ub-PA pull downs (in **A**) and in A549 iBAQ proteome expression dataset (Geiger et al., 2012). The number of DUBs identified in each proteomic dataset is indicated: sepharose-Ub-PA (dark grey circle), iBAQ expression (light grey circle) **C:** Histogram shows ranked iBAQ expression data for DUBs in A549 cells (Geiger et al., 2012). Dark grey bars (red text) represent Ub-PA tagged DUBs; light grey bars (black text) represent DUBs not identified in Ub-PA dataset. White bars (grey text) indicate DUBs unable to bind Ub-PA, including catalytically inactive USP54 and the JAMMs. * represent DUBs that bound in the 1.6:1 probe:protein condition.

4.3.3 Unbiased profiling of cell cycle-dependent DUB activity revealed increased activity regulation at checkpoint transitions

Having carefully optimised each aspect of the sepharose-Ub-PA assay, I was able to construct a protocol for screening DUB activity through cell cycle progression. The experimental design mirrors that used for the preliminary Ub-VME cell cycle screen (Figure 3.5A). For unbiased, quantitative, analysis of cell cycle-dependent DUB activity, I employed triplexed SILAC-MS to compare 3 different synchronised cell populations (see Section 3.3.4). To confirm that SILAC-labelling did not affect cell synchronisation, labelled A549 were synchronised (as described in Section 3.3.2) prior to separation by SDS-PAGE and immunoblotting for cell cycle phase-specific markers. Periodic expression of the cell cycle effectors CCNE and CCNB, and phosphorylation status of CDK1, mirrored the levels expressed in unlabelled A549 (compare Figure 4.4A and Figure 3.3B). SILAC labelling of A549 cells did not affect the profile of these markers, confirming that these synchronisation protocols could be used for the proteomic screen.

A matrix of four experiments were performed in parallel to enable quantitative analysis of 7 enriched cell cycle phases, each compared to an asynchronous control (Figure 4.4B). To identify any non-specific interactors, a control probe was used in the fifth experiment (Figure 4.4B, Run5). Sepharose-Ub-76 is a synthetic ubiquitin monomer in which the C-terminal carboxylate group has not been modified. Without the addition of a warhead group the ubiquitin monomer will only transiently interact with, but not covalently bind to, active DUBs. Therefore, pull down of sepharose Ub-76, after incubation with asynchronous

cell lysates, provided a list of proteins that bound to either to the sepharose beads or to synthetic ubiquitin in a non-catalytic manner. The experimental design is schematically represented in Figure 4.4C. SILAC-labelled A549 cells were synchronised following the matrix outlined in Figure 4.4B. Equal amounts of A549 cell lysates (1mg of each sample) were incubated with sepharose-Ub-PA or the sepharose-Ub-76 control. In the same manner as the preliminary Ub-VME screen, *in vitro* reactions were terminated prior to mixing samples (total of 3mg), preventing bias from cross-modification of proteins.

Spectra from the four experiments (Figure 4.4B, Run 1-4) were analysed together. Peptide hits from three technical replicates were compiled for each cell cycle phase. MaxQuant (version 1.4.1.2) was used to assign peptides to their protein identification (Protein ID) and quantitatively compare protein intensities between light, medium and heavy labelled samples. In total, 268 proteins were identified (Figure 4.5A, Appendix Table 3.1). This proteomic approach was targeted towards identifying DUBs and so I employed non-stringent criteria to select for proteins of interest. I selected for proteins that had at least one peptide observed at least once across the 12 datasets (the four experiment runs and their three individual technical replicates). This list was filtered for known contaminants (Mellacheruvu et al., 2013) and proteins that also appeared in sepharose-Ub-76 pull down (Run 5). This refined list had 144 sepharose-Ub-PA specific proteins. Thirty-two of these were associated with UPS, 23 of which were DUBs (ratios listed in Table 4.3, Log_2 ratios listed in Appendix Table 3.2).

As in Chapter 3 (Figure 3.6B), I have collated raw data from the MaxQuant analysis into a table (Table 4.3). The table displays the Protein IDs, the number of peptides identified and the protein ratios for each cell cycle phase for DUBs, UPS-associated and cell cycle-associated proteins. On comparison with the preliminary experiments (Figure 4.3), I identified the same 19 DUBs, plus an additional four DUBs: OTUD4, OTUD5, OTUD6B and USP9Y (Figure 4.5B). Three of which had not previously been identified in the A549 proteome expression dataset (Geiger et al., 2012) (Figure 4.5B and Figure 4.3D).

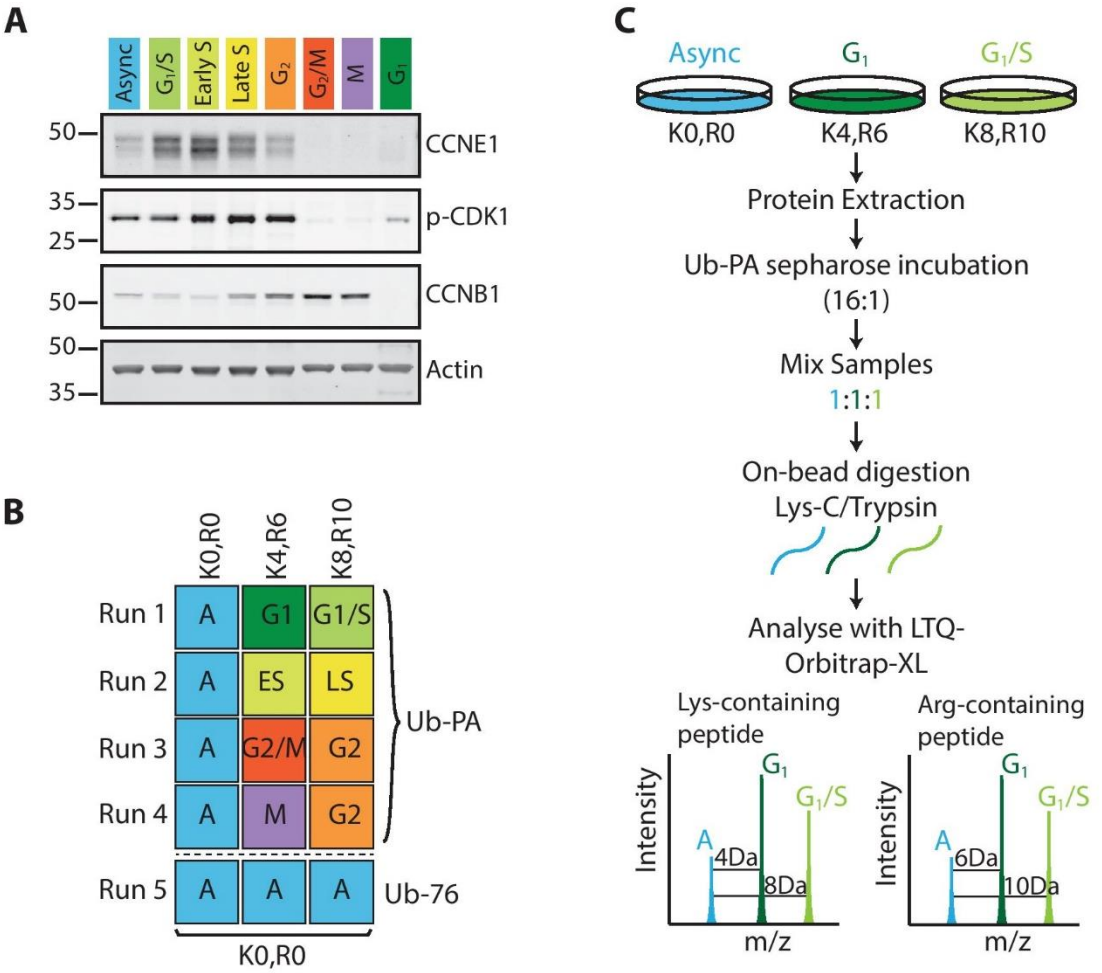

Figure 4.4: Experimental strategy for quantitative analysis of differential DUB activity across 7 enriched cell cycle phases.

A: SILAC labelled A549 cells can be effectively synchronised. Labelled A549 cells were synchronised using a double thymidine block (for G_1/S to G_2 enrichment) or a thymidine and nocodazole block (for G_2/M to G_1 enrichment) and sampled at indicated time of release. Equal amounts of synchronised lysate were separated by SDS-PAGE and immunoblotted for the specified cell cycle markers. **B and C**: Schematic illustrating the experimental strategy to analyse DUB activity using sepharose-Ub-PA triple-labelled SILAC-MS. **B:** A matrix of 5 runs was used to analyse DUB activity across all cell cycle phases (Runs 1-4) and to eliminate non-specific sepharose-Ub binding proteins (Run 5). **C:** Schematic representing the workflow for run 1 (from B) used to analyse DUB activity from synchronised cells. Equal amounts of synchronised SILAC-labelled A549 lysate (1mg) were incubated with 16mg sepharose-Ub-PA for 3 hours at 37°C with shaking. Reactions were supplemented with 0.4% SDS to terminate Ub-PA reactivity. Immobilised proteins from each run were washed, precipitated and mixed at equimolar ratios prior to on-bead digestion. Peptides were analysed on an LTQ-Orbitrap-XL.

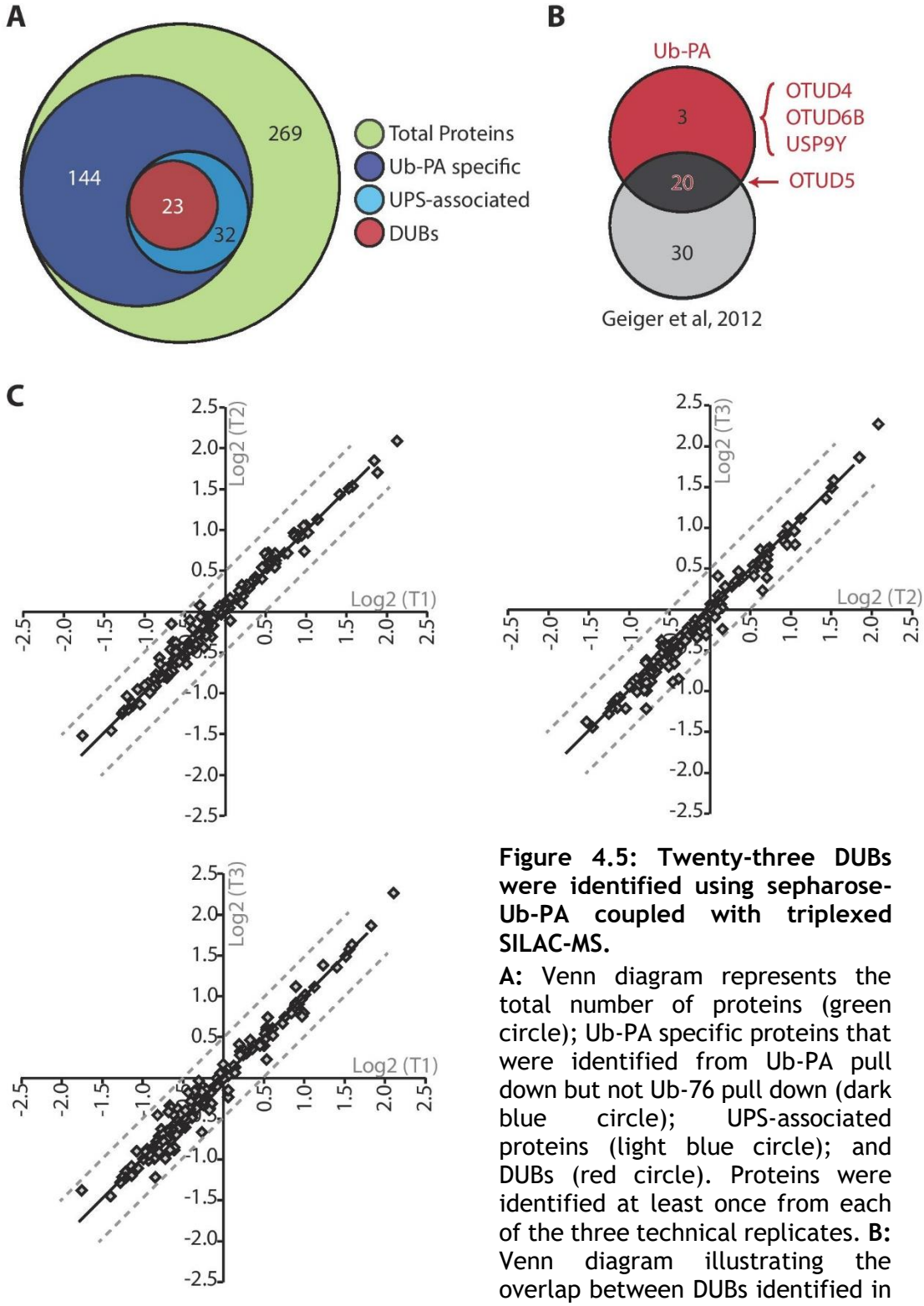

Figure 4.5: Twenty-three DUBs were identified using sepharose-Ub-PA coupled with triplexed SILAC-MS.

A: Venn diagram represents the total number of proteins (green circle); Ub-PA specific proteins that were identified from Ub-PA pull down but not Ub-76 pull down (dark blue circle); UPS-associated proteins (light blue circle); and DUBs (red circle). Proteins were identified at least once from each of the three technical replicates. **B:** Venn diagram illustrating the overlap between DUBs identified in Ub-PA pull downs (in A) and A549 iBAQ expression dataset (Geiger et al., 2012). The numbers represent DUBs identified in each proteomic dataset: sepharose-Ub-PA (red circle); iBAQ expression (light grey circle) and those identified in both (dark grey intersection, red text). **C:** Variation between technical repeats did not exceed ±1.5-fold change ($\pm Log_2 0.5$). DUB peptide ratios (M/L, H/L and M/H) measured from each MS run (T1, T2 and T3) were plotted against each other. Grey dashed lines represent the ±1.5-fold ($\pm Log_2 0.5$) threshold.

			G1 and G1/S		Early S and Late S		G2 and G2/M		G2 and M	
			Run1		Run2		Run3		Run4	
	Gene	Peptides	Ratio M/L	Ratio H/L	Ratio M/L	Ratio H/L	Ratio M/L	Ratio H/L	Ratio M/L	Ratio H/L
DUBs	**OTUB1**	12	1.10	0.66	0.72	0.72	0.75	0.64	0.80	0.66
	OTUD4	2	1.06	2.93	5.94	4.35	1.68	3.62	1.51	3.44
	OTUD5	1	0.51	0.70	1.06	1.50	0.61	1.18	0.89	1.17
	OTUD6B	3	0.56	0.66	0.88	0.91	0.44	0.75	0.53	0.78
	UCHL1	9	1.82	0.72	1.38	1.06	1.34	0.97	1.23	0.98
	UCHL3	1	2.48	0.84	0.39	0.57	3.06	2.02	1.03	0.68
	UCHL5	9	0.60	0.87	1.42	1.22	0.61	1.01	0.74	1.00
	USP11	17	0.67	1.31	1.66	1.83	0.82	1.49	0.86	1.47
	USP14	1	0.91	1.30	4.45	2.94	0.66	1.56	0.59	1.53
	USP15	30	0.82	0.81	0.74	0.73	0.60	0.79	0.62	0.74
	USP19	4	0.75	0.86	1.48	1.16	0.67	0.98	0.82	1.01
	USP24	17	0.98	0.84	0.42	0.44	0.68	0.77	0.54	0.56
	USP28	7	0.56	1.93	3.59	2.63	0.57	1.98	0.63	1.99
	USP34	5	0.67	1.63	1.77	1.53	0.45	1.53	0.45	1.45
	USP4	6	0.95	0.85	0.77	0.73	0.70	0.81	0.70	0.72
	USP40	8	0.84	0.60	0.34	0.47	0.62	0.52	0.68	0.53
	USP47	21	0.72	0.53	0.37	0.46	0.60	0.52	0.68	0.51
	USP5	36	1.00	1.22	1.45	1.28	0.69	1.20	0.67	1.11
	USP7	49	0.89	1.88	2.84	2.18	0.67	1.89	0.75	1.86
	USP8	4	0.52	0.54	0.95	0.73	1.00	0.64	1.40	0.66
	USP9X	55	1.03	1.03	0.43	0.57	0.71	0.96	0.53	0.69
	USP9Y	28	#DIV/0!	#DIV/0!	#DIV/0!	#DIV/0!	0.71	0.96	#DIV/0!	#DIV/0!
	VCPIP1	12	0.58	0.79	0.75	1.08	0.69	0.73	0.89	0.82
UPS	**HUWE1**	3	0.35	0.55	1.01	0.89	#DIV/0!	#DIV/0!	#DIV/0!	#DIV/0!
	NEDD4	1	0.20	0.17	#DIV/0!	#DIV/0!	0.29	0.43	#DIV/0!	#DIV/0!
	PSMB4	1	#DIV/0!	#DIV/0!	#DIV/0!	#DIV/0!	#DIV/0!	#DIV/0!	#DIV/0!	#DIV/0!
	PSMD13	1	#DIV/0!	#DIV/0!	#DIV/0!	#DIV/0!	#DIV/0!	#DIV/0!	#DIV/0!	#DIV/0!
	TRIM4	1	0.86	0.60	1.02	0.93	0.72	0.77	0.90	0.80
	UBA1	10	0.15	0.12	0.53	0.50	0.25	0.23	0.68	0.51
	UBC	8	0.03	0.02	0.06	0.05	0.05	0.01	0.05	0.02
	UBE2D3	1	0.16	0.16	#DIV/0!	#DIV/0!	0.27	0.22	#DIV/0!	#DIV/0!
	UBE2N	5	0.14	0.08	0.41	0.32	0.24	0.17	0.69	0.29
Cell Cycle	**CENPT**	1	#DIV/0	#DIV/0	#DIV/0	#DIV/0	0.25	0.44	#DIV/0	#DIV/0
	CLTC	8	0.36	0.76	1.43	1.63	0.34	0.95	0.59	1.08
	COPS6	1	#DIV/0	#DIV/0	#DIV/0	#DIV/0	#DIV/0	#DIV/0	#DIV/0	#DIV/0
	PGK1	2	0.75	0.41	1.17	0.99	0.80	0.80	0.70	0.65
	ZEB2	1	#DIV/0	#DIV/0	#DIV/0	#DIV/0	#DIV/0	#DIV/0	#DIV/0	#DIV/0

Table 4.3: UPS-associated and cell cycle-associated proteins identified from sepharose-Ub-PA cell cycle screen.
Ratios represent averaged data from three technical replicates.

Many proteomic studies apply an arbitrary cut-off value to assign proteins that are differentially expressed between samples. For my dataset, I determined the variance between each MS technical replicate and applied a cut-off based on this. To ascertain the variance between technical repeats, I compared Log_2 DUB peptide ratios (M/L, H/L and M/H) obtained from replicate MS analyses of each sample (Figure 4.5C). Analysis of these scatter plots revealed that all ratios for any given DUB, from triplicate MS runs, fell within a $\pm Log_2(0.5)$ limit, equivalent to a 1.4-fold change. This is represented as the grey dashed lines in Figure 4.5C. Therefore, in subsequent comparison of cell cycle data any ratio surpassing this 1.4-fold limit was considered as a difference in reactivity to Ub-PA compared to the asynchronous sample.

I was interested to see how these ratios, which were reflective of DUB reactivity to Ub-PA, differed throughout cell cycle progression. To investigate this, DUB peptide ratios were compared for two subsequent cell cycle phases. Values for the 7 cell cycle phase transitions are plotted in Figure 4.6A. Substantially changing values were identified using the 1.4-fold threshold, previously determined in Figure 4.5C. DUBs that exhibited differential Ub-PA reactivity were highlighted and numbered. The corresponding list of DUBs with their assigned numbers are tabulated in Figure 4.6B. DUBs that fall above the upper threshold exhibited an increase in reactivity to Ub-PA as the cell progressed from one cell cycle phase into the next. Conversely, DUBs that fell below the lower threshold displayed a decrease in reactivity to Ub-PA during the transition into the next phase of the cell cycle.

The schematic in Figure 4.6C collates all differential Ub-PA reactivity data from the entire cell cycle screen. It is evident that DUBs exhibited dynamic regulation throughout cell cycle progression, particularly at checkpoint transitions. The most profound regulation of DUB activity was observed as the cells entered mitosis; compare G_2 to G_2M (Figure 4.6A and C). Thirteen DUBs exhibited differential reactivity to Ub-PA probe; the majority of these DUBs were downregulated. Only USP8 and UCHL3 had higher reactivity to Ub-PA at G_2/M than G_2. It should be noted that two different synchronisation protocols are used to enrich for S-phase populations and mitotic populations (see Sections 2.1.2.1 and 2.1.2.2 respectively). The extensive regulation of DUB activity seen at the intersection of these protocols (G_1 to G_1/S and G_2 to G_2/M) could be an artefact of these different protocols. That being said, large-scale regulation of DUB activity was identified at transitions within synchronisation protocols. A large number of DUBs exhibited differential reactivity to Ub-PA as cells passed through the G_1/S transition into S-phase and as they exited mitosis into G_1 (Figure 4.6A and 4.6C). In both cases, there was an overall increase in DUB reactivity to Ub-PA. There were also periods of the cell cycle with little evidence of DUB regulation; there was no change in DUB reactivity to Ub-PA as cells progressed through S-phase. Furthermore, only modest changes in USP14, USP24 and UCHL3 reactivity were identified as cells approached G_2/M and only UCHL3 displayed an increase in reactivity to Ub-PA during cell division (Figure 4.6A and 4.6C).

Figure 4.6

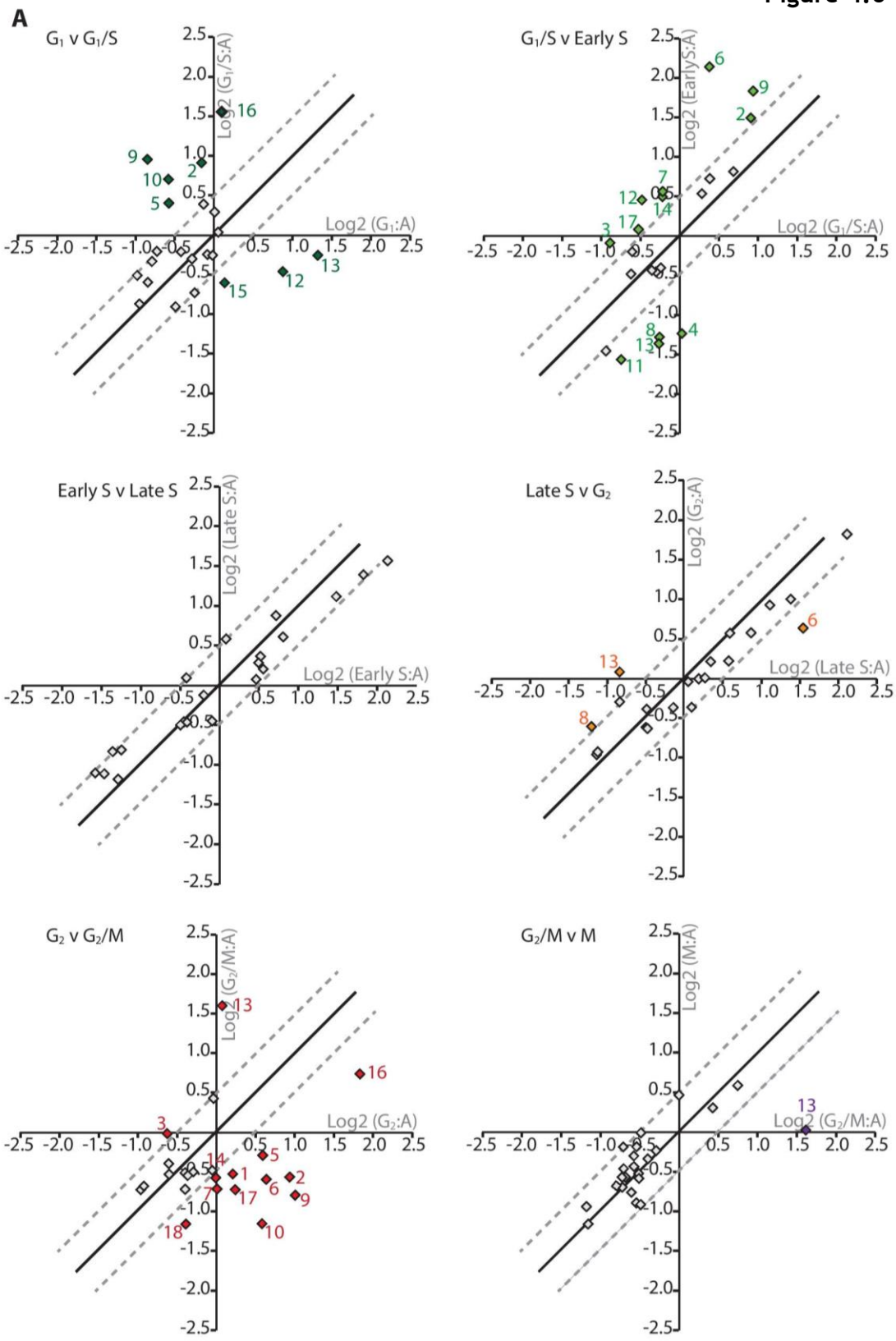
A
G1 v G1/S
Log2 (G1/S:A)
Log2 (G1:A)
G1/S v Early S
Log2 (Early S:A)
Log2 (G1/S:A)
Early S v Late S
Log2 (Late S:A)
Log2 (Early S:A)
Late S v G2
Log2 (G2:A)
Log2 (Late S:A)
G2 v G2/M
Log2 (G2/M:A)
Log2 (G2:A)
G2/M v M
Log2 (M:A)
Log2 (G2/M:A)

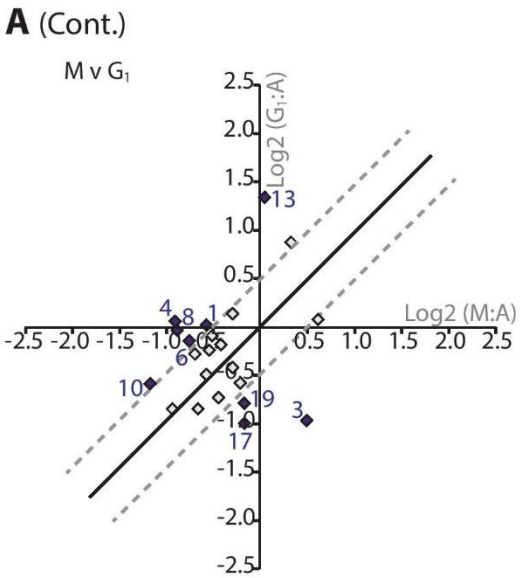

B

#	DUB	#	DUB
1	USP5	12	UCHL1
2	USP7	13	UCHL3
3	USP8	14	UCHL5
4	USP9X	15	OTUB1
5	USP11	16	OTUD4
6	USP14	17	OTUD5
7	USP19	18	OTUD6B
8	USP24	19	VCPIP1
9	USP28		
10	USP34		
11	USP40		

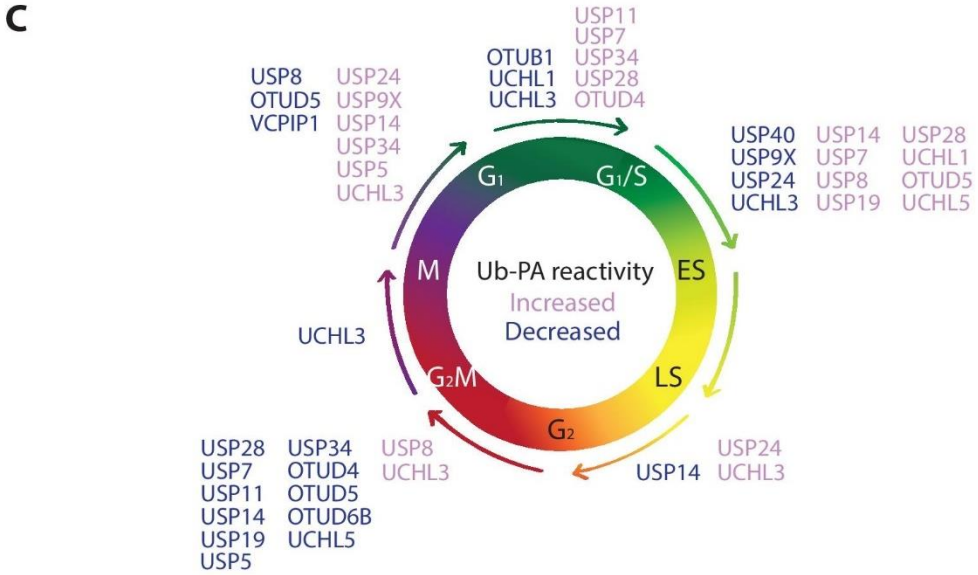

Figure 4.6: DUBs exhibited differential reactivity to Ub-PA in consecutive phases of the cell cycle.

A: DUB peptide ratios measured from consecutive cell cycle phases were plotted against each other as indicated. Each synchronised sample was first normalised to asynchronous cells prior to being plotted. Grey dashed lines represent the 1.4-fold change ($\pm Log_2 0.5$) threshold applied. DUBs that did not exceed this threshold are represented as grey diamonds. DUBs that did exceed this threshold are coloured and numbered. **B:** Table of DUBs that exhibited differential reactivity to Ub-PA throughout cell cycle, numbers correspond to DUBs indicated in A. **C:** Schematic overview of differential DUB activity between successive transitions in the cell cycle. DUBs with increased (pink text) or decreased (blue text) activity are listed for transitions between consecutive phases of the cell cycle.

4.3.4 Co-regulation of DUBs

It became apparent that certain DUBs displayed similar patterns of behaviour as the cell progressed through the cell cycle. This is exemplified by USP7 and USP28, which both exhibited increased reactivity to Ub-PA at the G_1 to G_1/S and G_1/S and Early S transitions and decreased reactivity to Ub-PA as the cell entered mitosis (Figure 6C). To identify the extent to which identified DUBs exhibited co-regulation, DUB peptide ratios were subject to hierarchal clustering (performed using Multi-experiment Viewer: MeV 4.8 – Version 10.2) and represented as a heat map (Figure 4.7A). This provided a holistic overview of differential DUB activity through the cell cycle and exposed a pervasive decrease in reactivity to Ub-PA as cells entered mitosis. Nineteen of the twenty-three DUBs identified (83%) were downregulated during mitosis (Figure 4.7A). Furthermore, cluster analysis highlighted six groups of co-regulated DUBs (Figure 4.7B).

Cluster 1 contains UCHL1 and OTUB1. Although they exhibit only modest changes in reactivity to Ub-PA, both displayed increased reactivity to Ub-PA at G_1 compared to the asynchronous control. DUBs in Cluster 2, the second largest group of co-regulated DUBs, all exhibited a substantial decrease in reactivity (mean of approximately 2.6-fold decrease) to Ub-PA during S-phase compared to asynchronous A549 cells. This was coupled with a moderate recovery in reactivity during G_2/M, though notably only UCHL3 had increased mitotic reactivity compared to the asynchronous control. Cluster 3 comprised two paralogs USP4 and USP15, which although exhibiting little variation in reactivity to Ub-PA, did map closely to each other through cell cycle progression. Cluster 4, the largest group with approximately half of the identified DUBs, shared the most oscillatory Ub-PA reactivity profile. There was increased reactivity in S-phase (mean of approximately 2.2-fold increase), coupled with a rapid decrease (mean of approximately 1.5-fold decrease) in Ub-PA reactivity as cells entered mitosis. This cluster contained USP28 and USP7, DUBs that were originally noted to exhibit similar behavioural patterns in cell cycle progression (Figure 4.6C).

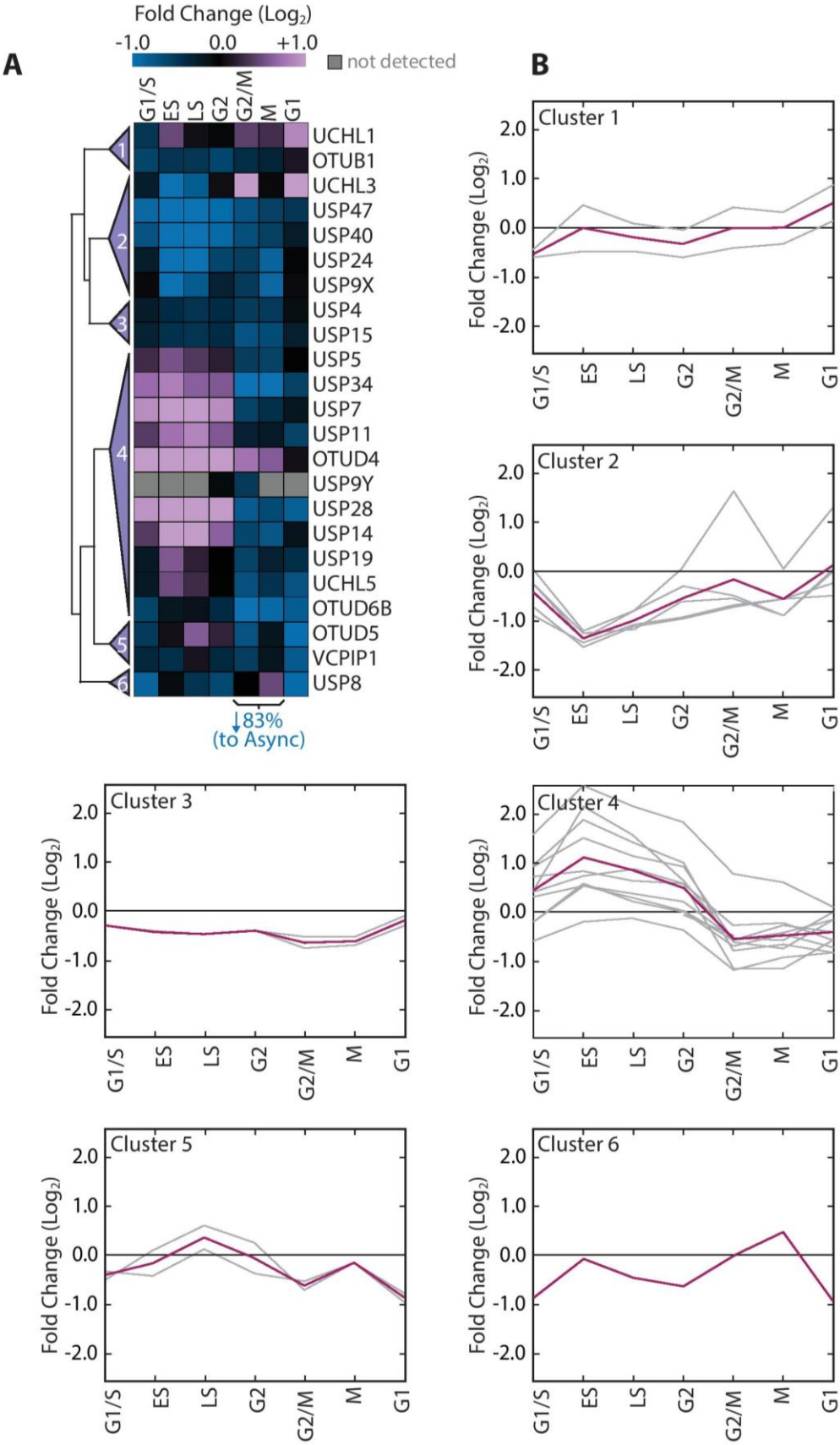

Figure 4.7: DUB activity was co-regulated throughout the cell cycle.

Figure 4.7: DUB activity was co-regulated throughout the cell cycle.

A: Ub-PA reactivity data were subjected to hierarchical clustering in MeV 4.8. Log_2 DUB peptide ratios, relative to the asynchronous control, are illustrated as a heatmap using a pink-to-blue colour scale to represent increased and decreased Ub-PA reactivity respectively. Clustering analysis, using an average linkage method coupled with a Pearson correlation, identified six groups of co-regulated DUBs. **B:** Line graphs for each cluster; grey lines represent Ub-PA reactivity for individual DUBs, the red line illustrates the cluster average.

Cluster 5, comprised of the Otubains OTUD5 and VCPIP1, exhibited a modest peak in activity at Late S, followed by decreased reactivity to Ub-PA at G_2/M and G_1 (mean of approximately 1.5-fold and 1.8-fold decrease respectively). Finally, USP8 the sole member of Cluster 6, displayed a peak of activity during mitosis; this profile agrees with its previously identified mitotic functions (Mizuno et al., 2007; Mukai et al., 2008).

There are a number of factors that can regulate DUB activity. One of the more fundamental aspects that can regulate catalytic activity is protein structure. This encompasses both the architecture of the catalytic domain and accessory protein domains, both of which may modulate DUB activity at an intramolecular level. This is exemplified by USP5, where an intrinsic ZnF domain binds to the catalytic core of USP5 increasing its activity (Avvakumov et al., 2012). To investigate whether intramolecular factors could regulate DUB activity throughout cell cycle progression, I analysed the proteomic data from the Ub-PA screen to identify any co-regulated activity for structurally similar DUBs.

4.3.4.1 DUB families

A distinguishing feature of any DUB is the architecture of its catalytic domain. Catalytic domains are highly conserved within each DUB family and have been used to study similarities between DUBs in phylogenetic analyses (Clague et al., 2013). Using the proteomic Ub-PA reactivity data, I collated reactivity profiles for three of the six DUB families: OTUs, UCHs and USPs. The relative proportion of each family identified using Ub-PA pull down is graphically represented in Figure 4.8A. With 56 members, the USPs are the largest DUB family. Fifteen

USPs were identified here giving approximately 27% coverage of the family (Figure 4.8A). However, the coverage increased to ~41% when considering only those DUBs previously identified in A549 cells by MS (Figure 4.8B)(Geiger et al., 2012). A third of the 15 OTUs were identified in this screen (Figure 4.8A). Only 6 of the 15 OTU family members were previously identified in A549 cells (Geiger et al., 2012) suggesting that OTUs, with the exception of OTUB1, are poorly expressed or poorly detected by MS in A549 cells. Of the five OTU family members, three were also identified in the A549 proteome study (Geiger et al., 2012). Interestingly, two OTUs were isolated by sepharose-Ub-PA pull down that were not previously identified by whole A549 proteome analysis (Figure 4.8B). There are only four members in the UCH DUB family; 3 of the 4 UCHs were profiled in this screen with BAP1 being the sole member not identified (Figure 4.8A and B).

To investigate whether DUBs within the same family, with conserved catalytic domains, exhibited similar Ub-PA reactivity during the cell cycle, I performed independent hierarchal clustering of the protein ratios for the OTU, UCH and USP DUB families (Figure 4.8C). The five members of the OTU family identified in this screen exhibited distinct activity profiles (Figure 4.8C). Interestingly, phylogenetic analysis revealed that these five OTUs shared a low sequence similarity (Figure 4.9B and reviewed in (Clague et al., 2013)).

The three members of the UCH family, UCHL1, UCHL3 and UCHL5, exhibited divergent activity profiles (Figure 4.8C). Interestingly, UCHL1 and UCHL3, the most similar UCHs (Figure 4.9A), were grouped after clustering analysis. Although their reactivity profiles differed in S phase, both exhibited increased activity at G_2/M and in early G_1. In contrast, UCHL3 and UCHL5 displayed inverse reactivity to Ub-PA during S-phase and mitosis.

The USP family, though larger and more diverse, exhibited distinct groups of co-regulated DUBs (Figure 4.8C). The largest cluster of USPs comprises DUBs from Figure 4.7, Cluster 4. In addition to this group, three pairs of USPs were also seen to be co-regulated: USP4 with USP15, USP9X with USP24 and USP40 with USP47 and will be discussed in more detail in Section 4.3.4.2.

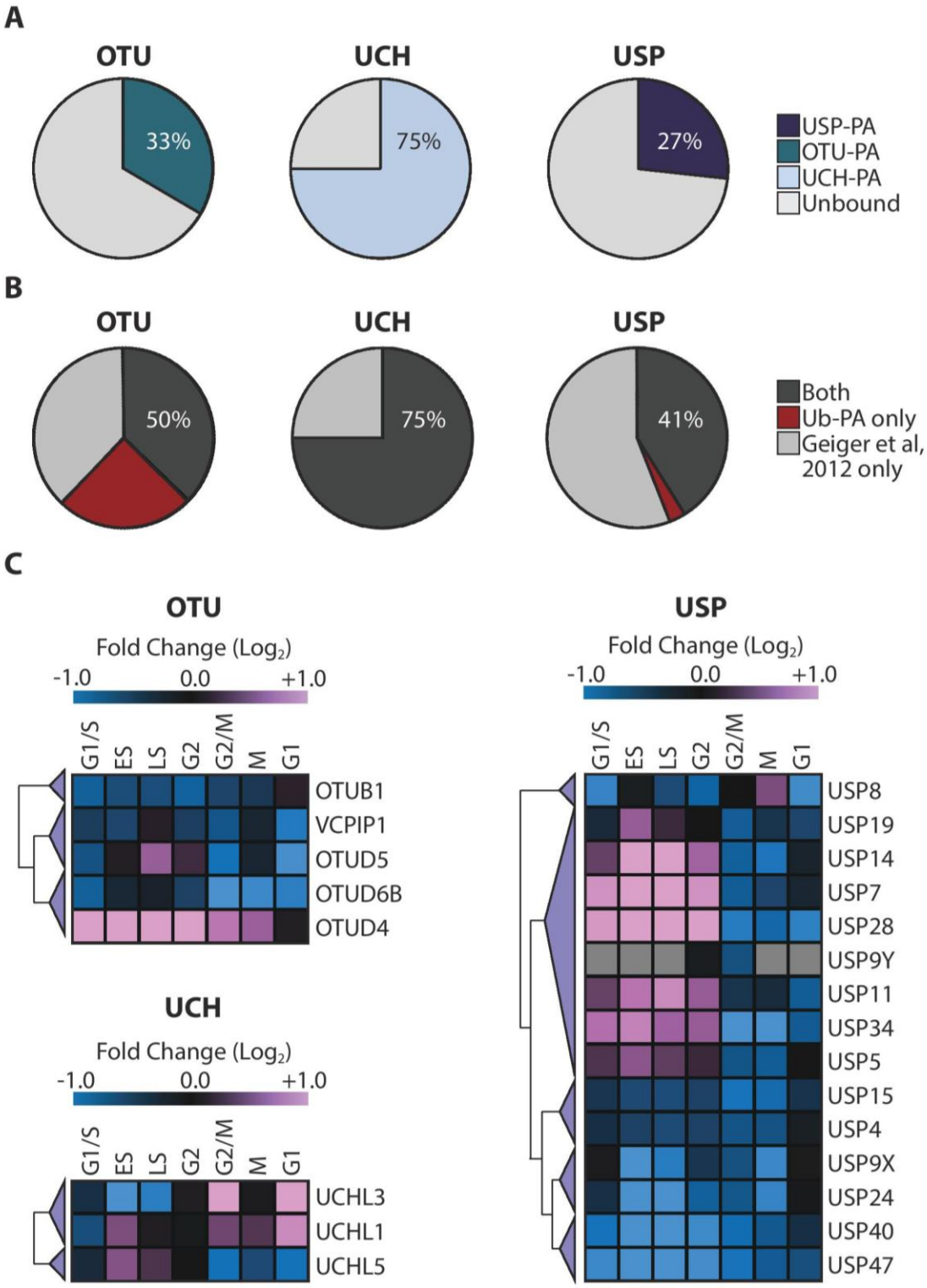

Figure 4.8: DUBs from three cysteine protease families were identified using sepharose-Ub-PA pull down.

A: Pie charts illustrate the proportion of DUBs bound by sepharose-Ub-PA for OTU, UCH and USP families. The percentage of Ub-PA bound DUBs are shown in coloured sections. **B:** Pie charts relate Ub-PA binding to previous mass spectrometry expression data (Geiger et al., 2012) for each of the OTU, UCH and USP families: dark grey sections represent the DUBs identified in both proteomic datasets, light grey sections represent DUBs from Geiger dataset that did not react with sepharose-Ub-PA, red sections illustrate the DUB identified using sepharose-Ub-PA pull down

that were not observed in the Geiger dataset. Numbers indicate the DUBs bound by sepharose-Ub-PA as a percentage of those that were previously identified by (Geiger et al., 2012). **C:** Heatmap of differential DUB activity for OTU, UCH and USP families. Data for each family were subjected to hierarchical clustering, using the average linkage method coupled with a Pearson correlation, to identify co-regulated DUBs in each family.

4.3.4.2 USP Paralogs

DUB reactivity to Ub-PA was divergent within DUB families (Figure 4.8). Although DUB families share a conserved catalytic domain, there can still be variations within catalytic domain structure between familial DUBs. Furthermore, there are a plethora of accessory domains that affect DUB activity, localisation and protein-protein interactions (Clague et al., 2013). Within each DUB family, there are frequent examples of DUB paralogs; these are DUBs that are genetically similar to each other and so share a high amino acid sequence similarity. To investigate whether DUB paralogs exhibited similar reactivity profiles, I extracted Ub-PA reactivity data from the cell cycle screen to compare activity profiles for genetically similar DUBs. I gathered data from an in-depth phylogenetic analysis of DUBs, which specifically compared the similarity of DUB catalytic domains (Clague et al., 2013). Phylogenetic trees for UCH, OTU and USP DUB families are represented in Figure 4.9A, B and C respectively based on the findings from that study.

Intriguingly, when studying the Ub-PA reactivity profiles for the USP family, it became apparent that all the 15 detected USPs belonged to two specific groups of related USPs (Figure 4.9C and (Clague et al., 2013)). The USP family harbours a number of DUB paralogs, those that were detected in Ub-PA screen are depicted in Figure 4.9D-F. USP15 is closely related to USP4 and USP11; sharing 71% sequence similarity with USP4 and 60% with USP11 (Faronato, 2011). As illustrated in Figure 4.9D, they share a split C-terminal USP domain, containing the catalytic triad, an N-terminal DUSP domain that is important for protein-protein interactions and two UBL domains, which can modulate activity by promoting ubiquitin exchange (Clerici et al., 2014; de Jong et al., 2006; Faronato, 2011; Harper et al., 2011). The two more closely related DUBs, USP15 and USP4, showed analogous Ub-PA reactivity throughout the cell cycle. In contrast, USP11, the less similar protein, had a contrasting profile with higher Ub-PA reactivity during S-phase (Figure 4.9D).

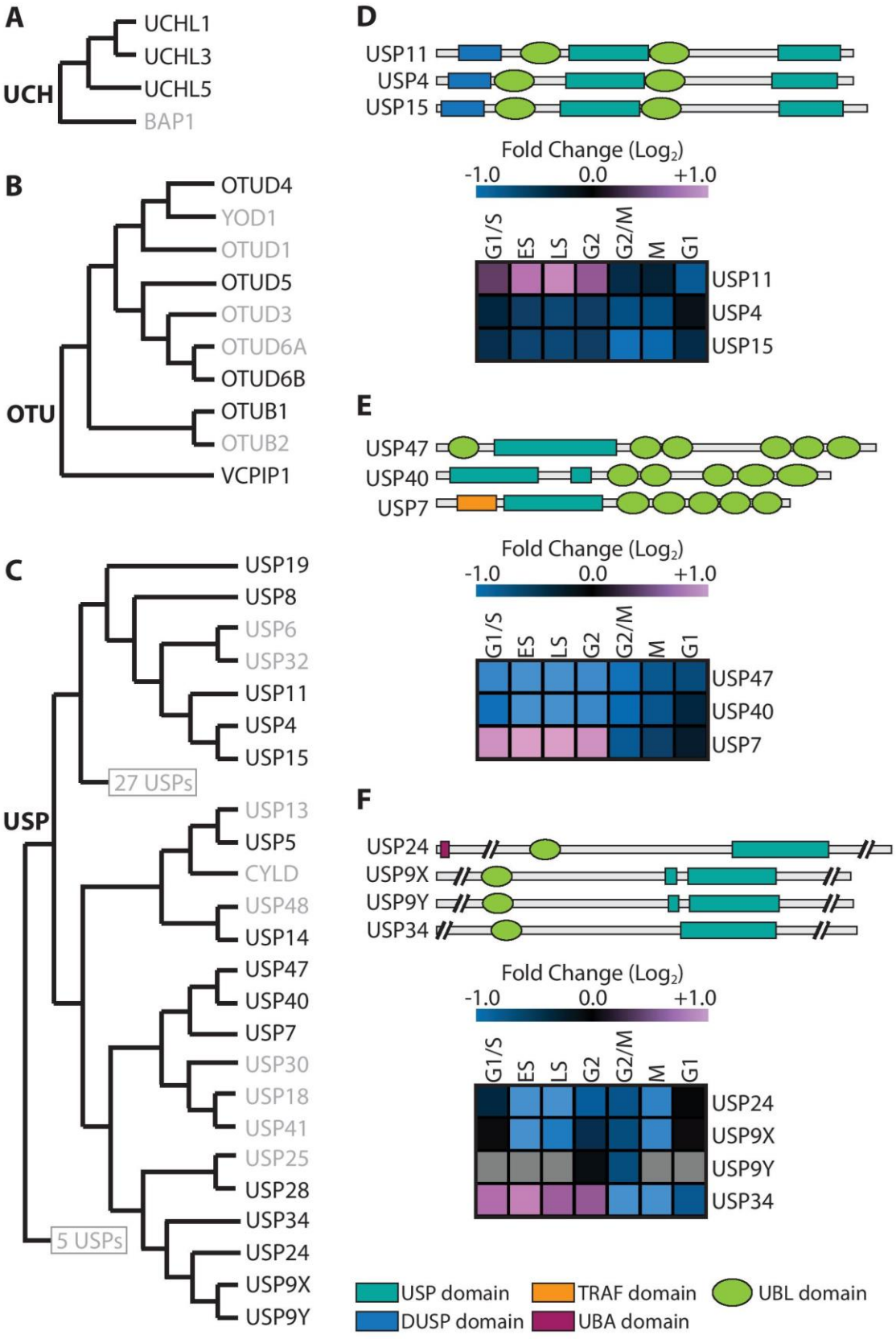

Figure 4.9: USP paralogs exhibited co-regulation through cell cycle progression.

Figure 4.9: USP paralogs exhibited co-regulation through cell cycle progression.

A-C: Phylogenetic analyses for UCH (A), OTU (B) and USP (C) DUB families based on their catalytic domains (adapted from (Clague et al., 2013)). Grey text represents DUBs not identified in Ub-PA proteomic screen. **D-F:** Hierarchal clustering of Ub-PA reactivity profiles for three groups of USP paralogs. Schematics of DUBs illustrate their domain structures. **D:** USP15, USP4 and USP11 **E:** USP40, USP47 and USP7 **F:** USP9X, USP9Y, USP24 and USP34, // represents >300 hidden amino acids.

USP40, USP47 and USP7 are a second group of genetically similar USPs: USP40 sharing amino acid sequence similarity of 53% with USP47 and 40% with USP7. Like all USPs, they contain a conserved catalytic domain, however in USP40 this USP domain contains an ~100aa insertion (Figure 4.9E). These paralogs share a string of five UBL domains in their C-terminal region. For USP7 these UBL domains have been shown to affect catalytic activity (Faesen et al., 2011a), although this has not been confirmed for USP40 or USP47. USP40 and USP47 exhibited similar activity profiles, with substantially decreased reactivity to Ub-PA during S-phase compared to asynchronous cells. Conversely, USP7 displayed a higher reactivity to Ub-PA at S-phase, prior to the decreased mitotic activity observed for all 3 paralogs (Figure 4.9E).

USP24, USP34, USP9X and USP9Y are another group of closely related USPs. USP9X shares sequence similarity of 95% with USP9Y, 63% with USP24 and 52% with USP34. They are the largest DUBs expressed in A549 cells, each containing a UBL domain upstream of the C-terminal catalytic USP domain. Like USP40, USP9X and USP9Y both contain short inserts (approximately 30 amino acids) within the USP domain (Figure 4.9F). USP24 and USP9X exhibit low reactivity to Ub-PA during S-phase, G_2 and mitosis with higher activity only at G_1 and G_1/S. Only G_2 and G_2/M reactivity data was obtained for USP9Y, again there was a concurrent decrease in mitotic reactivity to Ub-PA compared to asynchronous cells. Similarly, a low mitotic reactivity was observed for USP34, however, USP34 was the only DUB within this genetically similar group to exhibit high Ub-PA reactivity throughout S-phase (Figure 4.9F).

Within each group of paralogs, Ub-PA reactivity tracked most tightly through the cell cycle for the most closely related DUBs. Within each group, the one DUB that was least homologous did not conform to the collective activity profile: USP11 (Figure 4.9D), USP7 (Figure 4.9E) and USP34 (Figure 4.9F). Interestingly, each of these DUBs displayed the oscillatory reactivity profile seen in Figure 4.7, Cluster 4 suggesting that their activity, rather than being regulated by intramolecular factors, could be mediated through different mechanisms. Further layers of DUB regulation come from external factors; including sub-cellular localisation, allosteric protein interactions, substrate binding and PTMs. This has been discussed in Section 1.3.2 and comprehensively reviewed in (Sahtoe and Sixma, 2015). I wanted to investigate whether any of these factors could regulate this dynamic co-regulation of Ub-PA reactivity throughout the cell cycle.

4.3.4.3 DUB localisation

Structural similarity could not completely account for the co-regulation of DUB activity identified in Figure 4.7. One external factor that could affect DUB activity is subcellular localisation. There are several examples where regulated localisation modulates DUB activity towards specific target proteins. For example, BAP1 and USP8 had decreased activity towards known substrates when they are sequestered away from their usual subcellular compartment (Mashtalir et al., 2014; Mizuno et al., 2007). To ask whether DUBs that share subcellular compartmentalisation may be co-regulated during cell cycle progression, I grouped DUBs based upon their localisation within the cell (Urbe et al., 2012) and their Ub-PA reactivity. A recent global screen characterised the localisation of sixty-six exogenously expressed GFP-tagged DUBs. Using this data I assigned DUBs identified in my screen to five broad sub-cellular categories: nuclear, predominantly nuclear, cytoplasmic, predominantly cytoplasmic, and those DUBs with equivalent expression across both compartments (Figure 4.10A).

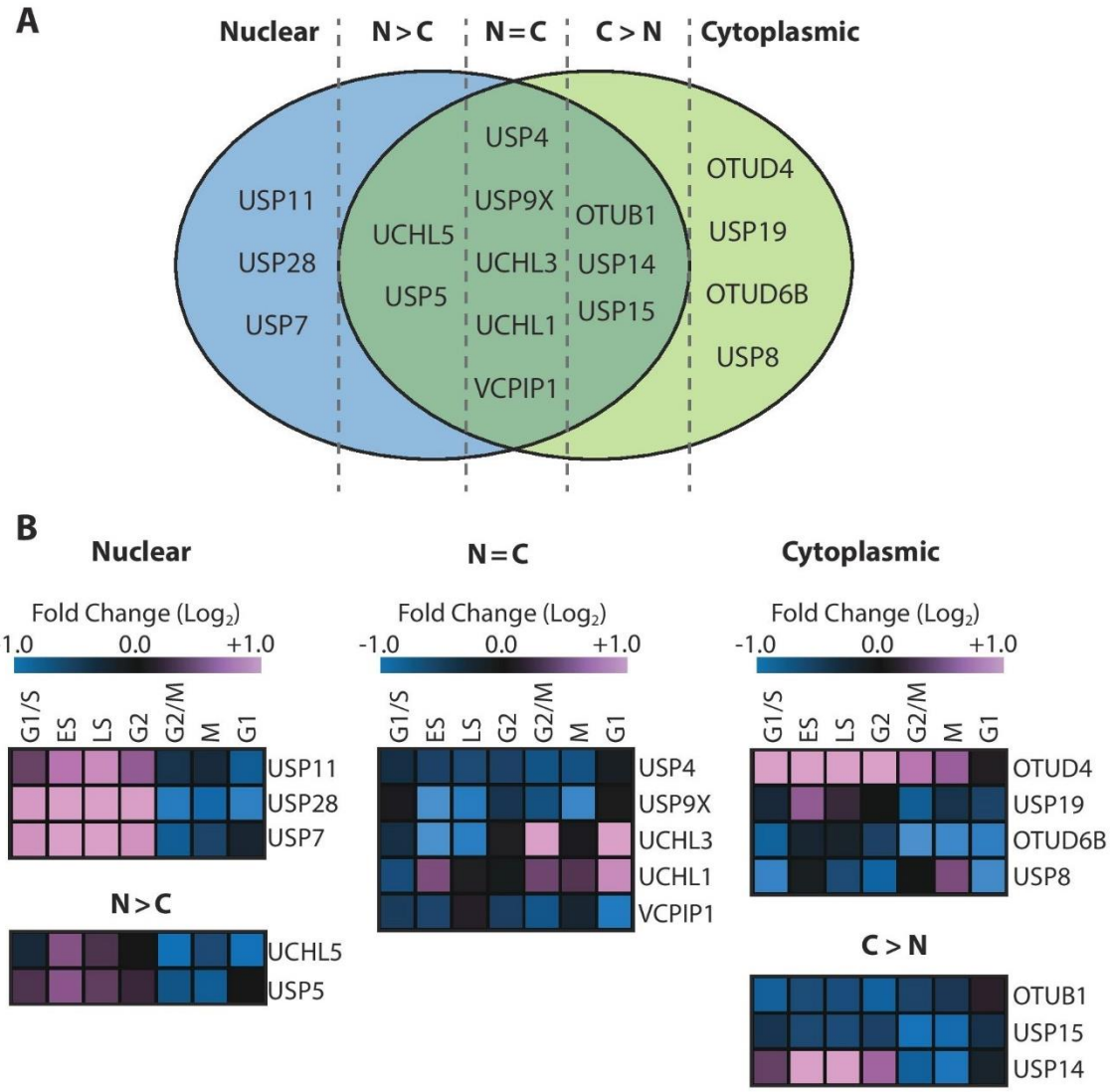

Figure 4.10: Nuclear, but not cytoplasmic, DUBs exhibited analogous reactivity to Ub-PA in synchronised A549 cells.

A: Venn diagram representing the subcellular distribution of DUBs based on (Urbe et al., 2012): Nuclear DUBs within the blue circle, cytoplasmic DUBs within the pale green circle. DUBs expressed in both subcellular compartments were further categorised in to five groups, separated by dashed grey lines: nuclear, predominantly nuclear (N>C), equivalent distribution (N=C), predominantly cytoplasmic (N<C), and cytoplasmic. **B:** Differential Ub-PA reactivity profiles for predominantly nuclear, equally distributed and predominantly cytoplasmic DUBs were illustrated in heatmaps. Hierarchical clustering was used to identify any co-regulated DUBs.

Interestingly, the predominantly nuclear DUBs displayed a high level of co-regulation during the cell cycle, with increased Ub-PA reactivity at S-phase followed by a decrease in reactivity during cell division (Figure 4.10B, left panel). Conversely, none of the DUBs that are equally expressed in both compartments exhibited comparable Ub-PA reactivity profiles throughout cell cycle progression (Figure 4.10B, middle panel). Furthermore, dissimilar Ub-PA reactivity profiles were observed for the predominantly cytoplasmic DUBs (Figure 4.10B, right panel). Taken together these data indicate that the catalytic activity of cytoplasmic DUBs was not temporally regulated through the cell cycle. In contrast, nuclear DUBs exhibited a high level of co-regulation, all displaying a striking reduction in reactivity to Ub-PA as the cells entered mitosis. Therefore, when the nuclear envelope dissolves in pro-metaphase and these nuclear DUBs are no longer spatially restricted, their activity decreases.

4.3.4.4 Interacting DUBs

Intermolecular protein-protein interactions are known to regulate DUB function. For example, UCHL5 interaction with DEUBAD domains within known allosteric regulators ADRM1 and INO80G can activate or inhibit UCHL5 activity in a context-dependent manner (Sahtoe et al., 2015). As neither intramolecular factors nor sub-cellular localisation could entirely account for the level of co-regulated DUB activity observed in Figure 4.7, I investigated whether there was co-regulation of interacting DUBs during the cell cycle. Interacting DUBs could be components of the same signalling pathway or bound in the same protein complex. This pathway/complex could have specific cellular functions and therefore could account for the co-regulated DUB activity identified throughout the cell cycle (Figure 4.7). One pioneering study defined the DUB interactome through an affinity-capture-MS approach to map proteins that interacted with 75 exogenously expressed DUBs (Sowa et al., 2009). A number of DUBs identified by Ub-PA pull down here, had been shown to interact with each other in that study. To investigate whether these interacting DUBs exhibited similar activity profiles, I compared their Ub-PA reactivity (Figure 4.11).

UCHL5 and USP14 are two of the three DUBs associated with the 19S regulatory subunit of the proteasome. The third, PSMD14, belongs to the JAMM family and

so does not bind to the Ub-PA probe. A number of interacting proteins, identified from UCHL5 pull down (Sowa et al., 2009), are illustrated in Figure 4.11A. Comparison of UCHL5 and USP14 reactivity to Ub-PA through the cell cycle revealed co-regulation (Figure 4.11A). They both exhibited the characteristic oscillatory binding profile attributed to Cluster 4 in Figure 4.7, suggesting that the deubiquitylating activity of the 19S subunit of the proteasome was upregulated during S-phase and subsequently downregulated during mitosis.

USP7 is one of the most highly connected DUBs with over 300 interacting proteins, some of which are important in cell cycle progression (BioGRID, 2016b). An abridged set of USP7 interactors is summarised in Figure 4.11B (BioGRID, 2016b; Sowa et al., 2009). Three other DUBs from my dataset were identified as USP7 interactors: USP11, USP14 and USP19. Interestingly, each exhibited similar Ub-PA reactivity throughout cell cycle progression with higher reactivity during S-phase and lower reactivity at mitosis (Figure 4.11B), despite being localised to different sub-cellular compartments (Figure 4.10). Approximately 30% of all identified OTUB1 interactors are components of the UPS (BioGRID, 2016a). Selecting for these UPS components, a simplified interaction map for OTUB1 is illustrated in Figure 4.11C. This includes two DUBs from my cell cycle dataset: USP8 and OTUD6B. However, these DUBs did not exhibit co-regulation during the cell cycle (Figure 4.11C).

4.3.4.5 Ubiquitin chain linkage specificities

DUBs can also be categorised based upon their affinity for different ubiquitin chain types. Ubiquitin monomers are conjugated to K residues within proteins. As discussed in Section 1.1.5 there are seven internal K residues within the ubiquitin peptide sequence enabling ubiquitin polymerisation on these seven residues (K6, K11, K27, K29, K33, K48 and K63) and M1 to produce ubiquitin chains. Linkage specific polyubiquitin chains regulate a diverse range of cellular functions, summarised in Figure 4.12A (Heride et al., 2014; Swatek and Komander, 2016; Ye and Rape, 2009).

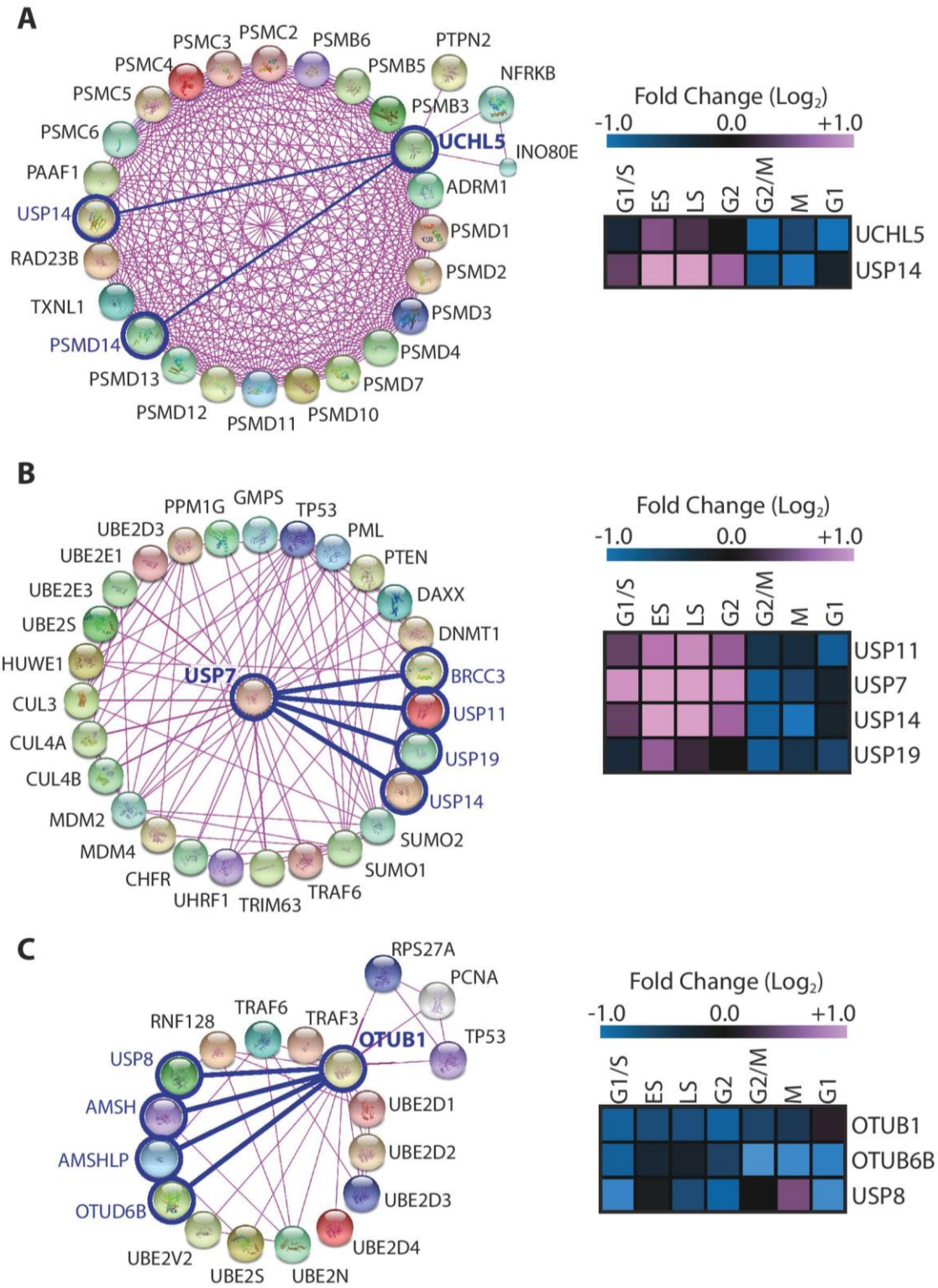

Figure 4.11: Proteasomal deubiquitylase activity was downregulated as cells entered mitosis.

Interaction maps for proteins identified by UCHL5 **(A)**, USP7 **(B)** or OTUB1 pull downs **(C)** (BioGRID, 2016a, b; Sowa et al., 2009). STRING network diagrams depict interactions within other UPS-associated proteins (left). Dark blue lines highlight interactions with other DUBs. Ub-PA reactivity profiles for DUBs within this network were represented in a heatmap (right). Profiles within this network were subjected to hierarchical clustering to identify any co-regulated Ub-reactivity throughout the cell cycle.

I was interested to see whether DUBs that shared chain linkage specificities or preferences would exhibit similar Ub-PA reactivity profiles during the cell cycle. To address this, I collated data from three studies that analysed the ubiquitin chain linkage specificities of OTUs (Mevissen et al., 2013), USPs (Faesen et al., 2011b) and a more global profile of the DUBome (Ritorto et al., 2014). The global screen analysed the activity of forty-two DUBs towards diubiquitin topoisomers by MALDI-TOF-mass spectrometry, whereas the investigations of OTU and USP families used a more classical approach, examining DUB activity through di-ubiquitin cleavage assays.

Only two DUBs within the Ub-PA dataset are restricted to cleavage of specific ubiquitin chain linkages, OTUB1 and OTUD4, which only cleave K48-linked ubiquitin chains (Mevissen et al., 2013; Ritorto et al., 2014). Both of these DUBs exhibited similar Ub-PA reactivity in G_1 sample compared to that in asynchronous cells, but for the rest of the cell cycle they are divergent with OTUB1 exhibiting low reactivity and OTUD4 exhibiting high reactivity to Ub-PA (Figure 4.12B).

One ubiquitin chain linkage of interest with respect to cell cycle progression is K11. As discussed in Section 1.5.3.2, the APC/C is a key regulator of mitotic progression. It has the capacity to assemble K11 and K48-linked chains (Wu et al., 2010). It tags target proteins with K11-linked chains, which acts as a signal for their K48-linked polyubiquitylation and subsequent degradation via the proteasome (Grice et al., 2015; Min et al., 2015). Numerous DUBs within the OTU and USP families can cleave K11-linked chains (Faesen et al., 2011b; Mevissen et al., 2013; Ritorto et al., 2014).

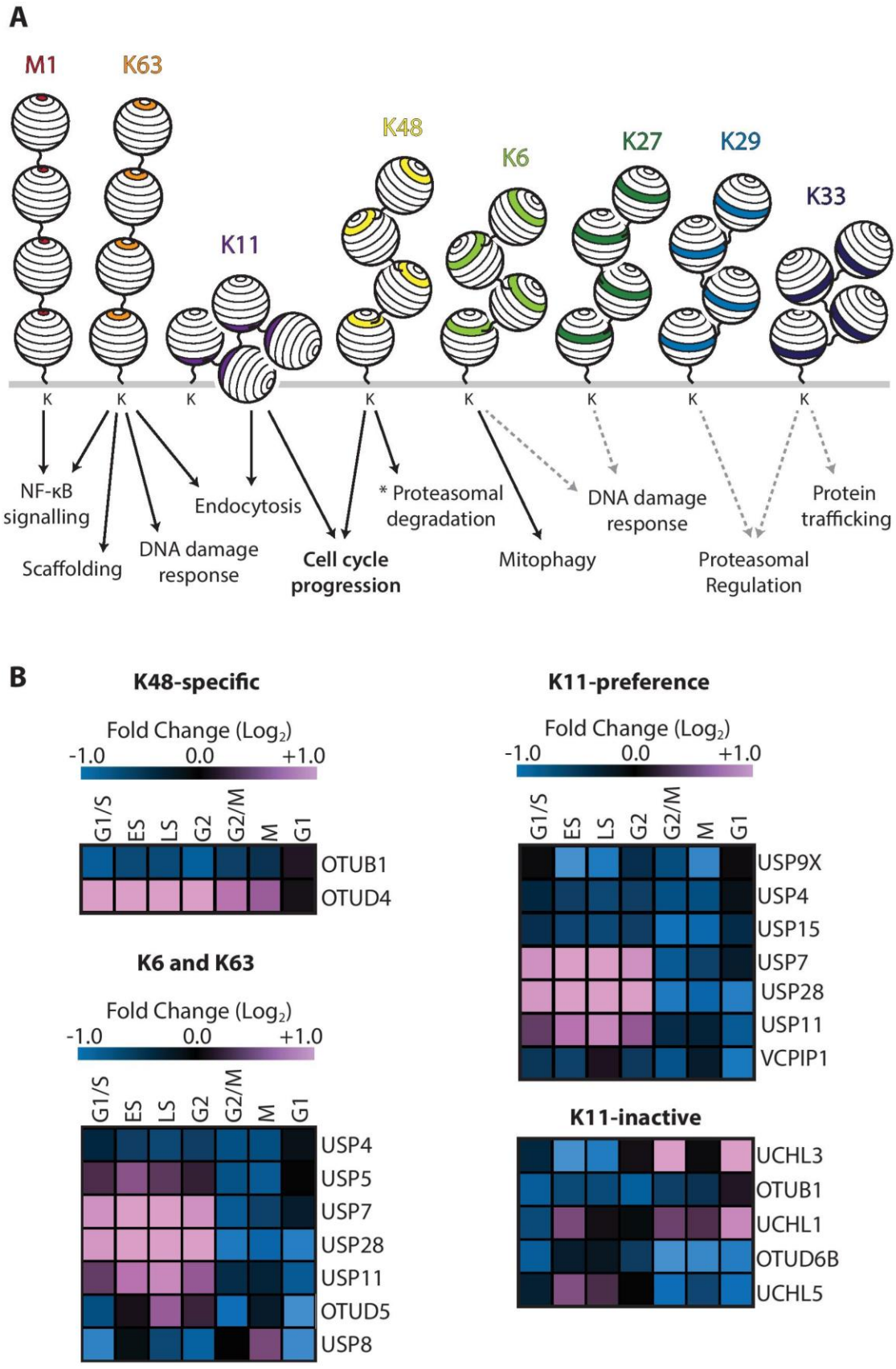

Figure 4.12: DUBs harbouring a cleavage preference for K11-linked ubiquitin chains were downregulated during cell division.

Figure 4.12: DUBs harbouring a cleavage preference for K11-linked ubiquitin chains were downregulated during cell division.

A: Schematic representing the eight possible ubiquitin chain types and their associated function in cells adapted from (Swatek and Komander, 2016; Ye and Rape, 2009). **B:** DUB activity profiles with known preferences to ubiquitin chain types were represented in heatmaps: K48-linked chains, K11-linked chains, K6-linked and K63-linked chains. Profiles within this network were subjected to hierarchical clustering to identify any co-regulation during cell cycle progression.

I wanted to investigate whether DUBs that cleave K11-linked chains shared a cell cycle-specific activity profile, particularly at mitosis. Seven DUBs within my dataset have a primary or secondary preference for K11-linked: USP4, USP7, USP9X, USP11, USP15, USP28 and VCPIP1 (Faesen et al., 2011b; Mevissen et al., 2013; Ritorto et al., 2014). There was a decreased Ub-PA reactivity for all seven DUBs during mitosis, although their activity profiles were more divergent during S-phase (Figure 4.12B). This may suggest that a temporal downregulation of DUBs with K11-linkage specificity could be required to ensure progression through mitosis.

To further this line of investigation, I decided to examine whether DUBs that are not able to cleave K11-linked ubiquitin chains were similarly regulated during cell division. USPs are a promiscuous family of DUBs and so none of the USPs identified from my screen were inactive towards K11-linked chains (Faesen et al., 2011b; Ritorto et al., 2014). In contrast, UCHs did not exhibit any reactivity towards K11-linked chains from the global screen (Ritorto et al., 2014) and OTU activity profiling revealed that OTUB1 and OTUD6B were also inactive towards K11-linked diubiquitin (Mevissen et al., 2013). Comparing the Ub-PA reactivity profiles of these five DUBs revealed less stringent co-regulation during mitosis, with further disparity at each stage of the cell cycle (Figure 4.12B).

The Ub-PA proteomic screen also exposed a high level of co-regulation during S-phase, with DUBs in cluster 4 exhibiting increased reactivity to Ub-PA relative to the asynchronous control (Figure 4.7). A number of these DUBs are known to regulate DNA damage response pathways. Certain ubiquitin chain linkages are prevalent in DNA damage responses (K6, K27 and K63) (Gatti et al., 2015; Morris

and Solomon, 2004; Schwertman et al., 2016; Wu-Baer et al., 2003) and so I wondered whether DUBs with preferences for these DNA damage-associated ubiquitin chains would exhibit co-regulation. Only one OTU exhibited a primary preference for K63-linked chains, OTUD5 (Mevissen et al., 2013), conversely a number of USPs within my dataset have a primary or secondary preference for K63-linked chains, USP4, USP5, USP7, USP8, USP11 and USP28 (Faesen et al., 2011b; Ritorto et al., 2014). The USP focussed study also saw that USP4, USP7, USP8 and USP11 were able to cleave K6 and K27-linked ubiquitin dimers (Faesen et al., 2011b). Interestingly, five of these seven DUB possessed high reactivity to Ub-PA during S-phase, with only USP4 and USP8 exhibiting decreased Ub-PA reactivity compared to the asynchronous control.

4.3.5 DUBs exhibited dynamic changes in phosphorylation status in a cell cycle-dependent manner

Phosphorylation plays a key role in cell cycle progression and is highly influential in regulating enzyme function. DUBs are not exempt from this. Large-scale phospho-proteomic studies have analysed global changes in protein phosphorylation at each stage of the cell cycle (Olsen et al., 2010). High-resolution MS-based proteomics, coupled with SILAC, was employed to investigate proteome and phospho-proteome dynamics in synchronised HeLa cells. Temporally regulated phospho-peptides were identified and analysed compared to an asynchronous control for relative quantification across the cell cycle (Olsen et al., 2010). Phospho-proteome data from this global study was made publicly available via the "Phosphorylation Site Database" (PHOSIDA) (Gnad et al., 2011). To investigate whether DUB phosphorylation is temporally regulated, I collated all cell cycle-specific data pertaining to DUBs from the Olsen dataset. A complete list of these data is available in Appendix Table 4.

Only sixteen of the twenty-three DUBs identified in the Ub-PA screen were also represented in the Olsen dataset. I extracted phosphorylation data for these sixteen DUBs and performed hierarchal clustering analysis, which is represented as a heat map in Figure 4.13A. To gain an overview of the overall phosphorylation profile of these DUBs through the cell cycle, I plotted data for

each phospho-residue identified on a line graph (Figure 4.13B). The centroid trace (red line), illustrates the overall trends in phosphorylation during cell cycle progression. Overall, relative to asynchronous cells, there was a ~3-fold decrease in phosphorylation during Early S-phase, mirrored by an ~3-fold increase during mitosis, for these DUBs.

The hierarchical analysis identified 5 clusters that exhibited similar trends in phosphorylation and 5 individual phospho-peptides with unique phosphorylation profiles throughout cell cycle progression. The five clusters are graphically represented in Figure 4.13C. Phospho-residues within DUBs in Cluster 2 exhibited decreased phosphorylation at the G_1/S transition coupled with a modest increase in phosphorylation during G_2. The inverse of this was observed for phospho-sites in Cluster 7. Phospho-residues in Cluster 8 underwent dynamic changes in phosphorylation during cell cycle progression; an ~8-fold decrease (centroid trace) in phosphorylation during Early S is reversed in mitosis with an equally large increase in phosphorylation. A similar profile was observed for residues in Cluster 9. There was a prolonged decrease in phosphorylation from S-phase to G_2, then increased mitotic phosphorylation extending into early G_1. In contrast, Cluster 10 exhibited only a moderate decrease in phosphorylation during Late S-phase, coupled with a modest increase in phosphorylation as the cells entered G_1.

Some DUBs were heavily phosphorylated during cell cycle progression. USP8 has the most phospho-sites of all the DUBs in this dataset; it harbours nine differentially phosphorylated residues that associate with five different clusters. Conversely, only one phospho-peptide was identified for UCHL1, which only exhibited negligible changes in phosphorylation and so does not appear to be cell cycle regulated (Figure 4.13A, Cluster 10 and Appendix Table 4).

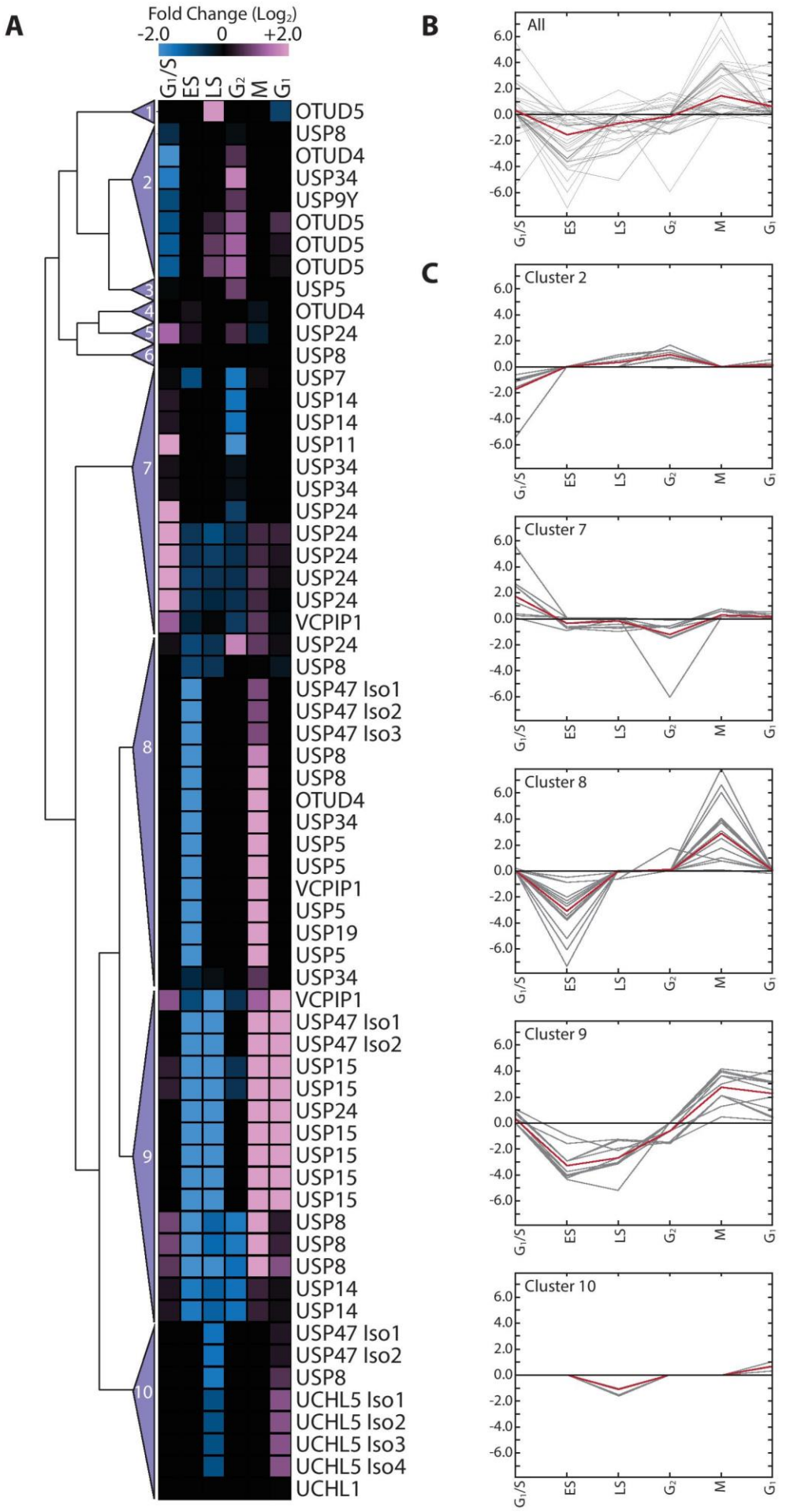
A
Fold Change (Log2)
-2.0
0
+2.0
G1/S
ES
LS
G2
M
G1
OTUD5
USP8
OTUD4
USP34
USP9Y
OTUD5
OTUD5
OTUD5
USP5
OTUD4
USP24
USP8
USP7
USP14
USP14
USP11
USP34
USP34
USP24
USP24
USP24
USP24
USP24
VCPIP1
USP24
USP8
USP47 Iso1
USP47 Iso2
USP47 Iso3
USP8
USP8
OTUD4
USP34
USP5
USP5
VCPIP1
USP5
USP19
USP5
USP34
VCPIP1
USP47 Iso1
USP47 Iso2
USP15
USP15
USP24
USP15
USP15
USP15
USP15
USP8
USP8
USP8
USP14
USP14
USP47 Iso1
USP47 Iso2
USP8
UCHL5 Iso1
UCHL5 Iso2
UCHL5 Iso3
UCHL5 Iso4
UCHL1
1
2
3
4
5
6
7
8
9
10
B
All
C
Cluster 2
Cluster 7
Cluster 8
Cluster 9
Cluster 10
6.0
4.0
2.0
0.0
-2.0
-4.0
-6.0

Figure 4.13: Identified DUBs exhibit dynamic changes in phosphorylation during the cell cycle.
Data for Ub-PA reactive DUBs was extracted from the cell cycle phospho-proteome of HeLa cells on the PHOSIDA database (Olsen et al., 2010). DUBs harbouring phospho-residues that were temporally phosphorylated were collated and subjected to hierarchical clustering. **A:** Differential phosphorylation was illustrated as a heatmap using a Log_2 colour scale to represent changes in phosphorylation relative to an asynchronous control. Clustering analysis identified 5 clusters of co-regulated phospho-sites and 5 individual phosphorylation profiles (average linkage method, Pearson correlation). Line graphs plotted changes in phosphorylation for all DUBs **(B)** or individual clusters **(C)**; grey lines represent the cell cycle phosphorylation profiles for individual phospho-residues, the red line illustrates the cluster average.

Phosphorylation can directly affect DUB activity; activating and inactivating phosphorylation events have been described for several DUBs, exemplified by OTUD5 and CYLD respectively. OTUD5 phosphorylation at S177 is essential for catalytic activity (Huang et al., 2012), whereas phosphorylation of CYLD at S148 decreased activity toward its substrate, NEMO (Reiley et al., 2005). In comparing Ub-PA reactivity with the Olsen phospho-proteome dataset, I noticed that there was often an inverse relationship between Ub-PA reactivity and phosphorylation particularly in mitotic extracts. There was a pervasive decrease in Ub-PA reactivity during M-phase (Figure 4.7A), yet phosphorylation increased for many DUB phospho-residues (Figure 4.13A). To identify whether DUB phospho-status correlated with activity, I compared phosphorylation data to Ub-PA reactivity data for individual DUBs at each phase of the cell cycle (Figure 4.14). I extracted phosphorylation data (Olsen et al., 2010) for all temporally regulated phospho-residues for the sixteen DUBs also identified in the Ub-PA screen. These values were subjected to hierarchal clustering analysis to identify co-regulated residues. DUBs were grouped according to clustered Ub-PA reactivity profiles (Figure 4.14).

One of the major inferences from the global phospho-proteome data was that the pervasive increase in mitotic phosphorylation was likely to be inhibitory (Olsen et al., 2010). Similarly, the inverse relationship between phosphorylation and Ub-PA reactivity data suggested that some phospho-residues may specifically inhibit DUB activity. This is best exemplified by USP15; there was little change in reactivity to Ub-PA during S-phase, yet a modest decrease in

activity was observed during mitosis. A number of phospho-peptides were identified for USP15 (Olsen et al., 2010), all exhibiting a substantial increase in mitotic phosphorylation (Figure 4.14C). Other potential examples of inhibitory phosphorylation events can be observed for UCHL5, USP5, USP19 and USP34 (Figure 4.14D). For these DUBs, mitotic and G_1 phosphorylation was coupled with S-phase dephosphorylation, with an inverse pattern in Ub-PA reactivity.

There are also examples potentially consistent with activating phosphorylation events for USP47 and OTUD5 (Figure 4.14B and E respectively). USP47 reactivity to Ub-PA was lowest during Early S phase and exhibited a modest increase as the cell entered mitosis. This pattern was mirrored by the phosphorylation status of all seven phospho-residues (Figure 4.14B). In contrast, only one of the four phospho-sites identified for OTUD5 (S450) correlated with its Ub-PA reactivity profile, exhibiting increased phosphorylation at S-phase coupled with a decrease in phosphorylation at G_1 (Figure 4.14E).

This correlative analysis of phosphorylation and activity also identified a number of potential priming phosphorylation events. A priming phosphorylation event provides a docking site for other proteins to interact and potentially regulate protein function. Potential priming phosphorylation events during the cell cycle were identified and underlined for USP5, USP7, USP9Y, USP11 and USP14 profiles (Figure 4.14D). All of these DUBs exhibited a significant decrease in reactivity to Ub-PA at the G_2/M boundary. In contrast, their phosphorylation status changed in G_2 samples (Figure 4.13, Cluster 7) preceding the decrease in DUB activity.

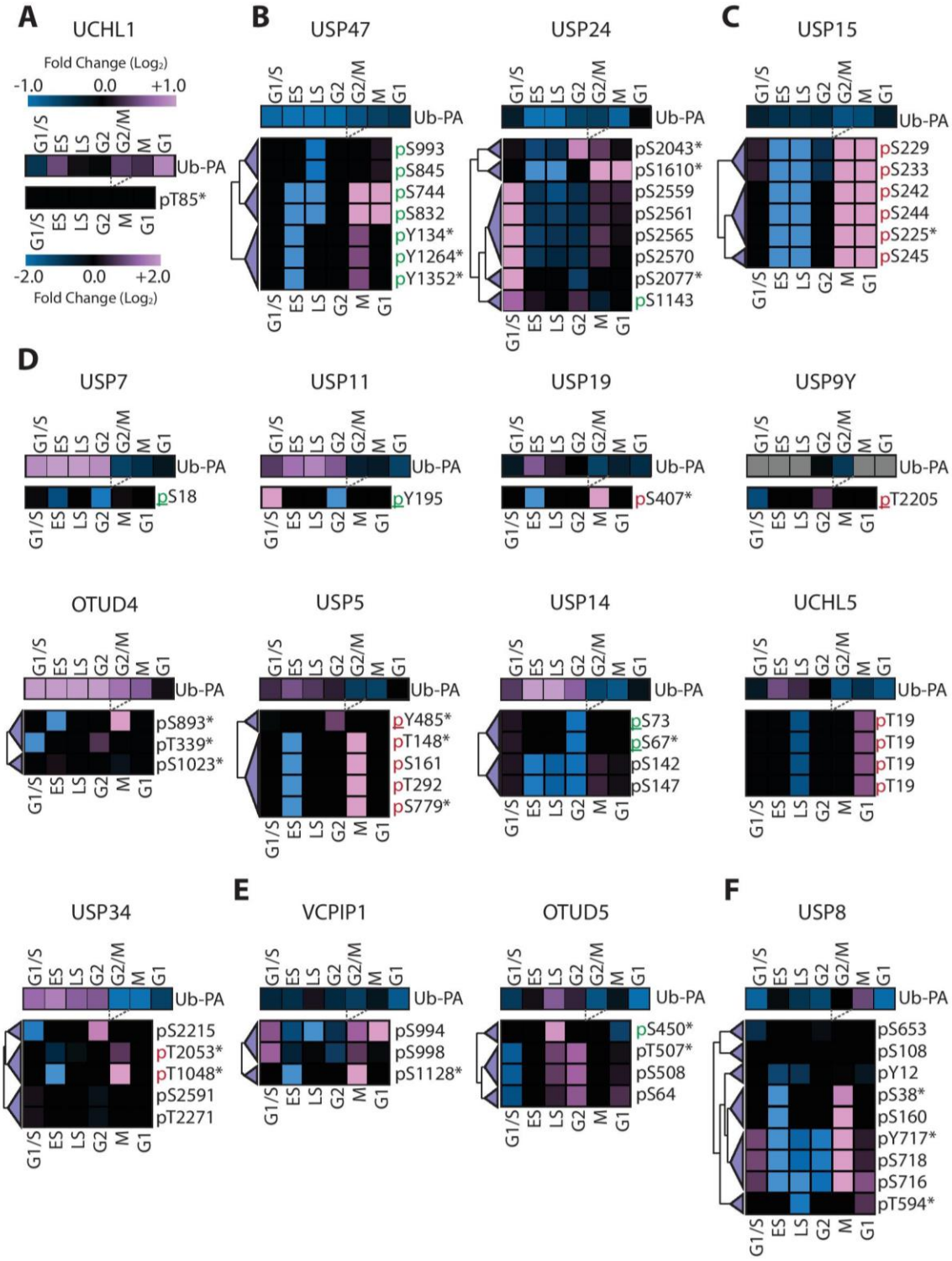

Figure 4.14: Comparative analysis of cell cycle-dependent Ub-PA reactivity and phosphorylation.

Ub-PA reactivity for individual DUBs was compared to their phosphorylation status at each stage of the cell cycle (Olsen et al., 2010), with the exception of G_2/M, which was not included in the Olsen dataset. Grey dashed lines show the exclusion of G_2/M data point within the phosphorylation heatmap. For each DUB, every residue exhibiting differential phosphorylation was compiled and subjected to hierarchical clustering to identify co-regulated residues. Log_2 scale bar illustrated in A applies to all data. DUBs were grouped by similar changes in Ub-PA reactivity as identified in Figure 4.7: Cluster 1 **(A)**, Cluster 2 **(B)**, Cluster 3 **(C)**, Cluster 4 **(D)**,

Cluster 5 **(E)** and Cluster 6 **(F)**. Phospho-residues in green (p) show positive correlation between Ub-PA reactivity and phosphorylation. Phospho-residues in red (p) show negative correlation. Underlined residues (p/p) illustrate a change in phosphorylation status that preceded a change in Ub-PA reactivity. Asterisks (*) were used to signify where phosphorylation data was linked to more than one phospho-residue within a phospho-peptide. The unabridged dataset can be found in Appendix Table 4.

In some cases, a DUBs phosphorylation status did not correlate to its Ub-PA reactivity profile during the cell cycle. Dynamic changes were observed in VCPIP1 phosphorylation status, yet there were only modest changes in Ub-PA reactivity (Figure 4.14E). This periodic phosphorylation could regulate other aspects of VCPIP1 function, including substrate interactions or subcellular localisation. A disparity between Ub-PA reactivity and phosphorylation was also observed for UCHL1, USP24, OTUD4 and USP8 (Figure 4.14A, B, D and F respectively) suggesting that other mechanisms were regulating DUB activity.

These data taken together suggest that DUB activity regulation throughout the cell cycle is a multi-layered and complex process. Both external and intramolecular factors play a role in governing DUB activity throughout cell cycle progression.

4.4 Discussion

In a process as dynamic and highly regulated as the cell cycle it was expected that some DUBs would exhibit differential reactivity towards the Ub-PA probe. However, it was surprising to identify large-scale co-regulation of DUB activity, with such substantial downregulation of activity at mitosis. To coordinate this, cells must employ a complex interplay of regulatory mechanisms. I will discuss possible cellular mechanisms at play, as well as comprehensively reviewing the Ub-PA reactivity data in Chapter 7.

Ub-PA proved to be an instrumental tool in profiling endogenous DUB activity. It possessed an unparalleled coverage of the cysteine protease DUBs (Abdul Rehman et al., 2016; Ekkebus et al., 2013; Mevissen et al., 2013), and in my

hands exhibited increased reactivity towards USPs, OTUs, UCHs and Josephins with faster binding kinetics than the Ub-VME probe (Figure 4.1). Cumulatively, this increased the recognition and retrieval of active DUBs, surpassing the benchmark set by Ub-VME in Chapter 3.

Three of the six DUB families were well represented in this activity screen; OTUs (33%), UCHs (75%) and USPs (27%) (Figure 4.8). Unfortunately, the Josephin, MINDY and JAMM families were not identified within this dataset. JAMMs, as metalloproteases, cannot bind to Ub-PA as explained in Section 3.1. It was disappointing not to identify any Josephins, as Ub-PA did bind efficiently to ATXN3 with prolonged *in vitro* incubation (Figure 4.1C). However, it should be noted that neither the Josephins nor MINDYs were identified in a previous A549 proteomic study (Geiger et al., 2012) suggesting that they are not highly expressed in this cell model, which may explain why they were not identified in this Ub-PA screen.

In addition to DUBs, sepharose-Ub-PA pull down identified 144 proteins that specifically interacted with Ub-PA or Ub-PA bound proteins (Figure 4.5), including 9 proteins associated with the UPS (Appendix Table 3.2). It was unsurprising that UPS-associated proteins were also identified in this global screen, as they also require a catalytic cysteine to mediate ubiquitin transfer along the E1-E2-E3 cascade. In fact, some of the studies that first pioneered activity-based profiling of endogenous proteins also identified other components of the UPS, most notably E3 ligase components (Altun et al., 2011).

As outlined in Section 4.2.1, the priority when designing the sepharose-Ub-PA screen was to increase the number of DUBs identified compared to the initial Ub-VME screen. I achieved this through prolonged Ub-PA incubation (3 hours) with cell lysates and ensured that the concentration of sepharose-Ub-PA would not limit the level of DUB binding. The optimum concentration to achieve this was a ratio of 16:1 sepharose-Ub-PA:protein (Figure 4.3). The lower concentration of 1.6:1 did limit the number of DUBs that could bind, with only

the four most abundantly expressed DUBs (Geiger et al., 2012) being identified here. Even using higher concentrations of Ub-PA probe in the reaction, Ub-PA still preferentially reacted with the higher abundance DUBs, with only two (USP10 and USP39) of the fifteen most abundant DUBs not binding to Ub-PA in my hands (Figure 4.3D). This could suggest that the activity of USP10 and USP39 is downregulated in A549 cells. In contrast, the Ub-PA screen isolated and identified three DUBs (OTUD4, OTUD6B and USP9Y) that had not previously been identified in this A549 MS-based proteome study (Geiger et al., 2012), suggesting that these DUBs may be more reactive than abundant in A549 cells.

There is one important consideration when analysing these Ub-PA reactivity profiles. The cell lysates were incubated with sepharose-Ub-PA for 3 hours, it is therefore likely that some DUBs, the more abundant and more reactive DUBs, will have bound to completion. This means that their cell cycle Ub-PA reactivity profile could be more reflective of their expression levels rather than cell cycle-dependent activity.

In summary, sepharose-Ub-PA, in conjunction with triplexed SILAC-MS, was successfully employed to profile DUB reactivity across seven cell cycle phases. Twenty-three DUBs were identified and most exhibited differential reactivity to Ub-PA, suggesting a high degree of regulated expression or activity throughout cell cycle progression. Further investigation into cell cycle-dependent DUB activity is required to understand the underlying mechanisms. I intend to independently validate and characterise the Ub-PA reactivity profiles seen in this chapter for a small selection of DUBs, ultimately focussing on USP7.

Chapter 5

Cell cycle periodicity of USP7 activity is mediated through protein abundance and S18 phosphorylation.

5.1 Introduction

USP7 is an extensively studied DUB with a plethora of roles within the cell, interestingly many of these have been linked to cell cycle progression. USP7 governs the G_1/S transition checkpoint, is integral during S-phase for many DNA damage response pathways and has also been found to have specific roles during mitosis. As a highly abundant DUB involved in a number of critically important signalling pathways, USP7 activity is carefully controlled through multiple mechanisms. For these reasons, I have decided to focus my investigation on the regulation of USP7 activity throughout the cell cycle.

USP7 regulates entry into the cell cycle through the G_1/S checkpoint by regulating Rb stability. Rb is targeted for proteasomal degradation by the E3 ligase MDM2. USP7 antagonises this polyubiquitylation, maintaining Rb levels and arresting the cells at G_1 until the checkpoint has been satisfied (Bhattacharya and Ghosh, 2014). USP7 has numerous roles in S-phase with links to DNA damage and repair pathways. The best characterised of which is its paradoxical relationship with the P53 and MDM2. USP7 directly stabilises P53 however depletion of USP7 resulted in an increase in P53 levels (Brooks et al., 2007). This was attributed to its preferential substrate MDM2 an E3 ligase that targets P53 for proteasomal degradation via K48-linked polyubiquitylation (Brooks et al., 2007). In normally cycling cells, P53 has a short half-life, a result of its continual polyubiquitylation by MDM2. During DNA damage, USP7 dissociates from MDM2 and upon binding with its allosteric activator GMPS preferentially stabilises P53 (Reddy et al., 2014). Recent studies have also linked USP7 to translesion DNA repair and DNA alkylation repair. (Zhao et al., 2015).

In addition to this, a number of roles have been identified for USP7 during mitosis. USP7, through its interactions with both the death domain-associated protein (DAXX) and BUB3, maintains genomic stability (Giovinazzi et al., 2013; Giovinazzi et al., 2014). DAXX interacts with USP7 specifically at mitosis and this increases USP7's activity towards the E3 ligase CHFR, stabilising CHFR levels throughout mitosis (Giovinazzi et al., 2013). Aurora A, a kinase essential for the correct maturation of the bi-polar spindle in mitosis, is a substrate for CHFR.

The temporal degradation of Aurora A prevents multipolar mitoses and subsequent genomic instability. Additionally, USP7 protects the cell from genomic instability though stabilising BUB3 levels (Giovinazzi et al., 2014). BUB3 is a key component of the mitotic spindle assembly checkpoint preventing the early onset of anaphase.

Intriguingly, USP7 exists in two conformations within the cell, one of which is severely catalytically impaired. Although the catalytic domain harbours the conserved USP fold, the residues comprising the catalytic triad are in a non-reactive conformation (Faesen et al., 2011a; Faesen et al., 2011b). The C-terminal domain of USP7 contains five UBL domains organised in a 2-1-2 conformation. The C-terminal di-UBL (UBL-45) is essential in activating USP7, increasing its activity ~100-fold. It relies upon an interaction between the C-terminus and a switching loop adjacent to the catalytic domain, inducing structural rearrangements and subsequent realignment of the catalytic triad into a reactive conformation (Faesen et al., 2011a). The metabolic enzyme GMPS can stabilise USP7 in this active conformation through its interaction with other UBL domains (UBL-123). In addition to this a more recent study by the same group has revealed that a linker helix between the catalytic domain and UBL-123 is essential in regulating USP7 activity in a charge-dependent manner (Kim et al., 2016). They have proposed that this is another possible site for allosteric regulation of USP7 activity.

Phosphorylation can also significantly modulate USP7 activity. Phosphorylation has been shown to regulate the activity of USP7 towards a number of substrates. BCR-ABL phosphorylation of multiple tyrosine residues within the catalytic and C-terminal domain of USP7 increased USP7 activity towards phosphatase and tensin homolog (PTEN) favouring nuclear exclusion of PTEN (Morotti et al., 2014). S18 phosphorylation can also regulate USP7 activity towards MDM2 and P53 in a DNA damage response pathway (Khoronenkova et al., 2012). This phosphorylation site was claimed to regulate USP7 stability, with dephosphorylated USP7 becoming K48-linked polyubiquitylated and

subsequently degraded in a proteasomal dependent manner (Khoronenkova et al., 2012).

5.2 Aims

5.2.1 To validate and further characterise DUB reactivity data from the Ub-PA cell cycle screen.

My first objective was to establish whether sepharose-Ub-PA activity profiling was reflective of regulated DUB activity or measured periodic DUB expression. To this end, I compared DUB reactivity data from the cell cycle screen to DUB expression levels and their reactivity towards Ub-VME in a carefully optimised reaction. These secondary activity assays, using Ub-VME, were specifically tailored to elicit a submaximal binding response (as described in Section 3.3). Using this approach, I aimed to characterise the differential activity of selected DUBs from the Ub-PA screen, representing each cluster in Figure 4.7.

5.2.2 To further characterise the periodic Ub-PA reactivity profile for USP7 to further understand its regulation through the cell cycle.

As a member of cluster 4 (Figure 4.7), USP7 exhibited an oscillatory Ub-PA reactivity profile, with peak activity during S-phase and a subsequent decrease in reactivity as the cells entered mitosis. A number of intramolecular and external factors have been identified to regulate the catalytic activity of USP7. Therefore, my second objective was to fully characterise USP7 expression and activity though the cell cycle and to investigate whether USP7 phosphorylation or GMPS-mediated allosteric activation contribute to periodic USP7 activity during cell cycle progression.

5.3 Characterisation of temporally regulated DUB activity

5.3.1 Sepharose-Ub-PA profiling reported changes in periodic DUB expression and activity.

Ub-PA profiling of cell cycle-dependent DUB activity revealed large-scale regulation of DUBs during cell cycle progression (Chapter 4). I had previously established that Ub-PA was a fast-reacting probe, binding active DUBs to completion after 5 minutes (Figure 4.1F). However, synchronised cell lysates were incubated with sepharose-Ub-PA for 3 hours to increase the number of

DUBs that could be tagged, retrieved and identified within the screen. It is therefore likely that highly active DUBs bound to completion so that their cell cycle Ub-PA reactivity profile could be more reflective of their expression levels rather than temporally regulated activity.

With this in mind, I next employed Ub-VME, in conjunction with DUB-specific immunoblotting, to more accurately measure DUB reactivity. As in Section 3.3.1, I tailored the *in vitro* reaction conditions for sub-maximal binding. With only a proportion of the available DUB becoming Ub-VME bound, any differences in reactivity to Ub-VME would be more reflective of regulated DUB activity rather than periodic expression. Ideally, reaction conditions would be optimised so that approximately half of the available DUB was covalently bound to Ub-VME in control reactions (in this case the asynchronous lysate). This would permit any increases or decreases in Ub-VME reactivity within a panel of synchronised cell lysates to be visualised and quantified.

Due to the covalent nature of the Ub-VME bond, it is important to remember that the level of DUB reactivity observed at the chosen incubation endpoint is subjective to both the Ub-VME concentration and the length of incubation. I performed a set of optimisation experiments to determine the conditions required for submaximal Ub-VME binding (Figure 5.1). I selected USP15 for optimisation because it was the most active DUB in earlier experiments (Figure 4.1E). USP15 exhibited decreased reactivity to Ub-PA during mitosis (Figure 4.7), and so I optimised Ub-VME reactions comparing asynchronous and G_2/M lysates.

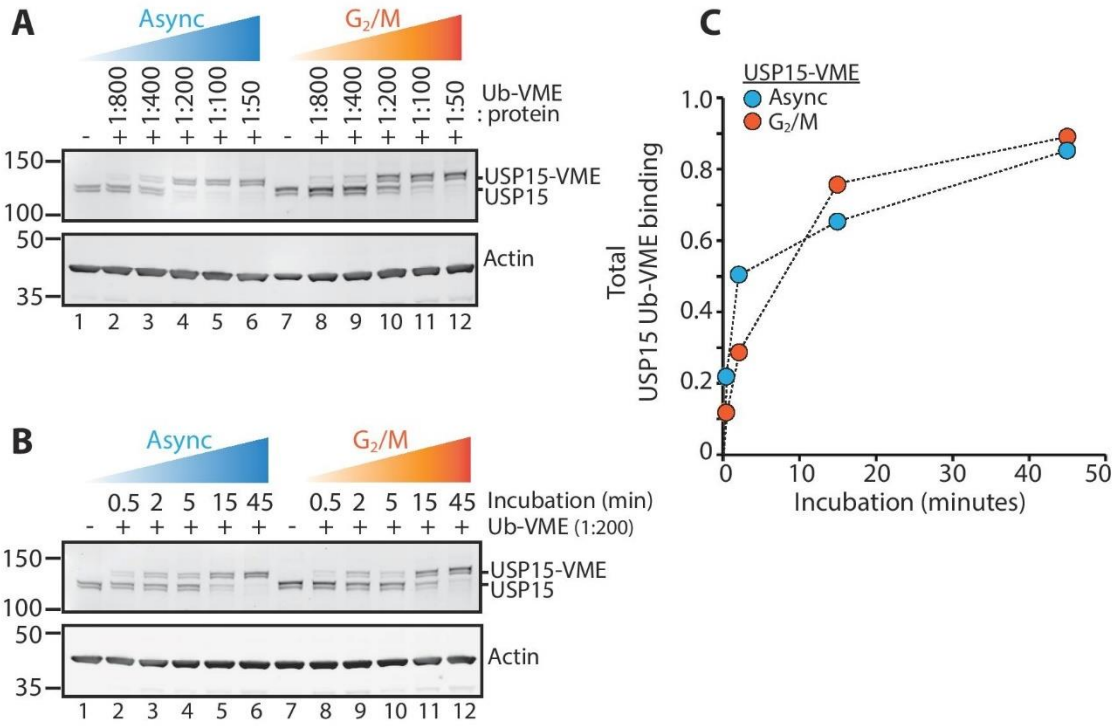

Figure 5.1: Developing a standard protocol to measure DUB reactivity to Ub-VME. **A-C:** Optimisation experiments for HA-Ub-VME *in vitro* reactions. All incubations were performed in asynchronous and G_2/M A549 cell extracts at 37°C and 300rpm in a thermo-shaker. Reactions were separated by SDS-PAGE on a 4-12% gradient gel and immunoblotted for USP15 to assess the level of Ub-VME binding. **A:** Titration of HA-Ub-VME concentration. 15µg lysate was incubated with increasing concentrations of HA-Ub-VME (from 1:800 to 1:50 Ub-VME: protein lysate) for 15 minutes. **B:** Time dependent Ub-VME binding. 15µg lysate was incubated with 75ng HA-Ub-VME (1:200) for increasing periods of time. **C:** Total reactivity of USP15 to Ub-VME was plotted over time for the 1:200 Ub-VME:protein concentration. Values for Ub-VME bound USP15 were normalised to actin and expressed relative to the no probe control (lanes 1 or 7).

As with prior optimisation experiments (Figure 3.2 and Figure 4.1), the first step was to titrate Ub-VME to find a concentration giving sub-maximal binding response (Figure 5.1A). Surprisingly, markedly more Ub-VME bound USP15 was evident at a probe:protein ratio of 1:200 than at 1:400 and so neither reaction resulted in a ~50% binding response (Figure 5.1A, Lane 3 and 4 respectively). However, in mitotic lysates approximately half of the available USP15 was Ub-VME bound after 15 minutes at 1:200 (Figure 5.1A, Lane 10) allowing differences in Ub-VME reactivity between asynchronous and mitotic lysates to be visualised and quantified. Such differences in reactivity would not have been evident at higher concentrations of Ub-VME (Figure 5.1A, Lane 11 and 12).

However, it was also important to ensure that this concentration of Ub-VME did not limit the total amount of DUB that could bind. Furthermore, I wanted to determine an appropriate incubation time that was short enough to prevent maximal DUB binding. To this end, I performed a time course for *in vitro* reactions at 1:200 Ub-VME:protein from 30 seconds to 45 minutes (Figure 5.1B and C). Time-dependent Ub-VME binding to USP15 was evident in both asynchronous and mitotic lysates. Importantly, USP15 bound Ub-VME to completion after 45 minutes in both asynchronous and mitotic reactions confirming that the probe was in excess for the earlier time points. The initial rate of reaction was much faster in asynchronous lysates compared to the G_2/M samples (Figure 5.1C), these reaction rates suggested that an incubation time of 2 or 5 minutes would be optimal for USP15. However, these optimisation experiments aimed to find a set of *in vitro* reaction conditions to suit four less reactive DUBs in addition to USP15. A short incubation would not benefit low abundance or low reactive DUBs. Increasing the reaction length to 15 minutes provided a compromise that still enabled a differential Ub-VME reactivity to be observed for USP15 (Figure 5.1B, compare lanes 5 and 11). In summary, 15 minute incubation coupled with a Ub-VME concentration of 1:200 (probe:protein) was chosen as the standard *in vitro* reaction to measure changes in Ub-VME reactivity.

To examine whether Ub-PA reactivity profiles were reflective of regulated activity or DUB abundance, I performed comparative analysis of periodic Ub-PA reactivity (from Chapter 4), DUB expression and Ub-VME reactivity for a small cohort of DUBs: UCHL1, USP47, USP15, UCHL5 and USP8. These DUBs represented five of the six clusters identified in Figure 4.7, but due to lack of specific antibodies I could not profile the expression or Ub-VME reactivity of either OTUD5 or VCPIP1 from Cluster 5. USP47 had relatively stable expression during the cell cycle but UCHL1, USP15, UCHL5 and USP8 protein abundance exhibited periodicity (Figure 5.2A).

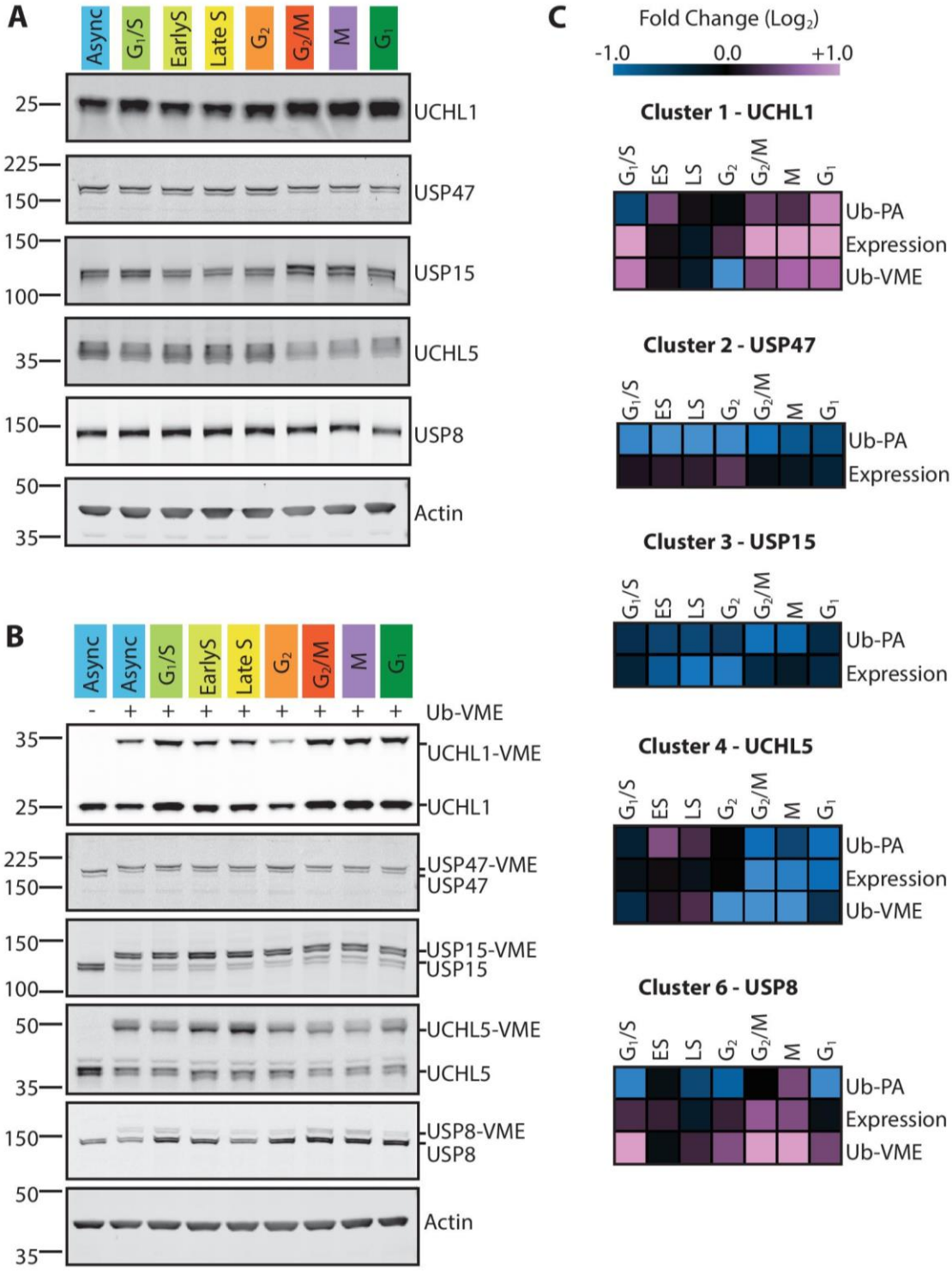

Figure 5.2: Profiling protein expression and Ub-VME reactivity through the cell cycle for a small DUB cohort.

A: DUB cell cycle expression profiles. Equal amounts of synchronised A549 cell lysate (20µg) were separated on a 4-12% gradient gel and immunoblotted for DUBs of interest: UCHL1, USP47, USP15, UCHL5 and USP8 **B:** Differential HA-Ub-VME reactivity throughout the cell cycle. Equal amounts of synchronised A549 cell extract (15µg) were incubated with 75ng HA-Ub-VME (1:200 Ub-VME:protein), or a vehicle control, for 15 minutes at 37ºC with shaking. Reactions were separated on a 4-12% gradient gel and subsequently immunoblotted for five DUBs of interest: UCHL1, USP47, USP15, UCHL5 and USP8. **C:** Heatmaps comparing sepharose-Ub-PA

reactivity data from the MS screen with expression and Ub-VME reactivity data. Both DUB protein levels and total Ub-VME reactivity levels were expressed relative to actin. Fold changes (Log_2), compared to the asynchronous control, were aligned next to the Ub-PA reactivity profiles extracted from the global dataset (Figure 4.7).

Periodic DUB activity was measured using Ub-VME coupled with DUB-specific immunoblotting across a panel of synchronised A549 lysates (Figure 5.2B). Each DUB displayed the characteristic 10kDa increase in molecular weight from covalent Ub-VME binding, with three of the five selected DUBs exhibiting a sub-maximal binding response in asynchronous lysates. These *in vitro* reactions used a different, more reactive, batch of Ub-VME and so both USP15 and USP47 bound Ub-VME completion after 15 minutes preventing the analysis of any cell cycle-dependent activity.

My objective was to examine whether Ub-PA reactivity profiles were reflective of periodic abundance or cell cycle-specific regulation of DUB activity. To achieve this I quantified differential DUB expression and Ub-VME reactivity across the panel of synchronised cell lysates (Figure 5.2A and B) and used heatmaps to represent the fold changes compared to the asynchronous control (Figure 5.2C). Within this small cohort of DUBs, there was evidence to show that the Ub-PA reactivity profiles were reflective of both periodic protein expression and post-translationally regulated activity.

UCHL1 reactivity to Ub-PA was high during mitosis, increasing further as cells entered G_1. This strongly correlated to an increase in protein abundance (Figure 5.2A and C). Similarly, the Ub-VME assay revealed that the amount of active UCHL1 was higher during mitosis than during S-phase (Figure 5.2B and C). From these profiles, it became clear that high UCHL1 activity during cell division was dependent upon increased protein expression. Expression-dependent regulation of DUB activity was also observed for USP8 during mitosis, where increased mitotic activity was reflective of high USP8 protein expression (Figure 5.2C). Interestingly, the correlation between USP8 abundance and Ub-VME reactivity was also observed at G_1/S and G_2, however this was not reflective of the Ub-PA reactivity (Figure 5.2C).

UCHL5 also underwent expression-dependent regulation of activity during mitosis. There was a substantial decrease in UCHL5 expression as cells entered mitosis (Figure 5.2A), this correlated with low levels of reactivity to both Ub-PA and Ub-VME (Figure 5.2C). Interestingly, UCHL5 abundance is stable as cells progressed through S-phase and into G_2 (Figure 5.2A), yet there was a modest increase in UCHL5 reactivity to Ub-PA and Ub-VME at S-phase compared to the asynchronous control (Figure 5.2B and C). This suggests that during S-phase UCHL5 activity is post-translationally regulated and is subsequently degraded during mitosis reducing the overall amount of active UCHL5.

It was unfortunate that Ub-VME reactivity data was not available for USP15 and USP47 as their cell cycle expression profiles revealed intriguing disparities to their Ub-PA reactivity profiles (Figure 5.2C). USP15 abundance peaked during mitosis, despite decreased reactivity to Ub-PA. Similarly, USP47 abundance peaked during G_2, a cell cycle phase where USP47 reactivity to Ub-PA was at its lowest.

These data suggest that the sepharose-Ub-PA profiling protocol could detect differential DUB activity, but cannot determine whether this activity is dependent or independent of protein expression. In order to more accurately characterise the regulation of DUB activity, these original Ub-PA reactivity profiles can be complemented with Ub-VME assays.

5.3.2 Increased USP7 activity during G_1/S is regulated independently of periodic protein expression.

USP7 is of particular interest to the ubiquitin community. It has been associated with a plethora of cellular processes (Nicholson and Suresh Kumar, 2011). Aberrant USP7 activity within cell signalling pathways caught the attention of numerous pharmaceutical companies resulting in the development of specific USP7 inhibitors (Fan et al., 2013; Reverdy et al., 2012). Furthermore, and of particular relevance to this project, intramolecular and external factors have been identified to modulate USP7 activity. Therefore, USP7 was selected for further characterisation of its cell cycle-dependent activity. In the screen, USP7

showed high reactivity towards Ub-PA from G_1/S through to G_2, followed by a substantial decrease in reactivity during mitosis and early G_1 (Figure 4.7, Cluster 4).

To analyse whether differential USP7 reactivity towards Ub-PA during the cell cycle was due to temporally regulated expression, I extracted mRNA and protein from synchronised cell lysates and subsequently analysed periodicity using qRT-PCR and immunoblotting. USP7 transcript levels remained stable during cell cycle progression, with no significant change identified at any cell cycle phase (Figure 5.3A). Conversely, USP7 protein expression did exhibit periodicity with peak abundance during S-phase (Figure 5.3B). Densitometry revealed USP7 protein expression significantly decreased as the cell progressed through G_2, mitosis and into early G_1. Expression remained low at G_1/S (Figure 5.3C). These data suggest that USP7 is the subject of periodic post-translational modification that affects protein stability. Interestingly, the periodicity in USP7 protein abundance mirrors that of Ub-PA reactivity with both exhibiting their highest levels during S-phase and lowest during mitosis (Figure 5.3D).

To investigate whether differential Ub-PA reactivity was regulated by USP7 abundance or was reflective of post-translationally regulated activity, I employed Ub-VME to profile USP7 reactivity during cell cycle progression. It was important to specifically optimise Ub-VME reaction conditions for USP7, and so I performed another set of optimisation experiments (Figure 5.4). I aimed to tailor the *in vitro* reaction conditions to elicit a sub-maximal binding response, in which ~50% of USP7 was Ub-VME bound in control reactions. USP7 exhibited a markedly lower reactivity to Ub-PA during mitosis (Figure 5.3D), therefore, I optimised *in vitro* Ub-VME reaction conditions in both asynchronous and G_2/M lysates.

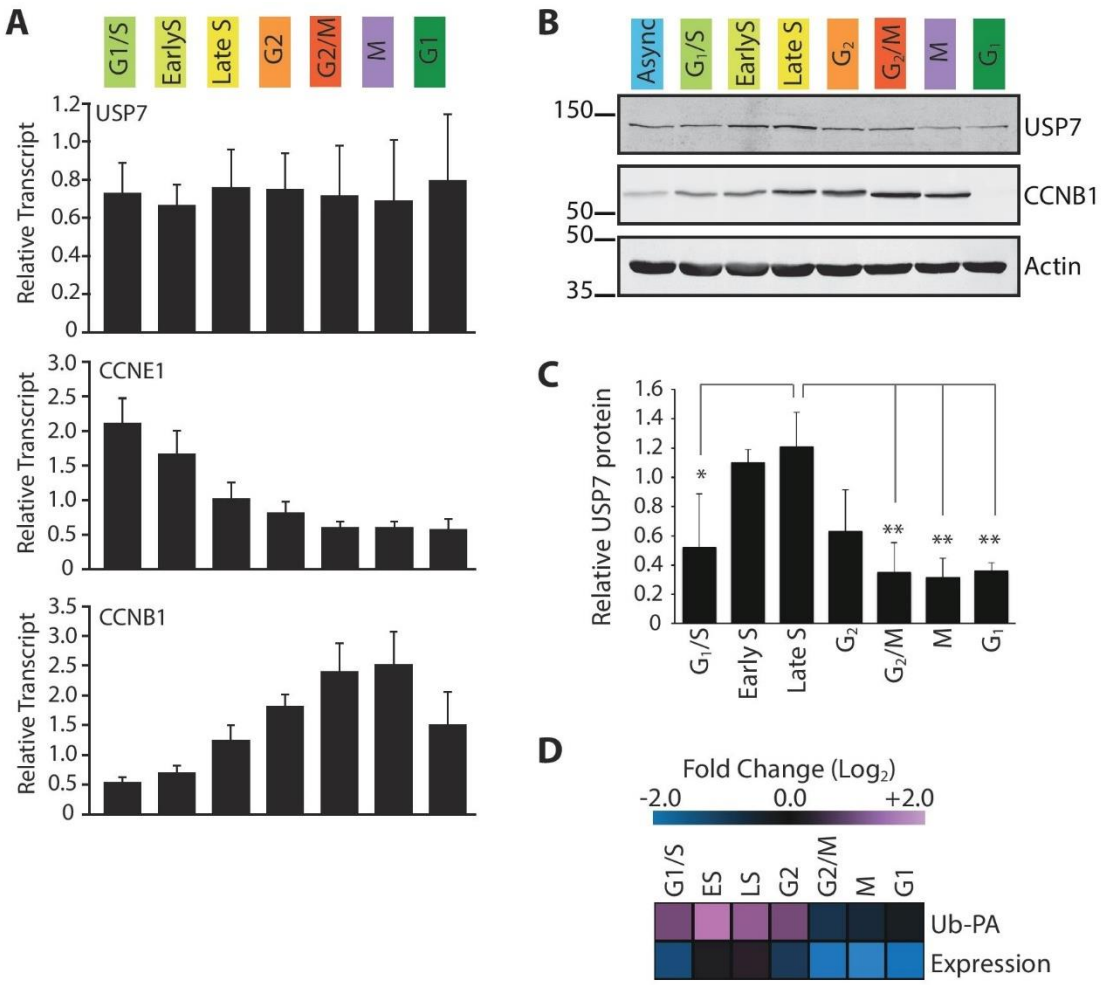

Figure 5.3: USP7 protein expression oscillates in a cell cycle-dependent manner, independent of transcript levels.

A: USP7 transcript levels are not cell cycle regulated. RNA was extracted from synchronised A549 cells. Equal amounts (1µg) were reverse transcribed to analyse USP7, CCNE1 and CCNB1 transcript abundance using qRT-PCR. Relative transcript levels ($2^{-\Delta\Delta Ct}$) were normalised using actin and asynchronous extracts as internal controls. Error bars indicate standard deviation from three independent experiments. **B-D:** USP7 protein expression is periodically regulated during the cell cycle. Equal amounts of synchronised A549 cell lysate (30µg) were resolved on an 8% polyacrylamide gel and immunoblotted for USP7, using CCNB1 and actin as synchronisation and loading controls respectively (**B**). Relative USP7 abundance was normalised to mean expression (**C**). Error bars indicate standard deviation from three independent experiments. Statistical significance was measured using a one-way ANOVA coupled with Tukey's post-hoc test (*p≤0.05; **p≤0.01). Statistical significance was also identified between Early S and G_2/M, M and G_1 samples (p≤0.05). **D:** Heatmap comparing USP7 Ub-PA reactivity and protein expression. Log_2 ratios compared USP7 protein expression to Ub-PA reactivity data extracted from the global activity screen.

I first titrated the concentration of Ub-VME to find the optimum ratio of probe to protein lysate that would bind ~50% of the available USP7 (Figure 5.4A). This was achieved using the 1:200 Ub-VME concentration (Figure 5.4A, Lane 3). Furthermore, there was a substantial decrease in reactivity to Ub-VME in G_2/M samples compared to the asynchronous control. This variation in proportional reactivity of USP7 would have been overlooked if the Ub-VME concentration were too high.

Again, it was important to ensure that the Ub-VME concentration was not limiting in these reactions and so I performed a time course of *in vitro* incubations from 2 to 45 minutes (Figure 5.4B). A 15 minute incubation was sufficient to elicit a half-maximal binding response (Figure 5.4B, Lane 4). To confirm that the concentration of Ub-VME (1:200) was not limiting during this incubation period, I quantified the total amount of reactive USP7 over time (Figure 5.4C). USP7 reactivity to Ub-VME continually increased from 2 to 45 minutes, binding to completion in asynchronous cell lysates. This confirmed that a 1:200 concentration of Ub-VME was not limiting for a 15 minute incubation. Cumulatively, these data determined that a 1:200 Ub-VME concentration coupled with a 15 minute incubation would accurately measure fluctuations in proportional USP7 reactivity.

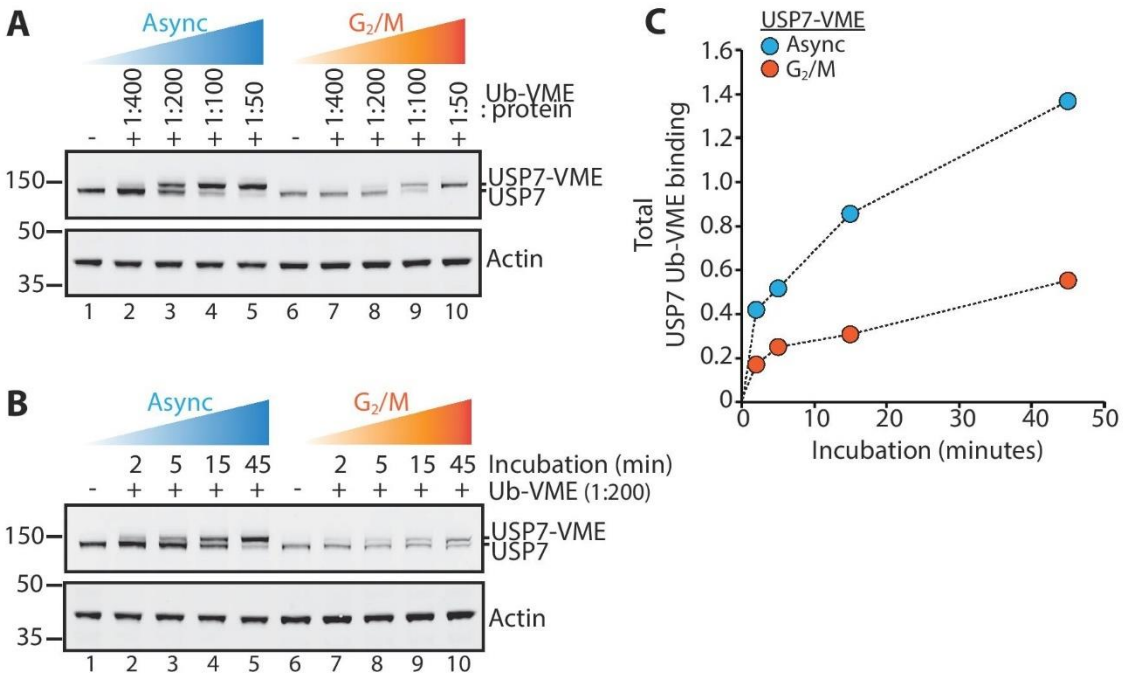

Figure 5.4: USP7-specific optimisation experiments for HA-Ub-VME *in vitro* reactions.

A-D: All incubations were performed in asynchronous and G_2/M A549 cell extracts at 37ºC and 300rpm in a thermo-shaker. Reactions were separated by SDS-PAGE on a 4-12% gradient gel and immunoblotted for USP7 to assess the level of Ub-VME reactivity. **A:** Titration of HA-Ub-VME concentration. 15µg lysate was incubated with increasing concentrations of HA-Ub-VME (from 1:400 to 1:50 Ub-VME:protein lysate) for 15 minutes. **B:** Time dependent Ub-VME binding. 15µg lysate was incubated with 75ng HA-Ub-VME (1:200) for increasing periods of time. **C:** Total reactivity of USP7 to Ub-VME was plotted over time for the 1:200 Ub-VME:protein concentration. Values for Ub-VME bound USP7 were first normalised to actin and then expressed relative to the no probe control (lanes 1 or 6).

Cell cycle-dependent USP7 activity was measured using these *in vitro* Ub-VME reaction conditions across a panel of synchronised A549 lysates (Figure 5.5A). I quantified USP7 reactivity to Ub-VME in two ways: the total amount of Ub-VME bound USP7 and the proportion of Ub-VME bound USP7. The total amount of reactive USP7 peaked during S-phase, significantly decreasing as the cell entered mitosis (Figure 5.5B). This periodicity mirrored the profiles observed for protein expression and Ub-PA reactivity (Figure 5.3D). I also analysed proportional reactivity of USP7, this takes periodic changes in USP7 expression in to account. Here, the amount of Ub-VME bound USP7 is divided by total USP7 expression (i.e. the sum of Ub-VME bound USP7 and the residual unbound USP7).

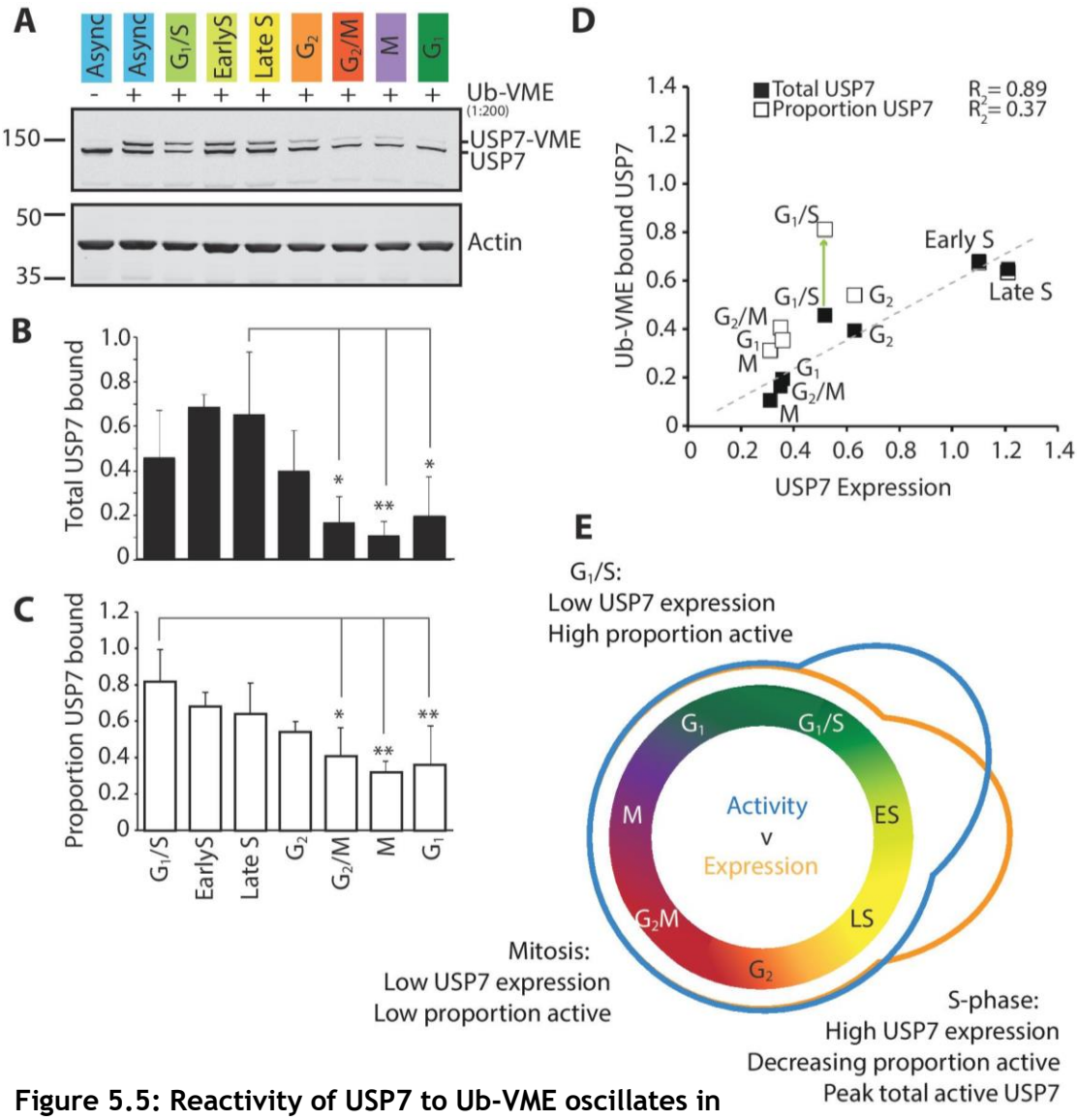

Figure 5.5: Reactivity of USP7 to Ub-VME oscillates in a cell cycle-dependent manner.

A-D: Differential reactivity of USP7 to HA-Ub-VME throughout the cell cycle. Equal amounts of synchronised A549 cell extract (15µg) were incubated with 75ng HA-Ub-VME, or a vehicle control, for 15 minutes at 37ºC with shaking. Reactions were separated on a 4-12% gradient gel and subsequently immunoblotted for USP7 using actin as a loading control (**A**). **B:** Levels of total Ub-VME bound USP7 were expressed relative to actin and normalised to experimental mean. **C:** Values for proportional HA-Ub-VME reactivity were generated by expressing Ub-VME bound USP7 as a fraction of total USP7 expression. Levels were normalised to the experimental mean. Error bars represent standard deviation from three independent biological replicates. Statistical significance was measured for B and C using a one-way ANOVA coupled with Tukey's post-hoc test (*p≤0.05; **p≤0.01). Statistical significance was also measured between Early S and M (p≤0.05) for total Ub-VME bound USP7 (B). **D:** Scatter plot comparing USP7 protein expression to the relative levels of total Ub-VME bound USP7 (black squares) and proportional Ub-VME bound USP7 (white squares). Dashed line represents the trendline for total Ub-VME bound USP7 dataset. **E:** Schematic representing the periodicity of USP7 protein expression (orange) and proportional activity (blue) during the cell cycle.

Interestingly, analysing the proportion of USP7 bound by Ub-VME revealed a similar profile, with one distinct difference at G_1/S. USP7 was most active during the G_1/S transition, with activity steadily decreasing throughout S-phase until a significant decrease was observed during mitosis and early G_1 (Figure 5.5C). This suggested that USP7 activity was regulated independently of its protein abundance specifically at G_1/S.

To confirm this, I performed a correlative analysis of USP7 protein expression against these two measures of USP7 activity (Figure 5.5D). The total amount of Ub-VME bound USP7 (black squares) positively correlated to protein expression with an R_2 of 0.89. There was a weaker correlation between the proportion of Ub-VME bound USP7 (white squares) and protein expression (R_2=0.37), notably if you remove G_1/S from this dataset the correlation increased (R_2=0.90). These data suggest there were three distinct phases of USP7 regulation during cell cycle progression, depicted in Figure 5.5E. During S-phase there was an increase in protein expression and an analogous increase in the amount of active USP7. In contrast, as the cell progressed through mitosis, there was a decrease in USP7 abundance, and a concurrent decrease in USP7 reactivity. The parallel between USP7 abundance and activity was disengaged at G_1/S, where the small reservoir of USP7 was highly active. This implied that external factors were potentiating USP7 activity in a G_1/S-specific manner.

5.4 Periodicity of USP7 regulatory mechanisms

5.4.1 Expression of GMPS, an allosteric activator of USP7, did not correlate with the periodic regulation of USP7 activity

The metabolic enzyme GMPS has been identified to allosterically regulate USP7 activity. Through an interaction with the UBL-123 domain in the C-terminal region of USP7, GMPS stabilises USP7 in an active conformation. To investigate whether GMPS might be responsible for increased USP7 reactivity to Ub-VME at G_1/S I first analysed whether GMPS protein expression was temporally regulated. GMPS protein expression showed limited periodicity, with a significant decrease in abundance in G_1 (Figure 5.6A and B). There was only a moderate correlation between GMPS expression and proportional USP7 activity (R_2=0.36) (Figure 5.6C). To further investigate the effect of GMPS on USP7 activity, I performed siRNA-mediated knockdown of GMPS and measured the differential reactivity of USP7 to the Ub-VME activity probe (Figure 5.6D). There was a slight, but insignificant, decrease in Ub-VME reactivity after a 5 minute *in vitro* incubation with Ub-VME (Figure 5.6E). Cumulatively, these data suggest that GMPS was not responsible for the potentiation of USP7 activity at G_1/S that was detected with the Ub-VME probe.

5.4.2 G_1/S-dependent potentiation of USP7 correlated to S18 phosphorylation

Phosphorylation has been shown to regulate the activity of USP7 towards a number of substrates. Multiple tyrosine residues within the catalytic and C-terminal domain regulate USP7 activity (Morotti et al., 2014). Similarly, S18 phosphorylation alters USP7 activity towards MDM2 in a DNA damage response pathway (Khoronenkova et al., 2012). S18 phosphorylation status was of particular interest, as serine and threonine phosphorylation predominates during cell cycle progression, therefore S18 was the most interesting candidate for further investigation.

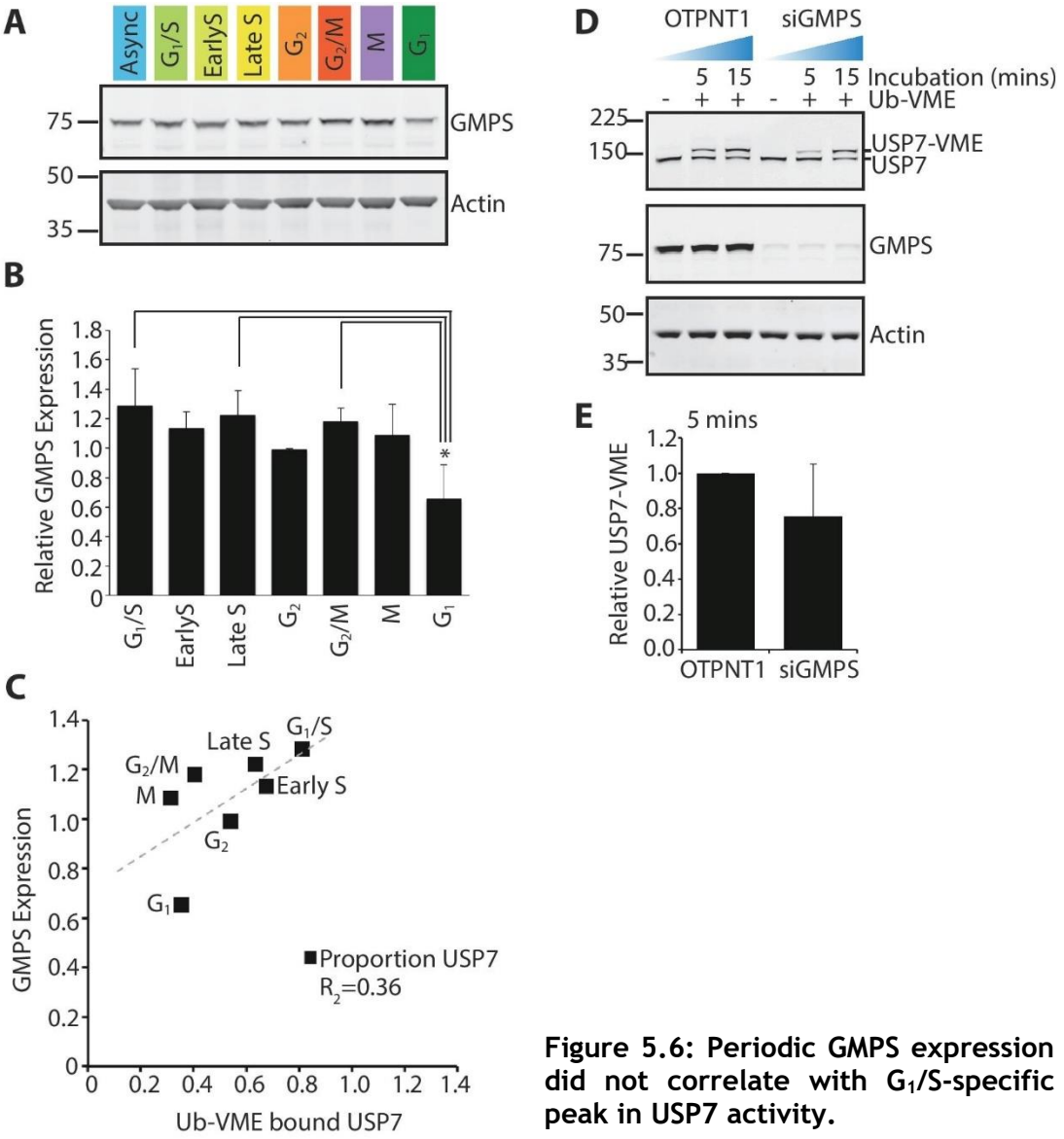

Figure 5.6: Periodic GMPS expression did not correlate with G_1/S-specific peak in USP7 activity.

A and B: GMPS protein expression is lowest during G_1. Equal amounts of synchronised A549 cell lysate (20µg) were separated on a 4-12% gradient gel and immunoblotted for GMPS, using actin as a loading control (**A**). Relative GMPS abundance was normalised to mean expression (**B**). Error bars indicate standard deviation from three independent biological replicates. Statistical significance was measured using a one-way ANOVA coupled with Tukey's post-hoc test (*$p \leq 0.05$) **C:** Scatter plot comparing GMPS protein expression to the proportion of Ub-VME bound USP7. Dashed line represents the trendline for this dataset. **D and E**: Depletion of GMPS does not significantly affect USP7 reactivity to Ub-VME. Asynchronous A549 cells were transfected with non-targeting control (OTPNT1) or GMPS-specific siRNA oligos for 72 hours prior to lysis. Equal amounts of lysate (15µg) were incubated with 75ng HA-Ub-VME, or a vehicle control, for 5 or 15 minutes at 37°C with shaking. Reactions were separated on a 4-12% gradient gel and subsequently immunoblotted for USP7, GMPS and actin (**D**). **E:** Quantitation of proportion of Ub-VME bound USP7 after 5 minute incubation. Levels were normalised to OTPNT1. Error bars indicate standard deviation from three independent biological replicates.

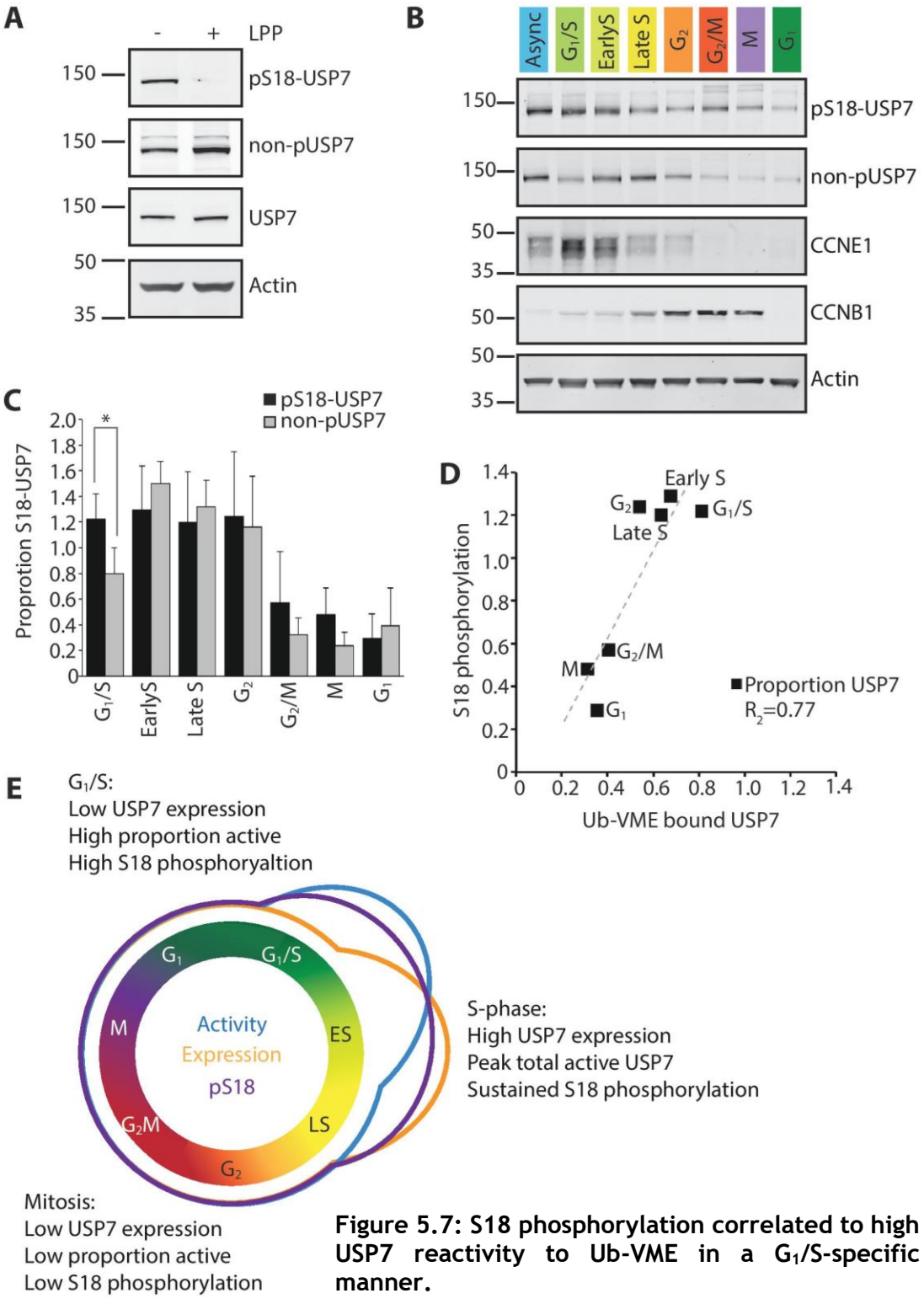

Figure 5.7: S18 phosphorylation correlated to high USP7 reactivity to Ub-VME in a G_1/S-specific manner.

A: Specificity of serine 18 (S18) phosphorylation specific antibodies. Asynchronous A549 cells were lysed in E1A lysis buffer. Cleared lysate (5µL, 2mg/mL) was mixed 1:1 with phosphatase reaction mix supplemented with 1mM $MnCl_2$ and 400U LPP. Phosphatase reactions were performed at 30°C for 30 minutes with shaking. Reactions were separated on a 4-12% polyacrylamide gel and immunoblotted for S18-phosphorylated USP7 (pS18-USP7), S18-unphosphorylated USP7 (non-pUSP7). Total USP7 (USP7) and actin were used as internal controls. **B and C:** S18 is

periodically phosphorylated through the cell cycle. Equal amounts of synchronised A549 cell lysate (20µg) were separated on a 4-12% gradient gel and immunoblotted for pS18-USP7 and non-pUSP7 using CCNE1, CCNB1 and actin as synchronisation and loading controls respectively (**B**). Relative levels of pS18-USP7 and non-pUSP7 abundance were normalised to the asynchronous control (**C**). Error bars indicate standard deviation from three independent biological replicates. Statistical significance was measured using a paired T-test (*p≤0.05). **D:** Scatter plot comparing S18-phosphorylation levels to the proportion of Ub-VME tagged USP7. Dashed line represents the trendline for this dataset. **E:** Schematic representing the periodicity of USP7 protein expression (orange), proportional activity (blue) and S18-phosphorylation (purple) during the cell cycle.

To elucidate whether S18 phosphorylation correlated with the potentiation of USP7 activity at G_1/S, I employed antibodies specific for S18-phosphorylated USP7 or S18-unphosphorylated USP7 (abbreviated to pS18-USP7 and non-pUSP7, respectively). The relative specificity of these antibodies was determined using LPP (Figure 5.7A). Upon phosphatase treatment, the pS18-USP7 signal disappeared, whereas the non-pUSP7 signal increased confirming the specificity of these commercially available antibodies. I analysed the extent of S18 phosphorylation across a panel of synchronised cell lysates (Figure 5.7B). The amount of S18-unphosphorylated USP7 peaked during S-phase and decreased during mitosis, mirroring the total USP7 expression profile (Figure 5.3B and C). A similar profile was observed for S18-phosphorylated USP7, however there was significantly more S18-phosphorylated than unphosphorylated USP7 at G_1/S (Figure 5.7C). This coincided with the higher proportion of active USP7 observed at G_1/S by Ub-based probe analysis. There was a strong correlation between pS18-USP7 levels and proportional USP7 reactivity (R2=0.77) suggesting a role for S18 phosphorylation in regulating USP7 activity (Figure 5.7D). Overlaying S18 phosphorylation status on to the schematic illustrates how S18 phosphorylation increases at G_1/S and bridges the gap between increased proportional activity of USP7 during G_1/S and the overall peak in USP7 activity observed at Early S-phase (Figure 5.7E).

5.5 Discussion

The data described in this chapter demonstrate that ubiquitin-based active site-directed probes can be used to accurately profile differential DUB activity in synchronised cell extracts. Ub-PA can be employed to globally profile DUB activity but is most effective when used in conjunction with carefully optimised Ub-VME incubations. Ub-PA profiling alone was not sufficient to determine whether changes in DUB activity were regulated by differential protein expression or regulated by external factors. It became evident that in order to characterise individual DUB activity throughout the cell cycle each DUB would have to undergo a separate set of Ub-VME optimisation experiments. It was important that these conditions would only result in submaximal Ub-VME binding, with approximately 50% of the target DUB Ub-VME bound in the asynchronous control.

Ub-PA reactivity profiling in synchronised cell lysates revealed an interesting pattern of USP7 activity throughout cell cycle progression. USP7 exhibited increased Ub-PA reactivity from G_1/S throughout S-phase, significantly decreasing as the cell entered mitosis (Figure 4.7). Further characterisation using Ub-VME confirmed this. When analysing the total amount of Ub-VME bound USP7 there was a significant increase in USP7 activity during S-phase, which significantly decreased during mitosis. This tightly correlated to the expression levels of USP7 protein but not mRNA (Figure 5.3), indicating that for the most part USP7 activity is regulated post-translationally through periodic regulation of USP7 protein levels. This relationship was only disengaged at G_1/S, where there was a significant increase in the proportional reactivity of USP7 to Ub-VME (Figure 5.5).

Data mining revealed that USP7 is post-translationally modified during the cell cycle at S18 (Olsen et al., 2010). I investigated the periodicity of S18 phosphorylation using phospho-specific antibodies. This antibody-based approach revealed a significant increase in the proportion of USP7 that was phosphorylated on S18 at G_1/S (Figure 5.7). This coincided with the increase in USP7 activity (Figure 5.7D). However, the cell cycle-dependent phosphorylation

profile identified from the global phospho-proteome study (Olsen et al., 2010) did not correlate to the antibody-based profile. Their study found a significant decrease in the level of S18-phosphorylated USP7 in G_2, coupled with a moderate decrease at Early S compared to an asynchronous control, a very different profile from that illustrated in Figure 5.7. This could result from the two different experimental approaches, mine a targeted antibody-based method, and the other a global overview of differential phosphorylation through the cell cycle (Olsen et al., 2010).

Evidently, USP7 phosphorylation is important in regulating USP7 activity. Phosphorylation can regulate a protein in a multitude of ways. It would be interesting to further investigate the role of this phosphorylation event on USP7 activation. Up to this point I have been studying the regulation of endogenous USP7 protein throughout cell cycle progression. However, to fully understand how S18 phosphorylation affects the behaviour of USP7 within cells, and could modulate USP7 catalytic activity, I will need to respectively utilise overexpression constructs, and an *in vitro* platform.

Chapter 6

CK2 phosphorylation of USP7 promotes nuclear localisation, affects USP7 protein interactions and potentiates catalytic activity.

6.1 Introduction

Phosphorylation is known to modulate a plethora of proteins in the UPS. Even ubiquitin is no exception; a recent pioneering study revealed many aspects of ubiquitin activity can be regulated by phosphorylation at S65 (Wauer et al., 2015). As outlined in detail in Section 1.3.2.4.3 phosphorylation mediates DUB activity in a number of ways. It can result in subcellular translocation (USP10 (Yuan et al., 2010) and USP4 (Zhang et al., 2012)) or sequester an active DUB from its substrates (USP8 (Mizuno et al., 2007)). In some cases phosphorylation is required for activation of the enzyme (OTUD5 (Huang et al., 2012) and USP37 (Huang et al., 2011)). A phosphorylation event at S177 on OTUD5 is sufficient to promote a large conformational change upon ubiquitin binding that augments catalytic activity (Huang et al., 2012).

In this thesis, I have made an exciting link between USP7 activity and S18 phosphorylation throughout the cell cycle, with both notably increasing at G_1/S (Figure 5.7). This phosphorylation site at the extreme N-terminus of USP7 is adjacent to a TNF receptor-associated factor (TRAF) domain that is important for protein and substrate interactions (Figure 6.1). Interestingly, the phosphorylation status of S18 does influence USP7 activity in DNA-damage dependent manner, S18 dephosphorylation decreases USP7 activity towards MDM2 resulting in an increase in P53 levels (Khoronenkova et al., 2012). A separate study suggests that the interaction of USP7 with MDM2 is also mediated in DNA-damage specific manner (Reddy et al., 2014). Taken together these two suggest could suggest that dephosphorylation of USP7 can also regulate its interaction with substrates, in addition to its activity. Surprisingly, this phosphorylation site was also demonstrated to regulate USP7 protein stability. A non-phosphorylatable variant of USP7 exhibited increased polyubiquitylation coupled with decreased steady-state expression levels (Khoronenkova et al., 2012). The same study identified that USP7 was phosphorylated at S18 by CK2, the ubiquitously expressed serine/threonine kinase.

Intriguingly, with regard to my investigation, CK2 plays a role at every stage of cell cycle progression, including the phosphorylation of proteins crucial to the

transition through the G_1/S boundary. Rather than driving cells from G_1 in to S-phase, CK2 acts as a moderator phosphorylating multiple regulatory proteins that govern G_1/S checkpoint signalling. A well-characterised CK2 target that regulates S-phase entry is P53. Upon DNA damage, CK2 both directly and indirectly increases P53 signalling, arresting cells at the G_1/S boundary until the checkpoint can be satisfied. P53 is phosphorylated at serine 392 (S392) by CK2 in response to UV irradiation; this phosphorylation promotes DNA binding and subsequently increases P53-dependent transcriptional activation (Kapoor and Lozano, 1998; Keller and Lu, 2002). Moreover, CK2 also phosphorylates MDM2, a negative regulator of P53 and a USP7 interactor. CK2 phosphorylates MDM2 at multiple residues within its acidic domain (serines 260, 267 and 269) perturbing the interaction with P53 and so resulting in increased P53 stability and signalling (Allende-Vega et al., 2005; Hjerrild et al., 2001).

It has been well established that USP7 antagonises MDM2 by deubiquitylating its substrates, as well as deubiquitylating auto-ubiquitylated MDM2 in cells (Brooks et al., 2007). The interplay of P53, MDM2 and USP7 is a critical axis for the regulation of P53 function in cells and, with respect to the cell cycle, regulation of the G_1/S checkpoint and progression into S-phase. CK2 has the capacity to phosphorylate all three of these proteins and so it will be interesting to investigate the effect of CK2-mediated S18 phosphorylation on USP7 activity.

6.2 Aims

6.2.1 Using site-directed mutagenesis to investigate the role of S18 phosphorylation on USP7 function in cells

As demonstrated in Chapter 5, there is a correlation between USP7 reactivity towards the Ub-VME probe and S18-phosphorylation levels, most notably at G_1/S. Classically, when a phospho-site is thought to have an effect on protein function that site is mutated, using site-directed mutagenesis, to observe whether the protein function has been altered. These can be non-phosphorylatable mutants in which the serine (S), threonine (T) or tyrosine (Y) amino acids are mutated to an alanine (A). Or a phospho-mimetic mutation can be made where the phospho-residue is mutated into a negatively charged amino acid (glutamic acid (E) or aspartic acid (D)). In the latter, the negative charge of the side chain mimics the charge of the phosphate group enabling the mutant to mimic the function of the phosphorylated protein. My first objective will be to create both non-phosphorylatable (S18A) and phospho-mimetic (S18E) USP7 mutants and examine exogenous USP7 activity, localisation and protein-protein interactions.

6.2.2 Using *in vitro* investigative tools to directly assess the effect of S18 phosphorylation on catalytic activity of USP7

To definitively answer whether the phosphorylation event at S18 increases the catalytic activity of USP7 I will move this line of investigation into an *in vitro* setting. Taking proteins out of their intracellular milieu eliminates the variables that can affect protein function. This will enable me to determine the direct effect of S18-phosphorylation on USP7 catalytic activity. I will measure USP7 activity using three separate *in vitro* assays: ubiquitin chain (Ub-chain) assays, Ub-VME assays and Ubiquitin 7-amido-4-methylcoumarin (Ub-AMC) assays.

Linkage-specific polyubiquitin chains are often used as substrates for *in vitro* reactions to analyse DUB activity. USP7 is a promiscuous DUB with high affinity towards numerous ubiquitin chain linkages, though it has been reported to exhibit a preference towards K48-linked ubiquitin (Faesen et al., 2011b) and so K48-linked tetra-ubiquitin chains (K48-Ub_4) were chosen as the substrate for this *in vitro* assay. The analysis of polyubiquitin hydrolysis into ubiquitin trimers,

dimers and monomers gives a succinct illustration of any differential DUB activity between different experimental conditions.

Ub-VME, depicted in Figure 3.1 and 3.2, is an active site-directed probe that reports the accessibility of a DUB's active site. Moreover, as a suicide probe that irreversibly binds to the catalytic cysteine, Ub-VME reactivity specifically relates to the rate of ubiquitin binding or "on-rate". This, coupled with the ubiquitin chain assays, will indicate whether S18 phosphorylation affects the on rate or catalytic turnover for USP7. Ub-VME has been repeatedly used throughout this investigation and so it is prudent to compare the *in vivo* Ub-VME reactivity data (see previous chapters) to Ub-VME reactivity in this *in vitro* setting.

Ub-AMC is a substrate that is classically used to assay DUB activity, including that of USP7 (Faesen et al., 2011a; Faesen et al., 2011b). The C-terminus of a synthetic ubiquitin monomer is covalently bound to a quenched AMC reporter molecule. Upon hydrolysis of this amide bond, the free AMC fluorophore emits a signal that is directly proportional to DUB activity. Furthermore, Ub-AMC hydrolysis follows Michaelis-Menten kinetics enabling the measurement of both catalytic turnover (K_{cat}) and substrate binding affinity (K_m), which provide quantification of enzyme efficiency. Combining the data obtained from these three *in vitro* approaches will elucidate whether and how phosphorylation at S18 affects the fundamental catalytic efficiency of USP7.

6.3 USP7 phosphorylation at S18 affects its behaviour in A549 cells

6.3.1 USP7 isoform 1, that can be phosphorylated at S18, is the major functional USP7 isoform expressed in A549 cells

There are eight protein coding splice variants of USP7 in the genome (Ensembl.), yet only one (USP7-001) encodes for the S18 phosphorylation site (Figure 6.1A and B). Only half of the eight splice variants encode for a functional enzyme: USP7-001, USP7-004, USP7-002 and USP7-201 (Figure 6.1B). The four remaining splice variants produce a truncated TRAF domain but are lacking the catalytic and C-terminal UBL domains. Previous studies using isoform specific antibodies have suggested that S18 phosphorylatable USP7 isoform 1 is not the major isoform of USP7 expressed in HeLa cells (Khoronenkova et al., 2012). To determine the expression of different USP7 transcripts, I designed primers to specifically amplify each of the four full protein-coding splice variants, as well as a primer pair that would amplify all transcripts as a control (Figure 6.1B – red and blue labels respectively). I extracted messenger RNA (mRNA) from A549, U2OS and HeLa cells and analysed USP7 transcript expression through end-point PCR (Figure 6.1C). The only USP7 isoform transcribed in all three cell lines was USP7-001. Even with prolonged UV exposure, no PCR product was identified for USP7-002, USP7-004 and USP7-201 isoforms. End point RT-PCR used in this manner does not provide a quantitative measurement of USP7 variant expression, however it was interesting to observe a difference between USP7-001 expression and USP7-all expression across the three cell lines. The increase observed in USP7-all expression (Figure 6.1C, right panel) compared to USP7-001 expression (Figure 6.1C, left panel) seen in A549 cells could suggest that A549 cells also express one or more of the TRAF-truncated USP7 splice variants (listed in (Ensembl.)). It should be noted that since performing these experiments the sequence for USP7-201 isoform has been removed from the Ensemble database. In summary, these data have showed that USP7-001, coding for the 1102aa protein, is the major splice variant in all three cell lines used in this study. This is the only splice variant that codes for the S18 phosphorylation site.

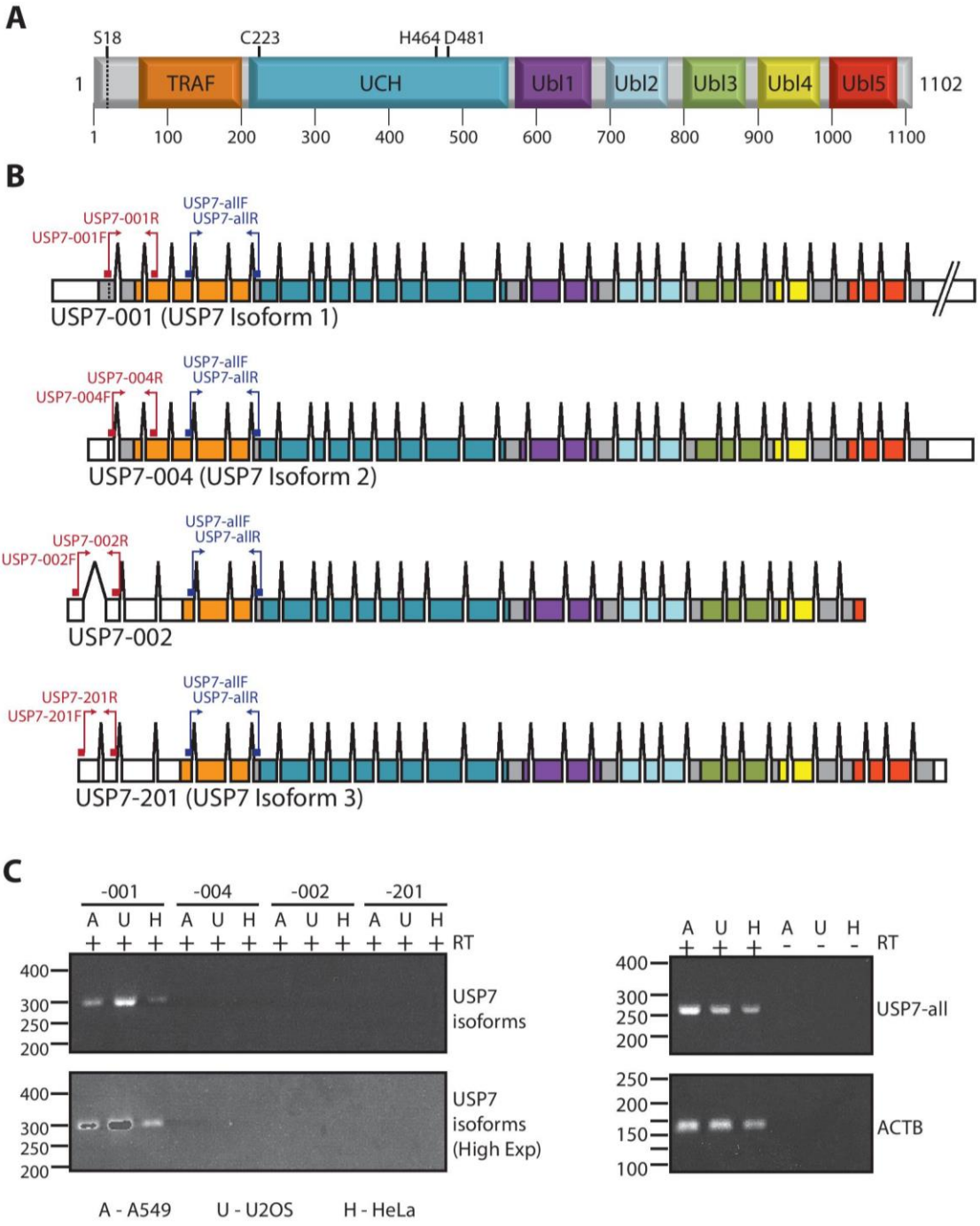

Figure 6.1: USP7 isoform 1 is expressed in A549, U2OS and HeLa cell lines.
A: Schematic depicting the protein domain structure of USP7 isoform 1. Each protein domain is colour coded: TRAF domain: orange, catalytic UCH domain: blue and the UBL domains 1-5: purple, light blue, green, yellow and red respectively. Four residues have been highlighted, the phosphorylation site at S18 (dotted line) and the catalytic triad: C223, H464 and D481. **B:** Schematic of the four functional protein coding USP7 splice variants. Genomic data for each variant was gathered from Ensembl (Ensembl). Exons have been colour-coded to match the protein domains in A. The dotted line in USP7-001 represents S18 codon. Annealing positions for isoform specific primer pairs have been highlighted on individual diagrams. **C:** Only USP7-001 is expressed A549, U2OS and HeLa cell lines. RNA was

extracted from asynchronous A549, U2OS and HeLa cells; equal amounts (1µg) were reverse transcribed to analyse USP7 splice variant transcript abundance for USP7-001, USP7-004, USP7-002, USP7-201 and total USP7 transcript levels (USP7-all) using end point RT-PCR. Actin (ACTB) was used as a housekeeping gene and RT- controls are included in the right panel.

6.3.2 Phospho-mimetic USP7 mutants exhibit increased activity and preferentially localise to the nucleus

Having demonstrated that the main isoform expressed in A549 cells carries the S18 phosphorylated site. It was important to know whether S18 phosphorylation can regulate USP7 function in cells. I generated four USP7 constructs using Gateway® cloning technology for transient overexpression studies (see Methods Section 2.3.5 to 2.3.7 for details). Wild type USP7 sequence was subject to site-directed mutagenesis to produce catalytically inactive (C223S), S18 non-phosphorylatable (S18A) and S18 phospho-mimetic (S18E) mutants. Through a second round of site-directed mutagenesis, each construct was made resistant to a USP7 siRNA (oligo #3), prior to the addition of an N-terminal GFP tag. Each USP7 construct was transiently expressed in U2OS cells (Figure 6.2A). Interestingly, both C223S and S18A expressed at lower levels suggesting that these point mutations may have a bearing on USP7 stability. Each of the four USP7 constructs expressed protein that exhibited resistance towards siUSP7_3, though expression levels were decreased compared to the OTP NT1 non-targeting control. With the successful creation of GFP-tagged catalytically inactive, non-phosphorylatable and phospho-mimetic USP7 mutants I could next investigate differential activity, localisation and protein-protein interactions.

The exogenous USP7 is under the control of a viral promoter and so expressed at 5-fold higher concentration than endogenous USP7 (Figure 6.2A). This required a re-optimisation for the Ub-VME activity assay. The higher the protein abundance, the higher the concentration of Ub-VME required to result in 50% of the exogenous USP7 binding Ub-VME. Exogenous GFP-USP7 required a ratio of 1:50 Ub-VME:protein to bind approximately half of the available GFP-tagged USP7 (Figure 6.2B). Using these newly optimised conditions, an activity assay was performed to measure the reactivity of the four GFP-USP7 constructs towards Ub-VME (Figure 6.2C and D). *In vitro* incubation was performed for 5 or

15 minutes, allowing for assessment of differential Ub-VME binding over time. Non-phosphorylatable USP7 (S18A) exhibited a significant decrease in Ub-VME binding, in comparison to the wild type USP7. This significant decrease mimics the decrease in Ub-VME binding seen for the catalytically inactive USP7 mutant (C223S). The phospho-mimetic USP7 (S18E) showed a similar profile of Ub-VME binding to wild type USP7. These data demonstrate that S18 phosphorylation is important for the activity status of USP7 in a cellular context.

Upon overexpression I noticed differential distribution of the four exogenous USP7 variants between nuclear and cytoplasmic compartments. To determine the effect of S18 phosphorylation status on USP7 localisation, I overexpressed each of the four GFP-tagged USP7 constructs in the U2OS osteosarcoma cell line and analysed compartmentalisation (Figure 6.3A). USP7 is predominantly a nuclear protein, though as no classical NLS has been identified it has been suggested that USP7 is dependent upon its interactors to translocate into the nucleus. As expected, wild type GFP-USP7 was predominantly expressed in the nucleus of transfected cells, 60% showed exclusively nuclear expression and a further 30% of cells displayed a predominantly nuclear (N>C) phenotype (Figure 6.3B). USP7 localisation appeared to be dependent on catalytic activity. There was a significant decrease in exclusive nuclear localisation from wild type (60%) to catalytically inactive USP7 (16%). This was coupled with a redistribution of USP7-C223S towards the cytoplasm (41% in N=C compartment) (Figure 6.3B). Interestingly, this activity-dependent localisation of USP7 was phenocopied by non-phosphorylatable USP7 (S18A). Again, a significant decrease (30%) was seen in exclusive nuclear USP7-S18A localisation compared to the wild type control. There was a concurrent increase (25%) in N=C USP7-S18A localisation, replicating the redistribution from the nucleus towards the cytoplasm seen in USP7-C223S expressing cells. In contrast, the phospho-mimetic S18E shared a similar distribution profile to the wild type, there was no significant difference in USP7 localisation in any cellular compartment (Figure 6.3B).

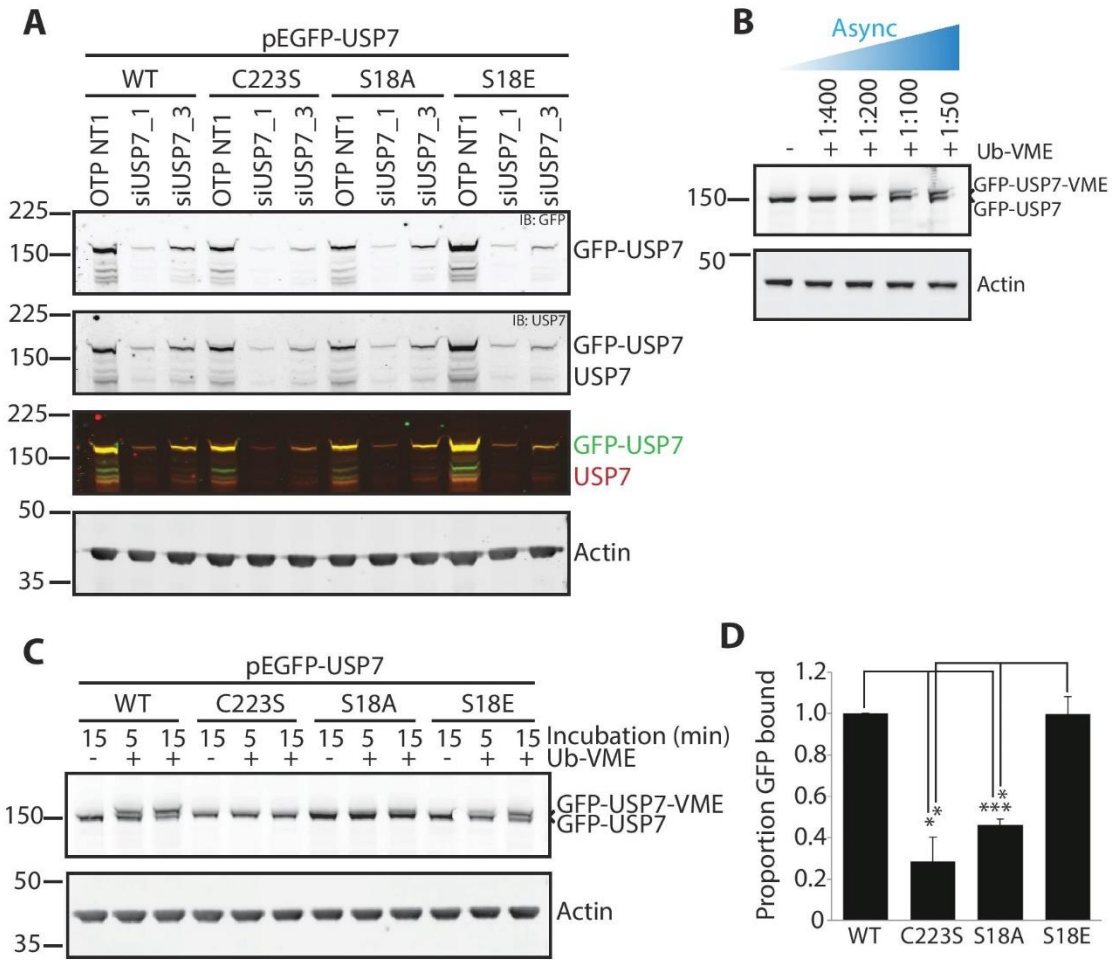

Figure 6.2: Non-phosphorylatable USP7 has limited reactivity to Ub-VME activity probe in cell lysates.

A: Exogenous expression of siRNA-resistant USP7 wild type and mutant constructs. Asynchronous U2OS cells were transfected with control or USP7-specific siRNA oligos for 72 hours prior to lysis. Cells were transfected with USP7 constructs 48 hours after siRNA transfection and 24 hours before lysis. Equal amounts of lysate (15µg) were separated on a 4-12% gradient gel prior to immunoblotting for GFP, USP7 and actin. The overlay of GFP (green) and USP7 (red) antibody staining distinguishes endogenous and exogenous USP7 bands (yellow) from the GFP degradation products. **B:** Optimisation of HA-Ub-VME assay conditions for exogenous USP7. A549 cells were transfected with GFP-USP7-WT plasmid for 24 hours prior to lysis. Equal amounts of lysate (20µg) were incubated with increasing concentrations of HA-Ub-VME, or a vehicle control, for 15 minutes at 37°C with shaking. Reactions were separated on a 4-12% gradient gel and subsequently immunoblotted for GFP and actin. **C:** Non-phosphorylatable USP7 exhibited decreased reactivity towards Ub-VME activity probe. Asynchronous A549 cells were transfected with GFP-USP7 constructs 24 hours prior to homogenisation. Equal amounts of cleared lysate (15µg) were incubated with 300ng HA-Ub-VME (1:50 probe:protein) for 5 or 15 minutes at 37°C with shaking. Reactions were separated on a 4-12% gradient gel and immunoblotted for GFP and actin. **D:** Quantitative densitometry of the proportion of Ub-VME bound GFP-USP7. Values are analysed from three independent experiments and have been normalised to GFP-USP7-WT. Error bars represent the standard deviation, statistical significance is determined by one-way ANOVA with Tukey's post-hoc test *p≤0.05 ***p≤0.005.

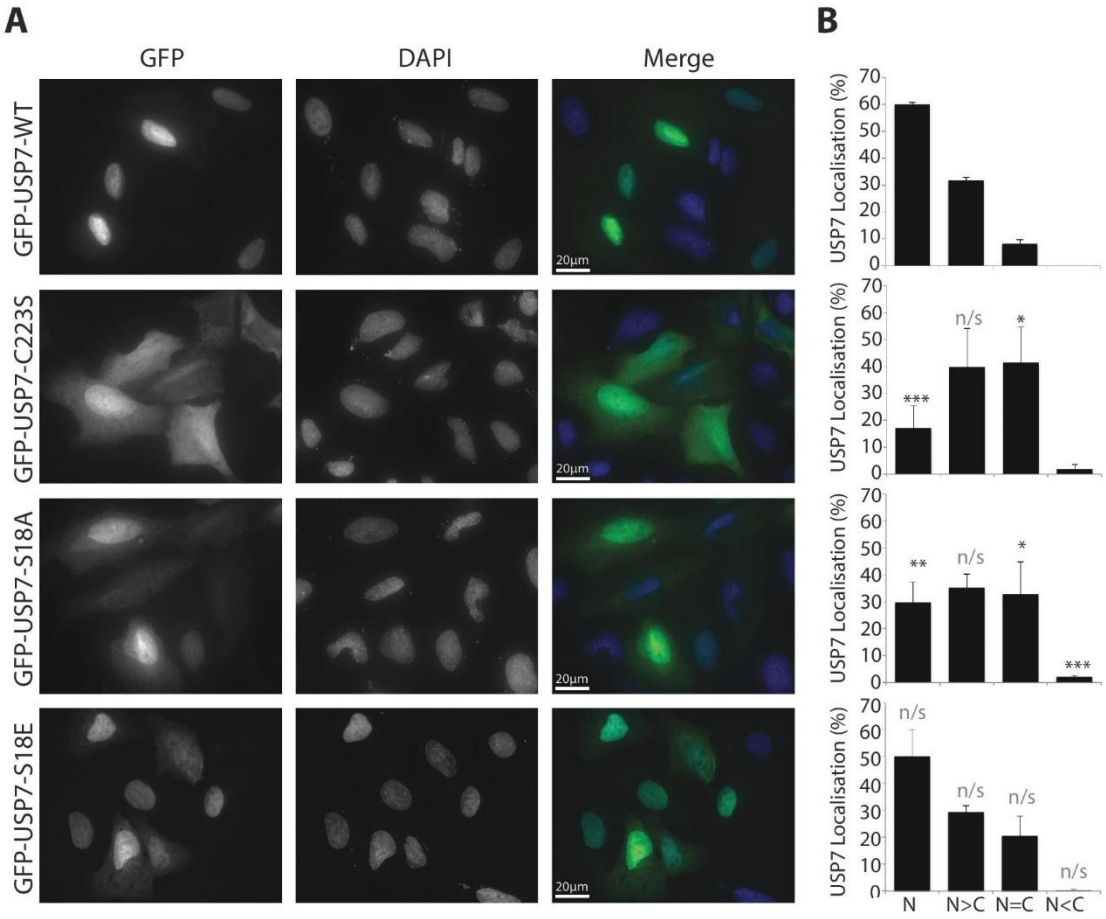

Figure 6.3: Catalytic activity and S18 phosphorylation status influence USP7 subcellular localisation.

A: Representative images of asynchronous U2OS cells transiently expressing GFP-tagged USP7 constructs. Cells were transfected 24 hours prior to PFA fixation. Fixed cells were quenched, Triton-X permeabilised, DAPI stained and mounted for imaging (scale bars are 20µm). **B:** Quantification of cellular distribution from three independent experiments, at least 100 cells were counted per condition. Error bars represent the standard deviation; statistical significance between subcellular compartments from individual GFP-USP7 transfections is indicated for one sample t-test (*p≤0.05, **p≤0.01 and ***p≤0.005). N, nucleus; C, cytoplasm.

6.3.3 S18 phosphorylation influences USP7 protein interactions.

The S18 phosphorylation site is at the extreme N-terminal of the protein adjacent to the TRAF domain (Figure 6.1A). The TRAF domain is essential for a number of protein and substrate interactions (Holowaty et al., 2003). As S18 phosphorylation affects activity (Figure 6.2C and D) and subcellular localisation (Figure 6.3) I was interested to see whether S18 phosphorylation could also affect the affinity of USP7 for its substrates. The cell cycle effector Rb is a key regulator of the G_1/S checkpoint and was recently discovered to interact with

USP7. This temporal interaction was described to regulate Rb stability throughout late G_1, governing the S-phase boundary.

As discussed in Section 5.4.2, there was a strong correlation between S18-phosphorylated USP7 and Ub-VME reactivity at G_1/S. I wanted to investigate whether S18 phosphorylation could promote the interaction between USP7 and Rb and in doing so could govern the G_1/S transition. Therefore, I performed a preliminary immunoprecipitation experiment analysing Rb interaction with the four exogenously expressed GFP-tagged USP7 constructs. I used the GFP tag on the exogenous USP7 constructs to immunoprecipitate USP7, and its interactors, and subsequently analysed Rb interaction through immunoblotting (Figure 6.4). To ensure an interaction between GFP-USP7 and Rb was specific to the USP7 protein, I performed a parallel immunoprecipitation from cells transfected with an EGFP expressing vector. Rb was not detected in the GFP control immunoprecipitation, indicating that any interaction identified was specific to the USP7 protein (Figure 6.4B). GFP immunoprecipitation efficiently pulled down each of the exogenously expressed USP7 constructs, as GFP-USP7 was not observed in the unbound flow through (Figure 6.4A). Rb was efficiently pulled down with all four USP7 constructs. To correct for differential expression of exogenous USP7, Rb interaction was normalised against the amount of GFP-USP7 within each sample. Rb interaction did not appear to be dependent upon USP7 phosphorylation or catalytic activity as there was little variation in the amount of Rb pulled down with each construct (Figure 6.4B).

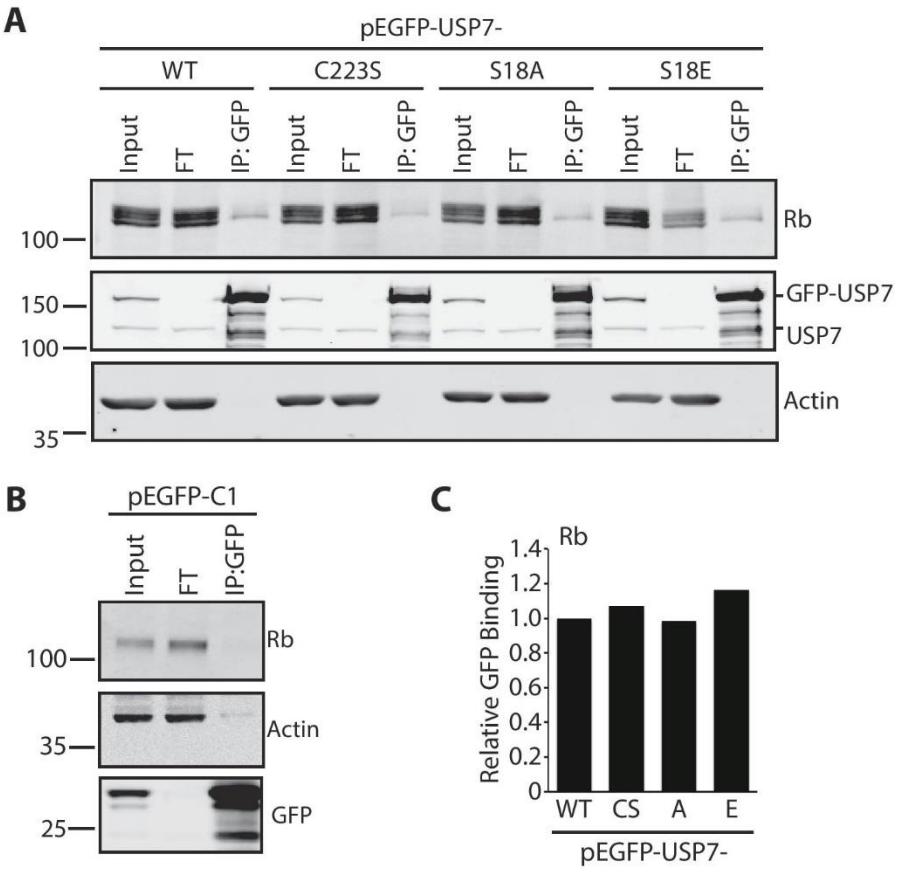

Figure 6.4: Rb interaction with exogenous USP7 is not dependent upon catalytic activity or S18 phosphorylation.

Co-immunoprecipitation of endogenous Rb with exogenous GFP-tagged USP7. **A and B**: A549 cells were transfected with GFP-tagged USP7 (A) or GFP only (B) constructs 24 hours prior to lysis. Equal amounts of cleared lysate (1mg) were incubated with 10µL GFP-NanoTrap beads for 16 hours at 4ºC with agitation. Immobilised proteins were released after SDS incubation at 95ºC for 5 minutes. Samples were separated on a 4-12% polyacrylamide gradient gel and immunoblotted for USP7, Rb, GFP and actin. Input: 1%, Flow through (FT): 1%, Eluate: 50%. **C:** Quantification of relative GFP binding for Rb (for two independent experiments).

Even though S18 phosphorylation did not mediate the interaction between USP7 and Rb, this TRAF domain adjacent phosphorylation site could still regulate binding to other substrates or interacting proteins. Therefore, I decided to investigate whether S18 phosphorylation could facilitate the interaction between USP7 and three well-established USP7 binding proteins: USP11, GMPS and P53. USP11 was originally shown to interact with USP7 in a large-scale DUB interactome study (Sowa et al., 2009). This interaction has since been identified

to play a role in the DNA damage response and epigenetic regulation (Ke et al., 2014; Maertens et al., 2010). Like USP7, it is a nuclear DUB that exhibited similar Ub-VME reactivity to USP7 throughout cell cycle progression (Chapter 4, Figure 4.10), this made it an interesting candidate for these interaction studies. GMPS was another obvious candidate to study as it has a well-defined role as an allosteric regulator of USP7 activity (Faesen et al., 2011a; Reddy et al., 2014). Finally, P53 is a classical substrate of USP7 and has been used as a readout of USP7 activity both in cells (Khoronenkova et al., 2012) and *in vitro* (Faesen et al., 2011a). It would be interesting to compare the S18-dependent binding profiles between a USP7 substrate (P53), an interacting protein (USP11) and an allosteric regulator (GMPS).

To elucidate whether S18 phosphorylation could affect the affinity of USP7 for these three proteins, I performed a preliminary experiment exogenously expressing the four GFP-tagged USP7 constructs and analysed USP7 protein interaction via GFP immunoprecipitation and immunoblotting (Figure 6.5). Again, I performed a parallel immunoprecipitation from cells expressing EGFP to validate whether an interaction was specific to the USP7 protein or the N-terminal GFP tag (Figure 6.5A, left panel). USP11, GMPS and P53 were not detected in the control immunoprecipitation, confirming that any interaction was specific to the exogenous USP7 variants. GFP immunoprecipitation efficiently pulled down exogenously expressed USP7, as GFP-USP7 was not observed in the unbound flow through after GFP immunoblotting. Furthermore, immunoblotting for endogenous USP7 revealed that USP7 does not appear to dimerise. A USP7 band was not identified in the eluate of any GFP-USP7 pull down, furthermore there was no decrease in the proportion of unbound endogenous USP7 in the flow through (Figure 6.5A, right panel).

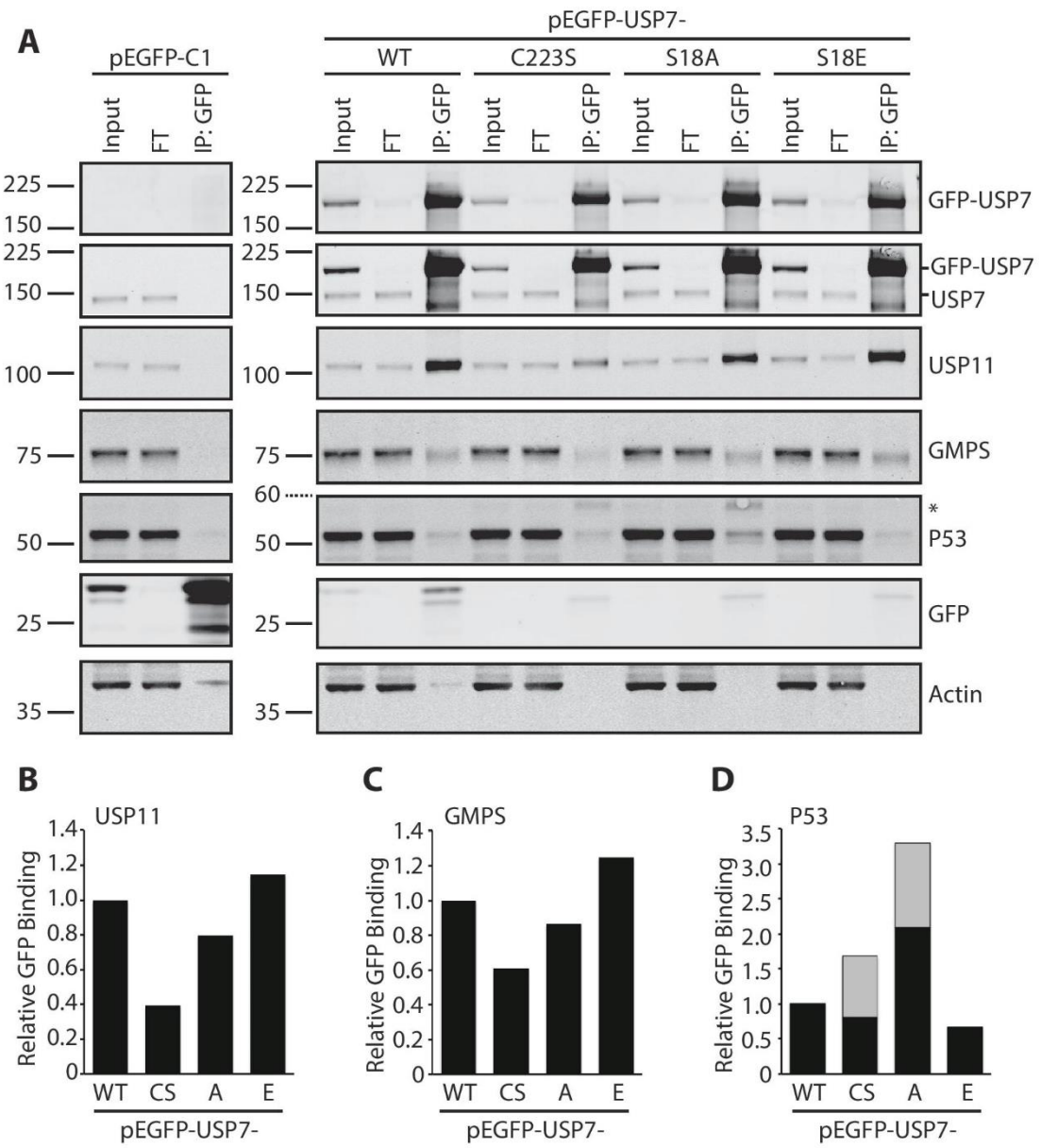

Figure 6.5: Catalytic activity and S18 phosphorylation status affect USP7 binding affinity for interacting proteins.

Co-immunoprecipitation of USP7 interactors and exogenous GFP-tagged USP7 **A:** A549 cells were transfected with GFP-tagged USP7 or GFP only constructs 24 hours prior to lysis. Equal amounts of cleared lysate (1mg) were incubated with 10µL GFP-NanoTrap beads for 16 hours at 4ºC with agitation. Immobilised proteins were released after 2% SDS incubation at 95ºC for 5 minutes. Samples were separated on a 4-12% polyacrylamide gradient gel and immunoblotted for GFP, USP7, USP11, GMPS, P53 and actin. The dotted molecular weight marker refers to where the membrane was cut at 60kDa. Input: 1%, Flow through (FT): 1%, Eluate: 50%. **B-D:** Quantification of relative GFP binding (normalised to GFP-USP7 pull down) for USP11 (**B**), GMPS (**C**) and P53 (**D**) from two independent experiments. Differential binding was set relative to the GFP-USP7-WT control. Quantification of a suspected monoubiquitylated form of P53 depicted in D (grey bars), modified P53 marked as a * in A.

Interestingly, USP11 interaction with USP7 appeared to be dependent upon catalytic activity of USP7 as there was a substantial decrease in USP11 immunoprecipitated with USP7-C223S compared to the wild type control. Additionally, a decrease in USP11 binding was observed with phospho-mutant (S18A) pull down compared to the wild type control and the phospho-mimetic USP7 (S18E) (Figure 6.5A and B). This is further evidence to suggest that the USP7-S18A mutant behaves in a similar manner to the inactive C223S mutant, as it was previously seen that non-phosphorylatable USP7 (S18A) exhibited decreased reactivity to Ub-VME (Figure 6.2C and D) phenocopying the USP7-C223S mutant. An intriguing link can perhaps be made between the activity-dependent interaction of USP7 and USP11 (Figure 6.5A and B) and activity-dependent USP7 localisation (Figure 6.3). USP11 is an exclusively nuclear DUB with predicted monopartite and bipartite NLSs (NLS predictions were performed using NLS Mapper (Kosugi et al., 2009a; Kosugi et al., 2009b)). As USP7 lacks a NLS, it likely uses an interaction with a nuclear protein to shuttle into the nucleus. Cumulatively, these data allow me to speculate that USP11 could be one such protein.

Intriguingly, GMPS exhibited a similar interaction profile to that of USP11. GMPS interaction with USP7 also appeared to be dependent on USP7 activity with a decrease in GMPS binding observed for the catalytically inactive (C233S) and non-phosphorylatable USP7 (S18A) (Figure 6.5A and C). In addition, the P53 interaction profile was particularly interesting. There was a sizeable increase in the amount of P53 that immunoprecipitated with non-phosphorylatable USP7 (S18A) compared to the wild type and phospho-mimetic USP7 (S18E) (Figure 6.5A and D). This aligns with previously published data. Upon DNA damage, USP7 preferentially interacted with P53 over MDM2, stabilising P53 levels to coordinate the DNA damage response (Reddy et al., 2014). Additionally, there was a second P53 immuno-reactive band (based on the 50kDa molecular weight marker, and the 60kDa cut used to section the nitrocellulose membrane, this band is approximately 8kDa heavier than unmodified P53). This band only appeared in GFP-USP7-C223S and –S18A immunoprecipitations (marked by * in

Figure 6.5A and grey bars in Figure 6.5D). This band is consistent with the expected molecular weight for monoubiquitylated P53, indicating that the C223S and S18A mutants of USP7 may act as a "substrate trap" whereby catalytically inactive USP7 is unable to deubiquitylate P53 resulting in prolonged binding and therefore in immunoprecipitation studies manifests as a tighter interaction.

The phosphorylation of S18 affects numerous aspects of USP7 behaviour within cells ranging from its subcellular localisation, and interactions with associated proteins, to its catalytic activity towards substrates. It remains unclear how a single phosphorylation event can regulate so many aspects of USP7 function in cells. Could S18 phosphorylation increase enzymatic activity, increasing the interaction and deubiquitylation of substrates, which upon binding shuttle USP7 into different subcellular compartments? Conversely, S18 phosphorylation could instead promote a protein-protein interaction that allosterically increases USP7 activity and enables subcellular compartment shuttling. Therefore, I next wanted to take a fundamental look at whether phosphorylation at S18 was sufficient to regulate the catalytic activity of USP7.

6.4 S18 phosphorylation potentiates USP7 catalytic activity but not substrate binding affinity *in vitro*

6.4.1 Development of an *in vitro* strategy to analyse the effect of CK2-mediated S18 phosphorylation on USP7 activity

CK2 is known to specifically phosphorylate USP7 at S18 (Khoronenkova et al., 2012). I developed an *in vitro* platform from which I could investigate the effects of S18 phosphorylation status on catalytic activity. Recombinant USP7 was extracted from bacterial cells and purified at the protein facility of the Netherlands Cancer Institute (NKI). The phospho-status of recombinant USP7 was unknown, although as *E. Coli* do not contain kinases that can phosphorylate CK2 consensus sites (Kallmeyer et al., 2006) it was assumed that S18 was not phosphorylated.

My first aim was to generate different pools of recombinant USP7, including a pool of S18-phosphorylated USP7, a pool of fully dephosphorylated USP7 and a pool of catalytically inhibited USP7. The catalytically inhibited USP7 was required as basal activity levels of recombinant USP7 were unknown and I needed a negative control that would represent diminished USP7 activity. P22077, a small molecular inhibitor that specifically binds to the USP7 active site (Altun et al., 2011), would be pre-incubated with recombinant USP7 to act as this negative control. I also intended to incubate recombinant USP7 with CK2 or LPP to generate the pools of S18-phosphorylated or dephosphorylated USP7 respectively. Subsequently, these pre-treated USP7 samples and untreated USP7 were to be analysed using three separate *in vitro* activity assays: Ub-chain catalysis, Ub-VME and Ub-AMC (Figure 6.6A). This would enable me to determine the effect of S18 phosphorylation on USP7 activity. Unfortunately, only a limited amount of recombinant USP7 was available and therefore I first optimised each of these assays with an alternative substrate.

Recombinant CK2 was obtained from the MRC Protein Phosphorylation and Ubiquitylation Unit at the University of Dundee. To determine how much CK2 was required in each reaction, I performed a titration of CK2 in a kinase assay against a synthetic peptide (RRRADDSDDDDD). This peptide contains a serine phosphorylation site surrounded by acidic amino acids that make it a highly specific substrate for CK2. The extent of peptide phosphorylation was measured using a luminescent kinase assay in which the level of phosphorylation was inversely proportional to the concentration of ATP remaining after the kinase reaction (Figure 6.6B). The normalised luminescent signal was represented as a proportion of the available ATP from each kinase assay (Figure 6.6C). 100ng CK2 was required to deplete the ATP pool, predicting that 100ng was sufficient to phosphorylate 99% the peptide substrate (grey dashed line). To ensure that the entire pool of recombinant USP7 would be fully S18-phosphorylated I selected a CK2 concentration of 500ng/10µL reaction.

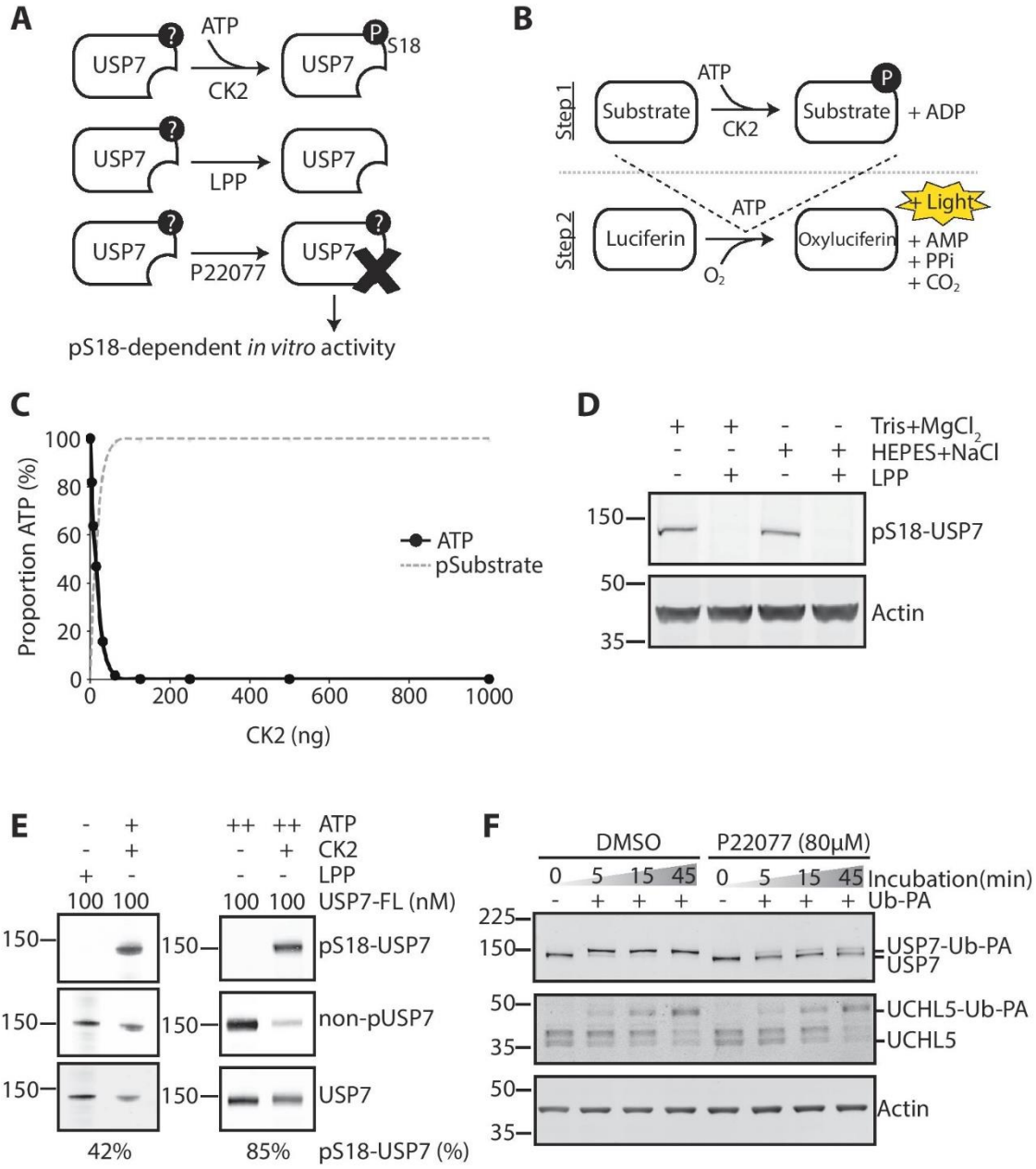

Figure 6.6: Optimisation of *in vitro* USP7 phosphorylation, dephosphorylation and inhibition.

A: Simplified workflow illustrating the generation of three pools of USP7 for *in vitro* activity assays: S18 phosphorylated, dephosphorylated and catalytically inhibited USP7. **B-C:** Optimisation of CK2 kinase assay. **B:** Schematic outlining the methodology of Kinase-Glo® luminescent kinase assay. **C:** Kinase reactions (Kinase buffer supplemented with 100mM synthetic substrate peptide, 10μM ATP and increasing amounts of recombinant CK2) were performed at room temperature (RT) for 60 minutes. Kinase-Glo® reagent was added to the CK2 kinase reaction at a 1:1 ratio and incubated for 10 minutes at RT prior to measuring luminescence. Luminescent signal represented the proportion of residual ATP (black line), the phosphorylation of the synthetic peptide (grey line) is the inverse. **D:** Optimisation of LPP dephosphorylation assay. Asynchronous A549 cells were lysed in E1A lysis buffer. Cleared lysate (5μL, 2mg/mL) was mixed 1:1 with phosphatase reaction mix (Tris-based or HEPES-based buffer supplemented with 1mM $MnCl_2$ and 400U LPP).

Phosphatase reactions were performed at 30ºC for 30 minutes with shaking. Reactions were separated on a 4-12% polyacrylamide gel and immunoblotted for pS18-USP7, non-pUSP7 and actin. **E:** S18-phosphorylation and dephosphorylation of recombinant USP7. Equal amounts (100nM) of full length USP7 (USP7-FL) were dephosphorylated with lambda phosphatase (LPP) or specifically phosphorylated at S18 using CK2, where indicated reactions were supplemented with ATP (concentrations: + 10μM, ++ 200μM). All reactions were incubated at 30ºC for 30min with shaking. Once terminated, the reactions were separated on a 4-12% gradient gel and immunoblotted for pS18-USP7, non-pUSP7 and total USP7 as a control. **F:** Optimisation of P22077 inhibition of USP7. Equal amounts (10μg) of homogenised A549 lysate were incubated with 80μM P22077 or DMSO vehicle control at 30ºC for 30 minutes with shaking. Each reaction was supplemented with 50ng Ub-PA (1:200 probe:protein ratio) and incubated for 5, 15 or 45 minutes at 37ºC with shaking. Reactions were separated by SDS-PAGE on a 4-12% gradient gel and immunoblotted for USP7, UCHL5 and actin.

Recombinant LPP was obtained from New England Bio Labs and was supplied with a HEPES-NaCl buffer, however as the other *in vitro* assays use a Tris-based buffer supplemented with $MgCl_2$ it would be preferable to perform the phosphatase treatment in a matching buffer. I compared phosphatase efficiency in these two different buffers. LPP efficiently dephosphorylated USP7 in both HEPES and Tris-based buffers (Figure 6.6D), enabling me to take forward the Tris-based buffer for future incubations.

Recombinant USP7 was pre-incubated with CK2 or LPP using the conditions defined in the previous experiments and S18 phosphorylation status was analysed using the phospho-specific antibodies validated in Chapter 5, Figure 5.8 (Figure 6.6E). Pre-incubation with CK2 resulted in increased pS18-USP7, and phosphatase treatment abolished S18 phosphorylation accordingly. Although CK2 incubation did result in S18 phosphorylation, the level of non-phosphorylated S18 did not decrease proportionally. I estimated from the residual non-pUSP7 antibody signal relative to total USP7 antibody signal that only 42% of the available USP7 was phosphorylated (Figure 6.6E, left panel). This suggested that under these conditions the pool of USP7 was not fully phosphorylated. This assay could have been limited by the concentration of CK2 or ATP, as I had already titrated the amount of CK2 in each reaction I next increased the concentration of ATP from 10μM to 200μM. The proportion of S18-phosphorylated USP7 increased with the increase in ATP concentration, with 85% of USP7 phosphorylated after a 30-minute incubation (Figure 6.6E, right panel). Furthermore, immunoblotting analysis of untreated USP7 revealed that

recombinant USP7 was not phosphorylated at S18 during expression in bacterial cells (Figure 6.6E, right panel).

P22077 inhibition of USP7 was optimised in A549 cell extracts using Ub-PA to measure the inhibition of USP7 activity (Figure 6.6F). A549 extracts were pre-incubated with P22077 or a DMSO vehicle control for 30 minutes prior to the addition of Ub-PA and were subsequently incubated over a time course to monitor binding. Pre-incubation with P22077 significantly reduced USP7 reactivity towards Ub-PA compared to the DMSO control. UCHL5, a DUB that is not inhibited by P22077 (Altun et al., 2011), was employed as a control. UCHL5 reactivity to Ub-PA did not decrease upon incubation with P22077, showing an identical activity profile to the vehicle control. This confirmed that P22077 inhibited USP7 catalytic activity under these conditions.

Taken together, these preliminary experiments revealed that recombinant USP7 was not phosphorylated at S18 after purification from an E. Coli system. I could manipulate this by pre-incubating with CK2 to increase the proportion of S18-phosphorylated USP7. Phosphatase treatment would abolish USP7 phosphorylation, therefore by comparing these two pools of pre-treated USP7 I could directly investigate the role of S18-phosphorylation on USP7 activity.

6.4.2 CK2 mediated phosphorylation of USP7 heightened USP7 activity towards a K48-linked ubiquitin chain substrate *in vitro*

USP7 activity was analysed in three *in vitro* assays the first of which employed recombinant K48-Ub_4 chains as a substrate to measure USP7 catalysis. Pre-incubation with CK2, LPP or P22077 produced five distinct pools of USP7 to be tested: untreated, S18-phosphorylated, dephosphorylated, catalytically inhibited, and S18-phosphorylated and catalytically inhibited USP7. Each pool of USP7 was incubated with equal amounts of K48-Ub_4 and catalysis was analysed through ubiquitin immunoblotting (Figure 6.7A).

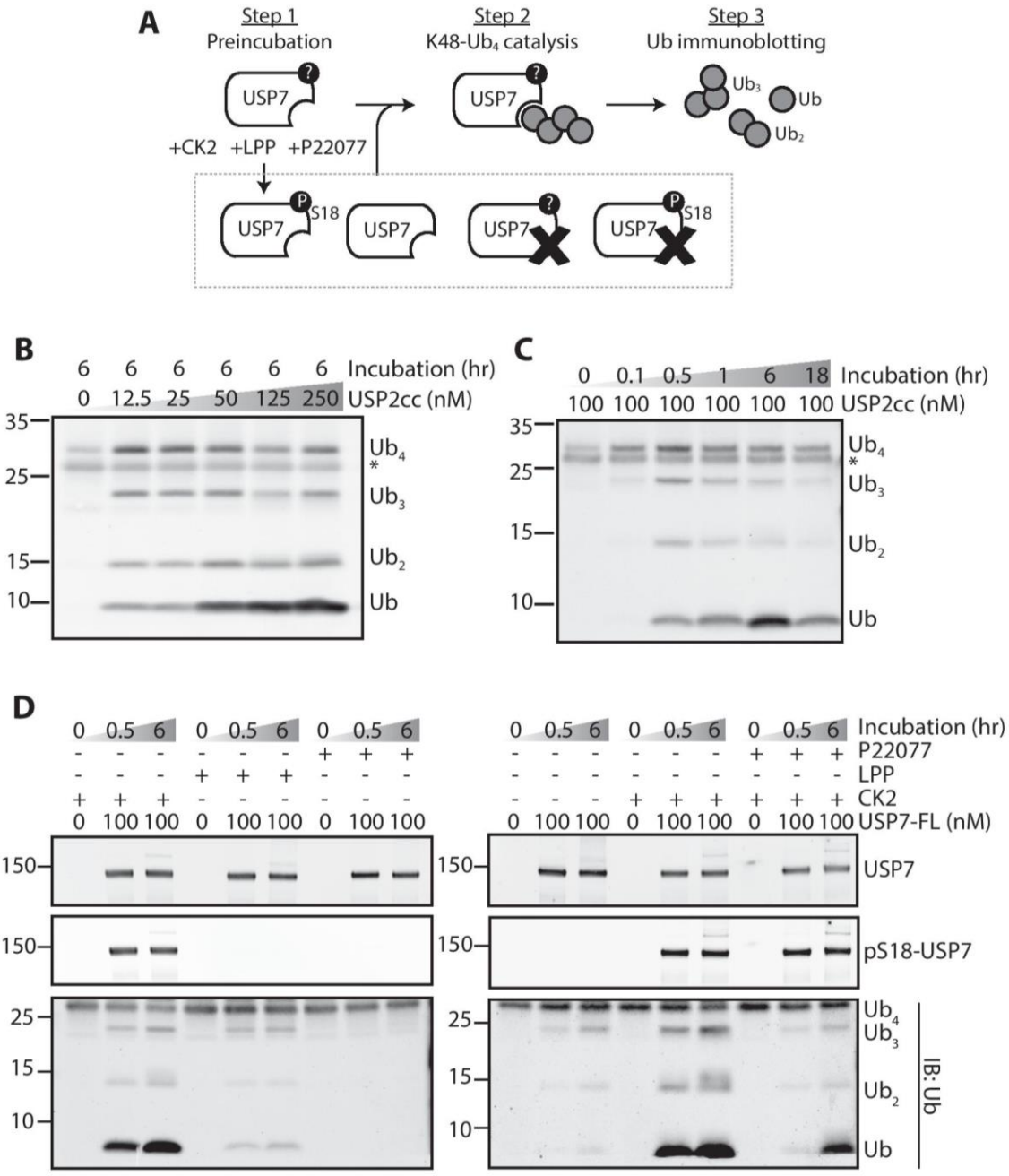

Figure 6.7: CK2 mediated S18-phosphorylation increases USP7 catalysis of K48-linked Ub chains.

A: Schematic representing experimental workflow. **B-C:** Optimisation of K48-Ub_4 activity assay using USP2cc. All reactions were incubated at 37ºC and 300rpm in a thermo-shaker. Once terminated, reactions were separated on a 4-12% polyacrylamide gel and immunoblotted for Ub. **B:** DUB concentration. Increasing concentrations of purified USP2cc (0-250nM) were incubated with 125ng K48-Ub_4 in DUB reaction buffer for 6 hours. **C:** Incubation time. Equal amounts of recombinant USP2cc (100nM) were incubated with 125ng K48-Ub_4 in DUB reaction buffer for increasing periods of time (5 minutes - 18 hours). **D:** S18-phosphorylation directly increases USP7 cleavage of K48-linked Ub chains. Equal amounts of recombinant USP7 (100nM) were pre-treated with CK2, LPP or P22077 for 30 minutes at 30ºC alongside an untreated control to generate the 5 pools of USP7 depicted in A (with

low ATP concentration (10μM in left panel) or high ATP concentration (200μM in right panel)). Each sample was supplemented with 25mM KCl and 125ng K48-Ub_4 and incubated for 30 minutes or 6 hours at 37ºC with shaking. Once terminated, reactions were separated on a 4-12% gradient gel and immunoblotted for USP7, pS18-USP7 and Ub.

The amount of recombinant USP7 available was limited and yet these *in vitro* assays required optimisation. To initially optimise the conditions for K48-Ub_4 assays I used the catalytic domain of USP2 (USP2cc), a highly active deubiquitylase. The concentration of USP2cc was titrated from 0-250nM, aiming to determine the lowest concentration that could be used to produce quantifiable chain catalysis. Increasing concentrations of USP2cc resulted in a decrease in K48-Ub_4 and concurrent accumulation of mono-ubiquitin (Figure 6.7B). Surprisingly, USP2cc was less reactive than expected, this may have been a result of poor quality or partially degraded recombinant protein. Nevertheless, after a 6 hour incubation with 125nM USP2cc there was a sizeable decrease in K48-Ub_4. Yet 50nM was still sufficient to accumulate monoubiquitin and so I decided to take forward a concentration of 100nM for future reactions. This concentration was used in a time course to help define a set of incubation conditions. Again, a 6 hour incubation resulted in a substantial increase in monoubiquitin levels (Figure 6.7C). Surprisingly, an overnight incubation did not further increase monoubiquitin accumulation. Instead there was a decrease in the overall level of ubiquitin, suggesting that prolonged reaction times result in protein degradation (Figure 6.7C). Therefore, a 6 hour time point was coupled with a shorter incubation period of 30 minutes for future assays.

Using these conditions, two separate K48-Ub_4 assays were performed for USP7. The first compared S18-phosphorylated and dephosphorylated USP7 to a P22077-inhibited control (Figure 6.7D left panel). The second compared untreated and S18-phosphorylated USP7 to a P22077-inhibited control that had also been phosphorylated by CK2 (Figure 6.7D, right panel). Untreated or phosphatase-treated USP7 exhibited minimal activity towards K48-Ub_4 with only a marginal increase in monoubiquitin accumulation compared the P22077 inhibited control in which no catalysis was observed (Figure 6.7D left panel). Pre-incubation with CK2 phosphorylated USP7 at S18, this was confirmed using phospho-specific

antibodies. Upon S18-phosphorylation there was a substantial reduction in K48-Ub_4 levels with a concurrent accumulation of tri-, di- and monoubiquitin bands. This clearly depicted a phosphorylation-dependent increase in catalytic activity. Moreover, S18-phosphorylated USP7 was less susceptible to P22077 inhibition, as monoubiquitin accumulation increased when catalytically inhibited USP7 was pre-treated with CK2 compared to the untreated sample (Figure 6.7D, right panel). The ability to cleave K48-Ub_4 chains *in vitro* was therefore markedly elevated by S18 phosphorylation, suggesting a direct link between S18 phosphorylation and USP7 activity.

6.4.3 S18-phosphorylation instigates a modest increase in USP7 reactivity to Ub-VME *in vitro*.

To further investigate this link and to establish whether this increase in activity was a result of an increased on-rate of ubiquitin binding, I took the same five pools of differentially modified USP7 to measure their reactivity towards Ub-VME activity probes *in vitro* by immunoblotting with phospho-specific antibodies (Figure 6.8A). Again, recombinant USP2cc was used initially to optimise the conditions for the *in vitro* Ub-VME reactions. The concentration of DUB used in each reaction was 100nM, to remain consistent with the previous concentrations used in Ub-chain assays. The concentration of Ub-VME was titrated to determine to optimal ratio of Ub-VME:DUB in these *in vitro* assays. We did not have an antibody that was raised against the catalytic domain of USP2cc and so I used a Coomassie stain to measure the extent of Ub-VME reactivity (Figure 6.8B). Approximately half of USP2cc was Ub-VME bound after a 30 minute incubation using a ratio of 2.5:1 Ub-VME: USP2cc. A time course was performed to determine a range of incubation periods for these *in vitro* assays. USPS2cc binding to Ub-VME was rapid with approximately half of USP2cc becoming bound after a 5 minute incubation. Prolonged incubation did not significantly increase the level of USP2cc reactivity towards the Ub-VME probe (Figure 6.8B). However, the amount residual Ub-VME suggests the probe was in large excess, implying that not all of the USP2cc was catalytically active. Using these preliminary experiments, the *in vitro* Ub-VME assay would use a ratio of 2.5:1 Ub-VME: USP7 with incubation periods of 5 or 45 minutes.

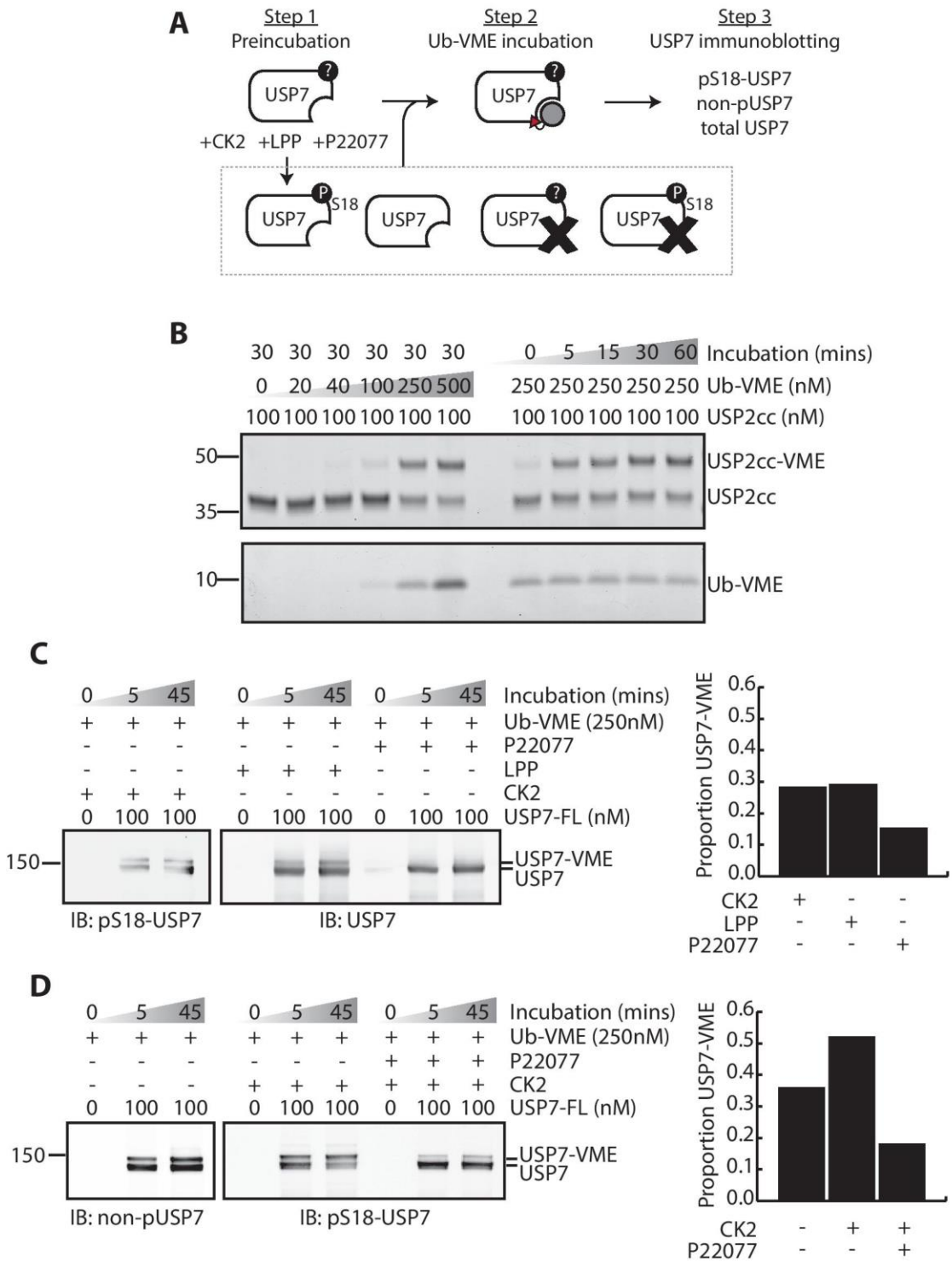

Figure 6.8: S18-phosphorylated USP7 exhibits increased reactivity towards Ub-VME.

A: Schematic representing experimental workflow. **B:** Optimisation of Ub-VME activity assay using USP2cc. All reactions were incubated at 37ºC and 300rpm in a thermo-shaker. Once terminated, reactions were separated on a 4-12% polyacrylamide gel, the gel was subsequently fixed and Coomassie stained to visualise USP2cc and residual HA-Ub-VME. Titration of HA-Ub-VME concentration (left): 100nM USP2cc was incubated with increasing concentrations of HA-Ub-VME. Incubation time (right): 100nM USP2cc was incubated with 250nM HA-Ub-VME (2.5:1 probe:DUB ratio) for increasing lengths of time (5-60 minutes). **C and D:** S18-

phosphorylation potentiates reactivity to Ub-VME reactivity probe. Equal amounts of recombinant USP7 (100nM) were pre-treated with CK2, LPP or P22077 for 30 minutes at 30ºC (with low ATP concentration (10μM in C) or high ATP concentration (200μM in D)) alongside an untreated control to generate the 5 pools of USP7 depicted in A. Each sample was supplemented with 250mM sucrose, 2mM ATP and 250nM HA-Ub-VME and incubated for 5 or 45 minutes at 37ºC with shaking (300rpm). Once terminated, reactions were separated on a 4-12% gradient gel and immunoblotted for USP7 and pS18-USP7 (C) or non-pUSP7 and pS18-USP7 (D). The proportion of Ub-VME bound USP7 (after 45 minutes) was quantified using densitometry and represented in the graphs (right).

Using these assay conditions, two separate Ub-VME assays were performed following the same pre-incubation conditions previously tested in the Ub-chain assays in Figure 6.7. The first assay was performed using USP7 that had been pre-incubated with CK2 in low ATP concentrations (10μM) in which only 42% of recombinant USP7 was phosphorylated at S18 (Figure 6.6E, left panel). S18-phosphorylated USP7 progressively bound to Ub-VME with approximately a third being Ub-VME bound over the 45-minute time course (Figure 6.8C). A similar profile was seen with the LPP-treated samples, un-phosphorylated USP7 was equally Ub-VME reactive over the time course, with a third being Ub-VME bound after 45 minutes (Figure 6.8C). P22077 treated samples were less reactive with only 15% Ub-VME bound after a 45 minute incubation.

A second Ub-VME assay was performed which used USP7 that had been pre-incubated with CK2 at a high ATP concentration (200μM) to achieve 85% S18-phosphorylation of USP7 (Figure 6.6E, right panel). Approximately 30% of USP7 bound to Ub-VME after 5 minutes in both untreated and CK2-treated samples (Figure 6.8D). There was only a small increase in reactivity of non-phosphorylated USP7 after 45 minutes, with 36% being Ub-VME bound. In contrast, S18-phosphorylated USP7 progressively bound over the time course with over 50% becoming Ub-VME bound after 45 minutes. P22077 effectively inhibited USP7 activity with only 18% of S18-phosphorylated and P22077-inhibited USP7 being bound after 45 minutes. In contrast to the K48-Ub_4 assay (Figure 6.7D, right panel), S18 phosphorylation was not sufficient to overcome P22077 inhibition (Figure 6.8D).

The increase in S18-phosphorylated USP7 reactivity towards Ub-VME *in vitro* is modest compared to the activity increase seen in the K48-Ub_4 assays. The Ub-VME assay measures the on-rate of ubiquitin binding and not the catalytic rate, suggesting that S18 phosphorylation may influence the latter stages of Ub catalysis (Figure 3.1) rather than the on-rate of ubiquitin binding.

6.4.4 CK2-mediated phosphorylation of S18 potentiates USP7 enzyme efficiency 5-fold towards an Ub-AMC substrate *in vitro*

To investigate this hypothesis and elucidate how S18 phosphorylation affects USP7 enzyme efficiency I performed an Ub-AMC activity assay, from which I could analyse substrate binding affinity (K_m) and catalytic turnover (K_{cat}). I pre-incubated recombinant USP7 with CK2, LPP or P22077 to generate 4 distinct pools of USP7: untreated, S18-phosphorylated, dephosphorylated and catalytically inhibited USP7. Ub-AMC catalysis was analysed, converting AMC fluorescence (Em:410nM) into the concentration of hydrolysed AMC (Figure 6.9A). Again, recombinant USP2cc was used initially to optimise the conditions for the *in vitro* Ub-AMC assay. The concentration of DUB (USP2cc) was titrated from 1-100nM, aiming to determine a concentration that resulted in a linear rate of reaction over the incubation time course. The lowest concentration of USP2cc (1nM) only resulted in a negligible increase in AMC fluorescence over a 60 minute incubation (Figure 6.9B). As expected, increasing the concentration of USP2cc increased AMC fluorescence, however emission from the highest concentration of USP2cc (100nM) plateaued after 30 minutes suggesting that the concentration of Ub-AMC was limiting for these assay conditions. Therefore, I decided to take forward a concentration of 10nM for future reactions with recombinant USP7. There was a linear rate of AMC fluorescence over the 60 minute time course, neither the concentration of DUB nor Ub-AMC was limiting throughout this incubation.

To quantify the effect S18 phosphorylation of USP7 had on Ub-AMC catalysis and to make the data comparable to previous USP7 activity studies (Faesen et al., 2011a; Faesen et al., 2011b), I converted the relative fluorescence emitted from the free AMC reporter into the concentration of hydrolysed AMC. To do this I

plotted the relative fluorescence of increasing amounts of free AMC to generate a standard curve (Figure 6.9C). All future experiments used the equation from this standard curve to convert relative fluorescence (AU) into the molar concentration of released AMC (μM).

Using these conditions, two separate Ub-AMC assays were performed for USP7. The first compared S18-phosphorlyated USP7 (using USP7 that had been pre-incubated with CK2 in low ATP concentrations) and LPP-dephosphorylated USP7 to a P22077-inhibited control. Even with sub-maximal phosphorylation of USP7 in the CK2-treated sample (42% S18-phosphorylated (Figure 6.6E, left panel)) there was a substantial increase in the amount of hydrolysed AMC released by CK2-treated USP7 compared to both LPP-treated (3.5-fold) and P22077-inhibited (5.4-fold) USP7 (Figure 6.9D).

A second Ub-AMC assay compared USP7 that had been pre-incubated with CK2 at the higher ATP concentration and achieved 85% S18-phosphorylation (Figure 6.6E, right panel) to untreated USP7 that was supplemented with the same concentration of ATP. Again, over a 90 minute incubation S18-phosphorylated USP7 hydrolysed significantly (1.9-fold) more Ub-AMC than the untreated USP7 (Figure 6.9E). Although the untreated USP7 (Figure 6.9E) was more active than the LPP-dephosphorylated USP7 (Figure 6.9D), catalysing approximately double the amount of Ub-AMC. This could be an artefact of differing ATP concentrations, or could suggest that recombinant USP7 is phosphorylated elsewhere and this marginally increases USP7 activity.

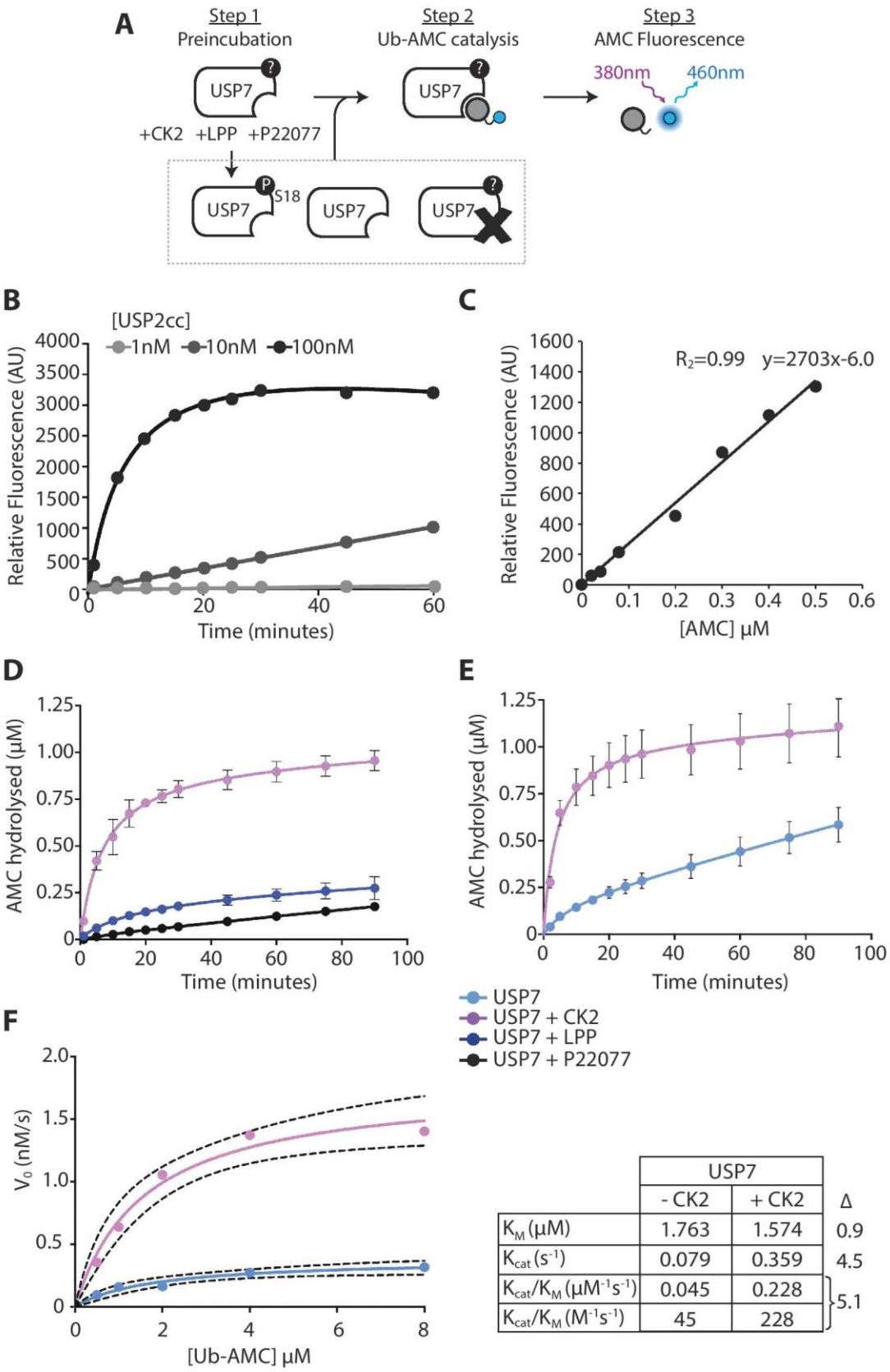

	USP7		
	- CK2	+ CK2	Δ
K_M (µM)	1.763	1.574	0.9
K_{cat} (s^{-1})	0.079	0.359	4.5
K_{cat}/K_M ($\mu M^{-1}s^{-1}$)	0.045	0.228	5.1
K_{cat}/K_M ($M^{-1}s^{-1}$)	45	228	

Figure 6.9: CK2-mediated S18-phosphorylation increases USP7 activity towards Ub-AMC 5-fold.

Figure 6.9: CK2-mediated S18-phosphorylation increases USP7 activity towards Ub-AMC 5-fold.

A: Schematic representing experimental workflow. **B-F:** All Ub-AMC reactions were performed in Ub-AMC reaction buffer and were aliquoted into a 96-well plate in triplicate prior to the addition of Ub-AMC. AMC fluorescence (Ex:365nm, Em:410nm) was measured at regular intervals. **B:** Optimisation of DUB concentration in Ub-AMC activity assay. 1nM, 10nM and 100nM USP2cc in Ub-AMC reaction buffer was incubated with 2μM Ub-AMC. **C:** RFU was converted to molar concentrations of hydrolysed AMC using an AMC standard curve (0-0.5μM AMC). **D-F:** Equal amounts of recombinant USP7 (10nM) were pre-treated with CK2, LPP or P22077 for 30 minutes at 30°C alongside an untreated control to generate the 4 pools of USP7 depicted in A (with low ATP concentration (10μM in D) or high ATP concentration (200μM in E and F)). Each sample was supplemented with 0.5% Tween-20 and 9mM DTT prior to aliquoting and further incubation with 2μM (D and E) or 0.5-8μM (F) Ub-AMC at 30°C. AMC fluorescence was periodically measured over 90 minutes and converted into molar concentrations of hydrolysed AMC. Line graphs depict AMC hydrolysis over time (D and E). Michaelis-Menten analysis provided enzyme kinetics for differentially phosphorylated USP7 (F).

Having demonstrated that CK2-mediated phosphorylation of USP7 increased its activity towards an Ub-AMC substrate, I now wanted to elucidate whether this was a result of decreased K_m or increased K_{cat}. Ub-AMC assays are a biochemical reaction involving a single substrate and as such follow Michaelis-Menten enzyme kinetics. I incubated recombinant USP7 with increasing concentrations of Ub-AMC and measured the initial velocity of each reaction (Figure 6.9F, graph). Non-linear regression software was used to calculate and compare the K_m and K_{cat} of untreated and CK2-treated USP7 (Figure 6.9F, table). CK2-mediated phosphorylation of S18 resulted in a marginal decrease in K_m from 1.76μM to 1.57μM (0.9-fold), suggesting a small increase in binding affinity or "on-rate". This mirrors the modest increase seen in Ub-VME reactivity of S18-phosphorylated USP7 (Figure 6.8D), which as a suicide substrate also reports the on-rate of ubiquitin binding. In contrast, S18-phosphorylation of USP7 considerably increased K_{cat} by 4.5-fold, increasing overall enzyme efficiency (K_{cat}/K_m) 5-fold. This substantial increase in pS18-USP7 efficiency correlates to the increased activity demonstrated towards the K48-Ub_4 substrates demonstrated in Figure 6.7D.

6.5 Discussion

This is the first report to show that the phosphorylation status of S18 intrinsically regulates USP7 catalytic activity and consequently its cellular behaviour. An *in vitro*-based investigation revealed that phosphorylation of S18 directly regulated the catalytic turnover of USP7. Moreover, when linking this data with the *in vivo* studies, it was evident that this potent regulation of USP7 activity influenced its interaction with other proteins as well as its subcellular localisation. It remains unclear how a single phosphorylation event can affect so many facets of USP7 function and would be interesting to understand how this activating phosphorylation connects with the network of mechanisms that regulate USP7 behaviour. I will discuss the possible interplay of S18 phosphorylation and other USP7 regulatory mechanisms in more detail in Chapter 7.

Examining the effect of S18 phosphorylation using parallel *in vitro* and *in vivo* approaches enabled me to determine whether S18 phosphorylation directly regulated USP7 activity and how this affected its role in the cell. Ub-VME was employed for both approaches, firstly to profile differential activity of the four overexpressed USP7 constructs in cell lysates (Figure 6.2) and secondly to measure the differential activity of phosphorylated and de-phosphorylated recombinant USP7-FL (Figure 6.8). The *in vivo* approach revealed that non-phosphorylatable USP7 exhibited decreased reactivity to Ub-VME when compared to the wild type control and the phospho-mimetic USP7 mutant (Figure 6.2C and D). Similarly, the *in vitro* approach showed phosphorylated USP7 was more reactive to Ub-VME than unphosphorylated USP7 (Figure 6.8D). Interestingly however, non-phosphorylatable USP7 exhibited lower relative Ub-VME reactivity in the cellular model than was seen for unphosphorylated USP7 *in vitro*. This suggests there could be additional cellular factors regulating USP7 reactivity towards ubiquitin that are dependent on S18 phosphorylation. Other external regulators of USP7 include protein-protein interactions and sub-cellular localisation. An obvious candidate is the allosteric activator of USP7, GMPS. GMPS preferentially interacted with the S18E phospho-mimetic USP7 compared to the S18A phospho-mutant (Figure 6.5C). Increased interaction of GMPS with

S18-phosphorylated USP7 could contribute to the larger phosphorylation-dependent differential Ub-VME reactivity *in vivo*.

The *in vitro* investigation showed that CK2-mediated phosphorylation of USP7 increased USP7 activity towards K48-Ub_4, Ub-VME and Ub-AMC synthetic substrates (Figure 6.7 – 6.9). However, it should also be noted that for the phosphorylation assay CK2 was in molar excess. A previous study used 1.3x more CK2 than USP7 when confirming that CK2 specifically phosphorylated S18 and no other USP7 residues (Khoronenkova et al., 2012). My investigation used 8x more CK2 than USP7 (Section 2.4.1.2). This could have resulted in multiple residues on USP7-FL becoming phosphorylated during the phosphorylation assay. Using a kinase-specific phosphorylation site prediction tool (KinasePhos 2.0), I identified five predicted phosphorylation sites (S18, S64, S601, S652, S1026) in USP7 (USP7-001, Figure 6.1A) based upon the CK2 consensus sequence S-X-X-E/D. It is yet to be confirmed whether CK2 can phosphorylate these serine residues or whether these phospho-residues can play a role in regulating USP7 catalytic activity. To further this line of investigation and answer definitively whether CK2 phosphorylation of the S18 residue specifically augments USP7 activity, I would assay a recombinant non-phosphorylatable S18A USP7 mutant in parallel with the USP7-WT and repeat these *in vitro* activity assays. However, it is evident from my data that S18 specifically regulates full length USP7 activity, as the non-phosphorylatable S18A USP7 mutant exhibited significantly lower reactivity towards Ub-VME when expressed in cell lysates (Figure 6.2C and D).

I noticed a minor disparity in USP7 activity between the untreated and LPP-treated samples in the Ub-AMC assay. Surprisingly, untreated USP7-FL was more reactive than de-phosphorylated USP7 towards the Ub-AMC substrate, hydrolysing nearly double the concentration of AMC during the 90 minute incubation (compare navy blue and light blue lines in Figure 6.9D and 6.9E). As highlighted previously, this could be an artefact of differing ATP concentrations, or could suggest that recombinant USP7 was phosphorylated in a manner that marginally increases USP7 activity. This was unexpected as the recombinant USP7-FL had been purified from a bacterial expression system (*E. Coli*) that does

not express CK2. However, analysis of the *E. Coli* phospho-proteome revealed that serine/threonine kinases are expressed in *E. Coli* (Macek et al., 2008), and so it is possible that USP7 was phosphorylated prior to the purification process. Immunoblotting recombinant USP7-FL using site-specific phospho-antibodies confirmed that USP7 was not phosphorylated at S18, however I did not confirm the phospho-status of other potential phosphorylation sites and so this could explain why dephosphorylated USP7-FL was less reactive to Ub-VME than the untreated control.

In summary, the methodology I developed to profile the DUBome through the cell cycle identified USP7 amongst a cluster of DUBs upregulated during S-phase and downregulated during mitosis. Having validated this finding, I showed that increased USP7 activity at G_1/S coincided with increased phosphorylation at S18. In this chapter I have shown that this phosphorylation event can influence USP7: (i) sub-cellular localisation, (ii) interaction with its allosteric regulator and key substrates including P53, and (iii) catalytic turnover. I will discuss the implications of these findings in more detail in Chapter 7.

Chapter 7

Discussion

This project aimed to generate the first unbiased global profile of DUB activity across each stage of the cell cycle. The use of Ub-based probes, in conjunction with triplexed SILAC-MS, was successfully employed to profile DUB activity throughout the cell cycle. Twenty-three DUBs were identified, across three of the six DUB families. This DUBome coverage is comparable to a study using HA-Ub-VME pull down for MS identification (Altun et al., 2011) and increases the previously reported coverage for Ub-PA pull down (Ekkebus et al., 2013) by more than 50%. The majority of the DUBs identified exhibited differential reactivity to Ub-PA. In a process as strictly controlled as the cell cycle it was expected that some DUBs would exhibit temporally regulated activity. Nonetheless, it was surprising to reveal the extent of co-regulation between DUBs.

7.1 Temporal co-regulation of DUB activity during the cell cycle

7.1.1 Co-regulated DUB activity during mitosis

Most notably, there was a pervasive downregulation of DUB activity as cells entered mitosis. Nineteen of the twenty-three Ub-PA reactive DUBs had decreased reactivity to Ub-PA in mitotic samples compared to the asynchronous control (Section 4.3.3, Figure 4.7). This was supported by data from the preliminary immunoblotting screen using HA-Ub-VME where a 51% decrease in Ub-VME reactivity at mitosis was identified (Section 3.3.3, Figure 3.4).

Mitotic progression relies upon the temporal proteasomal degradation of cell cycle effector proteins. As discussed in Section 1.5, this is coordinated though a complex interplay of phosphorylation and ubiquitylation (Mocciaro and Rape, 2012). E3 ligase activity is well studied throughout mitosis, best characterised is the role of the APC/C in governing progression through the latter stages of mitosis (Skaar and Pagano, 2009). One could hypothesise that the pervasive decrease in mitotic DUB activity identified here, is required to ensure unidirectional progression of mitosis, particularly as my data comprise the most abundant DUBs (Figure 4.3). The downregulation of DUB activity may remove potential antagonism of polyubiquitylation, so guaranteeing the timely degradation of cell cycle effectors. Unfortunately, the three DUBs known to directly antagonise the ligase activity of the APC/C, USP44, USP37 and USP22

(Huang et al., 2011; Lin et al., 2015; Stegmeier et al., 2007), were not identified in this screen. It would have been interestingly to see how their activity was regulated during mitosis when the APC/C is most active.

Counterintuitively however, amongst the DUBs with downregulated mitotic activity, were some with defined roles in mitosis. For example, USP9X regulates chromosomal alignment and segregation during anaphase through its interaction with Survivin (Vong et al., 2005). Yet, USP9X exhibited a significant decrease in Ub-PA reactivity in mitotic lysates. This could suggest that there is a pool of USP9X active at the mitotic spindle, whilst the majority of USP9X is downregulated.

One concern on seeing a global decrease in reactivity to Ub-PA during mitosis, was that this may be an artefact of nocodazole arrest. However, four DUBs showed increased mitotic reactivity towards Ub-PA compared to the asynchronous control: UCHL1, UCHL3, OTUD4 and USP8 (Figure 4.7). Significantly, USP8 was expected to have increased mitotic activity due to its well-defined role during the final stages of cytokinesis. USP8 is instrumental in regulating membrane scission, to separate the two daughter cells, through its interaction with VAMP8 (Mukai et al., 2008). Therefore, the observed mitotic increase in USP8 reactivity to Ub-PA provides evidence that Ub-PA can accurately profile temporally regulated DUBs, reflecting well-characterised *in vivo* DUB function.

UCHL1 is the most abundant DUB in A549 cells (Geiger et al., 2012) and its inactivation has been linked to the development neurodegenerative diseases, including Parkinson's and Alzheimer's (Leroy et al., 1998; Zhang et al., 2014). UCHL1 exhibited dynamic changes in Ub-PA reactivity as cells passed from G_2/M into G_1 with a notable decrease at mitosis (Figure 4.7). This reflected the modest increase in UCHL1 activity identified via HA-Ub-VME pull down in the preliminary screen (Figure 3.6). For UCHL1, we found increased expression during mitosis but restricted probe reactivity during G_2, preceding activation at G_2/M (Figure 5.2). This pattern is somewhat reminiscent of CCNB1-CDK1, where levels of the

activating CCN rise during G_2 but CDK1 is inactivated by phosphorylation, so that the kinase is poised for acute activation at mitosis. Thus, the UCHL1 profile reflects the hallmark sharp transitions that typify regulators of cell cycle progression.

In fact, UCHL1 can regulate cell cycle progression through the potentiation of CDKs, namely CDK1 and CDK4. Surprisingly, this effect is independent of UCHL1 catalytic activity but proportional to the physical interaction of UCHL1 with CDKs (Kabuta et al., 2013). The exact mechanism of UCHL1 potentiation of CDK activity is not known, however UCHL1 binds CDK4 within the T-loop domain. T-loops can conformationally regulate CDK activity (Jeffrey et al., 1995), and it has been proposed that UCHL1 allosterically increases CDK activity by stabilising this conformation. CCND-CDK4 complexes are active during G_1 governing the restriction point through the temporal phosphorylation of Rb (Section 1.5.2.1). Whereas CDK1, when associated with CCNB, regulates mitosis (Section 1.5.3.1). UCHL1 exhibited increased Ub-PA reactivity in both G_2/M and G_1 extracts compared to the asynchronous control, correlating with the cyclic activity of these CDKs (Figure 4.7).

UCHL1 was originally considered inactive towards ubiquitylated substrates due to a structurally limiting crossover loop which sits directly over the active site (Johnston et al., 1999). This results in the catalytic cysteine being 7.7Å away from the active histidine and is generally considered to be an inactive state (Boudreaux et al., 2010). UCHL1 can pivot into an active conformation upon ubiquitin binding to an exosite; the binding of the ubiquitin monomer reorients the misaligned active cysteine to within 4Å of the catalytic histidine (Boudreaux et al., 2010). UCHL1 has a proposed role in maintaining cellular pool of ubiquitin by inhibiting lysosomal degradation of free ubiquitin (Osaka et al., 2003), which may be shared by UCHL3, and this housekeeping role may account for their abundant expression (Figure 4.3, (Geiger et al., 2012)). Maintaining 'ready-to-use' ubiquitin is likely of greater importance during periods of intense polyubiquitylation like mitosis, and therefore could represent another mitosis-

associated function for UCHL1 and UCHL3, which exhibited the same the dynamic mitotic activity profile as UCHL1.

Currently there is no direct link between UCHL3 function and mitosis or subsequent mitotic exit. However, UCHL3 has deneddylating as well as deubiquitylating activity (Frickel et al., 2007). The predominant target proteins for neddylation are cullins, the scaffold component in CRLs (Merlet et al., 2009). Neddylation of CRLs potentiates their activity, increasing polyubiquitylation of substrates (Read et al., 2000; Wu et al., 2000). CRLs are influential in dynamic regulation during the cell cycle with transient $SCF^{-\beta TrCp}$ activity tightly controlling mitotic progression (Skaar and Pagano, 2009). It may therefore be important to modulate $SCF^{-\beta TrCp}$ activity through altering the balance of neddylation/deneddylation before and after mitosis, which could be hypothesised as a consequence of the observed fluxes in UCHL3 activity. Like UCHL3, there is no well-established cell cycle specific function for OTUD4. However, a recent study identified a role for OTUD4 in repairing DNA alkylation damage. Interestingly, OTUD4 catalytic activity was not required; instead OTUD4 acted as a scaffold, mediating the interaction of USP7 and USP9X with sites of DNA alkylation (Zhao et al., 2015).

7.1.2 Co-regulated DUB activity during S-phase.

There was an interestingly dichotomy observed during S-phase where two clusters of co-regulated DUBs exhibited either increased (Figure 4.7, Cluster 4) or decreased (Figure 4.7, Cluster 2) reactivity to Ub-PA in comparison to the asynchronous control. DUBs have been linked to DNA replication through the post-translational regulation of PCNA. During replication PCNA is constitutively deubiquitylated by USP1/UAF1 (Huang et al., 2006), only becoming ubiquitylated upon reaching a DNA lesion (Hoege et al., 2002). Unfortunately, USP1 was not identified in the Ub-PA reactivity dataset. Conversely, USP7, which exhibited a notable increase in S-phase activity (Figure 4.7), has recently been associated with PCNA activation. At stalled replication forks, DNA polymerase eta (Polη) is instrumental in coordinating PCNA-mediated translesion synthesis. USP7 directly stabilises Polη indirectly affecting PCNA function (Qian et al., 2015).

Dynamic regulation of DUB activity was observed as cells progressed though subsequent cell cycle phases, summarised in Figure 4.6C. This could suggest a role for DUBs in governing checkpoint transitions. Of the twenty-three DUBs profiled, seventeen have been predicted to influence cell cycle progression, half of which are known to regulate DNA damage response pathways to stall the cell cycle or the subsequent DNA repair pathways.

P53, a master regulator of the DNA damage response pathway, is a substrate for multiple DUBs including OTUB1, OTUD5, USP4, USP5, USP7 and USP11 (Brooks et al., 2007; Dayal et al., 2009; Ke et al., 2014; Li et al., 2015; Luo et al., 2013; Sun et al., 2012; Zhang et al., 2011). OTUB1 and USP4 did not exhibit a significant change in Ub-PA reactivity throughout the cell cycle (Figure 4.7, Cluster 1 and 3), suggesting their indirect effect on P53 abundance was not highly regulated in these normally cycling cells. Interestingly, four DUBs that directly interact with and deubiquitylate P53: OTUD5, USP5, USP7 and USP11 all shared increased Ub-PA reactivity during S-phase (Figure 4.7, Cluster 4 and 5).

USP34 Ub-PA reactivity peaked during Early S-phase (Figure 4.7), also reflecting its role during S-phase. USP34 has been identified as a regulator of the DNA damage response through RNF168 at the site of DNA double strand breaks (Sy et al., 2013). RNF168 mediates the assembly of damage repair factors at sites of double strand breaks through K63-linked polyubiquitylation (Doil et al., 2009; Huen and Chen, 2010) and USP34 plays a feed-forward role in this assembly. Taken together, my data for DUBs associated with DNA repair could suggest there is a low level of DNA damage occurring as synchronised cells progress through S-phase, a possible artefact of prolonged thymidine arrest during the cell synchronisation protocol.

7.2 Potential mechanisms for regulation of DUBs through the cell cycle

Analysing DUB expression levels in parallel with Ub-VME reactivity (Section 5.3.1, Figure 5.2) revealed that the dynamic profiles of Ub-PA reactivity (from Chapter 4) represented regulated protein expression in addition to post-

translationally regulated DUB activity. DUB protein expression profiles during the cell cycle represent novel data, as unbiased screens of cell-cycle dependent expression have largely relied on transcriptomics, and show that only USP1 exhibits cell cycle dependent transcription (Gauthier et al., 2008). Interestingly, UCHL1 activity during cell division was dependent upon increased protein expression rather than post-translational regulation. This correlates with its activity-independent function in regulating CDK1 and CDK4 (Kabuta et al., 2013).

Aside from regulated expression, as discussed in Section 1.3 there are a myriad of ways to regulate DUB activity that are broadly grouped into two areas: intramolecular mechanisms (directly pertaining to the DUB and its structure) and external mechanisms (relating to the effect of interacting proteins or protein modifications) (Sahtoe and Sixma, 2015). To investigate whether these mechanisms could account for the temporal co-regulation of DUB activity seen during the cell cycle, I compared Ub-PA reactivity data (Figure 4.7) to a number of characteristics known to moderate DUB behaviour.

7.2.1 Intramolecular mechanisms

First, I looked at intrinsic DUB properties, these included DUB structure (Figures 4.8 and 4.9) and affinity for differential ubiquitin chain linkages (Figure 4.12). Analysis of closely related DUBs revealed that structural similarities of the DUB catalytic domain could correlate to their Ub-PA reactivity in a cell cycle-dependent manner. This was observed for three pairs of USP paralogs: USP15 and USP4, USP40 and USP47, and USP9X and USP24 (Figure 4.9). In each case, these DUBs were the two most closely related paralogs, sharing a sequence similarity of over 50%. However, increased sequence similarity did not ensure co-regulated activity as UCHL1 and UCHL3 share a sequence similarity of 85% yet their Ub-PA reactivity profile although similar from G_2/M to G_1, was divergent throughout S-phase.

An interesting observation became apparent when analysing the phylogenetic tree of the DUBome (Clague et al., 2013). Of the twenty-three DUBs identified from the Ub-PA cell cycle screen, thirteen contained UBL domains. In fact, of the cysteine protease, and therefore Ub-PA reactive, DUBs only twenty contain internal UBL domains. Therefore, around two thirds of all UBL containing DUBs were isolated using the Ub-PA probe. It is not clear whether UBL domains can influence the binding of a DUB to Ub-PA, yet Ub-based probes have been shown to directly influence DUB activity when bound to distal protein domains. The interaction of Ub-VME with an exosite within UCHL1 was shown to orient the active site residues increasing its catalytic ability (Boudreaux et al., 2010).

Polyubiquitin chains form distinct structures dependent upon their chain linkage; K48-linked and K11-linked chains assume a more globular structure, whereas as M1 and K63 linked chains present a more open conformation (Varadan et al., 2002). Given the cell cycle-associated roles for certain ubiquitin chain linkages (Figure 4.12), I wondered whether DUBs with a shared affinity for these chain structures would share Ub-PA reactivity profiles during cell cycle progression. Only two DUBs within the cohort I identified by MS exhibit any chain type specificity: OTUB1 and OTUD4 specifically cleave K48-linked ubiquitin chains. They exhibited divergent cell cycle Ub-PA reactivity profiles. K48-linked polyubiquitylation is synonymous with proteasome-mediated protein degradation, which is widely employed to mediate a plethora of cell cycle-independent functions. A recent study characterised linkage specificity of forty-two cysteine protease DUBs; thirty-two exhibited *in vitro* activity, within this group 85% were able to cleave K48-linked chains (Ritorto et al., 2014). Therefore, it was unsurprising that ability to cleave K48-linked chains did not correlate with Ub-PA reactivity in a cell cycle-specific manner.

Ubiquitylation is a global process regulating a multitude of cellular activities, yet there are important examples of temporally regulated ubiquitylation during the cell cycle. K11-polyubuiquitlyation is upregulated during mitosis, correlating with degradation of APC/C substrates, which are labelled with K48/K11-linked branched ubiquitin chains, an enhanced signal for proteasomal degradation

(Grice et al., 2015; Matsumoto et al., 2010; Meyer and Rape, 2014; Min et al., 2015). It could be hypothesised that DUBs with higher affinity for K11 chains may antagonise the APC/C, rescuing the temporal degradation of APC/C substrates. Interestingly, the DUBs in my dataset that exhibit a preference for K11-linked chains (USP4, USP7, USP9X, USP11, USP15, USP28 and VCPIP1) all had decreased reactivity towards Ub-PA at mitosis (Figure 4.12B). These data support a theory where the pervasive downregulation of DUB activity, in combination with increased K11 and K48-linked branched polyubiquitylation, is required to ensure the unidirectional progression through mitosis.

Alongside K48/K11-linked branched ubiquitin chains, K6-linked, K27-linked and K63-linked ubiquitin chains are also linked to the cell cycle, due to their association with DNA repair. Interestingly, the majority of DUBs with a cleavage preference for K6-linked and K63-linked polyubiquitin chains exhibited increased reactivity towards Ub-PA at S-phase compared to the asynchronous control (Figure 4.12B). Moreover, as previously discussed, three of these DUBs (USP5, USP7 and USP11) all directly interact with and stabilise P53, an upstream coordinator of DNA repair pathways (Dayal et al., 2009; Ke et al., 2014; Li et al., 2002).

7.2.2 External mechanisms

Localisation can have a profound effect on DUB activity (Section 1.3.2.2). Sequestering a DUB away from its substrates or active sub-cellular compartment is a regulatory strategy employed during the cell cycle. USP8 is sequestered by 14-3-3 proteins during interphase in a phosphorylation-dependent manner (Mizuno et al., 2007). S680 phosphorylation promotes this interaction with 14-3-3ε, γ and ζ, whilst dephosphorylation during mitosis reverses this spatial restriction, increasing USP8 catalytic activity and enabling its role during cytokinesis (Mizuno et al., 2007; Mukai et al., 2008).

It should be noted that the subcellular DUB distribution in Figure 4.10 was identified in interphase cells (Urbe et al., 2012) and so any cell cycle-dependent subcellular compartment shuttling is not accounted for. Additionally, the Ub-PA

dataset is generated from detergent-free whole cell extracts, this will represent nuclear and cytoplasmic components, but could exclude proteins from compartments that would require harsher detergent extraction, like chromatin-associated proteins. Moreover, Ub-based probes were incubated with homogenised cell lysates, and so DUBs are no longer spatially restricted within their specific cellular compartments.

Within my dataset, there was no direct link between the subcellular distribution of a DUB at interphase and the Ub-PA reactivity profile during the cell cycle (Figure 4.10). However, the predominantly nuclear DUBs did exhibit some co-regulation with increased reactivity to Ub-PA during S-phase. This may infer that increased nuclear DUB activity is essential, and therefore upregulated, during DNA replication, however of these DUBs only USP7 has been directly linked to the activation of PCNA (Qian et al., 2015). Interestingly, the predominantly nuclear DUBs were also co-regulated at mitosis, where there was decreased reactivity to Ub-PA compared to the asynchronous control. During mitosis the nuclear envelope breaks down removing a barrier between cytosolic and nuclear components. It seems pertinent to downregulate the activity of nuclear DUBs during mitosis to prevent deubiquitylation of substrates from which they are spatially restricted for most of the cell cycle.

Intermolecular interactions are also known to modulate DUB behaviour (Section 1.3.2.3). A classic example is UAF1 allosteric activation of USP1 (Cohn et al., 2007), USP12 and USP46 (Cohn et al., 2009). There is also extensive intermolecular interplay between proteins in the UPS, for example E3 ligases and DUBs are often found in the same protein complexes (Sowa et al., 2009). Pairings between E3 ligases and DUBs, including MDM2:USP7, can regulate their partners stability as well as affect substrate ubiquitylation (Brooks et al., 2007). The interaction maps in Figure 4.11 illustrate some of the complex networks between UPS proteins. Interestingly, in my study some interacting DUBs exhibited analogous Ub-PA reactivity profiles. For example, UCHL5 and USP14 both exhibit increased reactivity during S-phase with a decrease during mitosis (Figure 11A). This was particularly interesting, as these are two of the three

DUBs in the regulatory subunit of the proteasome, insinuating that the deubiquitylating activity of the 19S subunit is subject to temporal regulation through the cell cycle. Unfortunately, the other DUB associated with the proteasome, PSMD14, is a metalloprotease and so could not be profiled in this screen.

Proteins must be unfolded to pass through the narrow axial channels into the 20S core of the proteasome, this rate-limiting step is hindered by substrate bound ubiquitin groups (Yao and Cohen, 2002). PSMD14 deubiquitylates proteins before they enter the proteolytic core of the proteasome (Lander et al., 2012; Lander et al., 2013). UCHL5 and USP14 are not situated at the substrate entry pore, instead they antagonise protein degradation (Schmidt and Finley, 2014). The 19S regulatory particle contains numerous ubiquitin receptors, which in binding ubiquitin can target non-proteolytic ubiquitin chains to the proteasome. It is thought that UCHL5 and USP14 prevent the degradation of these proteins, as K63-linked chains were deubiquitylated 6-fold faster than K48-linked chains resulting in ineffective degradation of K63-conjugated proteins (Jacobson et al., 2009). USP14 and UCHL5 both exhibited lower Ub-PA reactivity specifically at mitosis. As previously discussed, proteasome-mediated degradation of cell cycle effector proteins is essential for unidirectional progression through mitosis. As USP14 and UCHL5 antagonise proteasome activity, this may account for downregulation of these DUBs during mitosis. In contrast, it would be interesting to see whether PSMD14 exhibits increased mitotic activity.

A large-scale phospho-proteomic study, performed by (Olsen et al., 2010) analysed global changes in protein phosphorylation at each stage of the cell cycle. The authors employed high-resolution MS-based proteomics, coupled with SILAC, to investigate dynamic changes in the phospho-proteome during cell cycle progression (Olsen et al., 2010). Their main conclusion was that pervasive increase in mitotic phosphorylation was likely inhibitory to the function of modified proteins. Sixteen of the DUBs within my dataset were post-transitionally modified in a cell cycle-dependent manner with dynamic changes in phosphorylation occurring during cell cycle progression (Olsen et al., 2010).

There was a pervasive increase in the phosphorylation of DUBs during mitosis (Figure 4.13). Given the complex interplay of phosphorylation and the UPS during the cell cycle, one could speculate that this generic increase in mitotic phosphorylation may negatively correlate with the pervasive downregulation of DUB activity during mitosis. Indeed, this would be in agreement with the conclusions drawn from the global phospho-proteome study (Olsen et al., 2010).

The dataset, although extensive with over 24,000 phospho-residues identified (Olsen et al., 2010), did not report or confirm all previously reported cell-cycle phosphorylation events relating to DUB activity. For example, the dephosphorylation of S680 on USP8 during mitosis that releases it from an inhibitory interaction with 14-3-3 proteins (Mizuno et al., 2007; Mukai et al., 2008) was not reflected by global phospho-proteomics (Olsen et al., 2010), where data suggested an increase in mitotic modification of USP8. Furthermore, this increase in mitotic phosphorylation coincides with an increase in USP8 reactivity to Ub-PA (Figure 4.14), suggesting that in some cases mitotic phosphorylation may not inhibit DUB activity, but could potentiate it in a context-dependent manner.

Another phosphorylation event known to directly regulate DUB activity is for OTUD5, which requires phosphorylation at S177 in order to efficiently bind ubiquitin (Huang et al., 2012). This phospho-residue was not identified in the Olsen dataset (Olsen et al., 2010) (Appendix Table 4), yet OTUD5 exhibited dynamic changes in both Ub-PA reactivity and phosphorylation status (Olsen et al., 2010) during cell cycle progression (Figure 4.14).

This is the first report to reveal the extent of co-regulated DUB activity during cell cycle progression. The most striking discovery being the pervasive downregulation of DUB activity as the cell undergoes mitosis. I hypothesised that this temporal downregulation of DUB activity could help promote the timely polyubiquitylation of cell cycle effector proteins, as the degradation of these proteins is essential for the correct progression through each stage of cell division. However, it is also possible that once the nuclear envelope has

dissolved, and so the spatial restrictions of subcellular compartments removed, that DUB activity is downregulated to prevent the non-specific deubiquitylation of any ubiquitylated protein. In any case, the mechanisms involved in regulating DUB activity are complex, especially when relating to a dynamic and heavily regulated process like the cell cycle. It was unlikely that I could establish a unifying factor that globally regulated DUB activity in a cell-cycle specific manner and so it became evident that a focussed investigation into a DUB of interest would be a natural progression of this project.

7.3 USP7 activity is regulated in a cell cycle-specific manner

USP7 was the DUB selected for this more focused investigation. As outlined in Section 5.1, USP7 was already linked to a myriad of roles in cell cycle progression. In addition to this, USP7 activity is carefully controlled through multiple layers of regulation, including intramolecular as well as external mechanisms.

I performed an in-depth characterisation of USP7 expression, activity and regulation across the cell cycle phases. In summary, activity profiling in synchronised cell lysates revealed an interesting pattern. USP7 exhibited increased Ub-VME reactivity from G_1/S throughout S-phase, significantly decreasing as the cell entered mitosis (Figure 5.5). This tightly correlated to the expression levels of USP7 (Figure 5.3), indicating that for the most part USP7 activity is regulated post-translationally through periodic regulation of USP7 protein levels. However, at G_1/S, prior to increased USP7 expression, there was a significant increase in the proportion of USP7 that was reactive towards Ub-VME (Figure 5.5), suggesting additional regulation of USP7 activity at G_1/S.

USP7 exhibited a peak in total Ub-VME reactivity during S-phase (Figure 5.5), which was related to increased USP7 abundance. With such instrumental roles in orchestrating DNA repair it would be important for cells to maintain sufficient USP7 during S-phase. I hypothesize that a reservoir of available USP7 poised is to respond in case DNA damage is detected. However, in normally cycling cells, USP7 activity may need to be restricted to prevent hyper-activation of DNA

repair pathways. This could explain the observed decrease in the proportion of total USP7 that was reactivity during S-phase.

In contrast, the proportion of reactive USP7 was highest during G_1/S (Figure 5.5). I demonstrated that this increase in USP7 activity correlated with an increase in the proportion of S18-phosphorylated USP7 (Figure 5.7). CK2 phosphorylation of S18 has previously been linked to USP7 activity with specific reference to MDM2 and the ATM-dependent DDR (Khoronenkova et al., 2012). As outlined in Section 6.1, CK2 acts a moderator of the G_1/S transition; CK2 has the capacity to stall the cell cycle in G_1 in a P53-dependent manner (Kapoor and Lozano, 1998; Keller and Lu, 2002). The ubiquitylation status of P53 is regulated by a number of proteins, most notably MDM2, an E3 ligase, and USP7, a DUB. Interestingly, CK2-dependent phosphorylation of these two enzymes has been shown to regulate their behaviour, with respect to P53 stabilisation. CK2-mediated phosphorylation of MDM2 inhibits its association with P53 (Allende-Vega et al., 2005; Hjerrild et al., 2001), whereas CK2-mediated phosphorylation of USP7 increased its activity towards MDM2 (Khoronenkova et al., 2012).

Interestingly, preliminary data investigating the effect of S18 phosphorylation status on the interaction between USP7 and P53 revealed a sizeable increase in the amount of P53 that immunoprecipitated with non-phosphorylatable USP7 (S18A) compared to the wild type (Figure 6.5). Additionally, a monoubiquitylated form of P53 was observed to specifically interact with catalytically limited USP7 mutants (C223S and S18A) (Figure 6.5D, grey bars). I hypothesised in Section 6.3.3 that catalytically inactive C223S and S18A mutants of USP7 may act as "substrate traps", where their inability to remove the monoubiquitylation resulted in prolonged binding.

To date, this is the first report to suggest S18 phosphorylation of USP7 affects its interaction with P53 as well as monoubiquitylated P53. Of note, monoubiquitylation of P53 targets it for nuclear export and so this form is predominantly localised to the cytosol (Li et al., 2003). Intriguingly, the sub-cellular localisation of catalytically limited USP7 (C223S and S18A mutants)

exhibited redistribution from the nucleus to the cytosol (Figure 6.3), and so it is tempting to speculate this may be related to their increased interaction with monoubiquitylated P53.

MDM2 monoubiquitylates P53 in a dose-dependent manner; increased MDM2 levels result in more K48-linked polyubiquitylation, whereas low levels of cellular MDM2 promote monoubiquitylation of P53 and its subsequent translocation to the cytosol (Li et al., 2003). Given that (Khoronenkova et al., 2012) report S18-dephosphorylated USP7 has decreased activity towards MDM2, resulting in MDM2-autoubiquitylation and a subsequent decrease in MDM2 protein levels, this likely promotes monoubiquitylation of P53 and its subsequent nuclear export (Li et al., 2003). In addition, mitochondrial-associated cytosolic USP7 has been shown to interact with and deubiquitylate monoubiquitylated P53, enabling P53 to be functionally active in mitochondria (Marchenko et al., 2007). I speculate that these data, taken together with results from my project, could suggest a mechanism of nuclear export for inactive USP7. Data in Figures 6.7-6.9 show that S18 phosphorylation is important for USP7 catalytic activity, whilst interaction data in Figure 6.5 suggests that both the C223S catalytic site mutant and the S18A-USP7 non-phosphorylatable mutant may act as substrate traps for monoubiquitylated P53. The prolonged interaction between inactive USP7 and monoubiquitylated P53 could promote the nuclear export of USP7 in tandem with monoubiquitylated P53. Clearly further experimental work would be needed to prove this hypothesis.

Like the P53-MDM2-USP7 axis, CK2 can also regulate the activity of MDM2 and USP7 with respect to a second cell cycle effector, Rb. Rb levels are precisely regulated by MDM2-mediated polyubiquitylation; this is antagonised by USP7 (Bhattacharya and Ghosh, 2014). The CK2-mediated phosphorylation of S269 of MDM2 is situated in the protein-protein interaction domain and has been reported to decrease MDM2 affinity for Rb and stabilise Rb levels (Gotz et al., 2005). My *in vitro* investigations in Chapter 6 revealed for the first time that CK2-mediated phosphorylation of S18 directly potentiated USP7 catalytic activity (Figure 6.7-6.9). It may be interesting in future to see whether the G_1/S-

dependent increase in S18 phosphorylation on USP7 results in an increased deubiquitylation of Rb. As with P53, CK2 can regulate the ubiquitylation status of Rb through its phosphorylation of MDM2 and USP7 (Bhattacharya and Ghosh, 2014; Gotz et al., 2005; Hjerrild et al., 2001; Khoronenkova et al., 2012). This could suggest a role for these three enzymes in governing the transition from G_1 to S-phase. However, I saw no differential interaction of Rb with phospho-null or phospho-mimetic USP7 in preliminary immunoprecipitation experiments (Figure 6.4). These interaction studies were performed in asynchronous cells, so it could be interesting to further this line of investigation in G_1 synchronised cells.

Both the activity and expression of USP7 significantly decreased during mitosis (Figure 5.3 and 5.5). Yet, as highlighted in Section 5.1, a number of mitotic roles have been identified for USP7, particularly at metaphase where USP7 is an important regulator of genomic stability. USP7, through its interactions with both DAXX and BUB3, prevents the formation of multi-polar spindles as well as ensuring cells do not prematurely enter anaphase (Giovinazzi et al., 2013; Giovinazzi et al., 2014). Both of these events, if deregulated, increase the possibility of unequal division of sister chromatids during anaphase.

On the other hand, general downregulation of USP7 activity during mitosis is consistent with its behaviour towards other substrates. USP7 plays a role in controlling epigenetic modifications through stabilising UHRF1, an E3 ligase important in maintaining DNA methylation patterns. UHRF1 is subject to mitotic phosphorylation of serine 652 (S652), which prevents its protective interaction with USP7 resulting in mitotic degradation (Ma et al., 2012) and reduces the requirement for mitotic USP7 activity in this context.

These examples suggest that USP7 activity may need to be upregulated and downregulated during mitosis in a highly substrate-specific manner. Unbiased screening revealed that global USP7 activity was significantly reduced during mitosis (Figure 5.5), yet there is clear evidence that USP7 is important for the

metaphase-anaphase transition. USP7 is involved in a plethora of cellular functions, with a myriad of known interacting proteins including substrates. I hypothesise that the overall activity of cellular USP7 is restricted during mitosis, as upon the breakdown of the nuclear envelope the spatial restriction of USP7 is altered. With respect to specific mitotic functions, I suggest that when in complex with mitotic effectors, USP7 activity is maintained in a substrate-dependent manner.

7.4 Mechanisms for Regulating USP7 activity

In an attempt to understand how USP7 activity was regulated in a cell cycle-dependent manner I investigated two external factors that modulate USP7 activity: allosteric activation by GMPS and phosphorylation at S18 (Faesen et al., 2011a; Khoronenkova et al., 2012).

GMPS is a metabolic enzyme required for nucleotide biosynthesis, however an allosteric interaction with the UBL-123 domain of USP7 was found to stabilise USP7 in an active conformation increasing its activity 200-fold from its *apo*-conformation (Faesen et al., 2011a; van der Knaap et al., 2005). Interestingly, GMPS expression showed some periodicity with a significant decrease in expression at early G_1 (Figure 5.7A). This did not correlate to the G_1/S-specific increase in USP7 activity. As the major function of GMPS is in nucleotide biosynthesis, it is perhaps not surprising that there was little correlation of expression levels to USP7 activity. GMPS activity towards USP7 is reportedly regulated through a sequestration to the ER, mediated by a monoubiquitylation conferred by the Tripartite motif-containing protein 21 (TRIM21) (Reddy et al., 2014). TRIM21 exhibits cell cycle-specific changes in protein expression (Ly et al., 2014), and so it would be interesting in future to investigate whether TRIM21 expression correlates to USP7 activity. I directly tested whether GMPS affected USP7 reactivity towards Ub-VME and found that GMPS depletion did not have a significant effect (Figure 5.6D). As this assay reports the on-rate of ubiquitin binding for a DUB it essentially measures K_m. However, allosteric regulation of USP7 by GMPS is reported to predominantly increase its K_{cat}, rather than K_m

(Faesen et al., 2011a; Faesen et al., 2011b). This could explain why there was no significant change in USP7 activity with GMPS depletion.

To assess whether S18 phosphorylation of USP7 could affect USP7 function I combined both *in vivo* and *in vitro* approaches (Chapter 6). The *in vitro* approach employed recombinant CK2 to phosphorylate bacterially expressed USP7 and USP7 activity was analysed using three separate USP7 activity assays (Figure 6.7-6.9). In each case CK2-mediated phosphorylation of USP7 increased USP7 catalytic activity, moreover analysis of USP7 enzyme kinetics further elucidated that S18 phosphorylation predominantly increased USP7 K_{cat}, without a large effect on K_m.

How a single phosphorylation event could potently increase USP7 activity remains unclear. My initial hypothesis considered the N-terminal positioning of this phosphorylation, adjacent to the TRAF domain that is essential for the recruitment of numerous USP7 substrates, suggesting that phosphorylation could affect substrate binding. However, in the absence of other cellular proteins, these *in vitro* experiments definitively link S18 phosphorylation with direct potentiation of USP7 catalytic activity. This suggests that S18 phosphorylation can also affect USP7 activity through an intramolecular mechanism.

A number of investigations have studied the mechanisms that govern USP7 activity. As discussed in Section 1.3.2.1, the *apo*-structure of USP7 is considered inert due to the distance between the catalytic residues preventing the formation of a functional triad (Hu et al., 2002). However, upon ubiquitin binding structural rearrangements realign these residues enabling USP7 enzymatic activity. USP7 exists in equilibrium between these inactive and active states (Faesen et al., 2011a). The structural rearrangement is dependent on the C-terminal tail of USP7, with the catalytic domain of USP7 exhibiting 100-fold lower activity when compared to the full length protein (Faesen et al., 2011a; Fernandez-Montalvan et al., 2007; Rouge et al., 2016). As previously discussed, GMPS stabilises USP7 in this active conformation, additionally increasing USP7 activity 2-fold, making the allosterically stabilised USP7 200-fold more active

than the *apo*-structure of USP7 (Faesen et al., 2011a). Significantly, the pS18-dependent mechanism discussed in this study increased catalytic efficiency (K_{cat}/K_m) of full length USP7 by a higher margin of 5-fold, compared to its unphosphorylated USP7 counterpart (Figure 6.9).

In-depth structural analysis revealed that the intramolecular activation of USP7 relied the C-terminal di-UBL domains, UBL-45, as discussed in Section 1.3.1.1.2. More specifically, the rearrangement of these two UBL domains promoted the interaction of a C-terminal amino acid, isoleucine 1100 (I1100), with two residues in the switching loop that sits over the USP7 active site, tryptophan 285 (W285) and glutamic acid 286 (E286). In fact, single point mutations of these residues abolished USP7 catalytic activity (Faesen et al., 2011a). More recent studies have also identified a third region of interest within the USP7 structure that can regulate the interaction between these essential residues in the C-terminal tail and the switching loop. Between the catalytic domain and the first UBL domain in USP7 exists a 26 amino acid region that folds into a rigid helical structure. This linker region plays an important role in the correct positioning of the C-terminal element with respect to the catalytic site (Kim et al., 2016). Once more, mutational analyses revealed that the rigidity, the charge and the length of this rigid helical linker could affect the K_{cat}, but not the K_m, of USP7 activity.

A recent structural study proposed a model for the activation of full length USP7, furthering the knowledge from prior investigations (Faesen et al., 2011a; Kim et al., 2016). Here, the authors suggest that ubiquitin binding initiates the cascade of conformational rearrangements in USP7. The loop containing the catalytic cysteine converts into an α-helical structure, simultaneously exposing the switching loop (Rouge et al., 2016). This precedes this interaction with the C-terminal peptide, which then stabilises USP7 it this active conformation (Rouge et al., 2016). However, in proposing this model they discussed a previously published N-terminal USP7 structure from (Hu et al., 2006). This structure spans the N-terminal TRAF domain and the catalytic domain (residues 53-560), but excludes the extreme N-terminus. Consequently, the N-terminal S18

phosphorylation site still resides in an unstructured region of USP7 and so it is unknown which internal domains it lies adjacent to, or could interact with, when correctly folded.

There are a number of possible hypotheses to speculate how phosphorylation of S18 could so potently regulate catalytic activity of purified USP7. Phosphorylated S18 could either directly interact with the switching loop over the catalytic site, mirroring the role of I1100 at the C-terminal tail, or it could interact with I1100 and promote its interaction with W285 and E286. Moreover, the charge-sensitive region in the helical linker between the catalytic domain and UBL-123 could be involved. The negative charge of the phosphate group could interact with this positively charged region in the linker, and so facilitate the interaction of the C-terminal element with the switching loop.

Comparison of USP7 with the recently characterised phospho-activation of other DUBs may also shed light on the mechanism. OTUD5 is activated by phosphorylation at S177, which also lies in an unstructured N-terminal region (Huang et al., 2012). In this case, the phosphorylation of S177 promoted structural rearrangements upon ubiquitin binding and so increased its activity in a substrate-dependent manner (Huang et al., 2012). USP14 is activated by phosphorylation at serine 432 (S432). In this case the S432 residue lies within one of the blocking loops discussed in Section 1.3.1.2, S432 phosphorylation results in a charge-dependent structural rearrangement of the second blocking loop removing its inhibition of the active site (Xu et al., 2015). USP10 was also recently identified to be activated by single phosphorylation. Like USP7, the activating S76 phosphorylation site lies within an unstructured region towards the N-terminus of the protein and the mechanism outlining how this phosphorylation event increases activity remains unknown (Deng et al., 2016). It appears that without a full crystal structure of USP7, we can only speculate about how S18 phosphorylation could regulate USP7 catalytic activity.

7.5 Future work

My work throughout this investigation provided a novel insight into the extent of DUB regulation throughout the cell cycle, namely the dynamic co-regulation DUB expression and activity during mitosis and S-phase and the discovery that USP7 catalytic activity is regulated by phosphorylation. This has raised many interesting questions that could be addressed in future, for example to:

1. Fully characterise the phosphorylation-dependent potentiation of USP7 catalytic activity *in vitro* and explore the possible interplay with other regulatory mechanisms governing USP7 activity. This could include the structural regulation mediated by the UBL-123 linker helix and the C-terminal peptide in addition to allosteric activation by GMPS.

2. Understand the mechanistic consequences of S18 phosphorylation USP7 regulation *in vivo* by exploring the phosphorylation-dependent effect on cellular compartmentalisation and furthering the preliminary investigation into the interaction profile of phosphorylated USP7 with interacting proteins (GMPS and USP11) and cell cycle-relevant substrates (e.g. P53, MDM2, and Rb).

3. Finally, Ub-based probes proved to be a valuable tool in the unbiased global profiling of DUB expression and activity levels throughout the cell cycle. Twenty-three DUBs were identified in this study, yet with further optimisation of the screening protocols, including the use of more sensitive proteomic instruments, a more comprehensive overview of DUB activity could be obtained.

References

Abdul Rehman, S.A., Kristariyanto, Y.A., Choi, S.Y., Nkosi, P.J., Weidlich, S., Labib, K., Hofmann, K., and Kulathu, Y. (2016). MINDY-1 Is a Member of an Evolutionarily Conserved and Structurally Distinct New Family of Deubiquitinating Enzymes. Mol Cell *63*, 146-155.

Aktas, H., Cai, H., and Cooper, G.M. (1997). Ras links growth factor signaling to the cell cycle machinery via regulation of cyclin D1 and the Cdk inhibitor p27KIP1. Mol Cell Biol *17*, 3850-3857.

Akutsu, M., Dikic, I., and Bremm, A. (2016). Ubiquitin chain diversity at a glance. J Cell Sci *129*, 875-880.

Al-Hakim, A.K., Zagorska, A., Chapman, L., Deak, M., Peggie, M., and Alessi, D.R. (2008). Control of AMPK-related kinases by USP9X and atypical Lys(29)/Lys(33)-linked polyubiquitin chains. Biochem J *411*, 249-260.

Allende-Vega, N., Dias, S., Milne, D., and Meek, D. (2005). Phosphorylation of the acidic domain of Mdm2 by protein kinase CK2. Mol Cell Biochem *274*, 85-90.

Altun, M., Kramer, H.B., Willems, L.I., McDermott, J.L., Leach, C.A., Goldenberg, S.J., Kumar, K.G., Konietzny, R., Fischer, R., Kogan, E., *et al*. (2011). Activity-based chemical proteomics accelerates inhibitor development for deubiquitylating enzymes. Chem Biol *18*, 1401-1412.

Aressy, B., Jullien, D., Cazales, M., Marcellin, M., Bugler, B., Burlet-Schiltz, O., and Ducommun, B. (2010). A screen for deubiquitinating enzymes involved in the G_2/M checkpoint identifies USP50 as a regulator of HSP90-dependent Wee1 stability. Cell cycle *9*, 3815-3822.

Artavanis-Tsakonas, K., Misaghi, S., Comeaux, C.A., Catic, A., Spooner, E., Duraisingh, M.T., and Ploegh, H.L. (2006). Identification by functional proteomics of a deubiquitinating/deNeddylating enzyme in Plasmodium falciparum. Mol Microbiol *61*, 1187-1195.

Avvakumov, G.V., Walker, J.R., Xue, S., Allali-Hassani, A., Asinas, A., Nair, U.B., Fang, X., Zuo, X., Wang, Y.X., Wilkinson, K.D., *et al*. (2012). Two ZnF-UBP domains in isopeptidase T (USP5). Biochemistry *51*, 1188-1198.

Besche, H.C., Sha, Z., Kukushkin, N.V., Peth, A., Hock, E.M., Kim, W., Gygi, S., Gutierrez, J.A., Liao, H., Dick, L., *et al*. (2014). Autoubiquitination of the 26S proteasome on Rpn13 regulates breakdown of ubiquitin conjugates. EMBO J *33*, 1159-1176.

Bhattacharya, S., and Ghosh, M.K. (2014). HAUSP, a novel deubiquitinase for Rb - MDM2 the critical regulator. FEBS J *281*, 3061-3078.

Bilguvar, K., Tyagi, N.K., Ozkara, C., Tuysuz, B., Bakircioglu, M., Choi, M., Delil, S., Caglayan, A.O., Baranoski, J.F., Erturk, O., *et al*. (2013). Recessive loss of function of the neuronal ubiquitin hydrolase UCHL1 leads to early-onset progressive neurodegeneration. Proc Natl Acad Sci U S A *110*, 3489-3494.

BioGRID (2016a). OTUB1 (OTU deubiquitinase, ubiquitin aldehyde binding 1).

BioGRID (2016b). USP7 (ubiquitin specific peptidase 7) (BioGRID).

Blagosklonny, M.V., and Pardee, A.B. (2002). The restriction point of the cell cycle. Cell cycle *1*, 103-110.

Bonnet, J., Romier, C., Tora, L., and Devys, D. (2008). Zinc-finger UBPs: regulators of deubiquitylation. Trends Biochem Sci *33*, 369-375.

Borodovsky, A., Ovaa, H., Kolli, N., Gan-Erdene, T., Wilkinson, K.D., Ploegh, H.L., and Kessler, B.M. (2002). Chemistry-based functional proteomics reveals novel members of the deubiquitinating enzyme family. Chem Biol *9*, 1149-1159.

Bott, M., Brevet, M., Taylor, B.S., Shimizu, S., Ito, T., Wang, L., Creaney, J., Lake, R.A., Zakowski, M.F., Reva, B., *et al.* (2011). The nuclear deubiquitinase BAP1 is commonly inactivated by somatic mutations and 3p21.1 losses in malignant pleural mesothelioma. Nat Genet *43*, 668-672.

Boudreaux, D.A., Maiti, T.K., Davies, C.W., and Das, C. (2010). Ubiquitin vinyl methyl ester binding orients the misaligned active site of the ubiquitin hydrolase UCHL1 into productive conformation. Proc Natl Acad Sci U S A *107*, 9117-9122.

Brehm, A., Miska, E.A., McCance, D.J., Reid, J.L., Bannister, A.J., and Kouzarides, T. (1998). Retinoblastoma protein recruits histone deacetylase to repress transcription. Nature *391*, 597-601.

Bremm, A., Moniz, S., Mader, J., Rocha, S., and Komander, D. (2014). Cezanne (OTUD7B) regulates HIF-1alpha homeostasis in a proteasome-independent manner. EMBO Rep *15*, 1268-1277.

Brooks, C.L., Li, M., Hu, M., Shi, Y., and Gu, W. (2007). The p53--Mdm2--HAUSP complex is involved in p53 stabilization by HAUSP. Oncogene *26*, 7262-7266.

Cappadocia, L., and Lima, C.D. (2017). Ubiquitin-like Protein Conjugation: Structures, Chemistry, and Mechanism. Chem Rev.

Carbone, M., Yang, H., Pass, H.I., Krausz, T., Testa, J.R., and Gaudino, G. (2013). BAP1 and cancer. Nat Rev Cancer *13*, 153-159.

Chauhan, D., Tian, Z., Nicholson, B., Kumar, K.G., Zhou, B., Carrasco, R., McDermott, J.L., Leach, C.A., Fulcinniti, M., Kodrasov, M.P., *et al.* (2012). A small molecule inhibitor of ubiquitin-specific protease-7 induces apoptosis in multiple myeloma cells and overcomes bortezomib resistance. Cancer Cell *22*, 345-358.

Chen, J., Dexheimer, T.S., Ai, Y., Liang, Q., Villamil, M.A., Inglese, J., Maloney, D.J., Jadhav, A., Simeonov, A., and Zhuang, Z. (2011). Selective and cell-active inhibitors of the USP1/ UAF1 deubiquitinase complex reverse cisplatin resistance in non-small cell lung cancer cells. Chem Biol *18*, 1390-1400.

Chen, Z.J., and Sun, L.J. (2009). Nonproteolytic functions of ubiquitin in cell signaling. Mol Cell *33*, 275-286.

Choi, J., Levey, A.I., Weintraub, S.T., Rees, H.D., Gearing, M., Chin, L.S., and Li, L. (2004). Oxidative modifications and down-regulation of ubiquitin carboxyl-terminal hydrolase L1 associated with idiopathic Parkinson's and Alzheimer's diseases. J Biol Chem *279*, 13256-13264.

Ciechanover, A., Elias, S., Heller, H., and Hershko, A. (1982). "Covalent affinity" purification of ubiquitin-activating enzyme. J Biol Chem *257*, 2537-2542.

Ciechanover, A., Heller, H., Elias, S., Haas, A.L., and Hershko, A. (1980). ATP-dependent conjugation of reticulocyte proteins with the polypeptide required for protein degradation. Proc Natl Acad Sci U S A *77*, 1365-1368.

Clague, M.J., Barsukov, I., Coulson, J.M., Liu, H., Rigden, D.J., and Urbé, S. (2013). Deubiquitylases from genes to organism. Physiological reviews *93*, 1289-1315.

Clague, M.J., Heride, C., and Urbe, S. (2015). The demographics of the ubiquitin system. Trends Cell Biol *25*, 417-426.

Clague, M.J., and Urbe, S. (2006). Endocytosis: the DUB version. Trends Cell Biol *16*, 551-559.

Clerici, M., Luna-Vargas, M.P., Faesen, A.C., and Sixma, T.K. (2014). The DUSP-Ubl domain of USP4 enhances its catalytic efficiency by promoting ubiquitin exchange. Nat Commun *5*, 5399.

Cohn, M.A., Kee, Y., Haas, W., Gygi, S.P., and D'Andrea, A.D. (2009). UAF1 is a subunit of multiple deubiquitinating enzyme complexes. J Biol Chem *284*, 5343-5351.

Cohn, M.A., Kowal, P., Yang, K., Haas, W., Huang, T.T., Gygi, S.P., and D'Andrea, A.D. (2007). A UAF1-containing multisubunit protein complex regulates the Fanconi anemia pathway. Mol Cell *28*, 786-797.

Colland, F., Formstecher, E., Jacq, X., Reverdy, C., Planquette, C., Conrath, S., Trouplin, V., Bianchi, J., Aushev, V.N., Camonis, J., *et al*. (2009). Small-molecule inhibitor of USP7/HAUSP ubiquitin protease stabilizes and activates p53 in cells. Mol Cancer Ther *8*, 2286-2295.

Cope, G.A., Suh, G.S., Aravind, L., Schwarz, S.E., Zipursky, S.L., Koonin, E.V., and Deshaies, R.J. (2002). Role of predicted metalloprotease motif of Jab1/Csn5 in cleavage of Nedd8 from Cul1. Science *298*, 608-611.

Costa Mdo, C., and Paulson, H.L. (2012). Toward understanding Machado-Joseph disease. Prog Neurobiol *97*, 239-257.

Crasta, K., Lim, H.H., Giddings, T.H., Jr., Winey, M., and Surana, U. (2008). Inactivation of Cdh1 by synergistic action of Cdk1 and polo kinase is necessary for proper assembly of the mitotic spindle. Nat Cell Biol *10*, 665-675.

Crawford, L.J., Walker, B., and Irvine, A.E. (2011). Proteasome inhibitors in cancer therapy. J Cell Commun Signal *5*, 101-110.

Cunningham, C.N., Baughman, J.M., Phu, L., Tea, J.S., Yu, C., Coons, M., Kirkpatrick, D.S., Bingol, B., and Corn, J.E. (2015). USP30 and parkin homeostatically regulate atypical ubiquitin chains on mitochondria. Nat Cell Biol *17*, 160-169.

D'Arcy, P., Brnjic, S., Olofsson, M.H., Fryknas, M., Lindsten, K., De Cesare, M., Perego, P., Sadeghi, B., Hassan, M., Larsson, R., *et al*. (2011). Inhibition of proteasome deubiquitinating activity as a new cancer therapy. Nat Med *17*, 1636-1640.

Dayal, S., Sparks, A., Jacob, J., Allende-Vega, N., Lane, D.P., and Saville, M.K. (2009). Suppression of the deubiquitinating enzyme USP5 causes the accumulation of unanchored polyubiquitin and the activation of p53. J Biol Chem *284*, 5030-5041.

de Jong, A., Merkx, R., Berlin, I., Rodenko, B., Wijdeven, R.H., El Atmioui, D., Yalçin, Z., Robson, C.N., Neefjes, J.J., and Ovaa, H. (2012). Ubiquitin-based probes prepared by total synthesis to profile the activity of deubiquitinating enzymes. Chembiochem *13*, 2251-2258.

de Jong, R.N., Ab, E., Diercks, T., Truffault, V., Daniëls, M., Kaptein, R., and Folkers, G.E. (2006). Solution structure of the human ubiquitin-specific protease 15 DUSP domain. J Biol Chem *281*, 5026-5031.

Delston, R.B., Matatall, K.A., Sun, Y., Onken, M.D., and Harbour, J.W. (2011). p38 phosphorylates Rb on Ser567 by a novel, cell cycle-independent mechanism that triggers Rb-Hdm2 interaction and apoptosis. Oncogene *30*, 588-599.

den Elzen, N., and Pines, J. (2001). Cyclin A is destroyed in prometaphase and can delay chromosome alignment and anaphase. J Cell Biol *153*, 121-136.

Deng, M., Yang, X., Qin, B., Liu, T., Zhang, H., Guo, W., Lee, S.B., Kim, J.J., Yuan, J., Pei, H., *et al*. (2016). Deubiquitination and Activation of AMPK by USP10. Mol Cell *61*, 614-624.

Diehl, J.A., Zindy, F., and Sherr, C.J. (1997). Inhibition of cyclin D1 phosphorylation on threonine-286 prevents its rapid degradation via the ubiquitin-proteasome pathway. Genes Dev *11*, 957-972.

Doil, C., Mailand, N., Bekker-Jensen, S., Menard, P., Larsen, D.H., Pepperkok, R., Ellenberg, J., Panier, S., Durocher, D., Bartek, J., *et al*. (2009). RNF168 binds and amplifies ubiquitin conjugates on damaged chromosomes to allow accumulation of repair proteins. Cell *136*, 435-446.

Dumaz, N., Milne, D.M., and Meek, D.W. (1999). Protein kinase CK1 is a p53-threonine 18 kinase which requires prior phosphorylation of serine 15. FEBS Lett *463*, 312-316.

Edelmann, M.J., Iphofer, A., Akutsu, M., Altun, M., di Gleria, K., Kramer, H.B., Fiebiger, E., Dhe-Paganon, S., and Kessler, B.M. (2009). Structural basis and specificity of human otubain 1-mediated deubiquitination. Biochem J *418*, 379-390.

Edelmann, M.J., Nicholson, B., and Kessler, B.M. (2011). Pharmacological targets in the ubiquitin system offer new ways of treating cancer, neurodegenerative disorders and infectious diseases. Expert Rev Mol Med *13*, e35.

Ekkebus, R., van Kasteren, S.I., Kulathu, Y., Scholten, A., Berlin, I., Geurink, P.P., de Jong, A., Goerdayal, S., Neefjes, J., Heck, A.J., *et al.* (2013). On terminal alkynes that can react with active-site cysteine nucleophiles in proteases. J Am Chem Soc *135*, 2867-2870.

Eletr, Z.M., and Wilkinson, K.D. (2011). An emerging model for BAP1's role in regulating cell cycle progression. Cell Biochem Biophys *60*, 3-11.

Elia, A.E., Boardman, A.P., Wang, D.C., Huttlin, E.L., Everley, R.A., Dephoure, N., Zhou, C., Koren, I., Gygi, S.P., and Elledge, S.J. (2015). Quantitative Proteomic Atlas of Ubiquitination and Acetylation in the DNA Damage Response. Mol Cell *59*, 867-881.

Elliott, P.R., and Komander, D. (2016). Regulation of Met1-linked polyubiquitin signalling by the deubiquitinase OTULIN. FEBS J *283*, 39-53.

Ellisdon, A.M., Pearce, M.C., and Bottomley, S.P. (2007). Mechanisms of ataxin-3 misfolding and fibril formation: kinetic analysis of a disease-associated polyglutamine protein. J Mol Biol *368*, 595-605.

Ensembl. Ensembl. Gene: USP7 (ENSG00000187555). 11/2012.

Evert, B.O., Araujo, J., Vieira-Saecker, A.M., de Vos, R.A., Harendza, S., Klockgether, T., and Wullner, U. (2006). Ataxin-3 represses transcription via chromatin binding, interaction with histone deacetylase 3, and histone deacetylation. J Neurosci *26*, 11474-11486.

Faesen, A.C., Dirac, A.M., Shanmugham, A., Ovaa, H., Perrakis, A., and Sixma, T.K. (2011a). Mechanism of USP7/HAUSP activation by its C-terminal ubiquitin-like domain and allosteric regulation by GMP-synthetase. Mol Cell *44*, 147-159.

Faesen, A.C., Luna-Vargas, M.P., Geurink, P.P., Clerici, M., Merkx, R., van Dijk, W.J., Hameed, D.S., El Oualid, F., Ovaa, H., and Sixma, T.K. (2011b). The differential modulation of USP activity by internal regulatory domains, interactors and eight ubiquitin chain types. Chem Biol *18*, 1550-1561.

Fan, Y.H., Cheng, J., Vasudevan, S.A., Dou, J., Zhang, H., Patel, R.H., Ma, I.T., Rojas, Y., Zhao, Y., Yu, Y., *et al.* (2013). USP7 inhibitor P22077 inhibits neuroblastoma growth via inducing p53-mediated apoptosis. Cell Death Dis *4*, e867.

Faronato, M., Patel, V., Darling, S., Dearden, L., Clague, M.J., Urbe, S., and Coulson, J.M. (2013). The deubiquitylase USP15 stabilizes newly synthesized REST and rescues its expression at mitotic exit. Cell cycle *12*, 1964-1977.

Faronato, M.U., S and Coulson, JM. (2011). USP15 (ubiquitin specific peptidase 15). Altas Genet Cytogenet Oncol Haematol *15*, 654-651.

Farshi, P., Deshmukh, R.R., Nwankwo, J.O., Arkwright, R.T., Cvek, B., Liu, J., and Dou, Q.P. (2015). Deubiquitinases (DUBs) and DUB inhibitors: a patent review. Expert Opin Ther Pat *25*, 1191-1208.

Fernandez-Montalvan, A., Bouwmeester, T., Joberty, G., Mader, R., Mahnke, M., Pierrat, B., Schlaeppi, J.M., Worpenberg, S., and Gerhartz, B. (2007). Biochemical characterization of USP7 reveals post-translational modification sites and structural requirements for substrate processing and subcellular localization. FEBS J *274*, 4256-4270.

Finley, D., Sadis, S., Monia, B.P., Boucher, P., Ecker, D.J., Crooke, S.T., and Chau, V. (1994). Inhibition of proteolysis and cell cycle progression in a multiubiquitination-deficient yeast mutant. Mol Cell Biol *14*, 5501-5509.

Forbes, S.A., Tang, G., Bindal, N., Bamford, S., Dawson, E., Cole, C., Kok, C.Y., Jia, M., Ewing, R., Menzies, A., *et al*. (2010). COSMIC (the Catalogue of Somatic Mutations in Cancer): a resource to investigate acquired mutations in human cancer. Nucleic Acids Res *38*, D652-657.

Fournane, S., Krupina, K., Kleiss, C., and Sumara, I. (2012). Decoding ubiquitin for mitosis. Genes Cancer *3*, 697-711.

Frickel, E.M., Quesada, V., Muething, L., Gubbels, M.J., Spooner, E., Ploegh, H., and Artavanis-Tsakonas, K. (2007). Apicomplexan UCHL3 retains dual specificity for ubiquitin and Nedd8 throughout evolution. Cell Microbiol *9*, 1601-1610.

Fuchs, S.Y., Adler, V., Buschmann, T., Wu, X., and Ronai, Z. (1998). Mdm2 association with p53 targets its ubiquitination. Oncogene *17*, 2543-2547.

Garcia-Santisteban, I., Peters, G.J., Giovannetti, E., and Rodriguez, J.A. (2013). USP1 deubiquitinase: cellular functions, regulatory mechanisms and emerging potential as target in cancer therapy. Mol Cancer *12*, 91.

Gatti, M., Pinato, S., Maiolica, A., Rocchio, F., Prato, M.G., Aebersold, R., and Penengo, L. (2015). RNF168 promotes noncanonical K27 ubiquitination to signal DNA damage. Cell Rep *10*, 226-238.

Gauthier, N.P., Larsen, M.E., Wernersson, R., de Lichtenberg, U., Jensen, L.J., Brunak, S., and Jensen, T.S. (2008). Cyclebase.org--a comprehensive multi-organism online database of cell-cycle experiments. Nucleic Acids Res *36*, D854-859.

Geiger, T., Wehner, A., Schaab, C., Cox, J., and Mann, M. (2012). Comparative proteomic analysis of eleven common cell lines reveals ubiquitous but varying expression of most proteins. Mol Cell Proteomics *11*, M111.014050.

Giovinazzi, S., Morozov, V.M., Summers, M.K., Reinhold, W.C., and Ishov, A.M. (2013). USP7 and Daxx regulate mitosis progression and taxane sensitivity by affecting stability of Aurora-A kinase. Cell Death Differ *20*, 721-731.

Giovinazzi, S., Sirleto, P., Aksenova, V., Morozov, V.M., Zori, R., Reinhold, W.C., and Ishov, A.M. (2014). Usp7 protects genomic stability by regulating Bub3. Oncotarget *5*, 3728-3742.

Gnad, F., Gunawardena, J., and Mann, M. (2011). PHOSIDA 2011: the posttranslational modification database. Nucleic Acids Res *39*, D253-260.

Goldknopf, I.L., and Busch, H. (1977). Isopeptide linkage between nonhistone and histone 2A polypeptides of chromosomal conjugate-protein A24. Proc Natl Acad Sci U S A *74*, 864-868.

Goldstein, G., Scheid, M., Hammerling, U., Schlesinger, D.H., Niall, H.D., and Boyse, E.A. (1975). Isolation of a polypeptide that has lymphocyte-differentiating properties and is probably represented universally in living cells. Proc Natl Acad Sci U S A *72*, 11-15.

Gotz, C., Kartarius, S., Schwar, G., and Montenarh, M. (2005). Phosphorylation of mdm2 at serine 269 impairs its interaction with the retinoblastoma protein. Int J Oncol *26*, 801-808.

Grice, G.L., Lobb, I.T., Weekes, M.P., Gygi, S.P., Antrobus, R., and Nathan, J.A. (2015). The Proteasome Distinguishes between Heterotypic and Homotypic Lysine-11-Linked Polyubiquitin Chains. Cell Rep *12*, 545-553.

Harbour, J.W., Onken, M.D., Roberson, E.D., Duan, S., Cao, L., Worley, L.A., Council, M.L., Matatall, K.A., Helms, C., and Bowcock, A.M. (2010). Frequent mutation of BAP1 in metastasizing uveal melanomas. Science *330*, 1410-1413.

Harper, J.W., Adami, G.R., Wei, N., Keyomarsi, K., and Elledge, S.J. (1993). The p21 Cdk-interacting protein Cip1 is a potent inhibitor of G1 cyclin-dependent kinases. Cell *75*, 805-816.

Harper, S., Besong, T.M., Emsley, J., Scott, D.J., and Dreveny, I. (2011). Structure of the USP15 N-terminal domains: a β-hairpin mediates close association between the DUSP and UBL domains. Biochemistry *50*, 7995-8004.

Heideker, J., and Wertz, I.E. (2015). DUBs, the regulation of cell identity and disease. Biochem J *467*, 191.

Helin, K., Harlow, E., and Fattaey, A. (1993). Inhibition of E2F-1 transactivation by direct binding of the retinoblastoma protein. Mol Cell Biol *13*, 6501-6508.

Heride, C., Urbe, S., and Clague, M.J. (2014). Ubiquitin code assembly and disassembly. Curr Biol *24*, R215-220.

Hershko, A., and Ciechanover, A. (1998). The ubiquitin system. Annu Rev Biochem *67*, 425-479.

Hershko, A., Ciechanover, A., Heller, H., Haas, A.L., and Rose, I.A. (1980). Proposed role of ATP in protein breakdown: conjugation of protein with multiple chains of the polypeptide of ATP-dependent proteolysis. Proc Natl Acad Sci U S A *77*, 1783-1786.

Hershko, A., Heller, H., Elias, S., and Ciechanover, A. (1983). Components of ubiquitin-protein ligase system. Resolution, affinity purification, and role in protein breakdown. J Biol Chem *258*, 8206-8214.

Heyninck, K., and Beyaert, R. (2005). A20 inhibits NF-kappaB activation by dual ubiquitin-editing functions. Trends Biochem Sci *30*, 1-4.

Hjerrild, M., Milne, D., Dumaz, N., Hay, T., Issinger, O.G., and Meek, D. (2001). Phosphorylation of murine double minute clone 2 (MDM2) protein at serine-267 by protein kinase CK2 in vitro and in cultured cells. Biochem J *355*, 347-356.

Hoege, C., Pfander, B., Moldovan, G.L., Pyrowolakis, G., and Jentsch, S. (2002). RAD6-dependent DNA repair is linked to modification of PCNA by ubiquitin and SUMO. Nature *419*, 135-141.

Hoffmann, I., Clarke, P.R., Marcote, M.J., Karsenti, E., and Draetta, G. (1993). Phosphorylation and activation of human cdc25-C by cdc2--cyclin B and its involvement in the self-amplification of MPF at mitosis. EMBO J *12*, 53-63.

Holowaty, M.N., Sheng, Y., Nguyen, T., Arrowsmith, C., and Frappier, L. (2003). Protein interaction domains of the ubiquitin-specific protease, USP7/HAUSP. J Biol Chem *278*, 47753-47761.

Honma, K., Tsuzuki, S., Nakagawa, M., Tagawa, H., Nakamura, S., Morishima, Y., and Seto, M. (2009). TNFAIP3/A20 functions as a novel tumor suppressor gene in several subtypes of non-Hodgkin lymphomas. Blood *114*, 2467-2475.

Hornig, N.C., Knowles, P.P., McDonald, N.Q., and Uhlmann, F. (2002). The dual mechanism of separase regulation by securin. Curr Biol *12*, 973-982.

Hu, M., Gu, L., Li, M., Jeffrey, P.D., Gu, W., and Shi, Y. (2006). Structural basis of competitive recognition of p53 and MDM2 by HAUSP/USP7: implications for the regulation of the p53-MDM2 pathway. PLoS Biol *4*, e27.

Hu, M., Li, P., Li, M., Li, W., Yao, T., Wu, J.W., Gu, W., Cohen, R.E., and Shi, Y. (2002). Crystal structure of a UBP-family deubiquitinating enzyme in isolation and in complex with ubiquitin aldehyde. Cell *111*, 1041-1054.

Hu, M., Li, P., Song, L., Jeffrey, P.D., Chenova, T.A., Wilkinson, K.D., Cohen, R.E., and Shi, Y. (2005). Structure and mechanisms of the proteasome-associated deubiquitinating enzyme USP14. EMBO J *24*, 3747-3756.

Huang, H., Jeon, M.S., Liao, L., Yang, C., Elly, C., Yates, J.R., 3rd, and Liu, Y.C. (2010). K33-linked polyubiquitination of T cell receptor-zeta regulates proteolysis-independent T cell signaling. Immunity *33*, 60-70.

Huang, O.W., Ma, X., Yin, J., Flinders, J., Maurer, T., Kayagaki, N., Phung, Q., Bosanac, I., Arnott, D., Dixit, V.M., *et al.* (2012). Phosphorylation-dependent activity of the deubiquitinase DUBA. Nat Struct Mol Biol *19*, 171-175.

Huang, T.T., Nijman, S.M., Mirchandani, K.D., Galardy, P.J., Cohn, M.A., Haas, W., Gygi, S.P., Ploegh, H.L., Bernards, R., and D'Andrea, A.D. (2006). Regulation of monoubiquitinated PCNA by DUB autocleavage. Nat Cell Biol *8*, 339-347.

Huang, X., Summers, M.K., Pham, V., Lill, J.R., Liu, J., Lee, G., Kirkpatrick, D.S., Jackson, P.K., Fang, G., and Dixit, V.M. (2011). Deubiquitinase USP37 is activated by CDK2 to antagonize APC(CDH1) and promote S phase entry. Mol Cell *42*, 511-523.

Huen, M.S., and Chen, J. (2010). Assembly of checkpoint and repair machineries at DNA damage sites. Trends Biochem Sci *35*, 101-108.

Jacobson, A.D., Zhang, N.Y., Xu, P., Han, K.J., Noone, S., Peng, J., and Liu, C.W. (2009). The lysine 48 and lysine 63 ubiquitin conjugates are processed differently by the 26 s proteasome. J Biol Chem *284*, 35485-35494.

Jeffrey, P.D., Russo, A.A., Polyak, K., Gibbs, E., Hurwitz, J., Massagué, J., and Pavletich, N.P. (1995). Mechanism of CDK activation revealed by the structure of a cyclinA-CDK2 complex. Nature *376*, 313-320.

Jensen, D.E., and Rauscher, F.J., 3rd (1999). BAP1, a candidate tumor suppressor protein that interacts with BRCA1. Ann N Y Acad Sci *886*, 191-194.

Johnston, S.C., Riddle, S.M., Cohen, R.E., and Hill, C.P. (1999). Structural basis for the specificity of ubiquitin C-terminal hydrolases. EMBO J *18*, 3877-3887.

Juang, Y.C., Landry, M.C., Sanches, M., Vittal, V., Leung, C.C., Ceccarelli, D.F., Mateo, A.R., Pruneda, J.N., Mao, D.Y., Szilard, R.K., *et al.* (2012). OTUB1 co-opts Lys48-linked ubiquitin recognition to suppress E2 enzyme function. Mol Cell *45*, 384-397.

Kabuta, T., Mitsui, T., Takahashi, M., Fujiwara, Y., Kabuta, C., Konya, C., Tsuchiya, Y., Hatanaka, Y., Uchida, K., Hohjoh, H., *et al.* (2013). Ubiquitin C-terminal hydrolase L1 (UCH-L1) acts as a novel potentiator of cyclin-dependent kinases to enhance cell proliferation independently of its hydrolase activity. J Biol Chem *288*, 12615-12626.

Kaiser, S.E., Riley, B.E., Shaler, T.A., Trevino, R.S., Becker, C.H., Schulman, H., and Kopito, R.R. (2011). Protein standard absolute quantification (PSAQ) method for the measurement of cellular ubiquitin pools. Nat Methods *8*, 691-696.

Kallmeyer, A.K., Keeling, K.M., and Bedwell, D.M. (2006). Eukaryotic release factor 1 phosphorylation by CK2 protein kinase is dynamic but has little effect on the efficiency of translation termination in Saccharomyces cerevisiae. Eukaryot Cell *5*, 1378-1387.

Kane, L.A., Lazarou, M., Fogel, A.I., Li, Y., Yamano, K., Sarraf, S.A., Banerjee, S., and Youle, R.J. (2014). PINK1 phosphorylates ubiquitin to activate Parkin E3 ubiquitin ligase activity. J Cell Biol *205*, 143-153.

Kapoor, M., and Lozano, G. (1998). Functional activation of p53 via phosphorylation following DNA damage by UV but not gamma radiation. Proc Natl Acad Sci U S A *95*, 2834-2837.

Kattenhorn, L.M., Korbel, G.A., Kessler, B.M., Spooner, E., and Ploegh, H.L. (2005). A deubiquitinating enzyme encoded by HSV-1 belongs to a family of cysteine proteases that is conserved across the family Herpesviridae. Mol Cell *19*, 547-557.

Kawaguchi, Y., Okamoto, T., Taniwaki, M., Aizawa, M., Inoue, M., Katayama, S., Kawakami, H., Nakamura, S., Nishimura, M., Akiguchi, I., *et al.* (1994). CAG expansions in a novel gene for Machado-Joseph disease at chromosome 14q32.1. Nat Genet *8*, 221-228.

Kazlauskaite, A., Kondapalli, C., Gourlay, R., Campbell, D.G., Ritorto, M.S., Hofmann, K., Alessi, D.R., Knebel, A., Trost, M., and Muqit, M.M. (2014). Parkin is activated by PINK1-dependent phosphorylation of ubiquitin at Ser65. Biochem J *460*, 127-139.

Ke, J.Y., Dai, C.J., Wu, W.L., Gao, J.H., Xia, A.J., Liu, G.P., Lv, K.S., and Wu, C.L. (2014). USP11 regulates p53 stability by deubiquitinating p53. J Zhejiang Univ Sci B *15*, 1032-1038.

Kee, Y., and Huang, T.T. (2015). Role of Deubiquitinating Enzymes in DNA Repair. Mol Cell Biol *36*, 524-544.

Keller, D.M., and Lu, H. (2002). p53 serine 392 phosphorylation increases after UV through induction of the assembly of the CK2.hSPT16.SSRP1 complex. J Biol Chem *277*, 50206-50213.

Khoronenkova, S.V., Dianova, I.I., Ternette, N., Kessler, B.M., Parsons, J.L., and Dianov, G.L. (2012). ATM-dependent downregulation of USP7/HAUSP by PPM1G activates p53 response to DNA damage. Mol Cell *45*, 801-813.

Kim, R.Q., van Dijk, W.J., and Sixma, T.K. (2016). Structure of USP7 catalytic domain and three Ubl-domains reveals a connector alpha-helix with regulatory role. J Struct Biol *195*, 11-18.

Kim, W., Bennett, E.J., Huttlin, E.L., Guo, A., Li, J., Possemato, A., Sowa, M.E., Rad, R., Rush, J., Comb, M.J., *et al.* (2011). Systematic and quantitative assessment of the ubiquitin-modified proteome. Mol Cell *44*, 325-340.

Kirisako, T., Kamei, K., Murata, S., Kato, M., Fukumoto, H., Kanie, M., Sano, S., Tokunaga, F., Tanaka, K., and Iwai, K. (2006). A ubiquitin ligase complex assembles linear polyubiquitin chains. EMBO J *25*, 4877-4887.

Kobayashi, T., Masoumi, K.C., and Massoumi, R. (2015). Deubiquitinating activity of CYLD is impaired by SUMOylation in neuroblastoma cells. Oncogene *34*, 2251-2260.

Komander, D., and Barford, D. (2008). Structure of the A20 OTU domain and mechanistic insights into deubiquitination. Biochem J *409*, 77-85.

Komander, D., Clague, M.J., and Urbe, S. (2009). Breaking the chains: structure and function of the deubiquitinases. Nat Rev Mol Cell Biol *10*, 550-563.

Kosugi, S., Hasebe, M., Matsumura, N., Takashima, H., Miyamoto-Sato, E., Tomita, M., and Yanagawa, H. (2009a). Six classes of nuclear localization signals specific to different binding grooves of importin alpha. J Biol Chem *284*, 478-485.

Kosugi, S., Hasebe, M., Tomita, M., and Yanagawa, H. (2009b). Systematic identification of cell cycle-dependent yeast nucleocytoplasmic shuttling proteins by prediction of composite motifs. Proc Natl Acad Sci U S A *106*, 10171-10176.

Koyano, F., Okatsu, K., Kosako, H., Tamura, Y., Go, E., Kimura, M., Kimura, Y., Tsuchiya, H., Yoshihara, H., Hirokawa, T., *et al.* (2014). Ubiquitin is phosphorylated by PINK1 to activate parkin. Nature *510*, 162-166.

Kramer, E.R., Scheuringer, N., Podtelejnikov, A.V., Mann, M., and Peters, J.M. (2000). Mitotic regulation of the APC activator proteins CDC20 and CDH1. Mol Biol Cell *11*, 1555-1569.

Kristariyanto, Y.A., Abdul Rehman, S.A., Campbell, D.G., Morrice, N.A., Johnson, C., Toth, R., and Kulathu, Y. (2015). K29-selective ubiquitin binding domain reveals structural basis of specificity and heterotypic nature of k29 polyubiquitin. Mol Cell *58*, 83-94.

Kristariyanto, Y.A., Abdul Rehman, S.A., Weidlich, S., Knebel, A., and Kulathu, Y. (2017). A single MIU motif of MINDY-1 recognizes K48-linked polyubiquitin chains. EMBO Rep.

Lakin, N.D., and Jackson, S.P. (1999). Regulation of p53 in response to DNA damage. Oncogene *18*, 7644-7655.

Lander, G.C., Estrin, E., Matyskiela, M.E., Bashore, C., Nogales, E., and Martin, A. (2012). Complete subunit architecture of the proteasome regulatory particle. Nature *482*, 186-191.

Lander, G.C., Martin, A., and Nogales, E. (2013). The proteasome under the microscope: the regulatory particle in focus. Curr Opin Struct Biol *23*, 243-251.

Laoukili, J., Kooistra, M.R., Bras, A., Kauw, J., Kerkhoven, R.M., Morrison, A., Clevers, H., and Medema, R.H. (2005). FoxM1 is required for execution of the mitotic programme and chromosome stability. Nat Cell Biol *7*, 126-136.

Lee, J.G., Kim, W., Gygi, S., and Ye, Y. (2014). Characterization of the deubiquitinating activity of USP19 and its role in endoplasmic reticulum-associated degradation. J Biol Chem *289*, 3510-3517.

Leroy, E., Boyer, R., Auburger, G., Leube, B., Ulm, G., Mezey, E., Harta, G., Brownstein, M.J., Jonnalagada, S., Chernova, T., *et al.* (1998). The ubiquitin pathway in Parkinson's disease. Nature *395*, 451-452.

Li, M., Brooks, C.L., Wu-Baer, F., Chen, D., Baer, R., and Gu, W. (2003). Mono- versus polyubiquitination: differential control of p53 fate by Mdm2. Science *302*, 1972-1975.

Li, M., Chen, D., Shiloh, A., Luo, J., Nikolaev, A.Y., Qin, J., and Gu, W. (2002). Deubiquitination of p53 by HAUSP is an important pathway for p53 stabilization. Nature *416*, 648-653.

Li, W., Bengtson, M.H., Ulbrich, A., Matsuda, A., Reddy, V.A., Orth, A., Chanda, S.K., Batalov, S., and Joazeiro, C.A. (2008). Genome-wide and functional annotation of human E3 ubiquitin ligases identifies MULAN, a mitochondrial E3 that regulates the organelle's dynamics and signaling. PLoS One *3*, e1487.

Li, Z., Hao, Q., Luo, J., Xiong, J., Zhang, S., Wang, T., Bai, L., Wang, W., Chen, M., Gu, L., *et al.* (2015). USP4 inhibits p53 and NF-κB through deubiquitinating and stabilizing HDAC2. Oncogene.

Lin, J., Chen, J., Elenbaas, B., and Levine, A.J. (1994). Several hydrophobic amino acids in the p53 amino-terminal domain are required for transcriptional activation, binding to mdm-2 and the adenovirus 5 E1B 55-kD protein. Genes Dev *8*, 1235-1246.

Lin, S.C., Chung, J.Y., Lamothe, B., Rajashankar, K., Lu, M., Lo, Y.C., Lam, A.Y., Darnay, B.G., and Wu, H. (2008). Molecular basis for the unique deubiquitinating activity of the NF-kappaB inhibitor A20. J Mol Biol *376*, 526-540.

Lin, Z., Tan, C., Qiu, Q., Kong, S., Yang, H., Zhao, F., Liu, Z., Li, J., Kong, Q., Gao, B., *et al.* (2015). Ubiquitin-specific protease 22 is a deubiquitinase of CCNB1. Cell Discov *1*.

Lindon, C., and Pines, J. (2004). Ordered proteolysis in anaphase inactivates Plk1 to contribute to proper mitotic exit in human cells. J Cell Biol *164*, 233-241.

Lingaraju, G.M., Bunker, R.D., Cavadini, S., Hess, D., Hassiepen, U., Renatus, M., Fischer, E.S., and Thoma, N.H. (2014). Crystal structure of the human COP9 signalosome. Nature *512*, 161-165.

Littlepage, L.E., and Ruderman, J.V. (2002). Identification of a new APC/C recognition domain, the A box, which is required for the Cdh1-dependent destruction of the kinase Aurora-A during mitotic exit. Genes Dev *16*, 2274-2285.

Liu, Z., Chen, P., Gao, H., Gu, Y., Yang, J., Peng, H., Xu, X., Wang, H., Yang, M., Liu, X., *et al.* (2014). Ubiquitylation of autophagy receptor Optineurin by HACE1 activates selective autophagy for tumor suppression. Cancer Cell *26*, 106-120.

Loughery, J., Cox, M., Smith, L.M., and Meek, D.W. (2014). Critical role for p53-serine 15 phosphorylation in stimulating transactivation at p53-responsive promoters. Nucleic Acids Res *42*, 7666-7680.

Lu, S., and Wang, J. (2013). The resistance mechanisms of proteasome inhibitor bortezomib. Biomark Res *1*, 13.

Lu, Y., Lee, B.H., King, R.W., Finley, D., and Kirschner, M.W. (2015). Substrate degradation by the proteasome: a single-molecule kinetic analysis. Science *348*, 1250834.

Luchini, C., Veronese, N., Yachida, S., Cheng, L., Nottegar, A., Stubbs, B., Solmi, M., Capelli, P., Pea, A., Barbareschi, M., *et al.* (2016). Different prognostic roles of tumor suppressor gene BAP1 in cancer: A systematic review with meta-analysis. Genes Chromosomes Cancer *55*, 741-749.

Luo, J., Lu, Z., Lu, X., Chen, L., Cao, J., Zhang, S., Ling, Y., and Zhou, X. (2013). OTUD5 regulates p53 stability by deubiquitinating p53. PLoS One *8*, e77682.

Ly, T., Ahmad, Y., Shlien, A., Soroka, D., Mills, A., Emanuele, M.J., Stratton, M.R., and Lamond, A.I. (2014). A proteomic chronology of gene expression through the cell cycle in human myeloid leukemia cells. Elife *3*, e01630.

Ma, H., Chen, H., Guo, X., Wang, Z., Sowa, M.E., Zheng, L., Hu, S., Zeng, P., Guo, R., Diao, J., *et al.* (2012). M phase phosphorylation of the epigenetic regulator UHRF1 regulates its physical association with the deubiquitylase USP7 and stability. Proc Natl Acad Sci U S A *109*, 4828-4833.

Macek, B., Gnad, F., Soufi, B., Kumar, C., Olsen, J.V., Mijakovic, I., and Mann, M. (2008). Phospho-proteome analysis of E. coli reveals evolutionary conservation of bacterial Ser/Thr/Tyr phosphorylation. Mol Cell Proteomics *7*, 299-307.

Machida, Y.J., Machida, Y., Vashisht, A.A., Wohlschlegel, J.A., and Dutta, A. (2009). The deubiquitinating enzyme BAP1 regulates cell growth via interaction with HCF-1. J Biol Chem *284*, 34179-34188.

Maertens, G.N., El Messaoudi-Aubert, S., Elderkin, S., Hiom, K., and Peters, G. (2010). Ubiquitin-specific proteases 7 and 11 modulate Polycomb regulation of the INK4a tumour suppressor. EMBO J *29*, 2553-2565.

Malakhov, M.P., Malakhova, O.A., Kim, K.I., Ritchie, K.J., and Zhang, D.E. (2002). UBP43 (USP18) specifically removes ISG15 from conjugated proteins. J Biol Chem *277*, 9976-9981.

Maraganore, D.M., Lesnick, T.G., Elbaz, A., Chartier-Harlin, M.C., Gasser, T., Kruger, R., Hattori, N., Mellick, G.D., Quattrone, A., Satoh, J., *et al.* (2004). UCHL1 is a Parkinson's disease susceptibility gene. Ann Neurol *55*, 512-521.

Marchenko, N.D., Wolff, S., Erster, S., Becker, K., and Moll, U.M. (2007). Monoubiquitylation promotes mitochondrial p53 translocation. EMBO J *26*, 923-934.

Mashtalir, N., Daou, S., Barbour, H., Sen, N.N., Gagnon, J., Hammond-Martel, I., Dar, H.H., Therrien, M., and Affar, e.B. (2014). Autodeubiquitination protects the tumor suppressor BAP1 from cytoplasmic sequestration mediated by the atypical ubiquitin ligase UBE2O. Mol Cell *54*, 392-406.

Massoumi, R., Chmielarska, K., Hennecke, K., Pfeifer, A., and Fassler, R. (2006). Cyld inhibits tumor cell proliferation by blocking Bcl-3-dependent NF-kappaB signaling. Cell *125*, 665-677.

Massoumi, R., Kuphal, S., Hellerbrand, C., Haas, B., Wild, P., Spruss, T., Pfeifer, A., Fassler, R., and Bosserhoff, A.K. (2009). Down-regulation of CYLD expression by Snail promotes tumor progression in malignant melanoma. J Exp Med *206*, 221-232.

Matsumoto, M.L., Wickliffe, K.E., Dong, K.C., Yu, C., Bosanac, I., Bustos, D., Phu, L., Kirkpatrick, D.S., Hymowitz, S.G., Rape, M., *et al.* (2010). K11-linked polyubiquitination in cell cycle control revealed by a K11 linkage-specific antibody. Mol Cell *39*, 477-484.

Matsuyama, A., Shimazu, T., Sumida, Y., Saito, A., Yoshimatsu, Y., Seigneurin-Berny, D., Osada, H., Komatsu, Y., Nishino, N., Khochbin, S., *et al.* (2002). In vivo destabilization of dynamic microtubules by HDAC6-mediated deacetylation. EMBO J *21*, 6820-6831.

Maytal-Kivity, V., Reis, N., Hofmann, K., and Glickman, M.H. (2002). MPN+, a putative catalytic motif found in a subset of MPN domain proteins from eukaryotes and prokaryotes, is critical for Rpn11 function. BMC Biochem *3*, 28.

Meek, D.W. (2009). Tumour suppression by p53: a role for the DNA damage response? Nat Rev Cancer *9*, 714-723.

Meek, D.W., and Anderson, C.W. (2009). Posttranslational modification of p53: cooperative integrators of function. Cold Spring Harb Perspect Biol *1*, a000950.

Mellacheruvu, D., Wright, Z., Couzens, A.L., Lambert, J.P., St-Denis, N.A., Li, T., Miteva, Y.V., Hauri, S., Sardiu, M.E., Low, T.Y., *et al.* (2013). The CRAPome: a contaminant repository for affinity purification-mass spectrometry data. Nat Methods *10*, 730-736.

Meray, R.K., and Lansbury, P.T., Jr. (2007). Reversible monoubiquitination regulates the Parkinson disease-associated ubiquitin hydrolase UCH-L1. J Biol Chem *282*, 10567-10575.

Merlet, J., Burger, J., Gomes, J.E., and Pintard, L. (2009). Regulation of cullin-RING E3 ubiquitin-ligases by neddylation and dimerization. Cell Mol Life Sci *66*, 1924-1938.

Metzger, M.B., Pruneda, J.N., Klevit, R.E., and Weissman, A.M. (2014). RING-type E3 ligases: master manipulators of E2 ubiquitin-conjugating enzymes and ubiquitination. Biochim Biophys Acta *1843*, 47-60.

Meulmeester, E., Kunze, M., Hsiao, H.H., Urlaub, H., and Melchior, F. (2008). Mechanism and consequences for paralog-specific sumoylation of ubiquitin-specific protease 25. Mol Cell *30*, 610-619.

Mevissen, T.E., Hospenthal, M.K., Geurink, P.P., Elliott, P.R., Akutsu, M., Arnaudo, N., Ekkebus, R., Kulathu, Y., Wauer, T., El Oualid, F., *et al.* (2013). OTU deubiquitinases reveal mechanisms of linkage specificity and enable ubiquitin chain restriction analysis. Cell *154*, 169-184.

Meyer, H.J., and Rape, M. (2014). Enhanced protein degradation by branched ubiquitin chains. Cell *157*, 910-921.

Min, M., Mevissen, T.E., De Luca, M., Komander, D., and Lindon, C. (2015). Efficient APC/C substrate degradation in cells undergoing mitotic exit depends on K11 ubiquitin linkages. Mol Biol Cell.

Mizuno, E., Kitamura, N., and Komada, M. (2007). 14-3-3-dependent inhibition of the deubiquitinating activity of UBPY and its cancellation in the M phase. Exp Cell Res *313*, 3624-3634.

Mocciaro, A., and Rape, M. (2012). Emerging regulatory mechanisms in ubiquitin-dependent cell cycle control. J Cell Sci *125*, 255-263.

Monia, B.P., Ecker, D.J., Jonnalagadda, S., Marsh, J., Gotlib, L., Butt, T.R., and Crooke, S.T. (1989). Gene synthesis, expression, and processing of human ubiquitin carboxyl extension proteins. J Biol Chem *264*, 4093-4103.

Moniz, S., Bandarra, D., Biddlestone, J., Campbell, K.J., Komander, D., Bremm, A., and Rocha, S. (2015). Cezanne regulates E2F1-dependent HIF2alpha expression. J Cell Sci *128*, 3082-3093.

Morotti, A., Panuzzo, C., Crivellaro, S., Pergolizzi, B., Familiari, U., Berger, A.H., Saglio, G., and Pandolfi, P.P. (2014). BCR-ABL disrupts PTEN nuclear-cytoplasmic shuttling through phosphorylation-dependent activation of HAUSP. Leukemia *28*, 1326-1333.

Morreale, F.E., and Walden, H. (2016). Types of Ubiquitin Ligases. Cell *165*, 248-248 e241.

Morris, J.R., and Solomon, E. (2004). BRCA1 : BARD1 induces the formation of conjugated ubiquitin structures, dependent on K6 of ubiquitin, in cells during DNA replication and repair. Hum Mol Genet *13*, 807-817.

Mueller, P.R., Coleman, T.R., Kumagai, A., and Dunphy, W.G. (1995). Myt1: a membrane-associated inhibitory kinase that phosphorylates Cdc2 on both threonine-14 and tyrosine-15. Science *270*, 86-90.

Mukai, A., Mizuno, E., Kobayashi, K., Matsumoto, M., Nakayama, K.I., Kitamura, N., and Komada, M. (2008). Dynamic regulation of ubiquitylation and deubiquitylation at the central spindle during cytokinesis. J Cell Sci *121*, 1325-1333.

Nathan, J.A., Kim, H.T., Ting, L., Gygi, S.P., and Goldberg, A.L. (2013). Why do cellular proteins linked to K63-polyubiquitin chains not associate with proteasomes? EMBO J *32*, 552-565.

Ndubaku, C., and Tsui, V. (2015). Inhibiting the deubiquitinating enzymes (DUBs). J Med Chem *58*, 1581-1595.

Nicassio, F., Corrado, N., Vissers, J.H., Areces, L.B., Bergink, S., Marteijn, J.A., Geverts, B., Houtsmuller, A.B., Vermeulen, W., Di Fiore, P.P., *et al.* (2007). Human USP3 is a chromatin modifier required for S phase progression and genome stability. Curr Biol *17*, 1972-1977.

Nicholson, B., and Suresh Kumar, K.G. (2011). The multifaceted roles of USP7: new therapeutic opportunities. Cell Biochem Biophys *60*, 61-68.

Nishi, R., Wijnhoven, P., le Sage, C., Tjeertes, J., Galanty, Y., Forment, J.V., Clague, M.J., Urbe, S., and Jackson, S.P. (2014). Systematic characterization of deubiquitylating enzymes for roles in maintaining genome integrity. Nat Cell Biol *16*, 1016-1026, 1011-1018.

Nishikawa, K., Li, H., Kawamura, R., Osaka, H., Wang, Y.L., Hara, Y., Hirokawa, T., Manago, Y., Amano, T., Noda, M., *et al.* (2003). Alterations of structure and hydrolase activity of parkinsonism-associated human ubiquitin carboxyl-terminal hydrolase L1 variants. Biochem Biophys Res Commun *304*, 176-183.

Olsen, J.V., Vermeulen, M., Santamaria, A., Kumar, C., Miller, M.L., Jensen, L.J., Gnad, F., Cox, J., Jensen, T.S., Nigg, E.A., *et al.* (2010). Quantitative phosphoproteomics reveals widespread full phosphorylation site occupancy during mitosis. Sci Signal *3*, ra3.

Osaka, H., Wang, Y.L., Takada, K., Takizawa, S., Setsuie, R., Li, H., Sato, Y., Nishikawa, K., Sun, Y.J., Sakurai, M., *et al.* (2003). Ubiquitin carboxy-terminal hydrolase L1 binds to and stabilizes monoubiquitin in neuron. Hum Mol Genet *12*, 1945-1958.

Paiva, S.L., da Silva, S.R., de Araujo, E.D., and Gunning, P.T. (2017). Regulating the Master Regulator: Controlling Ubiquitination by Thinking Outside the Active Site. J Med Chem.

Palicharla, V.R., and Maddika, S. (2015). HACE1 mediated K27 ubiquitin linkage leads to YB-1 protein secretion. Cell Signal *27*, 2355-2362.

Parker, L.L., and Piwnica-Worms, H. (1992). Inactivation of the p34cdc2-cyclin B complex by the human WEE1 tyrosine kinase. Science *257*, 1955-1957.

Phillips, A.H., and Corn, J.E. (2015). Using protein motion to read, write, and erase ubiquitin signals. J Biol Chem *290*, 26437-26444.

Pinto-Fernandez, A., and Kessler, B.M. (2016). DUBbing Cancer: Deubiquitylating Enzymes Involved in Epigenetics, DNA Damage and the Cell Cycle As Therapeutic Targets. Front Genet *7*, 133.

Qian, J., Pentz, K., Zhu, Q., Wang, Q., He, J., Srivastava, A.K., and Wani, A.A. (2015). USP7 modulates UV-induced PCNA monoubiquitination by regulating DNA polymerase eta stability. Oncogene *34*, 4791-4796.

Rahighi, S., Ikeda, F., Kawasaki, M., Akutsu, M., Suzuki, N., Kato, R., Kensche, T., Uejima, T., Bloor, S., Komander, D., *et al.* (2009). Specific recognition of linear ubiquitin chains by NEMO is important for NF-kappaB activation. Cell *136*, 1098-1109.

Read, M.A., Brownell, J.E., Gladysheva, T.B., Hottelet, M., Parent, L.A., Coggins, M.B., Pierce, J.W., Podust, V.N., Luo, R.S., Chau, V., *et al.* (2000). Nedd8 modification of cul-1 activates SCF(beta(TrCP))-dependent ubiquitination of IkappaBalpha. Mol Cell Biol *20*, 2326-2333.

Reddy, B.A., van der Knaap, J.A., Bot, A.G., Mohd-Sarip, A., Dekkers, D.H., Timmermans, M.A., Martens, J.W., Demmers, J.A., and Verrijzer, C.P. (2014). Nucleotide biosynthetic enzyme GMP synthase is a TRIM21-controlled relay of p53 stabilization. Mol Cell *53*, 458-470.

Reddy, S.K., Rape, M., Margansky, W.A., and Kirschner, M.W. (2007). Ubiquitination by the anaphase-promoting complex drives spindle checkpoint inactivation. Nature *446*, 921-925.

Reiley, W., Zhang, M., Wu, X., Granger, E., and Sun, S.C. (2005). Regulation of the deubiquitinating enzyme CYLD by IkappaB kinase gamma-dependent phosphorylation. Mol Cell Biol *25*, 3886-3895.

Reverdy, C., Conrath, S., Lopez, R., Planquette, C., Atmanene, C., Collura, V., Harpon, J., Battaglia, V., Vivat, V., Sippl, W., *et al.* (2012). Discovery of specific inhibitors of human USP7/HAUSP deubiquitinating enzyme. Chem Biol *19*, 467-477.

Rhind, N., and Russell, P. (2012). Signaling pathways that regulate cell division. Cold Spring Harb Perspect Biol *4*.

Ritorto, M.S., Ewan, R., Perez-Oliva, A.B., Knebel, A., Buhrlage, S.J., Wightman, M., Kelly, S.M., Wood, N.T., Virdee, S., Gray, N.S., *et al.* (2014). Screening of DUB activity and specificity by MALDI-TOF mass spectrometry. Nat Commun *5*, 4763.

Rotin, D., and Kumar, S. (2009). Physiological functions of the HECT family of ubiquitin ligases. Nat Rev Mol Cell Biol *10*, 398-409.

Rouge, L., Bainbridge, T.W., Kwok, M., Tong, R., Di Lello, P., Wertz, I.E., Maurer, T., Ernst, J.A., and Murray, J. (2016). Molecular Understanding of USP7 Substrate Recognition and C-Terminal Activation. Structure *24*, 1335-1345.

Sacco, J.J., Coulson, J.M., Clague, M.J., and Urbe, S. (2010). Emerging roles of deubiquitinases in cancer-associated pathways. IUBMB Life *62*, 140-157.

Sacco, J.J., Yau, T.Y., Darling, S., Patel, V., Liu, H., Urbe, S., Clague, M.J., and Coulson, J.M. (2014). The deubiquitylase Ataxin-3 restricts PTEN transcription in lung cancer cells. Oncogene *33*, 4265-4272.

Sahtoe, D.D., and Sixma, T.K. (2015). Layers of DUB regulation. Trends Biochem Sci *40*, 456-467.

Sahtoe, D.D., van Dijk, W.J., Ekkebus, R., Ovaa, H., and Sixma, T.K. (2016). BAP1/ASXL1 recruitment and activation for H2A deubiquitination. Nat Commun *7*, 10292.

Sahtoe, D.D., van Dijk, W.J., El Oualid, F., Ekkebus, R., Ovaa, H., and Sixma, T.K. (2015). Mechanism of UCH-L5 activation and inhibition by DEUBAD domains in RPN13 and INO80G. Mol Cell *57*, 887-900.

Saito, S., Goodarzi, A.A., Higashimoto, Y., Noda, Y., Lees-Miller, S.P., Appella, E., and Anderson, C.W. (2002). ATM mediates phosphorylation at multiple p53 sites, including Ser(46), in response to ionizing radiation. J Biol Chem *277*, 12491-12494.

Schaeffer, V., Akutsu, M., Olma, M.H., Gomes, L.C., Kawasaki, M., and Dikic, I. (2014). Binding of OTULIN to the PUB domain of HOIP controls NF-kappaB signaling. Mol Cell *54*, 349-361.

Schlesinger, D.H., Goldstein, G., and Niall, H.D. (1975). The complete amino acid sequence of ubiquitin, an adenylate cyclase stimulating polypeptide probably universal in living cells. Biochemistry *14*, 2214-2218.

Schmidt, M., and Finley, D. (2014). Regulation of proteasome activity in health and disease. Biochim Biophys Acta *1843*, 13-25.

Schulz, S., Chachami, G., Kozaczkiewicz, L., Winter, U., Stankovic-Valentin, N., Haas, P., Hofmann, K., Urlaub, H., Ovaa, H., Wittbrodt, J., *et al.* (2012). Ubiquitin-specific protease-like 1 (USPL1) is a SUMO isopeptidase with essential, non-catalytic functions. EMBO Rep *13*, 930-938.

Schwanhäusser, B., Busse, D., Li, N., Dittmar, G., Schuchhardt, J., Wolf, J., Chen, W., and Selbach, M. (2011). Global quantification of mammalian gene expression control. Nature *473*, 337-342.

Schwertman, P., Bekker-Jensen, S., and Mailand, N. (2016). Regulation of DNA double-strand break repair by ubiquitin and ubiquitin-like modifiers. Nat Rev Mol Cell Biol *17*, 379-394.

Scott, D., Oldham, N.J., Strachan, J., Searle, M.S., and Layfield, R. (2015). Ubiquitin-binding domains: mechanisms of ubiquitin recognition and use as tools to investigate ubiquitin-modified proteomes. Proteomics *15*, 844-861.

Sdek, P., Ying, H., Chang, D.L., Qiu, W., Zheng, H., Touitou, R., Allday, M.J., and Xiao, Z.X. (2005). MDM2 promotes proteasome-dependent ubiquitin-independent degradation of retinoblastoma protein. Mol Cell *20*, 699-708.

Seki, T., Gong, L., Williams, A.J., Sakai, N., Todi, S.V., and Paulson, H.L. (2013). JosD1, a membrane-targeted deubiquitinating enzyme, is activated by ubiquitination and regulates membrane dynamics, cell motility, and endocytosis. J Biol Chem *288*, 17145-17155.

Sierra, M.I., Wright, M.H., and Nash, P.D. (2010). AMSH interacts with ESCRT-0 to regulate the stability and trafficking of CXCR4. J Biol Chem *285*, 13990-14004.

Skaar, J.R., and Pagano, M. (2009). Control of cell growth by the SCF and APC/C ubiquitin ligases. Curr Opin Cell Biol *21*, 816-824.

Sommer, S., Weikart, N.D., Linne, U., and Mootz, H.D. (2013). Covalent inhibition of SUMO and ubiquitin-specific cysteine proteases by an in situ thiol-alkyne addition. Bioorg Med Chem *21*, 2511-2517.

Sowa, M.E., Bennett, E.J., Gygi, S.P., and Harper, J.W. (2009). Defining the human deubiquitinating enzyme interaction landscape. Cell *138*, 389-403.

Spratt, D.E., Walden, H., and Shaw, G.S. (2014). RBR E3 ubiquitin ligases: new structures, new insights, new questions. Biochem J *458*, 421-437.

Stegmeier, F., Rape, M., Draviam, V.M., Nalepa, G., Sowa, M.E., Ang, X.L., McDonald, E.R., 3rd, Li, M.Z., Hannon, G.J., Sorger, P.K., *et al.* (2007a). Anaphase initiation is regulated by antagonistic ubiquitination and deubiquitination activities. Nature *446*, 876-881.

Stegmeier, F., Sowa, M.E., Nalepa, G., Gygi, S.P., Harper, J.W., and Elledge, S.J. (2007b). The tumor suppressor CYLD regulates entry into mitosis. Proc Natl Acad Sci U S A *104*, 8869-8874.

Stemmann, O., Zou, H., Gerber, S.A., Gygi, S.P., and Kirschner, M.W. (2001). Dual inhibition of sister chromatid separation at metaphase. Cell *107*, 715-726.

Stevenson, L.F., Sparks, A., Allende-Vega, N., Xirodimas, D.P., Lane, D.P., and Saville, M.K. (2007). The deubiquitinating enzyme USP2a regulates the p53 pathway by targeting Mdm2. EMBO J *26*, 976-986.

Stewart, M.D., Ritterhoff, T., Klevit, R.E., and Brzovic, P.S. (2016). E2 enzymes: more than just middle men. Cell Res *26*, 423-440.

Stewart, S., and Fang, G. (2005). Destruction box-dependent degradation of aurora B is mediated by the anaphase-promoting complex/cyclosome and Cdh1. Cancer Res *65*, 8730-8735.

Sudakin, V., Chan, G.K., and Yen, T.J. (2001). Checkpoint inhibition of the APC/C in HeLa cells is mediated by a complex of BUBR1, BUB3, CDC20, and MAD2. J Cell Biol *154*, 925-936.

Sudakin, V., Ganoth, D., Dahan, A., Heller, H., Hershko, J., Luca, F.C., Ruderman, J.V., and Hershko, A. (1995). The cyclosome, a large complex containing cyclin-selective ubiquitin ligase activity, targets cyclins for destruction at the end of mitosis. Mol Biol Cell *6*, 185-197.

Sun, X.X., Challagundla, K.B., and Dai, M.S. (2012). Positive regulation of p53 stability and activity by the deubiquitinating enzyme Otubain 1. EMBO J *31*, 576-592.

Swatek, K.N., and Komander, D. (2016). Ubiquitin modifications. Cell Res *26*, 399-422.

Sy, S.M., Jiang, J., O, W.S., Deng, Y., and Huen, M.S. (2013). The ubiquitin specific protease USP34 promotes ubiquitin signaling at DNA double-strand breaks. Nucleic Acids Res *41*, 8572-8580.

Testa, J.R., Cheung, M., Pei, J., Below, J.E., Tan, Y., Sementino, E., Cox, N.J., Dogan, A.U., Pass, H.I., Trusa, S., *et al.* (2011). Germline BAP1 mutations predispose to malignant mesothelioma. Nat Genet *43*, 1022-1025.

Thrower, J.S., Hoffman, L., Rechsteiner, M., and Pickart, C.M. (2000). Recognition of the polyubiquitin proteolytic signal. EMBO J *19*, 94-102.

Tian, Z., D'Arcy, P., Wang, X., Ray, A., Tai, Y.T., Hu, Y., Carrasco, R.D., Richardson, P., Linder, S., Chauhan, D., *et al.* (2014). A novel small molecule inhibitor of deubiquitylating enzyme USP14 and UCHL5 induces apoptosis in multiple myeloma and overcomes bortezomib resistance. Blood *123*, 706-716.

Todi, S.V., Winborn, B.J., Scaglione, K.M., Blount, J.R., Travis, S.M., and Paulson, H.L. (2009). Ubiquitination directly enhances activity of the deubiquitinating enzyme ataxin-3. EMBO J *28*, 372-382.

Uchida, C., Miwa, S., Kitagawa, K., Hattori, T., Isobe, T., Otani, S., Oda, T., Sugimura, H., Kamijo, T., Ookawa, K., *et al.* (2005). Enhanced Mdm2 activity inhibits pRB function via ubiquitin-dependent degradation. EMBO J *24*, 160-169.

Urbe, S., Liu, H., Hayes, S.D., Heride, C., Rigden, D.J., and Clague, M.J. (2012). Systematic survey of deubiquitinase localization identifies USP21 as a regulator of centrosome- and microtubule-associated functions. Mol Biol Cell *23*, 1095-1103.

Vader, G., Kauw, J.J., Medema, R.H., and Lens, S.M. (2006). Survivin mediates targeting of the chromosomal passenger complex to the centromere and midbody. EMBO Rep *7*, 85-92.

van der Knaap, J.A., Kumar, B.R., Moshkin, Y.M., Langenberg, K., Krijgsveld, J., Heck, A.J., Karch, F., and Verrijzer, C.P. (2005). GMP synthetase stimulates histone H2B deubiquitylation by the epigenetic silencer USP7. Mol Cell *17*, 695-707.

van Leuken, R.J., Luna-Vargas, M.P., Sixma, T.K., Wolthuis, R.M., and Medema, R.H. (2008). Usp39 is essential for mitotic spindle checkpoint integrity and controls mRNA-levels of aurora B. Cell cycle *7*, 2710-2719.

Varadan, R., Walker, O., Pickart, C., and Fushman, D. (2002). Structural properties of polyubiquitin chains in solution. J Mol Biol *324*, 637-647.

Vijay-Kumar, S., Bugg, C.E., and Cook, W.J. (1987). Structure of ubiquitin refined at 1.8 A resolution. J Mol Biol *194*, 531-544.

Villamil, M.A., Chen, J., Liang, Q., and Zhuang, Z. (2012a). A noncanonical cysteine protease USP1 is activated through active site modulation by USP1-associated factor 1. Biochemistry *51*, 2829-2839.

Villamil, M.A., Liang, Q., Chen, J., Choi, Y.S., Hou, S., Lee, K.H., and Zhuang, Z. (2012b). Serine phosphorylation is critical for the activation of ubiquitin-specific protease 1 and its interaction with WD40-repeat protein UAF1. Biochemistry *51*, 9112-9123.

Villamor, J.G., Kaschani, F., Colby, T., Oeljeklaus, J., Zhao, D., Kaiser, M., Patricelli, M.P., and van der Hoorn, R.A. (2013). Profiling protein kinases and other ATP binding proteins in Arabidopsis using Acyl-ATP probes. Mol Cell Proteomics *12*, 2481-2496.

Visconti, R., Palazzo, L., Della Monica, R., and Grieco, D. (2012). Fcp1-dependent dephosphorylation is required for M-phase-promoting factor inactivation at mitosis exit. Nat Commun *3*, 894.

Vong, Q.P., Cao, K., Li, H.Y., Iglesias, P.A., and Zheng, Y. (2005). Chromosome alignment and segregation regulated by ubiquitination of Survivin. Science *310*, 1499-1504.

Wang, C., Deng, L., Hong, M., Akkaraju, G.R., Inoue, J., and Chen, Z.J. (2001). TAK1 is a ubiquitin-dependent kinase of MKK and IKK. Nature *412*, 346-351.

Watanabe, N., Arai, H., Nishihara, Y., Taniguchi, M., Hunter, T., and Osada, H. (2004). M-phase kinases induce phospho-dependent ubiquitination of somatic Wee1 by SCFbeta-TrCP. Proc Natl Acad Sci U S A *101*, 4419-4424.

Wauer, T., Swatek, K.N., Wagstaff, J.L., Gladkova, C., Pruneda, J.N., Michel, M.A., Gersch, M., Johnson, C.M., Freund, S.M., and Komander, D. (2015). Ubiquitin Ser65 phosphorylation affects ubiquitin structure, chain assembly and hydrolysis. EMBO J *34*, 307-325.

Wiborg, O., Pedersen, M.S., Wind, A., Berglund, L.E., Marcker, K.A., and Vuust, J. (1985). The human ubiquitin multigene family: some genes contain multiple directly repeated ubiquitin coding sequences. EMBO J *4*, 755-759.

Wickliffe, K.E., Williamson, A., Meyer, H.J., Kelly, A., and Rape, M. (2011). K11-linked ubiquitin chains as novel regulators of cell division. Trends Cell Biol *21*, 656-663.

Wickstrom, S.A., Masoumi, K.C., Khochbin, S., Fassler, R., and Massoumi, R. (2010). CYLD negatively regulates cell-cycle progression by inactivating HDAC6 and increasing the levels of acetylated tubulin. EMBO J *29*, 131-144.

Wiener, R., Zhang, X., Wang, T., and Wolberger, C. (2012). The mechanism of OTUB1-mediated inhibition of ubiquitination. Nature *483*, 618-622.

Wiesner, T., Obenauf, A.C., Murali, R., Fried, I., Griewank, K.G., Ulz, P., Windpassinger, C., Wackernagel, W., Loy, S., Wolf, I., *et al.* (2011). Germline mutations in BAP1 predispose to melanocytic tumors. Nat Genet *43*, 1018-1021.

Wijnhoven, P., Konietzny, R., Blackford, A.N., Travers, J., Kessler, B.M., Nishi, R., and Jackson, S.P. (2015). USP4 Auto-Deubiquitylation Promotes Homologous Recombination. Mol Cell *60*, 362-373.

Wilkinson, K.D., Urban, M.K., and Haas, A.L. (1980). Ubiquitin is the ATP-dependent proteolysis factor I of rabbit reticulocytes. J Biol Chem *255*, 7529-7532.

Williamson, A., Banerjee, S., Zhu, X., Philipp, I., Iavarone, A.T., and Rape, M. (2011). Regulation of ubiquitin chain initiation to control the timing of substrate degradation. Mol Cell *42*, 744-757.

Wu, K., Chen, A., and Pan, Z.Q. (2000). Conjugation of Nedd8 to CUL1 enhances the ability of the ROC1-CUL1 complex to promote ubiquitin polymerization. J Biol Chem *275*, 32317-32324.

Wu, T., Merbl, Y., Huo, Y., Gallop, J.L., Tzur, A., and Kirschner, M.W. (2010). UBE2S drives elongation of K11-linked ubiquitin chains by the anaphase-promoting complex. Proc Natl Acad Sci U S A *107*, 1355-1360.

Wu-Baer, F., Lagrazon, K., Yuan, W., and Baer, R. (2003). The BRCA1/BARD1 heterodimer assembles polyubiquitin chains through an unconventional linkage involving lysine residue K6 of ubiquitin. J Biol Chem *278*, 34743-34746.

Xiao, Z.X., Chen, J., Levine, A.J., Modjtahedi, N., Xing, J., Sellers, W.R., and Livingston, D.M. (1995). Interaction between the retinoblastoma protein and the oncoprotein MDM2. Nature *375*, 694-698.

Xu, D., Shan, B., Lee, B.H., Zhu, K., Zhang, T., Sun, H., Liu, M., Shi, L., Liang, W., Qian, L., *et al.* (2015). Phosphorylation and activation of ubiquitin-specific protease-14 by Akt regulates the ubiquitin-proteasome system. Elife *4*, e10510.

Yang, Y., Liu, M., Li, D., Ran, J., Gao, J., Suo, S., Sun, S.C., and Zhou, J. (2014). CYLD regulates spindle orientation by stabilizing astral microtubules and promoting dishevelled-NuMA-dynein/dynactin complex formation. Proc Natl Acad Sci U S A *111*, 2158-2163.

Yao, T., and Cohen, R.E. (2002). A cryptic protease couples deubiquitination and degradation by the proteasome. Nature *419*, 403-407.

Yao, T., Song, L., Jin, J., Cai, Y., Takahashi, H., Swanson, S.K., Washburn, M.P., Florens, L., Conaway, R.C., Cohen, R.E., *et al.* (2008). Distinct modes of regulation of the Uch37 deubiquitinating enzyme in the proteasome and in the Ino80 chromatin-remodeling complex. Mol Cell *31*, 909-917.

Ye, Y., and Rape, M. (2009). Building ubiquitin chains: E2 enzymes at work. Nat Rev Mol Cell Biol *10*, 755-764.

You, J., and Pickart, C.M. (2001). A HECT domain E3 enzyme assembles novel polyubiquitin chains. J Biol Chem *276*, 19871-19878.

Yuan, J., Luo, K., Zhang, L., Cheville, J.C., and Lou, Z. (2010). USP10 regulates p53 localization and stability by deubiquitinating p53. Cell *140*, 384-396.

Yuan, W.C., Lee, Y.R., Lin, S.Y., Chang, L.Y., Tan, Y.P., Hung, C.C., Kuo, J.C., Liu, C.H., Lin, M.Y., Xu, M., *et al.* (2014). K33-Linked Polyubiquitination of Coronin 7 by Cul3-KLHL20 Ubiquitin E3 Ligase Regulates Protein Trafficking. Mol Cell *54*, 586-600.

Zhang, L., Zhou, F., Drabsch, Y., Gao, R., Snaar-Jagalska, B.E., Mickanin, C., Huang, H., Sheppard, K.A., Porter, J.A., Lu, C.X., *et al.* (2012). USP4 is regulated by AKT phosphorylation and directly deubiquitylates TGF-beta type I receptor. Nat Cell Biol *14*, 717-726.

Zhang, M., Cai, F., Zhang, S., and Song, W. (2014). Overexpression of ubiquitin carboxyl-terminal hydrolase L1 (UCHL1) delays Alzheimer's progression in vivo. Sci Rep *4*, 7298.

Zhang, X., Berger, F.G., Yang, J., and Lu, X. (2011). USP4 inhibits p53 through deubiquitinating and stabilizing ARF-BP1. EMBO J *30*, 2177-2189.

Zhao, Y., Majid, M.C., Soll, J.M., Brickner, J.R., Dango, S., and Mosammaparast, N. (2015). Noncanonical regulation of alkylation damage resistance by the OTUD4 deubiquitinase. EMBO J *34*, 1687-1703.

Zhen, Y., Knobel, P.A., Stracker, T.H., and Reverter, D. (2014). Regulation of USP28 deubiquitinating activity by SUMO conjugation. J Biol Chem *289*, 34838-34850.

Appendices

Appendix Table 1: A table representing the cellular abundance and molecular weight of DUBs, with and without the covalent Ub-VME addition.

All DUBs have been listed with their predicted molecular weight (from heaviest to lightest). Alongside this a value has been listed for their predicted molecular weight once covalently bound to HA-Ub-VME (an additional 10kDa). Cellular abundance values for DUBs was based on iBAQ data mined from A549 proteome studies (Geiger et al., 2012). The abundance ranking for each DUB is based upon these iBAQ values. DUBs that cannot interact with Ub-VME probe have been coloured, the JAMMs in red and the catalytically inactive in grey. The coloured regions in column 1 correspond to coloured arrows in Figure 3.4 and 3.6 and represent regions on interest from the HA immunoblot.

DUB		Molecular Weight (kDa)		iBAQ	Abundance Ranking
		Predicted	Predicted + Ub-VME (10kDa)		
	USP34	404.2	414.2	5.00	22
	USP24	294.4	304.4	5.19	20
*	USP9X	292.3	302.3	5.98	13
	USP9Y	291.1	301.1		
	USP54	187.4	197.4	1.41	45
	USP32	181.3	191.3	4.17	31
	USP6	158.7	168.7	1.46	44
	USP47	157.3	167.3	5.53	18
	USP19 (Iso5)	156.0	166.0		
	USP19 (Iso6)	151.9	161.9		
	USP19 (Iso7)	150.7	160.7		
	USP31	146.7	156.7		
	USP19	145.7	155.7	1.65	40
	USP42	145.4	155.4	1.58	41
	USP40	140.1	150.1	3.05	35
	USP52	135.4	145.4		
	VCPIP	134.3	144.3	4.82	24
*	USP7	128.3	138.3	6.47	8
	USP8	127.5	137.5	5.80	15
	OTUD4	123.9	133.9		
	USP43	122.8	132.8		
	USP36	122.7	132.7	5.02	21
	USP28	122.5	132.5	4.81	25
	USP25	122.2	132.2	4.67	27
	USP53	120.8	130.8		
	USPL1	120.4	130.4		
	USP48	119.0	129.0		
	USP38	116.5	126.5		
	USP35	113.4	123.4		
	USP38 (Iso2)	113.2	123.2		
*	USP15	112.3	122.3	6.16	12
	USP37	110.2	120.2		
	USP11	109.8	119.8	5.57	17

DUB		Molecular Weight (kDa)		iBAQ	Abundance Ranking
		Predicted	Predicted + Ub-VME (10kDa)		
	USP15 (Iso2)	109.4	119.4		
	USP4	108.6	118.6	4.29	29
	CYLD	107.3	117.3	2.38	38
	USP33	106.7	116.7	4.47	28
	USP29	104.2	114.2		
	USP26	104.0	114.0		
	USP20	102.0	112.0	1.66	39
	OTU7A	100.7	110.7		
	USP13	97.3	107.3	4.74	26
*	USP5	95.7	105.7	7.01	3
	MYSM1	95.0	105.0	1.16	46
	USP16	93.6	103.6	4.17	30
	OTU7B	92.5	102.5	2.91	36
	USP45	91.7	101.7		
	TNFAIP3	89.6	99.6		
	USP1	88.2	98.2	2.79	37
	USP10	87.1	97.1	6.55	6
	USP44	81.2	91.2		
	TRABID	81.0	91.0		
	BAP1	80.4	90.4	1.52	43
	USP51	79.8	89.8		
	USP49	79.2	89.2		
	USP2	68.1	78.1		
	USP39	65.4	75.4	6.52	7
	USP21	62.7	72.7		
	OTUD5	60.6	70.6	1.55	42
	OTUD5 (Iso6)	60.2	70.2		
	USP22	60.0	70.0	3.74	32
	USP17L2	59.6	69.6		
	USP3	58.9	68.9	5.69	16
	USP30	58.5	68.5	4.88	23
	USP39 (Iso3)	56.4	66.4		
	USP14	55.9	65.9	6.63	5
	USP3 (Iso2)	53.7	63.7		
	USP39 (Iso2)	53.5	63.5		
	USP14 (Iso2)	52.4	62.4		
	OTUD1	51.0	61.0		
	MNPD	50.7	60.7		
	STAMBLP	49.8	59.8	5.51	19
	USP27	49.6	59.6		
	STAMBP	48.0	58.0	5.93	14
	USP18	43.0	53.0		
	USP12	42.9	52.9	3.19	34
	USP46	42.4	52.4	3.58	33
	ATXN3	41.8	51.8		
	USP2 (Iso3)	41.7	51.7		

DUB		Molecular Weight (kDa)		iBAQ	Abundance Ranking
		Predicted	Predicted + Ub-VME (10kDa)		
	ATXN3L	40.7	50.7		
	EIF3H	39.9	49.9		
	ATXN3 (Iso4)	39.7	49.7		
	OTUD5 (Iso5)	39.2	49.2		
	PARP11	38.7	48.7		
	USP50 (Iso2)	38.4	48.4		
	YOD1 (OTU1)	38.3	48.3		
	UCHL5	37.6	47.6	6.27	11
	CSN5	37.4	47.4	6.41	9
	EIF3F	37.4	47.4		
	PSMD7	36.9	46.9		
	CSN6	36.2	46.2		
	BRCC3	35.9	45.9		
	USP4 (Iso3)	35.7	45.7		
	PSMD14 (POH1)	34.6	44.6	6.32	10
	OTU6B	33.8	43.8		
	OTU6A	33.3	43.3		
	OTUB1	31.2	41.2		
	OTUB2	27.2	37.2	7.21	2
	USP15 (Iso3)	27.1	37.1		
	UCHL3	26.2	36.2	6.8	4
*	UCHL1	24.6	34.6	8.05	1
	JOSD1	23.2	33.2		
	JOSD2	20.8	30.8		
	ATXN3 (Iso5)	20.6	30.6		

Appendix Table 2: List of MS-identified proteins from HA-Ub-VME pull down in G_1/S (medium) and mitotic (heavy) SILAC-labelled cell populations.

			Minus VME			Plus VME		
Gene name	Proteins	Peptides	Ratio M/L	Ratio H/L	Intensity	Ratio M/L	Ratio H/L	Intensity
ACTA2	12	7	0.9115	0.6281	605430	NaN	NaN	0
ACTN4	3	1	NaN	NaN	0	1.0602	0.3782	144320
ADO	1	1	NaN	NaN	0	NaN	NaN	0
AGPAT6	1	1	0.9740	0.6668	327420	NaN	NaN	0
AKR1B10	1	5	0.8041	1.0476	3336000	0.8785	1.1737	227540
AKR1C2	7	1	0.8262	1.0901	398460	NaN	NaN	0
AKR1D1	3	1	0.8043	1.1387	139040	NaN	NaN	0
ALMS1P	1	1	NaN	NaN	0	0.0510	0.2226	98728
ANKFY1	4	21	0.9608	0.5543	15123000	0.9326	0.5472	10398000
ASAP2	2	1	NaN	NaN	223110	NaN	NaN	0
C11orf74	3	1	NaN	NaN	0	NaN	NaN	275460
C13orf28	4	1	NaN	NaN	0	NaN	NaN	0
CAD	3	4	0.8893	1.7979	105910	0.8772	2.1561	500830
CAPZB	2	1	NaN	NaN	0	NaN	NaN	0
CARD9	3	1	NaN	NaN	0	NaN	NaN	0
CASQ1	1	1	NaN	NaN	0	NaN	NaN	0
CENPC1	1	1	NaN	NaN	0	NaN	NaN	0
CHD3	1	1	NaN	NaN	0	0.7931	0.3442	73319
CLCF1	2	1	0.1409	0.0768	410400	0.1457	0.0664	240350
DCAF15	1	1	NaN	NaN	0	NaN	NaN	0
DCD	2	1	NaN	NaN	0	NaN	NaN	62271
DCLRE1C	2	1	NaN	NaN	512170	NaN	NaN	0
DLG2	1	1	NaN	NaN	47467	NaN	NaN	0
DMD	6	1	NaN	NaN	0	17.8120	1.2544	653290
DOCK3	3	1	NaN	NaN	47465	NaN	NaN	0
EEF1A2	13	2	1.0761	0.7895	825510	1.6588	0.8588	421330
ENO1	2	2	1.0224	1.0316	312510	0.8704	1.0341	221760
EWSR1	8	1	NaN	NaN	0	0.5260	0.1164	254680
EXD3	1	1	1.6482	NaN	193590	NaN	NaN	0
F2R	1	1	NaN	NaN	0	NaN	NaN	150300
FAM154B	1	1	NaN	NaN	0	NaN	NaN	0
FAM54B	3	1	NaN	NaN	0	NaN	NaN	0
FASN	1	6	NaN	NaN	0	0.6186	0.6115	1343600
FGF11	1	1	NaN	NaN	0	NaN	NaN	0
FUS	7	3	NaN	NaN	0	0.5959	0.1487	2458500

			Minus VME			Plus VME		
Gene name	Proteins	Peptides	Ratio M/L	Ratio H/L	Intensity	Ratio M/L	Ratio H/L	Intensity
GAPDH	7	2	0.9050	0.7693	2275600	NaN	NaN	0
HERC6	2	1	NaN	NaN	0	NaN	NaN	0
HNRNPR	12	12	0.6817	1.3684	1200700	0.6245	1.4534	8134200
HNRNPU	5	5	0.8170	0.4338	297690	0.8059	0.5320	1300900
HSF1	1	1	NaN	NaN	832330	NaN	NaN	0
HSPA6	2	2	NaN	NaN	0	0.9092	0.6102	163120
HSPA8	23	3	0.9627	0.6442	283950	0.7900	0.5888	433600
HSPG2	2	1	NaN	NaN	0	NaN	NaN	0
IGKC	15	1	NaN	NaN	98448	NaN	NaN	0
IRF4	3	1	NaN	NaN	0	NaN	NaN	0
ITGA6	8	1	NaN	NaN	0	NaN	NaN	758450
KIAA0754	2	1	NaN	NaN	169770	NaN	NaN	0
KIT	2	1	0.0539	NaN	2071200	NaN	NaN	0
KLKB1	2	1	1.0277	10.4920	541650	NaN	NaN	0
KRT18	1	3	NaN	NaN	0	0.0270	0.0817	594890
LARGE	2	1	NaN	NaN	0	0.1082	0.0623	652480
LDHA	6	1	1.0536	1.0226	266980	NaN	NaN	0
LDHB	1	1	1.0211	0.9600	247940	NaN	NaN	0
LGALS12	7	1	NaN	NaN	0	NaN	NaN	127940
LOC283999	1	1	NaN	NaN	0	0.0495	0.1177	341290
LOC646048	2	2	1.0206	0.7060	211640	0.8349	0.6076	296350
LOC646057	2	1	NaN	NaN	0	NaN	NaN	212760
LOC646879	1	1	NaN	NaN	348900	NaN	NaN	490410
LOC647323	1	1	NaN	NaN	0	NaN	NaN	0
MAPKAPK2	2	1	NaN	NaN	375070	NaN	NaN	0
METTL2A	4	1	0.5764	0.5323	199740	NaN	NaN	0
MFAP1	1	1	NaN	NaN	0	NaN	NaN	0
MIA3	4	1	NaN	NaN	0	NaN	NaN	0
MLX	1	1	NaN	NaN	0	0.1389	0.0759	269220
MRPS9	1	1	NaN	NaN	0	NaN	NaN	0
NARG1L	5	2	0.8044	0.6558	180070	NaN	NaN	0
NAT6	1	1	NaN	NaN	64743	NaN	NaN	0
NCL	2	1	NaN	NaN	0	0.7833	0.4808	60048
NCRNA00185	1	1	NaN	NaN	0	NaN	NaN	181850
NPNT	5	1	NaN	NaN	0	0.0103	0.0107	14296000

Appendix Table 2 cont.

			Minus VME			Plus VME		
Gene name	Proteins	Peptides	Ratio M/L	Ratio H/L	Intensity	Ratio M/L	Ratio H/L	Intensity
OR3A3	1	1	NaN	NaN	214020	0.1103	0.3713	393090
OR4D6	1	1	NaN	NaN	0	NaN	NaN	0
PCNA	1	1	1.0257	0.5889	65868	NaN	NaN	0
PDE4D	3	1	NaN	NaN	0	NaN	NaN	483870
PKM2	13	2	1.1700	0.9972	363260	0.9367	0.8645	79190
PLOD2	1	1	NaN	NaN	0	NaN	NaN	37435
PLXNA1	1	1	NaN	NaN	65881	NaN	NaN	0
PPP2R1A	1	1	NaN	NaN	0	NaN	NaN	0
PRDM1	1	1	NaN	NaN	68122	NaN	NaN	0
RBMX	6	1	0.6068	1.9197	114680	NaN	NaN	0
REV1	2	1	NaN	NaN	0	NaN	NaN	0
RGAG1	2	1	NaN	NaN	3702700	196.1500	0.3710	11647000
RPL13A	6	2	0.7784	0.3019	671830	NaN	NaN	0
RPL14	1	1	0.8597	0.2433	203930	NaN	NaN	0
RPL24	4	1	0.7997	0.4399	236930	NaN	NaN	0
RPL27	2	1	0.7043	0.2268	219190	NaN	NaN	0
RPL28	5	2	0.7429	0.1959	403790	0.7019	0.1949	63755
RPL31	8	1	NaN	NaN	0	0.7300	0.2958	63789
RPL35A	1	1	NaN	NaN	0	NaN	NaN	0
RPL4	3	1	NaN	NaN	0	0.7378	0.3102	150190
RPL8	5	1	0.8315	0.2856	140500	NaN	NaN	0
RPS7	5	1	NaN	NaN	0	0.7055	0.2178	123770
RPS8	2	2	0.7526	0.2277	380060	NaN	NaN	0
SGOL2	4	1	NaN	NaN	0	NaN	NaN	0
SLA	3	1	NaN	NaN	0	NaN	NaN	0
SLC6A9	2	1	NaN	NaN	25221	NaN	NaN	0
SULT1C2	5	1	NaN	NaN	573470	NaN	NaN	1072800
SYNE1	1	1	NaN	NaN	0	0.1333	NaN	1069800
SYNE2	1	1	NaN	NaN	45934	NaN	NaN	0
TAF15	2	3	NaN	NaN	0	NaN	NaN	0
TKT	7	3	NaN	NaN	0	0.9151	0.5366	925420
TP53TG1	1	1	NaN	NaN	0	0.2586	2.5367	239970
TTC14	2	1	NaN	NaN	0	NaN	NaN	0
UCHL1	1	2	NaN	NaN	0	1.1067	1.3681	1638400
UCHL5	11	5	NaN	NaN	0	0.6845	0.4199	700690

			Minus VME			Plus VME		
Gene name	Proteins	Peptides	Ratio M/L	Ratio H/L	Intensity	Ratio M/L	Ratio H/L	Intensity
USP14	3	4	NaN	NaN	0	0.6174	0.4890	1302200
USP15	11	5	NaN	NaN	0	0.8493	0.4432	780510
USP24	2	1	NaN	NaN	0	0.7545	0.3465	127080
USP5	5	14	NaN	NaN	0	0.6409	0.3782	7188700
USP7	3	12	NaN	NaN	0	0.5489	0.2684	4087400
USP9X	5	18	NaN	NaN	0	0.8314	0.4537	5039000
XRCC2	1	1	0.1974	0.0135	251170	0.1180	0.0349	375820
ZEB2	1	1	NaN	NaN	0	NaN	NaN	143090
ZNF3	1	1	NaN	NaN	0	NaN	NaN	0
ZNF317	5	1	NaN	NaN	0	1.1492	1.4384	1930900
ZNF560	1	1	NaN	NaN	0	NaN	NaN	0
-	1	1	0.4207	4.2310	2104500	2.2673	2.2024	1149500
-	3	3	0.9141	0.6662	483300	NaN	NaN	0
-	11	1	0.7118	0.2833	305530	NaN	NaN	0
-	1	1	1.1398	0.5089	268440	NaN	NaN	0
-	6	1	0.6281	0.2025	89521	NaN	NaN	0
-	23	3	NaN	NaN	0	0.0717	0.0399	9653100
-	8	2	NaN	NaN	0	0.6422	0.5964	474220
-	4	1	NaN	NaN	0	NaN	NaN	271490
-	1	1	NaN	NaN	0	NaN	NaN	20038
-	5	1	NaN	NaN	0	NaN	NaN	0
-	1	1	0.1092	0.0852	1237700	NaN	NaN	0
-	6	1	0.6892	12.4740	559810	NaN	NaN	0
-	4	2	1.1088	1.1519	216810	1.1460	1.2115	96327
-	6	1	0.7346	0.1900	172390	NaN	NaN	0
-	1	1	NaN	NaN	136080	NaN	NaN	59688
-	1	1	NaN	NaN	0	0.0854	0.0082	4022700
-	1	1	NaN	NaN	0	0.0248	0.0167	293860
-	1	1	NaN	NaN	0	0.6887	0.9909	70287
-	1	1	NaN	NaN	0	NaN	NaN	0
-	1	1	NaN	NaN	0	NaN	NaN	0
-	1	1	NaN	NaN	0	NaN	NaN	0

Appendix 3: List of MS-identified proteins from sepharose-Ub-PA pull down across seven cell cycle phases.

Data from 4 triplexed-SILAC-MS experiments have been compiled. Run 1: G_1 (M) and G_1/S (H), Run 2: Early S (M) and Late S (H), Run 3: G_2/M (M) and G_2 (H), Run 4: M (M) and G_2 (H). Ratios listed in Appendix Table 3.1 and 3.2 are averages of three technical replicates (see Section 4.3.3).

Appendix Table 3.1: All proteins identified from sepharose-Ub-PA pull down (Runs 1 – 4).

		G1 and G1/S		Early S and Late S		G2 and G2/M		G2 and M	
		Run1		Run2		Run3		Run4	
Gene name	Peptides	Ratio M/L	Ratio H/L	Ratio M/L	Ratio H/L	Ratio M/L	Ratio H/L	Ratio M/L	Ratio H/L
ACLY	1	0.5920	0.6364	1.8096	1.3399	0.5907	0.8713	0.7434	1.0007
ACTA1	12	0.9925	0.5503	1.6057	0.7888	1.0488	0.7161	0.7320	0.5234
ACTB	17	1.0632	0.5915	1.7969	0.9021	1.1767	0.8671	0.6941	0.4923
ACTG1	17	1.0277	0.5397	1.6387	0.8262	1.0559	0.7082	0.7755	0.5827
ACTN1	1	0.3458	0.6456	1.0426	2.5506	0.6277	1.8195	0.4592	1.2945
AHCY	2	0.7157	0.7076	1.0721	1.3407	0.7146	1.0369	0.7516	0.8407
AKAP9	1	#DIV/0!	#DIV/0!	#DIV/0!	#DIV/0!	#DIV/0!	#DIV/0!	#DIV/0!	#DIV/0!
AKR1A1	1	1.5138	0.7800	1.6580	1.5989	1.5147	1.4889	1.2805	1.2049
AKR1B1	6	1.4996	0.8195	1.5995	1.7715	1.5906	1.6115	1.2669	1.2289
AKR1B10	16	0.5576	0.4218	0.5961	0.5276	0.6053	0.5787	0.5006	0.4682
AKR1B15	6	1.4346	0.7474	1.6755	1.4905	1.5144	1.4204	1.2024	1.1923
AKR1C2	8	0.6716	0.4129	0.8303	0.6940	0.6675	0.5981	0.5827	0.5177
AKR1C3	8	0.7412	0.5173	0.8454	0.7163	0.7755	0.7302	0.6398	0.5996
AKR1D1	2	0.7422	0.5175	1.0155	0.9474	0.7728	0.7979	#DIV/0!	#DIV/0!
ALDH1A1	20	0.7202	0.4724	0.6598	0.7807	0.8746	0.7774	0.8798	0.7468
ALDH3A1	4	0.7675	0.4980	1.3048	1.0461	0.7629	0.7615	0.8483	0.8414
ALDOA	3	0.6920	0.4651	0.6460	0.5139	0.5885	0.5883	0.6280	0.4942
ALPK1	1	#DIV/0!	#DIV/0!	#DIV/0!	#DIV/0!	#DIV/0!	#DIV/0!	#DIV/0!	#DIV/0!
ANP32B	1	#DIV/0!	#DIV/0!	3.2266	1.0574	1.4324	3.3348	#DIV/0!	#DIV/0!
ANXA2	5	0.7158	0.5679	2.1705	1.6939	1.7683	1.0054	0.7144	0.7512
API5	1	#DIV/0!	#DIV/0!	#DIV/0!	#DIV/0!	#DIV/0!	#DIV/0!	#DIV/0!	#DIV/0!
ARF1	3	0.5893	0.8091	1.7940	1.8445	0.6464	1.2855	0.8769	1.3076
ARMC2	1	#DIV/0!	#DIV/0!	#DIV/0!	#DIV/0!	#DIV/0!	#DIV/0!	#DIV/0!	#DIV/0!
ARNTL	1	#DIV/0!	#DIV/0!	#DIV/0!	#DIV/0!	#DIV/0!	#DIV/0!	#DIV/0!	#DIV/0!
ATPBD4	1	#DIV/0!	#DIV/0!	#DIV/0!	#DIV/0!	#DIV/0!	#DIV/0!	#DIV/0!	#DIV/0!
ATRX	1	#DIV/0!	#DIV/0!	2.2490	2.7070	0.3830	1.4247	0.4560	1.4147
BEST4	1	#DIV/0!	#DIV/0!	#DIV/0!	#DIV/0!	#DIV/0!	#DIV/0!	#DIV/0!	#DIV/0!
C12orf77	1	#DIV/0!	#DIV/0!	#DIV/0!	#DIV/0!	#DIV/0!	#DIV/0!	#DIV/0!	#DIV/0!
C5orf41	1	#DIV/0!	#DIV/0!	#DIV/0!	#DIV/0!	#DIV/0!	#DIV/0!	#DIV/0!	#DIV/0!
CCDC148	1	#DIV/0!	#DIV/0!	#DIV/0!	#DIV/0!	#DIV/0!	#DIV/0!	#DIV/0!	#DIV/0!
CD101	1	#DIV/0!	#DIV/0!	#DIV/0!	#DIV/0!	#DIV/0!	#DIV/0!	#DIV/0!	#DIV/0!
CDS1	1	0.8326	0.0213	0.1065	0.0370	0.1457	#DIV/0!	0.2586	0.0336
CENPT	1	#DIV/0!	#DIV/0!	#DIV/0!	#DIV/0!	0.2545	0.4404	#DIV/0!	#DIV/0!
CEP250	1	#DIV/0!	#DIV/0!	#DIV/0!	#DIV/0!	#DIV/0!	#DIV/0!	#DIV/0!	#DIV/0!

		G1 and G1/S		Early S and Late S		G2 and G2/M		G2 and M	
		Run1		Run2		Run3		Run4	
Gene name	Peptides	Ratio M/L	Ratio H/L	Ratio M/L	Ratio H/L	Ratio M/L	Ratio H/L	Ratio M/L	Ratio H/L
CLEC17A	1	#DIV/0!	#DIV/0!	#DIV/0!	#DIV/0!	#DIV/0!	#DIV/0!	#DIV/0!	#DIV/0!
CLGN	1	#DIV/0!	#DIV/0!	#DIV/0!	#DIV/0!	#DIV/0!	#DIV/0!	#DIV/0!	#DIV/0!
CLIP1	1	#DIV/0!	#DIV/0!	#DIV/0!	#DIV/0!	#DIV/0!	#DIV/0!	#DIV/0!	#DIV/0!
CLTC	8	0.3645	0.7592	1.4309	1.6314	0.3422	0.9509	0.5945	1.0777
COPS6	1	#DIV/0!	#DIV/0!	#DIV/0!	#DIV/0!	#DIV/0!	#DIV/0!	#DIV/0!	#DIV/0!
CR1L	1	#DIV/0!	#DIV/0!	#DIV/0!	#DIV/0!	#DIV/0!	#DIV/0!	#DIV/0!	#DIV/0!
CRY2	1	0.7210	0.5889	#DIV/0!	#DIV/0!	#DIV/0!	#DIV/0!	#DIV/0!	#DIV/0!
CSE1L	2	0.4751	1.5673	2.4976	2.4329	0.2744	0.7404	0.4874	0.8795
CUTC	1	#DIV/0!	#DIV/0!	#DIV/0!	#DIV/0!	#DIV/0!	#DIV/0!	#DIV/0!	#DIV/0!
DDX17	1	0.2899	1.7917	3.9070	3.8567	0.8524	3.1503	0.9644	3.1864
DDX3X	1	#DIV/0!	#DIV/0!	#DIV/0!	#DIV/0!	#DIV/0!	#DIV/0!	0.3870	1.0758
DHX57	1	#DIV/0!	#DIV/0!	#DIV/0!	#DIV/0!	#DIV/0!	#DIV/0!	#DIV/0!	#DIV/0!
DHX8	2	#DIV/0!	#DIV/0!	#DIV/0!	#DIV/0!	#DIV/0!	#DIV/0!	#DIV/0!	#DIV/0!
DLG4	1	#DIV/0!	#DIV/0!	#DIV/0!	#DIV/0!	#DIV/0!	#DIV/0!	#DIV/0!	#DIV/0!
DNAH1	1	#DIV/0!	#DIV/0!	#DIV/0!	#DIV/0!	#DIV/0!	#DIV/0!	#DIV/0!	#DIV/0!
EEF2	5	0.4535	0.4227	0.7266	0.6346	0.4729	0.7158	0.5361	0.5739
EIF4A1	2	0.2927	0.5296	0.8113	1.0878	0.5317	0.8621	0.6168	0.8981
ENO1	4	0.5862	0.3664	0.7588	0.9112	0.8153	0.6939	0.7671	0.6558
EPM2AIP1	1	#DIV/0!	#DIV/0!	#DIV/0!	#DIV/0!	#DIV/0!	#DIV/0!	#DIV/0!	#DIV/0!
FAM113A	1	#DIV/0!	#DIV/0!	#DIV/0!	#DIV/0!	#DIV/0!	#DIV/0!	#DIV/0!	#DIV/0!
FAM116A	2	#DIV/0!	#DIV/0!	#DIV/0!	#DIV/0!	0.5080	0.4567	#DIV/0!	#DIV/0!
FASN	2	0.4149	0.4259	0.5607	0.7359	0.3741	0.4650	0.5675	0.4760
FBXO24	1	#DIV/0!	#DIV/0!	#DIV/0!	#DIV/0!	#DIV/0!	#DIV/0!	#DIV/0!	#DIV/0!
FLNA	5	0.6997	0.9465	2.2881	1.9717	0.5834	1.6022	0.7287	1.3249
G6PD	11	0.7098	0.4337	0.6228	0.5167	0.7125	0.5780	0.7468	0.5249
GAL3ST4	1	#DIV/0!	#DIV/0!	#DIV/0!	#DIV/0!	#DIV/0!	#DIV/0!	#DIV/0!	#DIV/0!
GAPDH	8	0.5819	0.5165	0.8148	0.6711	0.6029	0.6892	0.5577	0.5642
GGT7	1	#DIV/0!	#DIV/0!	#DIV/0!	#DIV/0!	#DIV/0!	#DIV/0!	#DIV/0!	#DIV/0!
GNB2L1	2	0.2201	0.8201	2.1805	2.2646	#DIV/0!	#DIV/0!	0.3734	0.9942
GOLGB1	1	#DIV/0!	#DIV/0!	#DIV/0!	#DIV/0!	#DIV/0!	#DIV/0!	#DIV/0!	#DIV/0!
GPI	3	0.6275	0.4651	0.7296	0.8409	0.7081	0.7109	0.7660	0.6724
GPR111	1	0.7181	0.4726	0.6933	0.7939	#DIV/0!	#DIV/0!	0.8757	0.7852
GSTP1	2	#DIV/0!	#DIV/0!	#DIV/0!	#DIV/0!	0.7418	1.5313	1.5623	1.1900
H2AFX	2	0.4880	1.5782	3.2524	2.8903	0.8192	2.3815	0.4601	2.4118

Appendix Table 3.1 cont.

		G1 and G1/S		Early S and Late S		G2 and G2/M		G2 and M	
		Run1		Run2		Run3		Run4	
Gene name	Peptides	Ratio M/L	Ratio H/L	Ratio M/L	Ratio H/L	Ratio M/L	Ratio H/L	Ratio M/L	Ratio H/L
HIST1H1D	1	#DIV/0!	#DIV/0!	#DIV/0!	#DIV/0!	0.4539	2.0842	0.4546	1.7300
HIST2H2BF	2	0.4423	1.3448	2.3696	2.2706	0.8566	2.4935	0.5865	2.3608
HNRNPA2B1	2	#DIV/0!	#DIV/0!	4.3416	4.8542	2.2636	3.7627	#DIV/0!	#DIV/0!
HNRNPK	1	#DIV/0!	#DIV/0!	3.1480	2.8372	0.7803	2.9206	#DIV/0!	#DIV/0!
HNRNPU	4	0.4932	2.3424	4.8859	3.3991	1.1508	4.2077	1.0634	3.0951
HSPA6	1	0.5077	0.5967	2.1607	2.0164	1.1448	1.5523	1.1008	1.6168
HSPB1	3	1.0130	0.8619	1.1424	1.2784	0.7225	1.0110	1.2232	1.1651
HUWE1	3	0.3480	0.5512	1.0149	0.8902	#DIV/0!	#DIV/0!	#DIV/0!	#DIV/0!
ICAM3	1	#DIV/0!	#DIV/0!	#DIV/0!	#DIV/0!	#DIV/0!	#DIV/0!	#DIV/0!	#DIV/0!
IFNA2	1	#DIV/0!	#DIV/0!	#DIV/0!	#DIV/0!	#DIV/0!	#DIV/0!	#DIV/0!	#DIV/0!
JMJD1C	1	#DIV/0!	#DIV/0!	#DIV/0!	#DIV/0!	#DIV/0!	#DIV/0!	#DIV/0!	#DIV/0!
KCNJ1	1	#DIV/0!	#DIV/0!	#DIV/0!	#DIV/0!	#DIV/0!	#DIV/0!	#DIV/0!	#DIV/0!
KIAA0100	1	1.2344	0.6300	#DIV/0!	#DIV/0!	0.7460	0.5998	0.8108	0.6186
KIAA1109	1	#DIV/0!	#DIV/0!	#DIV/0!	#DIV/0!	#DIV/0!	#DIV/0!	#DIV/0!	#DIV/0!
KIT	1	#DIV/0!	#DIV/0!	#DIV/0!	#DIV/0!	#DIV/0!	#DIV/0!	#DIV/0!	#DIV/0!
KLHL13	1	#DIV/0!	#DIV/0!	#DIV/0!	#DIV/0!	#DIV/0!	#DIV/0!	#DIV/0!	#DIV/0!
KPNB1	4	0.3419	0.6945	1.2771	1.3928	0.3598	0.5565	0.5854	0.7708
KRT1	13	0.0544	0.0838	0.0795	0.1122	0.0642	0.1031	0.0685	0.0770
KRT10	15	0.2116	0.1315	0.1233	0.2633	0.2045	0.2105	0.1242	0.2053
KRT18	7	#DIV/0!	#DIV/0!	5.4156	1.2572	0.7058	0.4954	2.0856	1.0910
Krt19	3	0.2338	0.4443	#DIV/0!	#DIV/0!	0.1129	0.3934	#DIV/0!	#DIV/0!
KRT2	9	0.1576	0.0966	0.1182	0.1195	0.0788	0.1215	0.2313	0.1121
KRT8	6	0.9099	0.6014	3.9052	0.8967	0.4201	0.4583	0.9430	0.5210
KRT9	5	1.3901	0.2145	0.6240	0.1637	0.4051	0.2319	0.0620	0.1810
LDHA	12	0.6811	0.5491	0.7875	0.7875	0.6485	0.6726	0.7346	0.6652
LDHB	10	0.8605	0.4817	1.0363	0.8878	0.9058	0.7581	0.9336	0.7092
LOC81691	1	#DIV/0!	#DIV/0!	#DIV/0!	#DIV/0!	#DIV/0!	#DIV/0!	#DIV/0!	#DIV/0!
LPPR4	1	#DIV/0!	#DIV/0!	#DIV/0!	#DIV/0!	#DIV/0!	#DIV/0!	#DIV/0!	#DIV/0!
LUC7L2	1	#DIV/0!	#DIV/0!	0.5626	0.5172	0.3162	0.4244	0.3317	0.5895
MAGEF1	1	#DIV/0!	#DIV/0!	#DIV/0!	#DIV/0!	#DIV/0!	#DIV/0!	#DIV/0!	#DIV/0!
MAP2K4	1	#DIV/0!	#DIV/0!	#DIV/0!	#DIV/0!	#DIV/0!	#DIV/0!	#DIV/0!	#DIV/0!
MAVS	1	#DIV/0!	#DIV/0!	#DIV/0!	#DIV/0!	#DIV/0!	#DIV/0!	#DIV/0!	#DIV/0!
MFSD10	1	#DIV/0!	#DIV/0!	#DIV/0!	#DIV/0!	#DIV/0!	#DIV/0!	#DIV/0!	#DIV/0!
MLL5	1	#DIV/0!	#DIV/0!	#DIV/0!	#DIV/0!	#DIV/0!	#DIV/0!	#DIV/0!	#DIV/0!

		G1 and G1/S		Early S and Late S		G2 and G2/M		G2 and M	
		Run1		Run2		Run3		Run4	
Gene name	Peptides	Ratio M/L	Ratio H/L	Ratio M/L	Ratio H/L	Ratio M/L	Ratio H/L	Ratio M/L	Ratio H/L
MNX1	1	#DIV/0!	#DIV/0!	#DIV/0!	#DIV/0!	#DIV/0!	#DIV/0!	#DIV/0!	#DIV/0!
MTMR2	1	#DIV/0!	#DIV/0!	#DIV/0!	#DIV/0!	#DIV/0!	#DIV/0!	#DIV/0!	#DIV/0!
MYCBPAP	1	#DIV/0!	#DIV/0!	#DIV/0!	#DIV/0!	0.4338	1.2316	#DIV/0!	#DIV/0!
MYO1B	1	#DIV/0!	#DIV/0!	#DIV/0!	#DIV/0!	#DIV/0!	#DIV/0!	#DIV/0!	#DIV/0!
MYOM3	1	#DIV/0!	#DIV/0!	#DIV/0!	#DIV/0!	#DIV/0!	#DIV/0!	#DIV/0!	#DIV/0!
NBL1	1	#DIV/0!	#DIV/0!	#DIV/0!	#DIV/0!	#DIV/0!	#DIV/0!	#DIV/0!	#DIV/0!
NEDD4	1	0.1953	0.1655	#DIV/0!	#DIV/0!	0.2862	0.4310	#DIV/0!	#DIV/0!
NEU2	1	#DIV/0!	#DIV/0!	#DIV/0!	#DIV/0!	#DIV/0!	#DIV/0!	#DIV/0!	#DIV/0!
NFATC3	1	#DIV/0!	#DIV/0!	#DIV/0!	#DIV/0!	#DIV/0!	#DIV/0!	#DIV/0!	#DIV/0!
NQO1	7	0.6427	0.4331	0.5891	0.6094	0.6007	0.5597	0.6765	0.5682
OR13D1	1	#DIV/0!	#DIV/0!	#DIV/0!	#DIV/0!	#DIV/0!	#DIV/0!	#DIV/0!	#DIV/0!
OTUB1	12	1.1011	0.6599	0.7229	0.7196	0.7547	0.6417	0.8032	0.6641
OTUD4	2	1.0595	2.9340	5.9357	4.3541	1.6764	3.6242	1.5119	3.4411
OTUD5	1	0.5097	0.7035	1.0637	1.5041	0.6064	1.1828	0.8926	1.1685
OTUD6B	3	0.5628	0.6620	0.8827	0.9147	0.4408	0.7546	0.5268	0.7823
PARP1	1	#DIV/0!	#DIV/0!	#DIV/0!	#DIV/0!	#DIV/0!	#DIV/0!	#DIV/0!	#DIV/0!
PCBP2	1	#DIV/0!	#DIV/0!	#DIV/0!	#DIV/0!	#DIV/0!	#DIV/0!	#DIV/0!	#DIV/0!
PCDP1	1	#DIV/0!	#DIV/0!	#DIV/0!	#DIV/0!	#DIV/0!	#DIV/0!	#DIV/0!	#DIV/0!
PEX11B	1	#DIV/0!	#DIV/0!	#DIV/0!	#DIV/0!	0.6141	0.4986	#DIV/0!	#DIV/0!
PFN1	3	1.2115	0.5776	1.8467	1.7505	0.7774	1.1619	1.0485	0.9180
PGAM4	1	#DIV/0!	#DIV/0!	#DIV/0!	#DIV/0!	1.1676	1.0234	#DIV/0!	#DIV/0!
PGD	4	0.5359	0.4919	0.6599	0.7473	0.7138	0.6971	0.7503	0.6821
PGK1	2	0.7520	0.4058	1.1716	0.9855	0.7967	0.8040	0.7021	0.6453
PHC1	1	#DIV/0!	#DIV/0!	#DIV/0!	#DIV/0!	#DIV/0!	#DIV/0!	#DIV/0!	#DIV/0!
PHLDB1	1	#DIV/0!	#DIV/0!	#DIV/0!	#DIV/0!	#DIV/0!	#DIV/0!	#DIV/0!	#DIV/0!
PKM2	21	0.7222	0.4209	0.5884	0.5932	0.6926	0.6735	0.7667	0.6154
PLA2G6	1	0.4386	1.3269	2.2122	2.2563	0.2671	0.7298	0.5426	1.6362
PPIA	3	1.0119	0.5159	1.4065	1.9592	0.7056	1.1571	1.0089	0.8638
PRKAR1B	1	#DIV/0!	#DIV/0!	#DIV/0!	#DIV/0!	#DIV/0!	#DIV/0!	#DIV/0!	#DIV/0!
PRMT1	2	1.0223	1.2544	3.4271	2.1271	0.7297	1.7470	0.6173	1.5033
PSMB4	1	#DIV/0!	#DIV/0!	#DIV/0!	#DIV/0!	#DIV/0!	#DIV/0!	#DIV/0!	#DIV/0!
PSMD13	1	#DIV/0!	#DIV/0!	#DIV/0!	#DIV/0!	#DIV/0!	#DIV/0!	#DIV/0!	#DIV/0!
PTGR1	1	0.6926	0.5794	1.0143	0.9157	0.7076	0.9122	0.6880	0.7989
QRSL1	1	#DIV/0!	#DIV/0!	#DIV/0!	#DIV/0!	#DIV/0!	#DIV/0!	#DIV/0!	#DIV/0!

Appendix Table 3.1 cont.

		G1 and G1/S		Early S and Late S		G2 and G2/M		G2 and M	
		Run1		Run2		Run3		Run4	
Gene name	Peptides	Ratio M/L	Ratio H/L	Ratio M/L	Ratio H/L	Ratio M/L	Ratio H/L	Ratio M/L	Ratio H/L
RANP1;RAN	7	0.4728	0.5917	0.7332	1.1521	0.6030	0.9277	0.7135	0.9606
RDX	2	0.5583	0.5941	1.1293	1.1886	0.3878	1.0126	0.4723	0.9019
RIPK4	1	#DIV/0!	#DIV/0!	#DIV/0!	#DIV/0!	#DIV/0!	#DIV/0!	#DIV/0!	#DIV/0!
RPGRIP1	1	#DIV/0!	#DIV/0!	#DIV/0!	#DIV/0!	#DIV/0!	#DIV/0!	#DIV/0!	#DIV/0!
RPL10A	1	0.2005	1.0345	1.5556	2.6043	0.4730	1.4502	0.5098	1.4927
RPL11	2	0.2276	1.2871	1.9394	2.7316	0.4832	1.6530	0.5914	1.7725
RPL12	2	0.2467	1.2155	2.2020	2.8217	0.5110	1.6213	0.5678	1.5731
RPL13	4	1.1130	1.1099	2.2606	2.3926	0.4544	1.5910	0.5501	1.5075
RPL14	4	0.2376	1.0035	1.6520	2.4021	0.4355	1.5655	0.5020	1.4619
RPL18	4	0.3250	1.0722	2.7527	2.7045	0.4667	1.5496	0.5356	1.4995
RPL18A	4	0.2496	1.1557	2.1774	2.5206	0.4230	1.4609	0.4467	1.3191
RPL19	3	0.2595	1.0703	2.9928	2.9480	0.4644	1.5448	0.4864	1.5702
RPL22	2	0.2970	1.0099	2.3509	2.8743	0.4195	1.3609	0.4673	1.2488
RPL23	2	0.2998	0.9633	1.7481	2.0762	0.5166	1.0173	0.5758	1.0712
RPL24	3	0.2170	1.0398	2.1168	2.1929	0.4349	1.2680	0.4791	1.0983
RPL26	2	0.1789	0.9536	1.9378	2.0353	0.4459	1.4171	0.3665	1.1020
RPL27	4	0.3865	1.2103	2.6133	2.8476	0.6017	1.5581	0.5314	1.3924
RPL27A	2	0.4312	1.2295	2.8241	2.6906	0.5602	1.4905	0.7144	1.5029
RPL28	3	0.2437	1.1280	2.6989	2.9750	0.3850	1.5058	0.6104	1.5961
RPL31	1	0.2826	1.2825	2.7592	2.9668	0.5136	1.7379	0.5793	1.6547
RPL32	3	0.2516	1.0039	2.6165	2.8156	0.4177	1.7004	0.4759	1.6068
RPL35	1	0.2093	1.1520	3.3236	3.4406	0.4330	1.6039	#DIV/0!	#DIV/0!
RPL35A	2	0.2133	1.1991	2.9166	2.9939	0.5200	1.7388	0.5660	2.0446
RPL38	1	0.3075	0.5811	0.8690	1.5349	0.5076	1.0060	0.6713	0.9577
RPL4	4	0.2853	1.0534	2.1316	2.4235	0.4913	1.5619	0.5607	1.4822
RPL6	7	0.2526	1.0564	2.2337	2.5032	0.4580	1.5474	0.5041	1.5199
RPL8	2	0.2549	1.0719	1.9780	2.4710	0.4234	1.4196	0.4861	1.4683
RPL9	2	0.2705	1.2614	1.9873	2.5670	0.4491	1.4533	0.5035	1.4275
RPS10-NUDT3	1	0.2053	1.0244	1.8350	2.1851	0.3514	1.3706	0.4002	1.2772
RPS13	3	0.2276	0.9969	1.9752	2.3302	0.3777	1.3725	0.4261	1.2760
RPS15	1	#DIV/0!	#DIV/0!	2.1596	2.4052	0.4029	1.3729	#DIV/0!	#DIV/0!
RPS15A	3	0.2859	0.9008	2.3438	2.6941	0.4462	1.4294	0.5357	1.4388
RPS16	5	0.3066	1.1975	1.9575	2.2227	0.3487	1.3914	0.3976	1.2067
RPS19	5	0.2281	0.9512	1.9247	2.3345	0.3492	1.3565	0.4491	1.1903

		G1 and G1/S		Early S and Late S		G2 and G2/M		G2 and M	
		Run1		Run2		Run3		Run4	
Gene name	Peptides	Ratio M/L	Ratio H/L	Ratio M/L	Ratio H/L	Ratio M/L	Ratio H/L	Ratio M/L	Ratio H/L
RPS2	4	0.2133	1.0215	1.7014	2.2924	0.4037	1.3185	0.5261	1.4551
RPS23	1	0.2006	0.8314	1.8040	2.0461	0.3216	1.1454	0.3857	1.1184
RPS24	3	0.2573	0.9787	2.2542	2.5182	0.4372	1.4683	0.5402	1.3842
RPS25	3	0.2673	0.9560	2.9892	3.3736	0.4492	1.6978	0.5685	1.7425
RPS26	2	0.2495	0.9462	2.3797	2.5336	0.3943	1.4154	0.5075	1.4143
RPS3	4	0.2613	1.0598	1.6031	2.6147	0.4506	1.4762	0.6474	1.8289
RPS4X	2	0.1886	0.8620	1.7582	2.2282	0.4020	1.3363	0.5126	1.3086
RPS5	1	0.2625	1.1277	2.0483	2.4278	0.3470	1.6180	#DIV/0!	#DIV/0!
RPS6	3	0.2449	0.8871	1.4665	2.2565	0.4869	1.3672	0.5516	1.3267
RPS7	4	0.2319	0.9737	1.8782	2.4545	0.4537	1.4357	0.5699	1.4396
SAR1B	1	0.5674	0.6922	#DIV/0!	#DIV/0!	#DIV/0!	#DIV/0!	#DIV/0!	#DIV/0!
SETP20	1	#DIV/0!	#DIV/0!	#DIV/0!	#DIV/0!	#DIV/0!	#DIV/0!	2.6310	9.1503
SLC22A7	1	#DIV/0!	#DIV/0!	#DIV/0!	#DIV/0!	#DIV/0!	#DIV/0!	#DIV/0!	#DIV/0!
SLC25A41	1	1.0677	0.6381	0.7009	0.6863	0.7154	0.6248	0.7824	0.6168
SMARCA4	1	#DIV/0!	#DIV/0!	#DIV/0!	#DIV/0!	#DIV/0!	#DIV/0!	#DIV/0!	#DIV/0!
SNRPD1	1	0.5861	1.9417	5.0695	4.0521	1.2042	3.5620	1.6573	3.5698
SNRPE	1	0.5738	1.6045	4.9548	4.2346	1.2979	3.9537	1.5685	3.7042
SNX8	1	#DIV/0!	#DIV/0!	#DIV/0!	#DIV/0!	#DIV/0!	#DIV/0!	#DIV/0!	#DIV/0!
SPEF2	1	#DIV/0!	#DIV/0!	#DIV/0!	#DIV/0!	#DIV/0!	#DIV/0!	#DIV/0!	#DIV/0!
SPESP1	1	0.9886	0.5542	#DIV/0!	#DIV/0!	#DIV/0!	#DIV/0!	0.7369	0.5714
SRSF2	2	1.6980	1.8840	3.3452	3.1758	1.5667	2.0030	1.9684	2.4081
SRSF3	2	0.3872	0.5596	0.9563	0.9191	0.9957	0.8836	1.1173	1.0121
SYN1	1	#DIV/0!	#DIV/0!	#DIV/0!	#DIV/0!	#DIV/0!	#DIV/0!	#DIV/0!	#DIV/0!
TAF9B	1	#DIV/0!	#DIV/0!	#DIV/0!	#DIV/0!	#DIV/0!	#DIV/0!	#DIV/0!	#DIV/0!
TKT	12	0.4495	0.8772	2.6604	2.5278	0.4522	1.5760	0.4674	1.4544
TMEM52	1	#DIV/0!	#DIV/0!	#DIV/0!	#DIV/0!	#DIV/0!	#DIV/0!	#DIV/0!	#DIV/0!
TMPRSS12	1	#DIV/0!	#DIV/0!	#DIV/0!	#DIV/0!	#DIV/0!	#DIV/0!	#DIV/0!	#DIV/0!
TPI1;TPI1P1	2	0.8930	0.4875	1.5239	2.2211	1.5413	1.8799	1.1157	1.3850
TRIM4	1	0.8585	0.5995	1.0185	0.9254	0.7159	0.7709	0.8962	0.7953
TUBA1B	13	0.4043	0.4730	0.8109	0.7668	0.4071	0.7001	0.5348	0.8153
TUBA4A	3	#DIV/0!	#DIV/0!	#DIV/0!	#DIV/0!	#DIV/0!	#DIV/0!	0.9646	0.9084
TUBB2C	10	0.4105	0.6149	0.6865	0.6537	0.4198	0.7330	0.5625	0.9275
UBA1	10	0.1460	0.1174	0.5277	0.5034	0.2549	0.2314	0.6810	0.5126
UBC	8	0.0322	0.0239	0.0551	0.0478	0.0514	0.0146	0.0456	0.0247

Appendix Table 3.1 cont.

		G1 and G1/S		Early S and Late S		G2 and G2/M		G2 and M	
		Run1		Run2		Run3		Run4	
Gene name	Peptides	Ratio M/L	Ratio H/L	Ratio M/L	Ratio H/L	Ratio M/L	Ratio H/L	Ratio M/L	Ratio H/L
UBE2D3	1	0.1616	0.1583	#DIV/0!	#DIV/0!	0.2678	0.2241	#DIV/0!	#DIV/0!
UBE2N	5	0.1438	0.0752	0.4135	0.3235	0.2447	0.1684	0.6885	0.2880
UCHL1	9	1.8216	0.7214	1.3831	1.0557	1.3387	0.9684	1.2348	0.9754
UCHL3	1	2.4832	0.8389	0.3931	0.5666	3.0646	2.0218	1.0263	0.6820
UCHL5	9	0.6048	0.8672	1.4193	1.2176	0.6086	1.0068	0.7354	1.0012
UGDH	7	0.6099	0.7049	1.8149	1.5761	0.5622	1.1644	0.6884	1.1581
UMODL1	1	#DIV/0!	#DIV/0!	#DIV/0!	#DIV/0!	#DIV/0!	#DIV/0!	#DIV/0!	#DIV/0!
USP11	17	0.6695	1.3124	1.6643	1.8286	0.8196	1.4926	0.8553	1.4746
USP14	1	0.9101	1.3047	4.4483	2.9372	0.6584	1.5581	0.5941	1.5302
USP15	30	0.8237	0.8129	0.7377	0.7257	0.6012	0.7875	0.6237	0.7404
USP19	4	0.7513	0.8644	1.4847	1.1557	0.6682	0.9795	0.8193	1.0053
USP24	17	0.9839	0.8380	0.4165	0.4407	0.6841	0.7724	0.5441	0.5583
USP28	7	0.5601	1.9269	3.5880	2.6290	0.5740	1.9840	0.6329	1.9933
USP34	5	0.6718	1.6264	1.7705	1.5302	0.4470	1.5276	0.4491	1.4482
USP4	6	0.9466	0.8486	0.7710	0.7290	0.6991	0.8115	0.7026	0.7189
USP40	8	0.8449	0.6028	0.3430	0.4671	0.6182	0.5202	0.6796	0.5259
USP47	21	0.7161	0.5297	0.3699	0.4628	0.6005	0.5157	0.6760	0.5118
USP5	36	1.0030	1.2234	1.4456	1.2848	0.6913	1.2041	0.6700	1.1053
USP7	49	0.8867	1.8786	2.8354	2.1767	0.6706	1.8917	0.7482	1.8625
USP8	4	0.5227	0.5448	0.9547	0.7340	0.9993	0.6402	1.3965	0.6564
USP9X	55	1.0330	1.0258	0.4274	0.5699	0.7083	0.9599	0.5328	0.6878
USP9Y	28	#DIV/0!	#DIV/0!	#DIV/0!	#DIV/0!	0.7094	0.9607	#DIV/0!	#DIV/0!
VCPIP1	12	0.5803	0.7872	0.7475	1.0808	0.6873	0.7325	0.8865	0.8201
YPEL2	1	#DIV/0!	#DIV/0!	#DIV/0!	#DIV/0!	#DIV/0!	#DIV/0!	#DIV/0!	#DIV/0!
ZC3H14	1	#DIV/0!	#DIV/0!	#DIV/0!	#DIV/0!	#DIV/0!	#DIV/0!	#DIV/0!	#DIV/0!
ZEB2	1	#DIV/0!	#DIV/0!	#DIV/0!	#DIV/0!	#DIV/0!	#DIV/0!	#DIV/0!	#DIV/0!
ZFHX3	1	#DIV/0!	#DIV/0!	#DIV/0!	#DIV/0!	#DIV/0!	#DIV/0!	#DIV/0!	#DIV/0!
ZFP2	1	#DIV/0!	#DIV/0!	#DIV/0!	#DIV/0!	#DIV/0!	#DIV/0!	#DIV/0!	#DIV/0!
ZNF45	1	#DIV/0!	#DIV/0!	#DIV/0!	#DIV/0!	#DIV/0!	#DIV/0!	#DIV/0!	#DIV/0!
ZNF578	1	#DIV/0!	#DIV/0!	#DIV/0!	#DIV/0!	#DIV/0!	#DIV/0!	0.2181	0.1852
ZNF662	1	#DIV/0!	#DIV/0!	#DIV/0!	#DIV/0!	#DIV/0!	#DIV/0!	0.1202	0.1408

		G1 and G1/S		Early S and Late S		G2 and G2/M		G2 and M	
		Run1		Run2		Run3		Run4	
Gene name	Peptides	Ratio M/L	Ratio H/L	Ratio M/L	Ratio H/L	Ratio M/L	Ratio H/L	Ratio M/L	Ratio H/L
CON__P00761	3	0.0766	0.0103	0.0829	0.0166	0.1012	0.0194	0.0826	0.0100
CON__P02662	2	0.2354	0.1543	0.0807	0.0683	0.1300	0.0914	0.1105	0.1489
CON__P02666	1	#DIV/0!	#DIV/0!	#DIV/0!	#DIV/0!	#DIV/0!	#DIV/0!	#DIV/0!	#DIV/0!
CON__P02769	5	0.0862	0.0805	0.0773	0.1477	#DIV/0!	#DIV/0!	#DIV/0!	#DIV/0!
IPI00604550	1	#DIV/0!	#DIV/0!	#DIV/0!	#DIV/0!	#DIV/0!	#DIV/0!	#DIV/0!	#DIV/0!
IPI00003865	2	0.5919	0.6898	2.8315	2.7011	1.0106	1.5571	1.3355	1.9917
IPI00794659	2	0.3889	1.0802	2.2971	2.3362	0.4397	1.7355	0.6188	1.6273
IPI00013296	5	0.2575	1.0170	2.3935	2.5210	0.3765	1.3905	0.4390	1.3477
IPI00789159	2	0.2492	1.3264	2.2685	2.6745	0.4905	1.6750	0.4849	1.2464
IPI00022037	1	#DIV/0!	#DIV/0!	#DIV/0!	#DIV/0!	#DIV/0!	#DIV/0!	#DIV/0!	#DIV/0!
IPI00025849	1	#DIV/0!	#DIV/0!	8.1604	1.7199	#DIV/0!	#DIV/0!	#DIV/0!	#DIV/0!
IPI00604590	5	0.7413	0.4491	0.9263	0.8713	0.7071	0.8242	0.6739	0.5481
IPI00026271	1	0.2433	0.9717	2.0398	2.1665	0.3839	1.3245	0.4483	1.1877
IPI00030179	9	0.2749	1.1555	2.3601	2.8638	0.4636	1.5620	0.5235	1.6432
IPI00216587	5	0.2383	1.0670	1.8841	2.4923	0.3973	1.5126	0.4989	1.5531
IPI00221088	5	0.2434	1.0239	1.6712	2.3204	0.4183	1.2740	0.4701	1.3019
IPI00221093	1	#DIV/0!	#DIV/0!	2.2834	2.4691	0.3987	1.4160	0.5014	1.4866
IPI00221222	2	0.4826	0.4650	1.0476	0.9009	0.4261	0.6934	0.6064	0.6877
IPI00247583	1	0.3289	1.1740	2.4936	2.6644	0.4143	1.5349	0.5081	1.4477
IPI00299573	5	0.2992	1.0829	2.0067	2.6464	0.5012	1.6513	0.5252	1.5925
IPI00304588	1	#DIV/0!	#DIV/0!	#DIV/0!	#DIV/0!	#DIV/0!	#DIV/0!	#DIV/0!	#DIV/0!
IPI00304612	5	0.2759	1.0545	2.8389	2.9521	0.4351	1.4874	0.5224	1.5243
IPI00396485	9	0.7358	0.5632	0.8933	0.8518	0.7019	0.7486	0.7171	0.6948
IPI00413108	4	0.2698	1.0357	1.9871	3.0068	0.5169	1.4047	0.7913	1.8313
IPI00977661	1	0.3137	1.4495	#DIV/0!	#DIV/0!	0.4078	1.5566	#DIV/0!	#DIV/0!
IPI00419919	1	0.3337	1.6194	1.8779	3.0918	0.4739	1.5181	0.5111	1.2017
IPI00470528	4	0.2574	1.0914	2.3392	2.5239	0.4410	1.4612	0.4879	1.4040
IPI00550021	4	0.2679	1.2615	1.8368	2.3038	0.4414	1.5763	0.5879	1.8815
IPI01019113	13	0.3936	0.5425	0.7366	0.7072	0.4002	0.6891	0.5776	0.8771
IPI00447176	1	#DIV/0!	#DIV/0!	#DIV/0!	#DIV/0!	#DIV/0!	#DIV/0!	#DIV/0!	#DIV/0!
IPI00847466	1	#DIV/0!	#DIV/0!	#DIV/0!	#DIV/0!	#DIV/0!	#DIV/0!	9.8327	#DIV/0!
IPI00921993	1	#DIV/0!	#DIV/0!	#DIV/0!	#DIV/0!	#DIV/0!	#DIV/0!	#DIV/0!	#DIV/0!
IPI00922424	1	#DIV/0!	#DIV/0!	#DIV/0!	#DIV/0!	#DIV/0!	#DIV/0!	#DIV/0!	#DIV/0!

Appendix Table 3.2: Log2 ratios of all UPS-associated proteins identified from sepharose-Ub-PA pull down (Runs 1 – 4).

		G1 and G1/S			Early S and Late S			G2 and G2/M			G2 and M		
		Run1			Run2			Run3			Run4		
Gene name	**Peptides**	**Ratio M/L**	**Ratio H/L**	**Intensity**	**Ratio M/L**	**Ratio H/L**	**Intensity**	**Ratio M/L**	**Ratio H/L**	**Intensity**	**Ratio M/L**	**Ratio H/L**	**Intensity**
OTUB1	12	0.14	-0.60	9.11	-0.47	-0.47	9.07	-0.41	-0.64	9.15	-0.32	-0.59	9.10
OTUD4	2	0.08	1.55	6.98	2.57	2.12	7.17	0.75	1.86	6.76	0.60	1.78	6.83
OTUD5	1	-0.97	-0.51	6.89	0.09	0.59	6.86	-0.72	0.24	6.78	-0.17	0.22	6.86
OTUD6B	3	-0.83	-0.60	7.78	-0.18	-0.13	7.78	-1.18	-0.41	7.75	-0.92	-0.35	7.68
UCHL1	9	0.86	-0.47	8.72	0.47	0.08	8.58	0.42	-0.05	8.64	0.30	-0.04	8.45
UCHL3	1	1.31	-0.26	7.24	-1.35	-0.82	7.08	1.62	1.01	7.14	0.04	-0.55	7.43
UCHL5	9	-0.73	-0.21	8.02	0.50	0.28	8.28	-0.72	0.01	8.13	-0.44	0.00	8.12
USP11	17	-0.58	0.39	8.49	0.73	0.87	8.61	-0.29	0.58	8.56	-0.23	0.56	8.39
USP14	1	-0.14	0.38	7.20	2.15	1.55	7.32	-0.61	0.64	7.04	-0.75	0.61	6.95
USP15	30	-0.28	-0.30	8.81	-0.44	-0.46	8.80	-0.73	-0.34	8.83	-0.68	-0.43	8.78
USP19	4	-0.41	-0.21	7.28	0.57	0.21	7.37	-0.58	-0.03	7.26	-0.29	0.01	7.22
USP24	17	-0.02	-0.26	8.06	-1.26	-1.18	7.97	-0.55	-0.37	8.12	-0.88	-0.84	8.16
USP28	7	-0.84	0.94	7.89	1.84	1.39	8.19	-0.80	0.99	7.85	-0.66	0.99	7.81
USP34	5	-0.58	0.70	7.50	0.82	0.61	7.61	-1.16	0.61	7.57	-1.16	0.53	7.29
USP4	6	-0.09	-0.24	7.48	-0.39	-0.46	7.46	-0.52	-0.30	7.58	-0.51	-0.48	7.29
USP40	8	-0.24	-0.73	7.76	-1.55	-1.10	7.56	-0.69	-0.94	7.78	-0.56	-0.93	7.70
USP47	21	-0.48	-0.92	8.52	-1.43	-1.11	8.32	-0.74	-0.96	8.49	-0.56	-0.97	8.38
USP5	36	0.00	0.29	9.54	0.53	0.36	9.62	-0.53	0.27	9.47	-0.58	0.14	9.43
USP7	49	-0.17	0.91	9.32	1.50	1.12	9.51	-0.58	0.92	9.29	-0.42	0.90	9.26
USP8	4	-0.95	-0.88	7.24	-0.07	-0.46	7.31	-0.01	-0.65	7.36	0.47	-0.62	7.34
USP9X	55	0.05	0.04	9.07	-1.23	-0.81	9.03	-0.50	-0.06	9.09	-0.91	-0.54	9.05
USP9Y	28	#VALUE!	#VALUE!	#NUM!	#VALUE!	#VALUE!	#NUM!	-0.50	-0.06	6.91	#VALUE!	#VALUE!	#NUM!
VCPIP1	12	-0.79	-0.35	8.26	-0.42	0.11	8.23	-0.54	-0.45	8.28	-0.17	-0.29	8.22

Appendix Table 3.2 cont.

			G1 and G1/S			Early S and Late S			G2 and G2/M			G2 and M		
			Run1			Run2			Run3			Run4		
Gene name	**Function**	**Peptides**	**Ratio M/L**	**Ratio H/L**	**Intensity**	**Ratio M/L**	**Ratio H/L**	**Intensity**	**Ratio M/L**	**Ratio H/L**	**Intensity**	**Ratio M/L**	**Ratio H/L**	**Intensity**
HUWE1	E3	3	-1.52	-0.86	6.84	0.02	-0.17	6.95	#VALUE!	#VALUE!	#NUM!	#VALUE!	#VALUE!	#NUM!
NEDD4	E3	1	-2.36	-2.60	6.94	#VALUE!	#VALUE!	#NUM!	-1.80	-1.21	6.63	#VALUE!	#VALUE!	#NUM!
PSMB4	Proteasomal	1	#VALUE!	#VALUE!	#NUM!	#VALUE!	#VALUE!	#NUM!	#VALUE!	#VALUE!	#NUM!	#VALUE!	#VALUE!	#NUM!
PSMD13	Proteasomal	1	#VALUE!	#VALUE!	#NUM!	#VALUE!	#VALUE!	#NUM!	#VALUE!	#VALUE!	#NUM!	#VALUE!	#VALUE!	#NUM!
TRIM4	E3	1	#VALUE!	#VALUE!	#NUM!	0.02	-0.12	7.35	-0.48	-0.38	7.49	-0.16	-0.33	7.55
UBA1	E1	10	-2.78	-3.09	8.35	-0.92	-1.00	7.27	-1.98	-2.12	7.82	-0.55	-0.96	7.50
UBC	Ubiquitin	8	-5.10	-5.42	9.25	-4.54	-4.72	8.86	-4.34	-6.22	9.40	-4.62	-5.39	8.82
UBE2D3	E2	1	-2.63	-2.68	7.25	#VALUE!	#VALUE!	#NUM!	-1.90	-2.16	7.27	#VALUE!	#VALUE!	#NUM!
UBE2N	E2	5	-2.80	-3.74	8.06	-1.27	-1.63	7.24	-2.04	-2.59	7.69	-0.54	-1.80	7.29

Appendix Table 4: Phospho-proteomic data from (Olsen et al., 2010), listing the cell cycle-dependent phosphorylation sites on DUBs.

Tabulated values refer to Log_2 ratios from synchronised cell populations compared to an asynchronous control (Olsen et al., 2010) (represented in the heat map in Figure 4.13).

DUB	Residue	G_1/S	Early S	Late S	G_2	M	G_1
ATXN3	-	-	-	-	-	-	-
ATXN3L	-	-	-	-	-	-	-
BAP1	S528	0	1.36	0	0	-1.36	0
BRCC3 (Iso1)	S28	0	0	-10.83	0	0	-2.8
BRCC3 (Iso1)	S43	-0.4	0	-10.83	3.01	0	-2.8
BRCC3 (Iso1)	S44	-0.4	0	-10.83	3.01	0	-2.8
BRCC3 (Iso1)	S48	-0.4	0	0	3.01	0	0
BRCC3 (Iso1)	S50	-0.4	0	0	3.01	0	0
BRCC3 (Iso1)	Y54	-0.4	0	0	3.01	0	0
BRCC3 (Iso1)	T55	-0.4	0	0	3.01	0	0
BRCC3 (Iso1)	T57	-0.4	0	0	3.01	0	0
BRCC3 (Iso1)	T61	-0.4	0	0	3.01	0	0
BRCC3 (Iso1)	T204	0	1.39	0	0	-2.32	0
BRCC3 (Iso2)	S28	0	0	-10.83	0	0	-2.8
BRCC3 (Iso2)	S43	-0.4	0	-10.83	3.01	0	-2.8
BRCC3 (Iso2)	S44	-0.4	0	-10.83	3.01	0	-2.8
BRCC3 (Iso2)	S48	-0.4	0	0	3.01	0	0
BRCC3 (Iso2)	S50	-0.4	0	0	3.01	0	0
BRCC3 (Iso2)	Y54	-0.4	0	0	3.01	0	0
BRCC3 (Iso2)	T55	-0.4	0	0	3.01	0	0
BRCC3 (Iso2)	T57	-0.4	0	0	3.01	0	0
BRCC3 (Iso2)	T61	0	0	0	0	0	0
BRCC3 (Iso2)	T229	0	1.39	0	0	-2.32	0
COPS5	-	-	-	-	-	-	-
COPS6	Y241	0	0	0	0	0	0
CYLD (Iso1)	-	-	-	-	-	-	-
CYLD (Iso2)	-	-	-	-	-	-	-
EIF3F	S233	0	0	0	0	0	0
EIF3F	T234	0	0	0	0	0	0
EIF3F	T270	0	-3.35	-2.44	0	2.57	1.6
EIF3F	T273	0	-2.89	2.44	0	2.89	2.44
EIF3F	T310	-0.32	0	0	-0.04	0	0
EIF3H	S197	2.21	-3.69	-4.31	-3.72	2.25	2.78
JOSD1	-	-	-	-	-	-	-
JOSD2	-	-	-	-	-	-	-
MPND							
MYSM1	-	-	-	-	-	-	-
OTUB1	-	-	-	-	-	-	-
OTUB2	-	-	-	-	-	-	-
OTUD1	-	-	-	-	-	-	-
OTUD4 (Iso1)	T339	-5.54	0	0	0.65	0	0
OTUD4 (Iso1)	S341	-5.54	0	0	0.65	0	0
OTUD4 (Iso1)	S893	0	-3.83	0	0	3.81	0
OTUD4 (Iso1)	S900	0	-3.83	0	0	3.81	0
OTUD4 (Iso1)	S1023	0	0.17	0	0	-0.19	0
OTUD4 (Iso1)	S1024	0	0.17	0	0	-0.19	0
OTUD5	S64	-1.05	0	0.42	1.12	0	0.6
OTUD5	S450	0	0	1.87	0	0	-0.85

DUB	Residue	G_1/S	Early S	Late S	G_2	M	G_1
OTUD5	S452	0	0	1.87	0	0	-0.85
OTUD5	T507	-1.19	0	0.86	1.26	0	0.16
OTUD5	S508	-1.19	0	0.75	1.26	0	0.27
OTUD5	S512	-1.19	0	0.86	1.26	0	0.16
OTUD6A	-	-	-	-	-	-	-
OTUD6B	-	-	-	-	-	-	-
OTUD7A	-	-	-	-	-	-	-
OTUD7B	S114	0	-2.76	0	0	2.52	0
OTUD7B	S463	0	1.5	-0.15	0	-1.74	0.38
OTUD7B	T465	0	1.5	-0.15	0	-1.74	0.38
PAN2 (USP52)	-	-	-	-	-	-	-
PARP11	-	-	-	-	-	-	-
PRPF8							
PSMD14	-	-	-	-	-	-	-
PSMD7	T182	0	0	0	0	0	0
PSMD7	S203	0	-0.45	0	0	-0.18	0
STAMBP	-	-	-	-	-	-	-
STAMBPL1 (Iso1)	S242	0	-4.93	0	0	1.01	0
STAMBPL1 (Iso2)	S242	0	-4.93	0	0	1.01	0
TNFAIP3	S573	0	-3.42	-0.29	0	3.42	0.29
TNFAIP3	S575	0	-3.36	-0.29	0	3.36	0.29
TNFAIP3	S578	0	-3.77	-0.29	0	3.37	0.29
TNFAIP3	S645	1.7	0	-1.71	-1.7	0	1.71
TNFAIP3	T647	-	-	-	-	-	-
TNFAIP3	S649	1.7	0	-1.71	-1.7	0	1.71
UCHL1	T85	0	0	-0.01	0	0	0.01
UCHL1	S89	0	0	-0.01	0	0	0.01
UCHL3	-	-	-	-	-	-	-
UCHL5 (Iso1)	T19	0	0	-1.05	0	0	1.05
UCHL5 (Iso2)	T19	0	0	-1.05	0	0	1.05
UCHL5 (Iso3)	T19	0	0	-1.05	0	0	1.05
UCHL5 (Iso4)	T19	0	0	-1.05	0	0	1.05
USP1	S7	0	-3.6	-3.32	0	0.42	0.15
USP1	S13	0	-3.6	-3.32	0	0.42	0.15
USP1	S16	0	-3.6	-3.32	0	0.42	0.15
USP1	S42	0	0	0	0	0	0
USP1	T307	0	-4.35	-3.82	0	1.17	0.64
USP1	S308	0	-4.35	-3.32	0	1.17	0.64
USP1	T310	0	-4.35	-3.32	0	1.17	0.64
USP1	S313	0	-4.35	-3.76	0	1.17	0.59
USP1	T529	0	0	-3.65	0	0	0.48
USP1	S768	0	-4.67	-4.66	0	1.49	1.49
USP1	S770	0	-4.67	-4.92	0	1.49	1.74
USP1	T771	0	-4.67	-4.92	0	1.49	1.74
USP1	S772	0	-5	-5.28	0	1.82	2.1
USP1	T774	0	-4.45	-4.92	0	1.27	1.74
USP1	S775	0	-4.67	-4.92	0	1.49	1.74
USP10	S10	0	-4.41	-2.73	0	3.94	2.59
USP10	Y13	0	-4.41	-3.29	0	3.94	3.16
USP10	S19	0	-4.41	-2.8	0	3.94	2.64
USP10	T29	0	-3.91	0	0	3.44	0
USP10	Y82	0	-3.91	0	0	3.44	0
USP10	S86	0	-3.91	0	0	3.44	0
USP10	T87	0	-3.91	0	0	3.44	0
USP10	S216	0.63	0	0	-1.89	0	0
USP10	S220	0.63	0	0	-1.89	0	0

DUB	Residue	G_1/S	Early S	Late S	G_2	M	G_1
USP10	S223	0.63	0	0	-1.89	0	0
USP10	S359	0	-4.06	0	0	3.59	0
USP10	S360	0	-4.06	0	0	3.59	0
USP10	S370	-0.92	-11.52	-1.78	-0.34	11.05	1.65
USP10	S552	0	-3.55	-3.97	0	3.08	3.83
USP10	S554	0	-3.55	-1.84	0	3.08	1.7
USP10	S568	0.21	0.44	0.42	-1.46	-0.91	-0.56
USP10	S576	-	-	-	-	-	-
USP10	S581	0.17	0.44	0.42	-1.42	-0.91	-0.56
USP10	T774	0	0	0	0	0	0
USP11	Y195	5.58	0	0	-6.11	0	0
USP11	S942	0	0	0	0	0	0
USP11	S943	0	0	0	0	0	0
USP11	S948	0	0	0	0	0	0
USP11	S952	0	0	0	0	0	0
USP11	S953	0	0	0	0	0	0
USP11	S956	0	0	0	0	0	0
USP12	T258	0	0	-1.54	0	0	-0.16
USP12	T259	0	0	-1.54	0	0	-0.16
USP13	S228	0	0	0	0	0	0
USP14	T67	0.3	0	0	-1.53	0	0
USP14	S73	0.27	0	0	-1.5	0	0
USP14	S82	0.3	0	0	-1.53	0	0
USP14	S142	0.27	-1.6	-1.27	-1.49	0.43	0.15
USP14	S147	0.27	-1.62	-1.27	-1.49	0.46	0.15
USP14	S227	0	0	0	0	0	0
USP14	S228	0	0	0	0	0	0
USP14	S229	0	0	0	0	0	0
USP14	S231	0	0	0	0	0	0
USP14	T234	0	0	0	0	0	0
USP14	S236	0	0	0	0	0	0
USP15 (Iso1)	S102	0	0	0	0	0	0
USP15 (Iso1)	Y104	0	0	0	0	0	0
USP15 (Iso1)	T105	0	0	0	0	0	0
USP15 (Iso1)	S225	0	-4.11	-3.09	0	3.98	3.07
USP15 (Iso1)	T226	0	-4.11	-3.09	0	3.98	3.07
USP15 (Iso1)	S229	0.38	-3.72	-3.09	-0.65	3.58	3.07
USP15 (Iso1)	S233	0.38	-3.76	-3.09	-0.65	3.62	3.07
USP15 (Iso1)	S242	0	-4.03	-3.18	0	3.89	3.16
USP15 (Iso1)	S244	0	-4	-3.1	0	3.87	3.08
USP15 (Iso1)	S245	0	-4.27	-2.71	0	4.13	3.69
USP15 (Iso1)	S961	0	0	0	0	0	0
USP15 (Iso1)	S965	0	0	0	0	0	0
USP15 (Iso2)	S102	0	0	0	0	0	0
USP15 (Iso2)	Y104	0	0	0	0	0	0
USP15 (Iso2)	Y105	0	0	0	0	0	0
USP15 (Iso2)	S932	0	0	0	0	0	0
USP15 (Iso2)	S936	0	0	0	0	0	0
USP15 (Iso3)	S102	0	0	0	0	0	0
USP15 (Iso3)	Y104	0	0	0	0	0	0
USP15 (Iso3)	Y105	0	0	0	0	0	0
USP15 (Iso3)	S936	0	0	0	0	0	0
USP15 (Iso3)	S940	0	0	0	0	0	0
USP16	T550	0	0.04	0.29	0	0.49	-0.08
USP16	S551	0	0.49	0.29	0	0.04	-0.08
USP16	S552	0	0.03	0.23	0	0.5	-0.02

DUB	Residue	G_1/S	Early S	Late S	G_2	M	G_1
USP16	T554	0	0.04	0.1	0	0.49	0.11
USP16	T600	0	-2.68	0	0	3.21	0
USP18	-	-	-	-	-	-	-
USP19	S406	0	-5.3	0	0	5.98	0
USP19	T407	0	-5.3	0	0	5.98	0
USP2	-	-	-	-	-	-	-
USP20	-	-	-	-	-	-	-
USP21	-	-	-	-	-	-	-
USP22	-	-	-	-	-	-	-
USP24	S1143	1.29	0.25	0	0.55	-0.41	0
USP24	S1610	0	-3.75	-3.05	0	3.59	2.51
USP24	S1612	0	-3.75	-3.05	0	3.59	2.51
USP24	S1616	0	-3.75	-2.68	0	3.59	2.14
USP24	S2043	0.14	-0.93	-0.66	1.7	0.76	0.12
USP24	S2047	2.39	-0.93	-0.66	-0.55	0.76	0.12
USP24	S2077	2.65	0	0	-0.82	0	0
USP24	S2080	2.65	0	0	-0.82	0	0
USP24	S2081	2.65	0	0	-0.82	0	0
USP24	T2559	2.46	-0.7	-1.01	-0.62	0.54	0.47
USP24	S2561	2.46	-0.69	-0.81	-0.62	0.53	0.27
USP24	T2565	2.46	-0.83	-0.67	-0.62	0.67	0.13
USP24	T2570	2.46	-0.7	-0.51	-0.62	0.54	-0.03
USP25	-	-	-	-	-	-	-
USP26	-	-	-	-	-	-	-
USP27X	-	-	-	-	-	-	-
USP28	-	-	-	-	-	-	-
USP29	-	-	-	-	-	-	-
USP3	-	-	-	-	-	-	-
USP30	-	-	-	-	-	-	-
USP31	-	-	-	-	-	-	-
USP32	-	-	-	-	-	-	-
USP33	-	-	-	-	-	-	-
USP34	T1048	0	-3.48	0	0	3.66	0
USP34	Y1049	0	-3.48	0	0	3.66	0
USP34	T2053	0	-0.53	-0.14	0	0.7	-0.02
USP34	Y2060	0	-0.53	-0.14	0	0.7	-0.02
USP34	T2061	0	-0.53	-0.14	0	0.7	-0.02
USP34	S2063	0	-0.53	-0.14	0	0.7	-0.02
USP34	S2215	-1.65	0	0	1.65	0	0
USP34	T2217	0.18	0	0	-0.18	0	0
USP34	S2591	0.18	0	0	-0.18	0	0
USP35	-	-	-	-	-	-	-
USP36	Y60	1.83	0	0	-4.11	0	0
USP36	S464	0	0	0	0	0	0
USP36	S467	0	0	0	0	0	0
USP36	S580	0	-2.05	-4.59	0	0.6	2.11
USP36	T581	0	-1.93	-3.74	0	0.49	1.27
USP36	S582	0	-5.21	0	0	3.76	0
USP36	S667	0	-5.32	0	0	3.88	0
USP36	S671	0	-5.32	0	0	3.88	0
USP36	T673	0	-5.32	0	0	3.88	0
USP36	T674	0	-5.32	0	0	3.88	0
USP36	T675	0	-5.32	0	0	3.88	0
USP36	T680	0	-5.37	0	0	3.92	0
USP36	S682	0	-5.27	0	0	3.83	0
USP36	S692	0	0	0	0	0	0

DUB	Residue	G_1/S	Early S	Late S	G_2	M	G_1
USP36	S713	0	-3.98	-4.59	0	2.54	2.11
USP36	S742	-0.35	0	0	-1.93	0	0
USP36	T1067	0	0	0	0	0	0
USP36	S1118	-2.01	-1.71	-0.65	-0.27	0.27	-1.82
USP36	S1120	-2.01	-1.71	-0.65	-0.27	0.27	-1.82
USP36	Y1121	-2.01	-1.71	-0.65	-0.27	0.27	-1.82
USP37	-	-	-	-	-	-	-
USP38	-	-	-	-	-	-	-
USP39	S192	-1.62	0	-0.4	3.13	0	1.62
USP39	T197	0	0	-0.4	0	0	1.62
USP4	-	-	-	-	-	-	-
USP40	-	-	-	-	-	-	-
USP41	-	-	-	-	-	-	-
USP42	S611	-0.36	0	0	0.39	0	0
USP42	S612	-0.36	0	0	0.39	0	0
USP42	S615	-0.36	0	0	0.39	0	0
USP42	S754	-1.11	0	-0.64	1.05	0	-6.4
USP42	S759	-1.11	0	-0.64	1.05	0	-6.4
USP42	T772	-1.11	0	-0.64	1.05	0	-6.4
USP42	S829	1.31	0	0	-1.38	0	0
USP42	S832	1.31	0	0	-1.38	0	0
USP42	S856	-0.34	-0.12	1.55	0.27	0.75	-8.6
USP42	S1115	0	0	-0.84	0	0	0.82
USP42	S1227	0	0	0	0	0	0
USP42	S1281	0	0	-2.19	0	0	-4.86
USP43	-	-	-	-	-	-	-
USP44	-	-	-	-	-	-	-
USP45	-	-	-	-	-	-	-
USP46	-	-	-	-	-	-	-
USP47 (iso1)	S832	0	-4.35	-5.22	0	2.96	3.99
USP47 (iso1)	S933	0	0	-1.51	0	0	0.28
USP47 (iso1)	Y1352	0	-2.35	0	0	0.96	0
USP47 (iso1)	S1353	0	-2.35	0	0	0.96	0
USP47 (iso2)	S744	0	-4.35	-5.22	0	2.96	3.99
USP47 (iso2)	S845	0	0	-1.51	0	0	0.28
USP47 (iso2)	Y1264	0	-2.35	0	0	0.96	0
USP47 (iso2)	S1265	0	-2.35	0	0	0.96	0
USP47 (iso3)	Y134	0	-2.35	0	0	0.96	0
USP47 (iso3)	S135	0	-2.35	0	0	0.96	0
USP48 (iso1)	S287	0	-0.09	0	0	-1.61	0
USP48 (iso2)	S287	0	-0.09	0	0	-1.61	0
USP48 (iso3)	S287	0	-0.09	0	0	-1.61	0
USP48 (iso4)	S287	0	-0.09	0	0	-1.61	0
USP48 (iso7)	S287	0	-0.09	0	0	-1.61	0
USP49	-	-	-	-	-	-	-
USP5	T148	0	-7.39	0	0	7.83	0
USP5	S149	0	-7.39	0	0	7.83	0
USP5	S156	0	-7.39	0	0	7.83	0
USP5	S161	0	-6.16	0	0	6.6	0
USP5	T292	0	-3.52	0	0	3.96	0
USP5	Y485	-0.06	0	0	0.86	0	0
USP5	Y505	-0.06	0	0	0.86	0	0
USP5	S779	0	-2.07	0	0	2.5	0
USP5	S783	0	-2.07	0	0	2.5	0
USP50	-	-	-	-	-	-	-
USP51	-	-	-	-	-	-	-

DUB	Residue	G_1/S	Early S	Late S	G_2	M	G_1
USP53	-	-	-	-	-	-	-
USP54	-	-	-	-	-	-	-
USP6	-	-	-	-	-	-	-
USP7	S18	0.06	-1	0	-1.58	0.1	0
USP8	Y12	0	-0.89	-0.67	0	0.03	-0.25
USP8	S108	0	0	0	0	0	0
USP8	S160	0	-3.72	0	0	2.86	0
USP8	S378	0	0	0	0	0	0
USP8	T379	0	0	0	0	0	0
USP8	S287	0	0	0	0	0	0
USP8	S389	0	-2.57	0	0	1.71	0
USP8	S392	0	-2.57	0	0	1.71	0
USP8	T594	0	0	-1.58	0	0	0.65
USP8	S599	0	0	-1.58	0	0	0.65
USP8	S653	-0.61	0	0	-0.11	0	0
USP8	S716	0.73	-2.95	-1.95	-1.45	2.09	1.02
USP8	Y717	0.9	-2.95	-1.29	-1.62	2.09	0.36
USP8	S718	0.9	-2.95	-1.37	-1.62	2.09	0.44
USP8	S719	0.9	-2.95	-1.29	-1.62	2.09	0.36
USP9X	-	-	-	-	-	-	-
USP9Y	T2205	-0.98	0	0	0.7	0	0
USPL1	-	-	-	-	-	-	-
VCPIP1	S131	0	0	0	0	0	0
VCPIP1	S994	1.07	-0.96	-2.13	-0.62	1.24	1.99
VCPIP1	S998	1.22	-0.45	-0.05	-0.76	0.73	-0.09
VCPIP1	S1128	0	-2.76	0	0	3.05	0
VCPIP1	S1132	0	-2.76	0	0	3.05	0
VCPIP1	S1134	0	-2.76	0	0	3.05	0
VCPIP1	S1198	0	0	0	0	0	0
YOD1	-	-	-	-	-	-	-
ZRANB1	-	-	-	-	-	-	-
USP17L2 (DUB3)	-	-	-	-	-	-	-
USP17	-	-	-	-	-	-	-